Physical Features of Ultrasound-Enhanced Desulfurization of Liquid Fuels

A
Thesis
Submitted in
Fulfillment of the
Requirements for the Degree of

DOCTOR OF PHILOSOPHY

Jaykumar B. Bhasarkar

DEPARTMENT OF CHEMICAL ENGINEERING
Indian Institute of Technology Guwahati
Guwahati – 781 039, Assam, India

January 2016

Dedicated

to

My Parents

&

My Lovely Wife

who Mean the World to me

INDIAN INSTITUTE OF TECHNOLOGY GUWAHATI

DEPARTMENT OF CHEMICAL ENGINEERING

STATEMENT

I do hereby declare that the content embodied in this thesis entitled "**PHYSICAL FEATURES OF ULTRASOUND-ENHANCED DESULFURIZATION OF LIQUID FUELS**" is the result of investigations carried out by me at Department of Chemical Engineering, Indian Institute of Technology Guwahati, Guwahati, India, under the guidance of Prof. Vijayanand S. Moholkar.

In keeping with the general practice of reporting scientific observations, due acknowledgements have been made wherever the work described is based on the findings of other investigators.

January 2016

Jaykumar B. Bhasarkar

(Roll No.: 11610715)

INDIAN INSTITUTE OF TECHNOLOGY GUWAHATI

DEPARTMENT OF CHEMICAL ENGINEERING

CERTIFICATE

It is certify that the work contained in the thesis entitled " **PHYSICAL FEATURES OF ULTRASOUND-ENHANCED DESULFURIZATION OF LIQUID FUELS**", by **Jaykumar B. Bhasarkar** (Roll No: 11610715), has been carried out under my supervision and that this work has not been submitted elsewhere for a degree

Prof. Vijayanand S. Moholkar
Professor
Department of Chemical Engineering
Indian Institute of Technology,Guwahati
Guwahati – 781 039
Assam, India

CONTENTS

LIST OF TABLES

LIST OF FIGURES

Chapter 1

Chapter 2

Chapter 1

Introduction and Literature Review

Introduction and Literature Review

1.1 INTRODUCTION

Clean energy production is one of the most pressing issues of modern times – in view of environmental concerns, in addition to cater growing energy needs of society (domestic usage), agriculture and industry. Producing energy in a clean manner can be accomplished in a number of ways. A possible solution to this issue is renewable (non–fossil fuel) energy sources such as solar, wind, and nuclear power, which are being increasingly used globally. The convectional technique for producing energy, i.e. combustion of fossil fuels, has adverse effects on the environment due to emission of greenhouse gas CO_2, which contributes to global warming. In addition, emissions of other gases such as SO_x and NO_x during combustion of fossil fuels also cause enormous damage to environment. These gases react with water in the atmosphere to form sulfates and acid rain, which acidifies soil leading to loss of arable land with

removal of soil nutrients such as calcium and magnesium, loss of forests due to weakening of trees' natural defenses, in addition to acidification of other aquatic ecosystems such as lakes, rivers and streams, which causes enormous harm to fish and other aquatic life. Acid rain also has other destructive effects such as damage to the building materials and paints. Sulfur emissions cause respiratory illnesses, aggravate heart disease, trigger asthma, and contribute to formation of atmospheric particulates. SO_x and NO_x emissions during combustion of fossil fuels are a consequence of presence of contaminants in the fuel in the form of sulfur and nitrogen containing compounds. Oxidation of these sulfur/nitrogen compounds during combustion of fuel leads to the emissions of SO_x and NO_x gases. large number of sulfur compounds in the form of thiols, sulfides, disulfides and thiophene originally present in crude oil end up in liquid transportation fuels (diesel and petrol) produced by refining of crude oil. In order to curb the environmental pollution due to emissions of SO_x and NO_x gases through vehicular exhaust, stringent restrictions have been imposed by many countries on sulfur content of the fuel. U.S. Environmental Protection Agency has mandated the sulfur content of common liquid transportation fuels, viz. diesel and petrol/gasoline, as 15 and 30 ppm, respectively.

Presence of sulfur compounds in crude oil is also highly undesirable due to adverse effects of these compounds on the catalysts used in different processes of crude oil refining such as fluidized catalytic cracking (FCC), catalytic reforming, hydrocracking and steam–cracking. Therefore, effective removal of these compounds is utmost essential for the stability and durability of the catalyst, which is a cost intensive component of the refining processes.

Due to these reasons, much attention has been focused on desulfurization and even deep desulfurization of crude oil. In gasoline fraction of crude oil, more than 90%

sulfur present is in the form of thiophene and its derivatives, while in diesel fraction, thiophene sulfur is reported to contribute 80% of the total sulfur, with benzothiophene and dibenzothiophene as main components (Lin et al., 2009).

1.1.1 Environmental Legislation

The linear relationship observed between sulfur level in the diesel fuel and the particulates and other harmful pollutants in the emissions are the main reasons for targeting sulfur content in diesel fuel specifications, and reducing it to as low level as possible, in many countries worldwide. Significant reduction in sulfur induced corrosion and slower acidification of engine lubricating oil (which leads to longer maintenance intervals and lower maintenance costs), are additional benefits of using ultra low sulfur diesel in vehicles. Sulfur specifications for diesel used in vehicles in many countries are shown in Table 1.1.

Table 1.1: Sulfur emission standards for diesel for different countries

Region	Country	Sulfur (ppm)	Year of implementation
South America	Argentina	50	2008
	Brazil	50	2009
	Chile	50	2010
	Mexico	15	2009
Asia pacific	China	50	2012
	Hong Kong	350	2005
	India	50	2010
	Singapore	50	2007
	Taiwan	50	2007
	Australia	10	2009
Middle East	Kuwait	50	2010
	Saudi Arabia	10	2013
	Qatar, UAE	10	2010
	Bahrain	10	2013
EU	Germany, France, Denmark, Sweden	< 10	2010

(Source: Fuel Regulations, www.dieselnet.com/standards/fuels.html.)

1.1.2 Petroleum Refining

Refining crude liquid fuel is a complicated series of chemical processes & operations designed to separate petroleum into a variety of useful products, each meeting certain compositional criteria. Refining begins by fractionating (distilling) crude oil into a series of streams with defined boiling ranges. Table 1.2 shows some of the fractions and their boiling ranges.

Table 1.2: Fractions of crude oil and their boiling ranges (Pafko, 2000)

Distillate Fraction	**Boiling Point (^{o}C)**
Gases / LPG	< 30
Straight–run gasoline	30–210
Naphtha	100–200
Kerosene	150–250
Diesel & fuel oil	160–400
Heavy fuel oil	315–540

In this chapter, a brief description and overview of the basic scientific and technical details of various techniques for desulfurization currently practiced in petroleum refineries has been given. In addition, a description of alternate techniques of desulfurization, viz. oxidative and bio–desulfurization, along with review and analysis of the contemporary literature employing these techniques is presented. Finally, a brief review of state–of–the–art research on the convention desulfurization technique of hydrodesulfurization is also presented. On the basis of this literature review and analysis, the purpose of the present thesis has been justified, followed by description of aim, approach and scope (or content) of the thesis.

1.2 CONVENTIONAL TECHNIQUES FOR DESULFURIZATION OF FUEL

As noted in preceding section, several processes have been developed and practiced for removal of sulfur compounds from fuel. Depending on the predominant mechanism of transformation of sulfur compounds, these processes can be divided into three groups: decomposition, separation without decomposition and decomposition with separation. Fig. 1.1 shows categorization of different sulfur removal techniques into the above three groups.

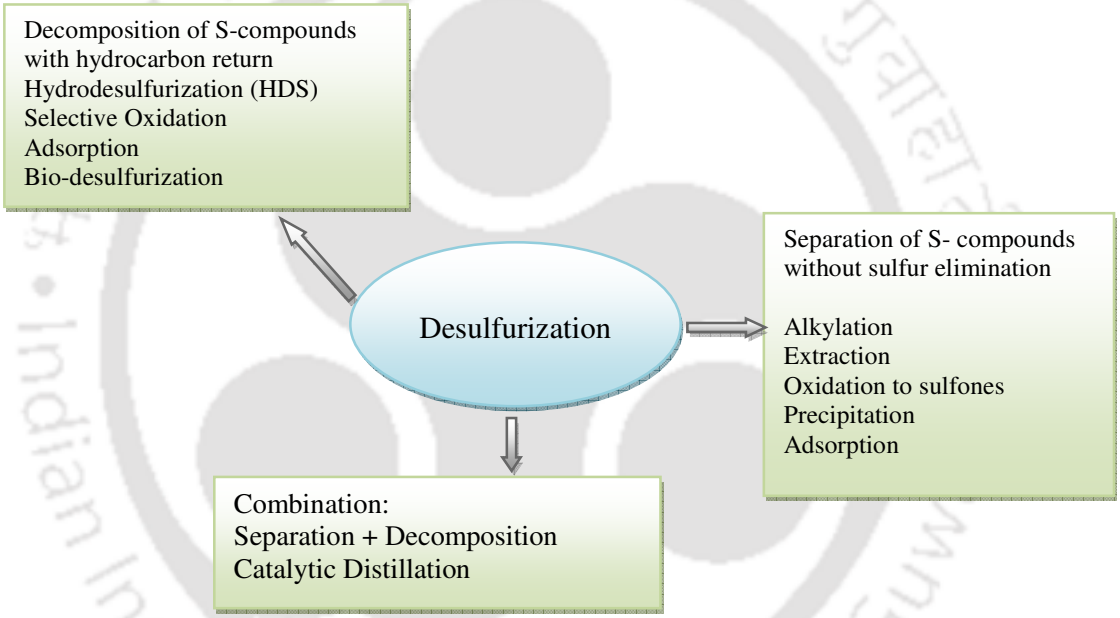

Figure 1.1: Categorization of different sulfur removal techniques

Desulfurization techniques practiced in petroleum refineries are broadly divided into two categories: (a) Hydrodesulfurization process (HDS), and (b) Non–HDS processes. HDS is the most common and widely practiced industrial process, which involves treating the fuel under high temperatures and high pressures with hydrogen. This process is called hydrodesulfurization (HDS). Non HDS processes include: (1) Adsorption desulfurization, (2) Oxidative desulfurization, and (3) Microbial

desulfurization.

1.3 Hydrodesulfurization (HDS) Process

As noted earlier, hydro–desulfurization is the convectional process widely used in refinery industry, and it essentially involves reaction of the sulfur containing compounds in liquid fuel with hydrogen under high temperatures (300°–450°C), and high pressures (3–5 MPa) that results in removal of sulfur present in the hydrocarbons as H_2S. In HDS process, generally Co–Mo/Al_2O_3 or Ni–Mo/Al_2O_3 catalysts are used for desulfurization of liquid fuels (Whitehurst et al., 1998, Shafi and Hutchings, 2000). Due to very harsh conditions, olefins in the crude oil also get hydrogenated in the process, leading to loss of octane rating and excess hydrogen consumption. Under mild operating conditions, H_2S can react with olefins in the feed to create recombinant mercaptans, which are linear or branched thiols of typically 5–12 carbons. The formation of recombinant mercaptans causes sulfur to be retained in the product, limiting the effectiveness of the HDS process. Further research in HDS catalysis and process designs are being carried out so as to increase the extent of sulfur removal, while maintaining the fuel quality at required specification. A typical flowsheet of the HDS process is shown in Fig. 1.2. In this process, light oil is heated and mixed with hydrogen, and fed to a reactor packed with pelleted catalysts. Temperatures in the reactor typically range from 300° to 380°C. At these temperatures, some or all of the feed is vaporized, depending on the boiling range of the feed and the pressure in the unit. For heavier feeds with high boiling points, hydrodesulfurization could also be a liquid–phase process. Reaction pressures range from as low as 15 to 90 bars depending on the difficulty of reaction of sulfur compound with hydrogen (Babich et al., 2003). In the hydro–desulfurization of light fractions of crude oil (such as

gasoline, diesel or jet fuel), pressures higher than 30 bar are commonly used. In the older processes, the reactor operation was downdraft (i.e. feed and hydrogen mixture flow downward through the fixed bed reactor), passing through the particulate catalyst. In new processes (Synsat process), however, the flow of reaction mixture is upwards from the bottom of the reactor (Babich et al., 2003). The reactor effluent (i.e. mixture of treated fuel and unreacted hydrogen) flows through a series of mechanical devices to separate and recycle the unreacted hydrogen, remove the H_2S generated in the reaction, and recover the desulfurized products. It is well established mechanism / pathway of HDS for DBT and alkyl DBT molecules proceed mainly via two parallel routes as shown in Fig. 1.3. The first route involves direct desulfurization leading to the formation of biphenyl, while the second route involves hydrogenation of one of the benzene rings of the DBT producing tetrahydro dibenzothiophene in the first step, which is further desulfurized to cyclohexyl benzene (Shafi and Hutchings, 2000, Girgis and Gates, 1991).

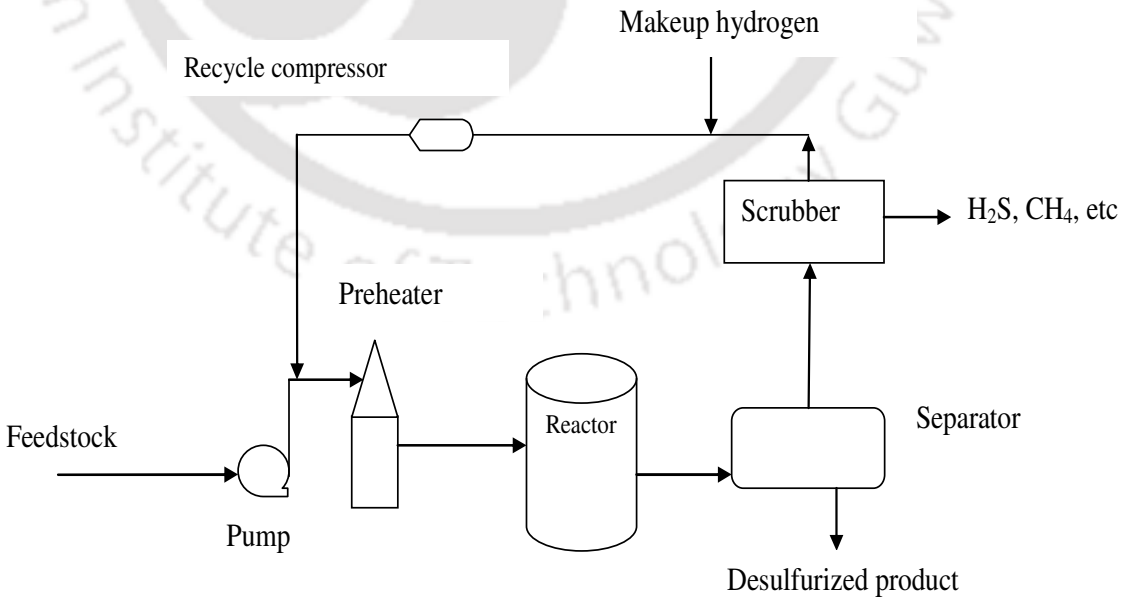

Figure 1.2: Typical flowsheet of hydrodesulfurization process

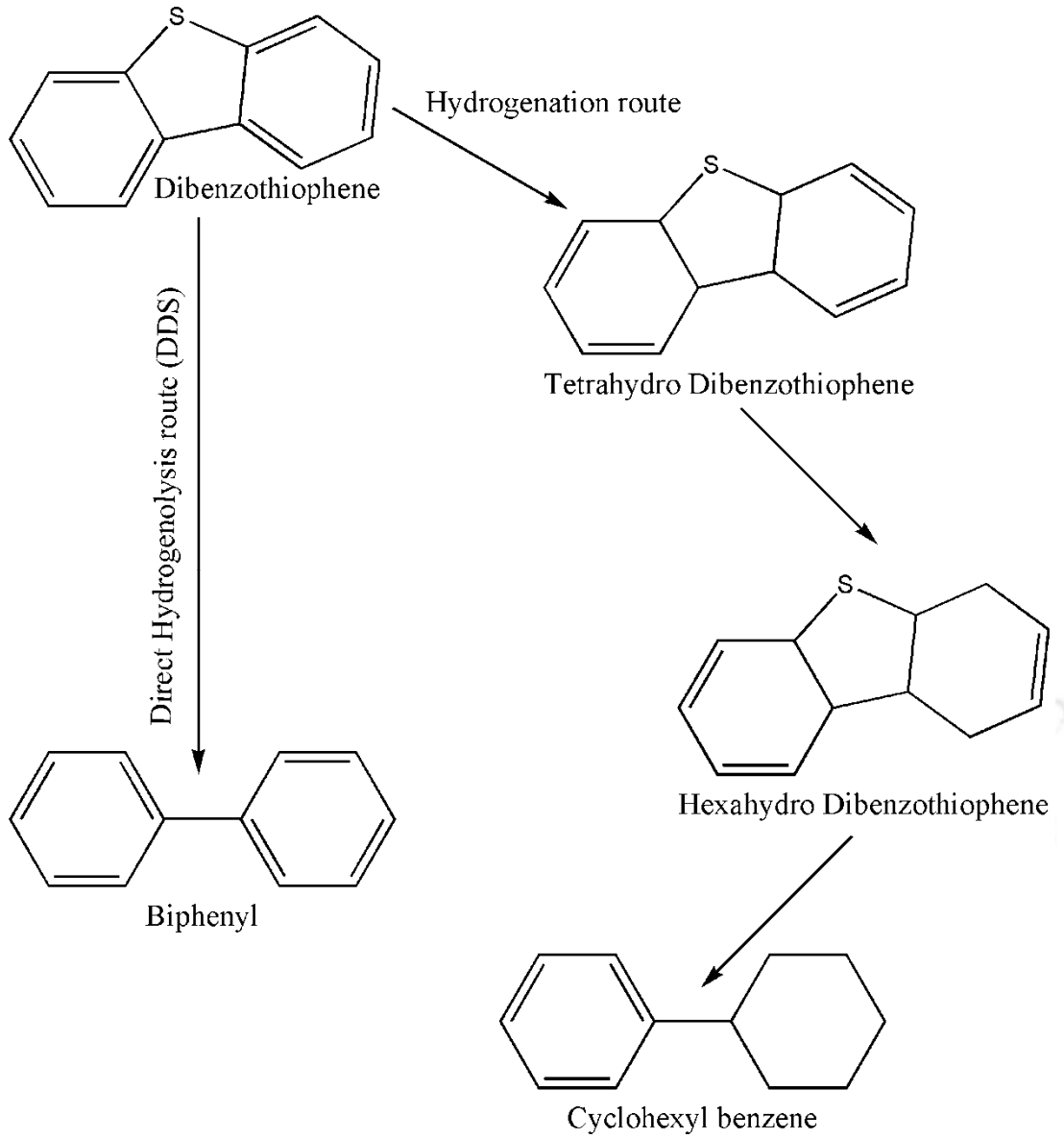

Figure 1.3: Reaction mechanism / pathway of HDS for DBT (Fuentes and Bartholomew, 1997)

1.3.1 Effect of refractory organosulfur compounds on HDS

The major limitation of hydro–desulfurization process is that it is not capable of removing all sulfur compounds in diesel fuel such as benzothiophene, alkyl dibenzothiophene and alkyl derivatives of dibenzothiophene. The major cause leading to this effect is presence of alkyl group at the 4 and 6 positions relative to sulfur atom

(Song et al., 2006). The reactivity chart of different sulfur compounds under hydro–desulfurization process is given in Fig. 1.4. Sulfur compounds found in fuels are usually H_2S, mercaptans, sulfides, disulfides, thiophene, benzothiophene (BT) and its derivative. The reactivities of the sulfur compounds take the following sequence: Sulfides > mercaptans > thiophenes > BT > DBT > 4MDBT > 4,6 DMDBT (Andari et al., 1996; Torrisi and Gunter, 2004).

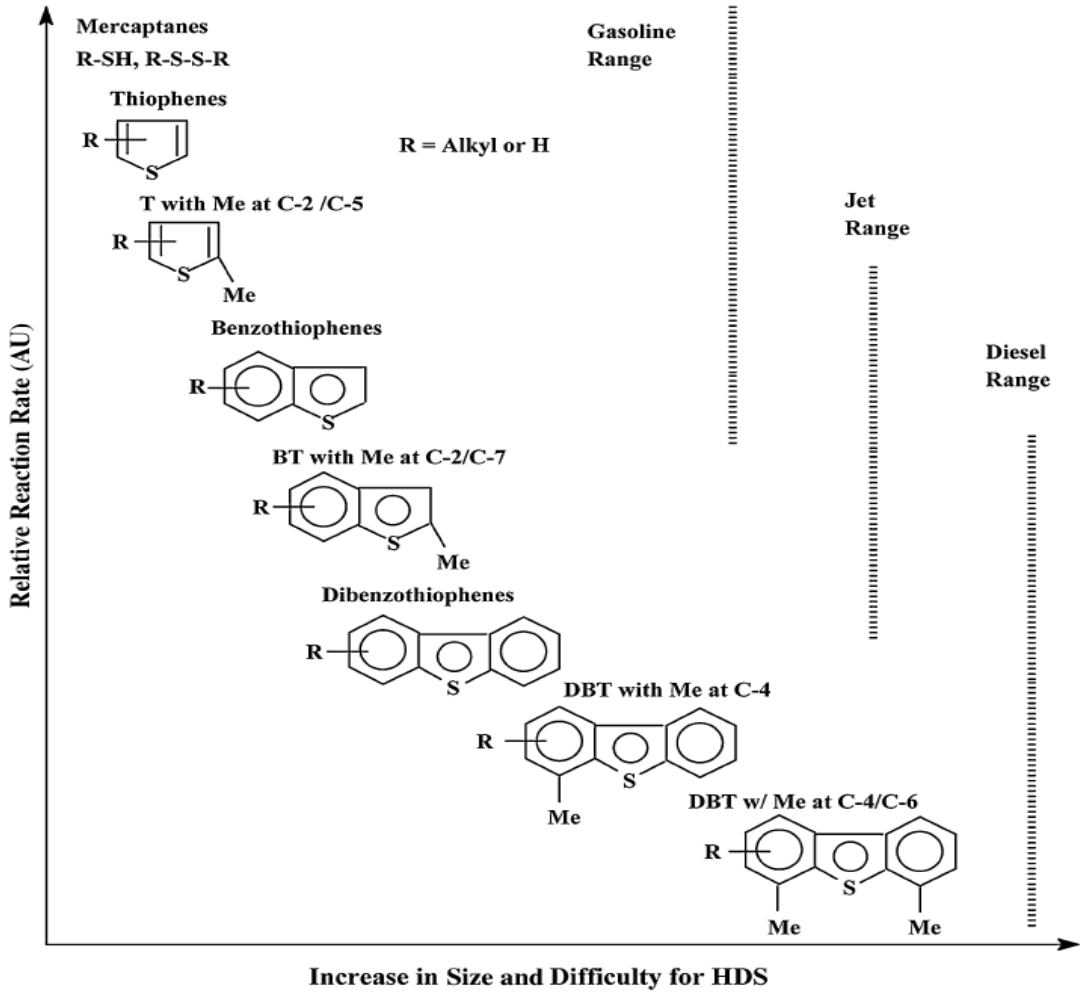

Figure 1.4: Reactivity chart of different sulfur compounds in desulfurization as a function of their molecular size and positions of alkyl substituents in the ring (Song et al., 2006).

1.3.2 Catalyst for Hydrodesulfurization (HDS)

Catalysts play an important role in various petroleum processes including diesel feedstocks hydrotreatment to produce clean fuels. Catalysts consisting of molybdenum supported on γ–alumina and promoted with cobalt or nickel are mostly used in the hydro–treating processes. The role of the catalyst is to enhance removal of sulfur, nitrogen and other undesirable contaminants present in the refinery streams by promoting hydrodesulfurization. Co–Mo and Ni–Mo based hydrotreating catalysts are highly active in reducing sulfur compounds such as, mercaptans, thiophenes, thioethers, and disulfides; however, they require severe operating conditions such as high temperature, low space velocity and high hydrogen partial pressure. Several studies have been shown that the CoMo catalysts are about 4 times more active than NiMo under normal operating conditions (Knudsen et al., 1999). Improvement in catalyst activity is necessary when the sulfur content is to be reduced upto < 15 ppm. Intensive efforts have been devoted by researchers worldwide to develop highly active hydrotreating catalysts for deep desulfurization of diesel to ultralow levels as required (Topsoe et al., 2005; Costa et al., 2008; Knudsen et al., 1999; Fujikawa et al., 2006 Wan et al., 2009). HDS catalysts have mainly two components, *viz.* support and active metals. Alumina is conventionally used as a support for HDS catalysts for its stability under harsh conditions, but many other supports based on mixed oxides and zeolites have been developed in recent years (Oyama et al., 2009; Perot et al., 2003; Muralidhar et al., 2003).

1.3.3 Support for HDS catalyst

In HDS catalysts, the active components (mixed sulfides of Mo and Co or Ni as Co–Mo–S or Ni–Mo–S phases) are supported on a carrier. The carrier or support material

usually provides high surface area and also provides mechanical strength to the catalyst. Al_2O_3 is the most widely used support material for HDS catalysts due to highly stability, content of acidic and basic sites, high surface area and porosity. New supports for HDS catalysts, viz. TiO_2, ZrO_2, MgO, carbon, SiO_2, zeolites etc., are being explored for better catalytic activity, higher surface area and other suitable properties as catalyst support for given application (Rayo et al., 2009; Rana et al., 2005; Al–Dolama et al., 2006; Zhao et al., 2008). Okamoto and coworkers (2008, 2010) have studied the effect of nature of support (Al_2O_3, TiO_2, ZrO_2 and SiO_2) using supported Mo–sulfide and of supported Co–Mo sulfide model catalysts on catalytic activity in two cases, viz. (1) HDS of thiophene, and (2) hydrogenation of butadiene. Co–Mo catalysts were prepared by chemical vapor deposition of $Co(CO)_3NO$ on supported Mo–sulfide. Authors concluded that the Co species deposited in this way were located at the edges of the MoS_2 particles. For HDS of thiophene, most active catalyst was SiO_2–supported MoS_2, while least active catalyst was Al_2O_3–supported MoS_2. On the other hand, for hydro–genation of butadiene, most active catalyst was ZrO_2–supported MoS_2, while SiO_2– supported MoS_2 catalyst was the least active catalyst.

A few studies have also treated the matter of acidic and basic nature of support, and its effect on the nature of interaction with the active metal. TiO_2 mixed oxide received relatively higher attention because it shows higher activity. Detailed explanation of characterization of hydrotreating catalysts supported on TiO_2–Al_2O_3 binary oxides was given by Ramirez et al. (1993). The catalytic behavior over the TiO_2–Al_2O_3 supported Mo catalysts, in particular for the 4,6–dimethyl–DBT, was much higher than that obtained over Al_2O_3 supported Mo catalyst. Muralidhar et al. (1984) have studied separately the HDS of thiophene and the hydrocracking of 2,4,4–

trimethylpentene over various supported CoMo catalysts. They compared the catalysts CoMo supported on different types of alumina to CoMo supported on SiO_2–Al_2O_3, SiO_2–MgO and TiO_2. They concluded that the CoMo–Al_2O_3 catalysts were most active for HDS. However, the Al_2O_3–supported catalysts were less active in hydrocracking, which is an indication that they were less acidic than the other catalysts. The authors found that increasing the SiO_2 content in SiO_2–Al_2O_3 support decreased both the HDS and hydrogenation activities but increased the hydrocracking activity. Wang et al. (2015) have studied the Co–Mo–S catalysts supported on tri–modal porous Al_2O_3 for the hydrodesulfurization of fluid catalytic cracking gasoline. To improve the performance of CoMoS catalysts applied to the hydrodesulfurization (HDS) of fluid catalytic cracking (FCC) gasoline, a series of CoMoS/Al_2O_3 catalysts were prepared with alumina of different pore structures, and their HDS performance was evaluated with real FCC gasoline. This study indicated that CoMoS/Al_2O_3 catalysts prepared with micro or meso–porous alumina possessed high HDS activity but low selectivity, whereas macro–porous alumina enhanced the selectivity of CoMoS catalysts. Flego et al. (2001) aimed at improving the activity of CoMo catalysts in view of deep desulfurization of fuels. The authors prepared CoMo catalysts with various supports containing metal (viz. Zr, Si, and B) oxides having different acid–base properties and measured their activity in the HDS of thiophene. The authors also estimated the hydrogenation activity of the catalysts from the butane selectivity in the HDS products. Both HDS and hydrogenation activities increased with increasing acid site density. The authors interpreted the relative decrease in hydrogenation activity of the samples containing boron oxide by supposing that the olefins were too strongly adsorbed on the acid sites to migrate to the sulfide phase. Klimova et al. (1998) used Mg–Al mixed oxides prepared by the sol–gel method as

supports for Mo and NiMo catalysts. The results indicated that even with the incorporation of small amounts of magnesia in alumina, the hydrogenation function of the un–promoted Mo–catalyst was substantially reduced, while the thiophene conversion was much less affected. The gain in HDS/hydrogenation selectivity resulting from the addition of magnesia was attributed to the fact that the size of MoS_2 crystallites increased with increasing magnesia content, as compared to their size on pure alumina. This interpretation implies that hydrogenation takes place at corner sites, the addition of magnesia leads to an increased proportion of edge versus corner sites. However, with Ni promoted catalysts with Ni/ (Ni + Mo) ratio of 0.3, there was continuous and substantial drop in HDS activity with increasing magnesia loading, which paralleled the decrease in hydrogenation activity. Kagami et al. (2005) also studied the catalytic activities of $NiMo/Al_2O_3$ catalysts on various model compounds like thiophene, tetrahydrothiophene, dibenzothiophene and 4,6–dimethyldibenzothiophene.

The use of zeolites and amorphous silica–alumina as supports for HDS active phases (e.g. Mo, CoMo, NiMo etc.) have been the subject of many studies. Zeolites are highly acidic and contain Bronsted acidity that can improve the HDS activity for refractory sulfur compounds such as DBT, 4,6–DMDBT. The Bronsted acidity of the support can promote isomerization of the alkyl groups in the alkyl DBTs and suppress their steric hindrance (Perot, 2003). The main problem in using zeolites as supports for HDS catalysts is the difficulty in the impregnation and dispersion of the active phase (*e.g.* MoS_2, Co–Mo–S or Ni–Mo–S) on the support surface. Another type of HDS catalyst, nano–porous alumino–silicate based materials such as MCM–41, Al–MCM–41, SBA–15 have received considerable attention as supports for Co and Ni promoted MoS_2 catalysts (Corma et al., 1995, 1996; Song et al., 1999; Klimova et al.,

1998; Gutierrez et al., 2008; Ren et al., 2008). Carbon–supported catalysts have also been found to show high HDS activity with reduced deactivation by coke deposition due to a lower acidity of the carbon support (Kouzu et al., 2004). Rapid sintering of the active phase under reaction conditions and its unsuitability for regeneration (after deactivation) are major disadvantages in using this support.

1.3.4 Unsupported catalysts for HDS

Unsupported transition metal sulfides, have also attracted a great deal of attention in recent years as potential new catalysts for HDS reactions (Ho, 2003; Oyama et al., 2009; Yoosuk et al., 2008; Ho, 2008, Chianelli et al., 2009). The materials tested include RuS_2, V_2S_3, NbS_3, mixed sulfides of Co–Mo, Ni–Mo, Ni–W, Ni–Mo–W, Fe–W, Fe–Mo, Ni–Ru. RuS_2, Rh_2S_3 and NbS_3 were found to exhibit improved HDS performance over the traditional Co–Ni and Mo–W metal sulfides (Hermann et al., 2000; Plantenga et al., 2003). Unsupported tri–metallic Ni–Mo–W sulfide exhibited at least 3 times higher activity than the alumina supported NiMo and CoMo catalysts (Soled et al., 2000; Soled et al., 2005). Unsupported Ni–Mo–W sulfide composition is commercially used for deep HDS of diesel under the commercial trade name NEBULA (Plantenga et al., 2003). Apart from the unsupported transition metal sulfides, the hydrotreating activities of carbides and nitrides of Mo and W have also been investigated (Zhong and Wang, 2012). Unsupported metal phosphides have also received much attention due to their high activity for hydrodesulfurization (HDS) and hydrodenitrogenation of petroleum feedstocks (Nozaki et al. 1980; Li et al. 1998, Kanda et al. 2010). It has been shown that MoP, and WP have moderate activity and Ni_2P has better activity in hydroprocessing. The overall activity was found to be in the order: $Fe_2P < CoP < MoP < WP < Ni_2P$ for simultaneous HDS of dibenzothiophene

and HDN of quinoline. Table 1.3 summarizes recent literature in the area of optimization of HDS processes utilizing various catalysts.

1.4 ADSORPTIVE DESULFURIZATION

Adsorptive desulfurization has been used for removal of sulfur compounds from liquid hydrocarbon fuels. Removal of thiophene, dibenzothiophene and other sulfur compounds has been studied over zeolites, aluminosilicates, activated carbon (AC), alumina, zinc oxide, TiO_2–CeO_2 and light irradiation. Only few adsorbents have shown high selectivity for sulfur compounds such as 4,6–dimethyldibenzothiophene, benzothiophene, dibenzothiophene, 4,6–dimethyldibenzothiophene, which are difficult to remove through hydrotreating.

1.4.1 Adsorbent

Significant research has been dedicated for development of adsorbents with large capacities and selectivities towards sulfur compounds in fuel. Adsorptive desulfurization has the following advantages over HDS (Samokhvalov and Tatarchuk, 2010, Pawelec et al., 2011, Srivastava, 2012): (1) Low temperature; (2) Absence or low consumption of hydrogen for nonreactive and reactive desulfurization; (3) Ability to remove refractory sulfur.

Solid adsorbents are used in granular form with varying size. They must have adequate strength and hardness. Adsorptive desulfurization can be divided into non-reactive and reactive adsorptive desulfurization (Samokhvalov and Tatarchuk 2010, Pawelec et al. 2011). A porous zeolite catalytic support, mainly composed of alumina and silica has been synthesized, and this catalytic support has been loaded with single walled carbon nanotubes (SWNT's) to enhance the catalyst adsorption capability. Other adsorbents with high sulfur removal efficiency are commercial grade activated carbon in powder form, and acid activated bentonite clay. Hernandez-Maldonado and

Yang (2004) have reviewed adsorptive desulfurization of transportation fuel using zeolite adsorbents. The main focus of this review is on π-complexation sorbents. The refractory thiophenic compounds (such as 4-methyldibenzothiophene and 4,6-dimethyldibenzothiophene, which are difficult to remove through hydrodesulfurization) bind selectively to the sorbents through π-complexation because of better electron donation/ back donation ability. The authors have reviewed zeolite based sorbents such as Ag-Y, Cu(I)-Y, Ni(II)-Y and Ni(II)-X synthesized using vapor and solid state ion exchange techniques, which result in high loading of the transition metals. Among these sorbents, the best sulfur removal performance was obtained for vapor phase ion exchanged Cu(I)-Y sorbent. This sorbent could produce 38 cm^3 fo desulfurized fuel per g of sorbent with sulfur content < 0.2 ppm (wt). The desulfurization capacity of this sorbent was enhanced when used in layered bed matrices. More recently, Ahmad et al. (2014) have reported adsorptive desulfurization of diesel and kerosene using Zn-impregnated montmorillonite (MMT) clay. Among different metals, such as Fe, Cr, Ni, Co, Mn, Pb impregnated on the MMT clay, the highest desulfurization was achieved by Zn-MMT clay at 25^oC for 1 h of treatment in batch mode. Characterization of the impregnated clay revealed that surface area, pore size and pore volume of MMT clay increased several times with Zn impregnation. The surface morphology of the MMT clay also improved with Zn impregnation leading to high adsorptive removal of DBT.

For a porous sorbent, the size of the microspores determines the accessibility of adsorbate molecules to the internal adsorption surface. Thus, pore size distribution of microspores is another important property for characterizing adsorptivity of adsorbents. Especially materials such as zeolite and carbon molecular sieves can be specifically engineered with precise pore size distributions, and hence, tuned for a

particular separation.

1.4.2 Processes Employing Adsorptive Desulfurization

Adsorptive desulfurization technology is considered promising evidenced by the fact that two processes, IRVAD and Philips S–Zorb, were developed based on it (Irvine and Varraveto 1999, Velu et al. 2003, Pawelec et al. 2011).

S Zorb process: In the S-Zorb process, desulfurization takes places in presence of hydrogen so as to accelerate the reaction between sulfur compounds and adsorbing agent. However, as compared to HDS process, the hydrogen consumption is much lesser. Different configurations of process flow have been used such as fluidized bed, moving bed and slurry column to transport the adsorption agent through reaction column and regeneration column. Regeneration of the adsorbent is carried out by subjecting it to air oxidation followed by processing by sulfur collector. The sorbent is purged with nitrogenand returned to its original state using hydrogen – before returning it to the reaction column. A possible chemical mechanism of adsorption in the S Zorb process is as follows: The hydrogen attacks sulfur compounds and weakens the atomic bonds of the sulfur atoms, which promotes their reactive adsorption on to the sorbent. In this mechanism, benzothiophene after desulfurization is converted into ethyl benzene. It is claimed that S zorb process does not involve any loss of hydrogen through olefins hydrogenation.

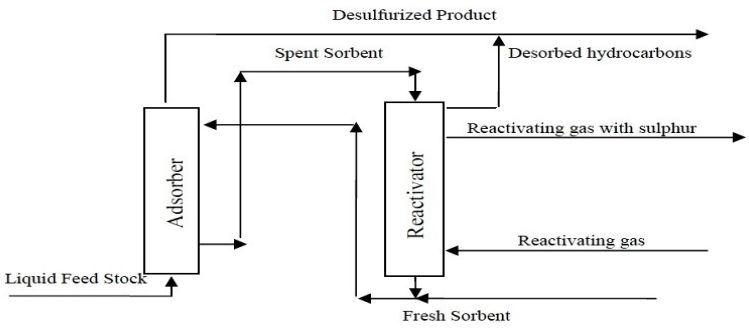

Figure 1.5: Adsorptive desulfurization – IRVAD (Irvine and Varraveto, 1999)

IRVAD process: Irvine (1998) and Irvine and Varraveto (1999) have reported an adsorptive desulfurization process called IRVAD. This process is claimed to remove wide spectrum of organosulfur compounds from various refinery streams including FCC gasoline. This process employs a moving bed of solid sorbent. This bed is brought in countercurrent contact with sulfur rich hydrocarbon stream. The desulfurized hydrocarbon stream emerges from the top of absorber. The sorbent loaded with sulfur compounds leaves from bottom. The spent sorbent is sent to the regeneration chamber where organosulfur compounds absorbed on the surface of sorbent are desorbed. The sorbent employed in this process is alumina, which can operate upto 240oC at low pressure with hydrocarbon/sorbent weight ratio of 1.4. This technology has been tested in pilot plant experiments in order to desulfurize the FCC feedstock (1276 ppm) and coker naphtha (2935 ppm Sulfur) which resulted in a 90% decrease in sulfur content. The IRVAD method is limited by the sorbent capacity and its selectivity, as adsorption of sulfur compounds occurs parallel to the surface of the sorbent. For example, dibenzothiophene gets attached parallel to the surface of the catalyst via π–electron of the aromatic ring (Xiaoliang et al., 2000). So, the sorbent requirement for effective operations is very high. Other limitation that has hampered commercial application of IRVAD adsorptive desulfurization technology is high pressure hydro-treatment required to eliminate organosulfur compounds concentrated on the adsorbent. However, optimization of some properties of adsorbent and process conditions (e.g. sorbent particle size and reactivation step temperature) can increase the efficiency and potentially make the process commercially viable. Table 1.4 summarizes some of the researchers conducted for the sulfur removal with different types of adsorbents at optimized condition.

1.5 OXIDATIVE DESULFURIZATION (ODS)

Oxidative desulfurization has been introduced as a new technology for deep desulfurization of diesel oil, and has proven to be an attractive alternative to hydrodesulfurization.

- It does not require expensive hydrogen, but instead uses (relatively much cheaper) oxidant such as peracids and hydrogen peroxide.
- In the ODS process, the hydrocarbon fraction containing sulfur compound is extracted from the feedstock, instead of converting to hydrogen sulfide as in HDS process.
- ODS process operates near atmospheric pressure and relatively mild temperature (<100^{o}C), and as a result, capital cost of the process is substantially lower than HDS process.

Table 1.3: Summary of Sulfur removal by Hydrodesulfurization process

Sulfur Compound	Catalyst	Operating condition	% Sulfur removal	Reference
DBT	Al_2O_3–ZrO_2 supported CoMo catalyst	Temp:350^o C Pressure: 8 MPa	90 %	Sintarako et al. 2015
DBT	NiMo catalysts supported on Al_2O_3/MgO	Temp = 300^o C Pressure = 3 MPa	75 %	Mogica–Betancourt et al. 2014
BT, DBT	NiMoW catalyst dispersed by diatomite	Temp = 340^o C Pressure = 4 MPa	63.8 %	Di and Chenguang 2013
Alkyl DBTs Diesel	CoMoP/nanoAl_2O_3, CoMoB/nanoAl_2O_3, CoMo/nanoAl2O_3, and CoMoP/microAl_2O_3	Temp = 310^{o}C Pressure = 3 MPa	CoMo/ nanoAl_2O_3 = > 98 %	Rashidi et al. 2013
Alkyl DBTs Diesel	Al_2O_3–TiO_2, Al_2O_3–TiO_2–SiO_2 Supported Bimetallic Pt–Pd Catalysts	Temp= 330 ^{o}C Pressure= 5 MPa	Pt–Pd/ Al_2O_3–TiO_2–SiO_2 = 95 %	Wan et al. 2009
Alkyl DBT	NiW/TiO_2–Al_2O_3	Temp = 350 ^{o}C Pressure = 5 MPa	100 %	Duan et al. 2009
Alkyl DBTs Diesel	P and Ni–Al_2O_3 supported Mo Oxycarbides	Temp= 340 ^{o}C Pressure= 4 MPa	50 %	Costa et al. 2009
Thiophene	FeS–MoS supported on Al_2O_3 and carbon	Temp= 280 ^{o}C Pressure = 0.1 MPa	30 %	Hubaut et al .2007
Alkyl DBTs	Co–Mo supported on MCM–41	Temp = 350 Pressure = 4.5 MPa	57%	Turaga et al. 2003

Notation: DBT: Dibenzothiophene; BT: Benzothiophene; HDS: Hydrodesulfrurization; Temp: Temperature

Table 1.4: Summary of Sulfur removal by Adsorptive desulfurization process

Sulfur compound	Adsorbent	Operating conditions	% Sulfur removal	Reference
DBT	Mesoporous carbon (CMK–3)	Temp = 25 ^{o}C	67 %	Shi et al., 2015
Hydrodesulfurized diesel fuel	Activated carbon	Temp= 25 ^{o}C	90 %	Selvavathi et al., 2009
DBT	Mesoporous aluminosilicates	Temp = 25 ^{o}C Oil : Adsorbents ratio= 20 mL/g	87 %	Tang et al., 2009
4–6 DMDBT	Y zeolite	Temp = 60 ^{o}C	97 %	Tang et al., 2008
4–6 DMDBT	NiMoP/Al_2O_3 + NaY zeolites	Temp= 340 ^{o}C Pressure = 40 (atm)	56 %	Richard et al., 2007
Thiophene	Activated Carbon	Two step process Temp= 70 Pressure = 1.5 (atm)	88 %	Sano et al., 2005
DBT sulfone	Alumina	Temp = 200 ^{o}C	30 %	Larrubia et al., 2002

1.5.1 Basic principles of oxidative desulfurization

In ODS, sulfur–containing compounds are oxidized using a selective oxidant to form compounds that can be favorably extracted from diesel oil using suitable solvents due to their relative polarity. General oxidants employed in ODS process are peroxyorganic acids, hydroperoxides, nitrogen oxides, peroxy salts and ozone etc. Such oxidants donate oxygen atom to sulfur in thiols, sulfides, disulfides and thiophenes to form sulfoxides or sulfones. The reaction scheme is given in Fig. 1.6.

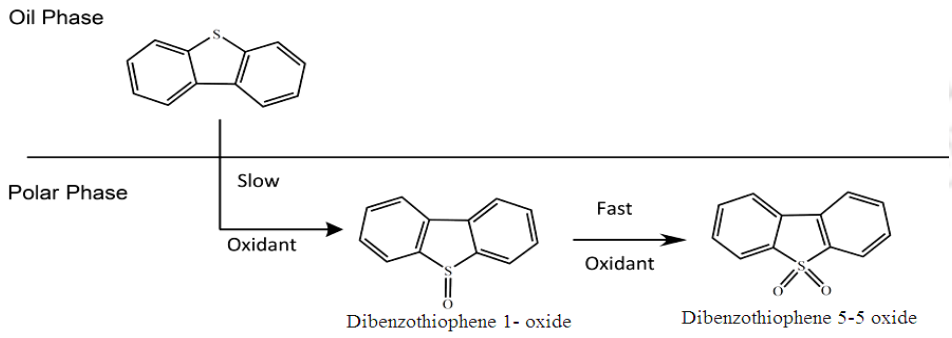

Figure 1.6: Reaction chemistry of oxidation desulfurization

Oxidation is accomplished by contacting an oxidant with light oil under optimum conditions, and continuing the reaction until the complete oxidation of S–containing compounds to corresponding sulfones is achieved. The sulfones can be extracted from feed using simple solvents such as methanol or acetonitrile. Oxidative desulfurization process has capability of removing sulfur compounds from fuel to the required low levels. Among different chemical oxidants like organic peracids, organic hydroperacids and hydrogen peroxide etc., the best option is hydrogen peroxide for desulfurization of fuel. Oxidation and extraction is simultaneously carried out with H_2O_2, and very high level of sulfur removal can be achieved (Ali et al., 2009). Various ODS processes reported in literature have used different oxidizing agents,

such as H_2O_2, organic oxidants and photochemical oxidation. More recently, several studies have also dealt with application of sonolysis (or ultrasound treatment) for oxidative desulfurization.

1.5.2 Oxidant Selection

Oxidizing agent is one of the key elements in any oxidative desulfurization process. To effective desulfurization, the oxidant is required to oxidize organic sulfur compounds to the corresponding sulfoxides or sulfones with higher polarity. With higher polarity than other hydrocarbons, sulfoxides or sulfones can be easily removed from fuel by extraction, adsorption or other post–treatments.

The oxidants employed in oxidative desulfurization process are concentrated nitric acid (Tam et al., 1990), organic hydroperoxides (Boikov et al., 2008), peroxyacids (Tetsuo et al., 1994), hydrogen peroxide (Mei et al., 2003), permanganate (Dehkordi et al., 2009), ozone (Otsuki et al., 1999) and oxygen (Campos–Martin et al., 2004). Among these, hydrogen peroxide is considered to be the most promising oxidant in terms of selectivity, availability, safety, cost effectiveness and environmental influence in presence of some catalysts (Filippis et al., 2003). Typically this catalyst is an organic acid that forms a peroxy–acid in the presence of H_2O_2 as the active oxidant. The most commonly employed acid catalysts are formic acid and acetic acid.

H_2O_2 oxidation method **:** H_2O_2—organic acid was the earliest oxidative desulfurization system for liquid fuel, and the mechanism of reactions is considered as: in the reaction system, H_2O_2 fist reacts with organic acid quickly and generates peroxide acid, and then the acid reacts with nonpolar sulfur compounds and form relative sulfone or sulfoxide. After the desulfurization reaction, H_2O_2 decompose to

H_2O and O_2, so there is no secondary pollution. Proper quantities catalysts can accelerate reaction and increase oxidation efficiency. A typical reaction scheme for oxidation of sulfur compound with H_2O_2 is shown in Fig. 1.7.

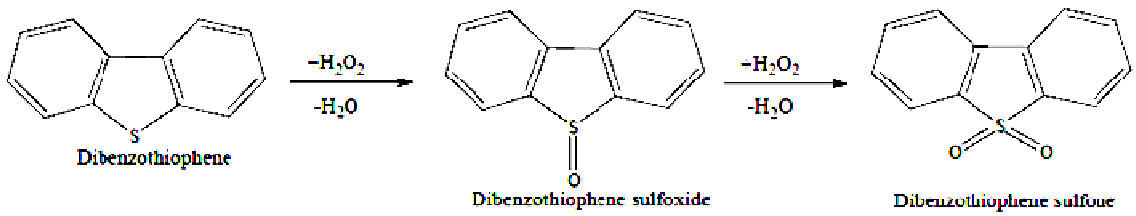

Figure 1.7: Typical reaction scheme for oxidation of sulfur compound

H_2O_2–Acetic acid oxidation system: Zannikos et al. (1995) have studied the desulfurization of crude oil using an oxidative desulfurization process. The experiments were conducted by dissolving the gas oil (Arab medium crude oil A and mixture of high sulfur crude B) having sulfur content 0.87 and 2.40 wt% respectively, in an equal volume of acetic acid at 90°C. To this, a solution of aqueous hydrogen peroxide (H_2O_2) was added drop wise with stirring for 30 min. Authors discovered that the oxidation process itself lead to removal of substantial portion of sulfur without any negative effects on other fuel properties. For solvent to gas oil volume ratio of 0.25, 98.5% sulfur was removed using methanol as a solvent (in comparison with other solvents like N–methylpyrolidone (NMP) and N–dimethylformamide (DMF)). Similarly, for gas oil B at same volume ratio, the sulfur removal was found to be 89.2% using methanol as a solvent. Shiraishi et al. (2002) have also studied the H_2O_2–acetic acid system for oxidative desulfurization of DBT, BT and 4,6 DMDBT as model sulfur compounds. Authors mixed model sulfur compounds (BT, DBT and

their methyl–substituted derivatives) with H_2O_2 solution and heated the mixture to 323 K. Acetic acid was then added to the mixture. Authors found that the sulfur content did not reduce to the required level of deep desulfurization (0.05 wt%), only by oxidative desulfurization process due to production of alkyl substituted sulfone. Hence, the oxidation was followed by extraction using an acetonitrile/ water azeotropic mixture, such that sulfur content of the light oil decreased to < 0.05 wt%, while maintaining high oil recovery. Authors reported the desulfurization efficiency to be 96.5% at temperature of 323 K in 8 h reaction time, with initial concentration of sulfur compound = 1.35 mmol, H_2O_2 = 135 mmol, and acetic acid = 67.5 mmol. Lu et al. (2006) have studied desulfurization process with improved H_2O_2/ acetic acid oxidant system. They developed H_2O_2/ acetic anhydride system to oxidize sulfur compounds in diesel, followed by extraction of oxidized diesel with ethyl cyanide. The experimental data showed that oxidation–extraction combination was an efficient desulfurization method. Optimal conditions for this process were: temperature = 80^{o}C, reaction time = 2 h, and volume ratio of diesel oil:H_2O_2: acetic acid was 10:1:1. With this method, the total sulfur content of diesel can be reduced from 2623.6 mg/kg to 270.3 mg/kg, with diesel yield of 95%. The main oxidation products of sulfur compounds were sulfone, and traces of SO_4^{2-} were found in the oxidant phase. Dehkordi et al. (2009) have studied the oxidative desulfurization of non–hydrotreated kerosene using hydrogen peroxide and acetic Acid as an oxidant system. The influences of various operating parameters such as reaction temperature and O/S ratio on the performance of ODS process were examined. Authors found that sulfur removal rate increased with temperature due to an increase in rate of oxidation of sulfur compounds present in kerosene. Optimum O/S ratio for the oxidation of sulfur–containing compounds of untreated kerosene was dependent on reaction temperature

to some extent. The optimum O/S ratio was revealed to be 8 and 23 at 25º and 60ºC, respectively.

H_2O_2—formic acid oxidation system : The reactivity of sulfur compounds towards oxidation increases with electron density on sulfur atom. The reactivities of DBT derivatives are influenced by the electron donation of substituted methyl groups. Hence, the reactivity decreases in the order 4,6–DMDBT > 4–MDBT > DBT, which is essentially inverse of the reactivity order for HDS. Otsuki et al. (2000) have applied H_2O_2 as oxidant with formic acid as catalyst to oxidize the sulfur `compounds. Authors dissolved 10 representative model sulfur compounds (viz. methyl phenyl sulfide, thiophenol, diphenyl sulfide, 4,6–DMDBT, 4–MDBT, DBT and BT) into cis- and trans- decahydronaphthalene (decalin) to make the model oil. The results showed that sulfur oxidation rate decreased in the order: 4,6–DMDBT > 4–MDBT > DBT > BT. Thiophene derivatives with 5.69 to 5.71 electron density on the sulfur atoms could not be oxidized at 50ºC. BT with 5.73 electron density and other benzothiophene and dibenzothiophene with higher electron densities could be oxidized. Yao et al. (2004) have applied formic acid as catalyst and H_2O_2 solution as oxidant to oxidize sulfur compounds. Model sulfur compounds of BT, DBT, 4,6–DMDBT were dissolved in n–heptane to simulate the light oil. The results showed that under the condition of reaction temperature of 60ºC, molar ratio of hydrogen peroxide to sulfur as 7:1, volume ratio of hydrogen peroxide to formic acid of 1:1, and reaction time of 40 min, the desulfurization yields for 4,6–DMDBT, DBT and BT were 100%, 96% and 58%, respectively. The addition of naphthalene and tetralin resulted in decrease of BT desulfurization yield, while small rise in desulfurization of DBT was observed. They also found addition of both cyclodexene and indole decreased the removal of BT and DBT, with desulfurization yield of BT decreasing

faster than that of DBT. Lu et al. (2001) adopted H_2O_2–HCOOH as oxidation system for catalytic oxidation of sulfur compounds in diesel oil. After oxidation, the oxidized organic sulfur compounds were separated by solvent extraction. The results show that different solvents have different abilities to extract sulfones from the diesel. Among various solvents attempted, N, N–dimethyl formamide (DMF) and dimethly sulfoxide (DMSO) gave best results. The total sulfur concentration of feed could be reduced from 0.8% to 0.3% for extract to diesel ratio of 1:2 (v/v), water content of solvent as 5%, and extraction time of 10 min. Bunthid et al. (2010) have studied the oxidative desulfurization of tire pyrolysis naphtha with formic acid/ H_2O_2 oxidant system. pH of reaction mixture was maintained at 4 with addition of formic acid. The results of this study showed that in presence of formic acid at pH = 4, removal level of 75% for sulfur compounds in the pyrolysis naphtha was achieved via ODS process using HNO_3 and H_2O_2 surface modified char. Mamaghani et al. (2013) have also studied desulfurization of DBT in presence of formic acid/ H_2O_2 oxidant system. The main objective of this study is to optimize the operating conditions including H_2O_2/S molar ratio, formic acid/S molar ratio and oxidation reaction time. The optimum operating conditions were determined as O/S = 15, formic acid/S = 22, reaction time = 56 min and temperature = 65°C to achieve 100% sulfur removal from the fuel.

H_2O_2–organic acid oxidant system has relatively mild reaction condition and strong oxidation potential to achieve high desulfurization rate. The liquid organic acids have several disadvantages such being non-renewable and a high replacement cost. The catalysts which can be recovered for reuse is are preferred choice.

1.6 OXIDATION BY OTHER METHODS

1.6.1 Ultrasound Assisted Oxidative desulfurization

Ultrasound irradiation (or sonication) is a well–known technique for enhancing the interphase mass transfer through generation of strong convection in the system. The ultrasonic wave generates very fine emulsion that improves the liquid–liquid interfacial area through enhancement of (i) interfacial area available for reaction, (ii) effective local concentration of the reactive species, and (iii) mass transfer in the interfacial region (Mei et al., 2003; Dai et al., 2008). This results in increase in reaction rate, and this is evidenced by the short reaction times (7–20 min) for achieving 85–99% conversion (Mei et al., 2003; Etemadi and Yen, 2007; Wan and Yen, 2007). The main mechanism through which convection is generated in the system during ultrasound irradiation is micro–streaming by ultrasound wave, and microturbulence and micro–jets by transient cavitation, which is secondary effect of ultrasound. Transient cavitation also generates highly reactive radicals through dissociation of solvent vapor entrapped in it, which is the well known sonochemical effect. The intensity of the physical and chemical effects of ultrasound and cavitation is influenced by physical properties of the fuel such as density, viscosity and surface tension. Oxidative systems such as H_2O_2/ acetic acid, H_2O_2/ formic acid, H_2O_2/ phosphotungstic acid and Fenton reagent have all been tested. Phase transfer agents have also been used to promote ultrasound assisted oxidative desulfurization (UAOD). Wan and Yen (2007) have studied the effect of phase transfer agents used simultaneously with ultrasound on desulfurization. According to these authors, desulfurization rate increases with the carbon chain length of the cation, and decreases with increase in the molecular size of the anion. A review by Wu and Ondruschka (2010) indicated that the optimum temperature for the ultrasound-assisted oxidative

desulfurization process lies between 25° - 70°C due to the competitive effects of higher decomposition of H_2O_2 and reduction in the intensity of collapsing cavitation bubbles with increasing temperature. It was also shown that sulfur removal rate at low frequency (20 kHz) is higher than at higher frequency (40 kHz). The % sulfur removal increases with increase in ultrasonic power till 200 W, and decreases above this value due to the formation of cavitation shielding (Wu and Ondruschka 2010).

The mechanism involved in this process was presented by Wan and Yen (2007) and Wan et al. (2012). The main features of the mechanism are as follows: (1) in presence of excess H_2O_2, the catalyst is peroxidized to peroxometal complex bearing an active oxygen, (2) the resulting peroxo compound undergoes an ion exchange with the phase transfer agent, and subsequently gets transferred to an organic phase, (3) the sulfur compounds are oxidized by the peroxometal complex in the organic phase to their corresponding sulfones, (4) the reduced peroxo compound exchanges an ion with the phase transfer agent and is transferred back to aqueous phase, where it is regenerated with the H_2O_2, and (5) ultrasound increases desulfurization efficiency by allowing for effective mass transfer between biphasic layers. Sun et al. (2008) have applied this method to remove organosulfur compounds from diesel fuel. H_2O_2 was employed as the oxidant, and ultrasound irradiation was introduced into the system to provide energy for the reaction. Phosphoric or acetic acid was used as a catalysts. The authors achieved optimal desulfurization degree after 10 min at 50°C. Yen and coworker conducted similar experiments to remove sulfur from model oil, in which DBT was dissolved in toluene (Wan and Yen 2007). DBT was completely oxidized to DBTO after 7 min at 73–77°C. Some recent studies on phase transfer agent assisted desulfurization are given in Table 1.5. Table 1.5 represents a summary of the results of previous literature in oxidative desulfurization with phase transfer agent.

1.6.2 Photochemical desulfurization

In photochemical desulfurization, the sulfur compound present in liquid fuel is photo–excited using light of appropriate wavelength. The transient photo-excited state of sulfur aromatic compound such as singlet state reacts with the oxidant. Reactive intermediates lead to molecular reaction products, such as sulfones and sulfoxides of aromatic sulfur compounds (Tao et al., 2009). These sulfones and sulfoxides are removed by adsorption method. both Both ultraviolet and visible light irradiation has been used for the improvement of ODS (Hirai et al., 1997; Shiraishi et al., 1998, 2001). High–pressure mercury and Xe–Hg lamps have also been used in the ultraviolet (UV) region ($\lambda > 290$ nm) for direct oxidation of DBT and its alkyl derivatives (Hirai et al., 1996, Tao et al., 2009). UV ($\lambda > 290$ nm) has been used for indirect photo–oxidation and photocatalytic oxidation of sulfur compounds (Paybarah et al., 1982). The indirect oxidation constitutes the *in situ* generation of the oxidizing agent. Titanium–based catalysts have been studied in photocatalytic oxidation (Abdel–Wahab and Gaber, 1998; Wang et al., 2006). The performance of photocatalyst-assisted oxidative desulfurization has been revealed to be better than oxidative process alone (Robertson and Bandosz 2006). The mechanism involved in photocatalytic oxidation of DBT using titanium–based (TS–1) catalyst has been reported by Juan and coworkers (2010). Ultraviolet light with wavelength < 280 nm has also been used to study the mechanisms involved in the photo–oxidation of sulfur compounds. Visible light has also employed with mixed–phase Fe_2O_3 photo–catalyst for removal of sulfur from model fuel (n–octane) under simulated solar irradiation. In this process, 92% sulfur removal has been achieved in 90 min. The kinetics of photooxidation followed pseudo first–order profile with an apparent rate constant of 0.0287 min^{-1} (Li et al., 2012). According to the authors, electron transfer from the α–

Fe_2O_3 conductive band to the β–Fe_2O_3 conductive band effectively separates the photo–generated electrons and holes, which thereby reduces their recombination. The α–Fe_2O_3–originating holes will then move from the valence band of α–Fe_2O_3 to β–Fe_2O_3 phase, and then react with OH^- to form OH radical to participate in the oxidation reaction. However, when the β–Fe_2O_3 phase content exceeded 36.6%, photocatalytic activity slightly decreased because its band gap is narrower than that of the α–Fe_2O_3 phase and the recombination rate of the electron–hole pairs during the β–Fe_2O_3 phase is faster than that in the α–Fe_2O_3 phase.

1.7 MICROBIAL / ENZYMATIC DESULFURIZATION

An alternative means to the chemical methods of HDS and ODS for removal of sulfur from fossil fuel is the biological method of microbial or enzymatic desulfurization. Microorganisms require sulfur for their growth and biological activities. Sulfur generally occurs in the structure of some enzyme cofactors (such as coenzyme A, thiamine and biotin), amino acids and proteins (cysteine, methionine, and disulfur bonds).

Several microorganisms, depending on their enzymes and metabolic pathways, have the ability to acquire and metabolize carbon and sulfur from different sources. Some microorganisms, such as *Arthrobacter, Brevibacterium, Pseudomonas, Gordona*, and *Rhodococcus spp.* can consume the sulfur in heterocyclic thiophenic compounds such as DBT, and reduce the sulfur content in fuel. For microbial desulfurization, two main pathways have been reported: (1) ring–destructive Kodama pathway (degradation) and, (2) sulfur–specific (desulfurization) 4S pathways.

Table 1.5: Summary of the literature in PTA–assisted oxidative desulfurization

Sl. No	Authors	Model Sulfur Compound & Solvent	PTA (concentration)	Reaction Conditions	Oxidation System	Method of Treatment	% Reduction of Sulfur compound
1.	Mei et al., 2003	DBT (400 ppm) Toluene	TOAB (7.32 mM)	React Vol: 50 mL; Temp: 75 ± 2 °C; pH: NA; Time: 7 min; US Freq: 20 kHz	H_2O_2/ Phospho–tungstic acid	US/ Oxidation/ Extraction	98 % (After Extraction); 2.5% (After oxidation)
2.	Chen et al., 2007	Thiophene or 3–methyl thiophene (500 ppm) n–Heptane	TBAB (0.5 g)	React Vol: 50 mL; Temp: 50 °C Time: 120 min; Str: 1500 rpm; Metal oxide loaded molecular sieve	H_2O_2/ Formic acid	Oxidative Desulfurization in H_2O_2	Best with formic acid Thiophene: 78.4% 3–Methyl thiophene 82.3%
3.	Li et al., 2010	Thiophene (800 µL/L ≈1200 ppm) n–Octane	TBAB (0.1 g)	React Vol: 50 mL; pH: 12; Temp: NA; Time: 120 min; Air Flow 150 ml/min	Photo–oxidative 365 nm, 500 W	US	80.6%
4.	Chen et al., 2010	Thiophene, BT, DBT (960 ppm) Toluene	TOAB (0.1 g)	Temp: 88 ± 2°C Freq: 20 kHz	H_2O_2/Phospho–tungstic acid	US/ Oxidation/ Extraction	88.4%
5.	Zhao et al., 2007	Thiophene (~ 1200 ppm); n–Heptane	TBAB, TEAB, TMAB, TPAB (0.0116 mol/L)	React Vol: 24 mL; Time:120 min; Temp: 50 °C	H_2O_2/ HCOOH	US/Oxidation–Extraction: TPAB– 86.5% TEAB– 42.37 %; without PTA: 28.3%	No PTA: 28.4% TMAB: 42.4% TEAB: 70% TPAB: 86.6% TBAB: 94.7%

Table 1.5: *Continued…*

Sl. No	Authors	Model Sulfur Compound & Solvent	PTA (concentration)	Reaction Conditions	Oxidation System	Method of Treatment	% Reduction of Sulfur compound
6.	Wan and Yen, 2007	Benzothiophene; 2 – methyl benzo–thiophene; Dibenzothiophene; 4–MDBT, Toluene	MBAH; TOAB; TOAF; TODAB; TBAB; TMAF; MTAC (0.1 g)	Temp: 70 ± 2°C; Time:10 min; Freq: 20 kHz	H_2O_2/Phospho–tungustic acid	US–assisted Oxidation followed by extraction	TOAF: 90.3% TODAB: 56.9% TOAB: 49.6% TBAB: 38.3% MBAC: 11.4% MBAH: 11.1% TMAF: 8.2%
7.	Sachdeva and Pant, 2010	DBT (325 ppm); n–Decane	TOAB (0.006g/g S)	React Vol: 120 mL; Temp: 70°C; pH: NA; Stirring: 1000 rpm; Time: 200 min	H_2O_2/Phospho–tungustic acid	Conventional Oxidative desulfurization	98%
8.	Zhao et al., 2009	Thiophene, DBT (600 ppm); n–Heptane (24 mL)	TBSB (0.0123 mol/L)	React Vol: 36 mL; Temp: 45°C; Time: 90 min; pH: NA; Stirring: ~200 rpm	H_2O_2/ HCOOH	Mechanical Stirring	Thiophene: 86.4 % DBT: 97.5%
9.	Zhao et al., 2008	Thiophene (500 ppm); n–Octane + Xylene (1:1 vol)	HTMAB or TBAB (1.5 g)	React Vol: 130 mL; Temp: 40°C; pH: NA; Time: 150 min; US Freq: NA	H_2O_2/ phospho–tungstic acid	Mechanical Stirring	96.3% with HTMAB 91.5% with TBAB

Note: The concentration given in the table for S compound is by default in ppmw. Abbreviations: TPAB – tetrapropyl ammonium bromide, TEAB – tertraethyl ammonium bromide, TMAB – tetramethyl ammonium bromide, HTMAB – hexadecyltrimethyl ammonium bromide, TBAB – tetrabutyl ammonium bromide, MBAH – methyltributyl ammonium hydroxide, TODAB – tetraoctadecyl ammonium bromide, TOAF – tetraoctyl ammonium fluoride, MTAC – methyltributyl ammonium chloride, TBSB – tetrabutyl ammonium bisulfate. US – ultrasound

1.7.1 Destructive Biodesulfurization (Oxidative C–C bond cleavage)

Kodama pathway was essentially developed for dibenzothiophene as the model sulfur compound. Kodama first reported the oxidative cleavage of DBT (Kodama et al. 1970, 1973) in which the initial attack is directed against one of the carbon atoms, preferentially one of the DBT phenyl rings. Kodama identified various intermediates, which are generated during the oxidation and proposed the well-known Kodama pathway shown in Fig. 1.9. Initial enzyme attack directed against one of the carbon atom results in undesirable breakage of carbon–carbon bond in phenyl ring. The series of enzymatic reactions in the microbial metabolism that results in successive carbon bond breakage and oxidation is called Kodama pathway (Srivastava, 2012).

The Kodama pathway essentially comprises three steps, viz. hydroxylation, ring cleavage and hydrolysis. In this pathway, initial deoxygenation occurs at the peripheral aromatic ring of DBT, followed by cleavage of the ring. This process leads to formation of 3–hydroxy–2–formyl–benzothiophene as a water soluble end product with lower carbon content than dibenzothiophene. For methyl-DBT as substrate, the carbon-carbon cleavage occurs on the benzene ring. Essentially, due to attack on carbon atoms and cleavage of C-C bonds in aromatic rings, the Kodama pathway of desulfurization is a destructive process.

For its destructive nature that results in reduction of the fuel value, biodesulfurization by Kodoma pathway is not commercially viable. Various microorganisms are known to follow this pathway. The two microorganisms reported in 1970 were *Pseudomonas jijani* and *P. abikonesis* (Kodama et al. 1970, 1977), which follow the Kodama pathway. The products of DBT oxidation through Kodama pathway are water soluble, and hence, inhibitory to both cell growth and further DBT oxidation.

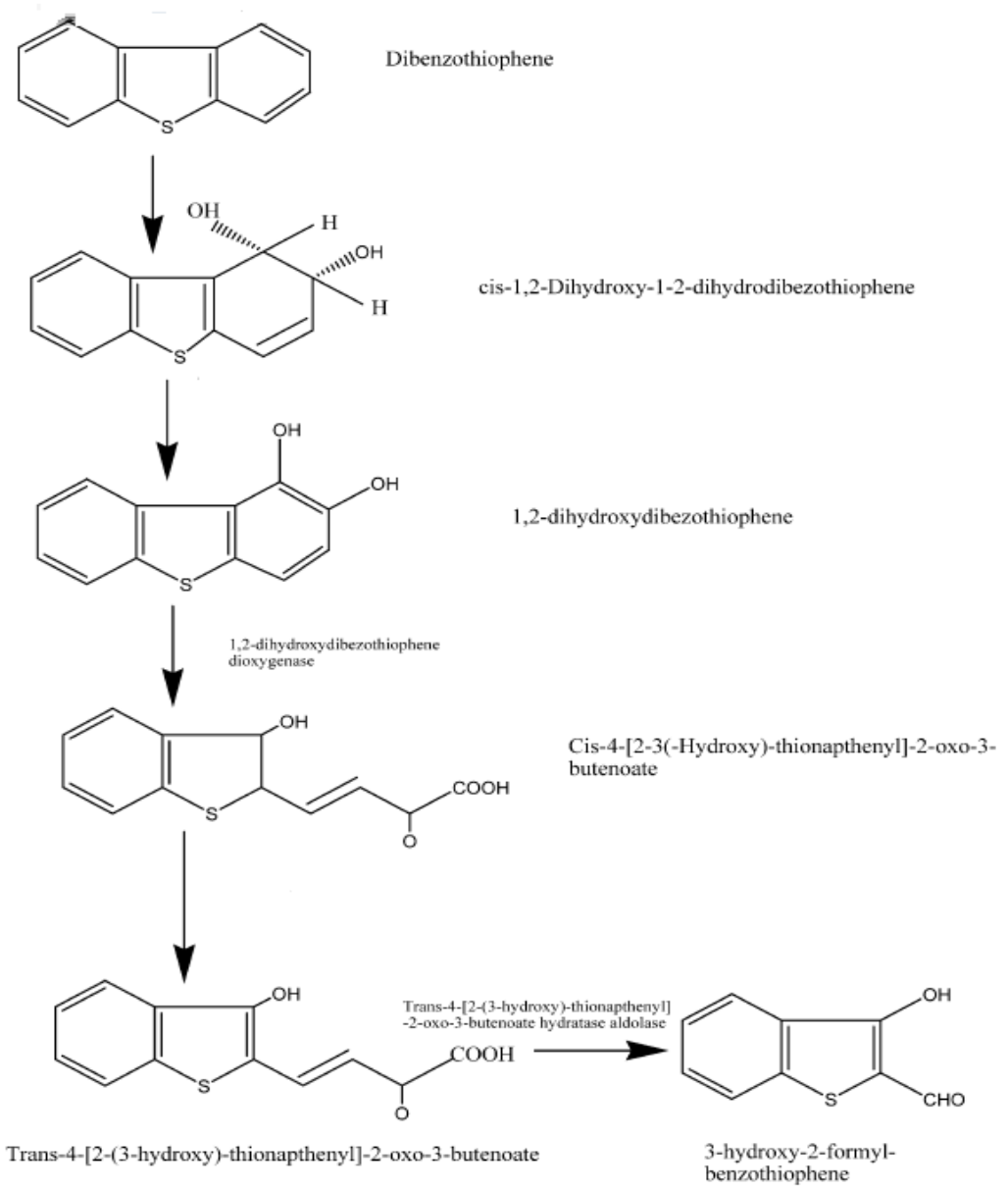

Figure 1.8: Sulfur specific DBT degradation *via* the Kodama pathway

1.7.2 4S pathway (Oxidative C–S bond cleavage)

This metabolic pathway results in sulfur removal from dibenzothiophene through 4 sulfur containing intermediates, viz. DBT-sulfoxide, DBT-sulfone, DBT-sulfinate and the final product hydroxybiphenyl, and hence, it draws its name as 4-S pathway. A peculiarity of this pathway is that the basic carbon skeleton of the sulfur compound remains unaffected, and thus, there is no reduction in calorific value of fuel during

desulfurization, as in case of the Kodama pathway. The schematic of this pathway is shown in Fig. 1.9.

This metabolic pathway for sulfur removal was first reported for *Rhodococcus rhodochrous* IGTS8 by Gallagher et al. (1993). Besides *Rhodococcus rhodochrous* IGTS8 (Kilbane and Jackowski 1992; Mohebali et al. 2007), other bacteria, which follow the 4S pathway are *R. erythropolis* D1 (Izumi et al. 1994; Ohshiro et al. 1994), *Rhodococcus* ECRD1 (Grossman et al. 1999), *Gordona* CYKS1 (Rhee et al. 1998), *Xanthomonas* (Constanti et al. 1994), *Nocardia globelula* (Wang and Krawiee 1994), *Paenibacillus* strain (Konishi et al. 1997), and *Mycobacterium sp*. (Li et al. 2003).

The 4S pathway proceeds *via* two cytoplasmic monooxygenases supported by flavin reductase and a desulfinase. Two step action of DBT monooxygenase catalyzes the sequential conversion of DBT to DBT sulfoxide, and DBT sulfoxide to DBT sulfone, respectively. These reactions require flavin mononucleotide for the activity, which is provided by the enzyme flavin mononucleotide oxidoreductase. Conversion of DBT sulfone to hydroxyl-phenyl benzene sulfonate is catalyzed by DBT sulfone monooxygenase. This reaction also requires reduced flavin mononucleotide which is provided by the flavin oxidoreductase enzyme. The fourth enzyme HPBS desulfinase completes the pathway by converting hydroxyl phenyl benzene sulfonate to HBP and sulfite. HBP is highly soluble in oil and readily diffuses back into the oil phase. Thus the fuel value of the oil is conserved during the 4-S pathway. There are several resistances that put limit on the overall kinetics of the 4S pathway. The main rate limiting step is the transfer of polyaromatic sulfur heterocycle from oil phase into the cell. The supply of reducing equivalents and enzyme turnover rate is another hindrance for kinetic of the 4S pathway.

The genes responsible for the4S pathway were discovered in the species *Rhodococcus erythropolis* IGTS8. However, in the past several years of research these genes have been cloned, sequenced and engineered from several microbial species. These have also been transferred to other species.

Most of the microorganisms showing 4S metabolic pathway are mesophiles, i.e. the ability of DBT desulfurization is higher at temperature around 30°C and decreases with higher temperatures. If the biodesulfurization process is to be integrated with conventional HDS process, thermophillic biodesulfurization at higher temperatures is desired. If biodesulfurization could be performed around 50°C, it would obviate the need to cool the HDS treated diesel oil to ambient temperature. In addition, contamination by undesirable bacteria, which affects the BDS process, would be avoided at high temperature. Only a few microorganisms, such as a *Paenibacillus strain* (Konishi et al. 1997), *Bacillus subtilis* WU–S2B (Kirimura et al. 2001), *Mycobacterium sp*. X7B (Li et al. 2003), *Mycobacterium sp*. GTIS 10 (Kayser et al. 2002), and *Mycobacterium pheli* WU–F1 (Furuya et al. 2001) are reported to show desulfurization at high temperature. Table 1.6 shows the summary of the literature on biodesulfurization follow 4S pathway.

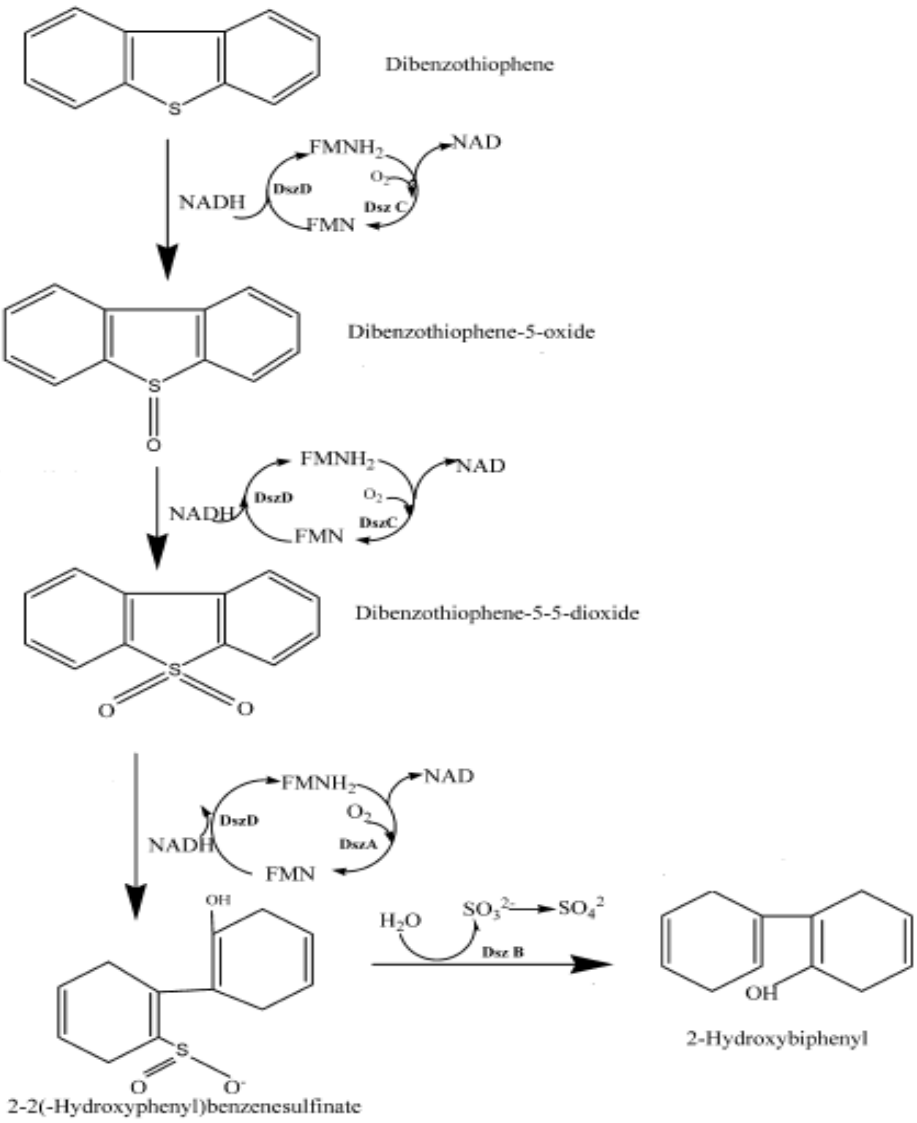

Figure 1.9: Sulfur specific DBT degradation *via* the 4S pathway

Table 1.6: Summary of the literature on biodesulfurization

Model oil	Microorganism	Experimental system and conditions	%DBT removal	Reference
Hexadecane	*Gardonia alkanivorans RIPI90A*	Batch process with mechanical agitation (30°C, 120 rpm, pH 7.0, 10 days), Initial DBT concn: 100 ppm	90%	Mohebali et al. 2007
n–Hexadecane	*Mycobacterium sp. ZD–19*	Batch process with mechanical agitation (30°C, 180 rpm, pH range 6.5 – 7.5, 4–7 days), Initial DBT concn: 92 ppm	100%	Chen et al. 2008
Hexadecane	*Rhodococcus erythropolis IGTS8*	Batch process with mechanical agitation (30°C, 200 rpm, 24 h, oil:water volume ratio 1:1), Initial DBT concn: 50 ppm	80%	Caro et al. 2007
n–Heptane	*Gardonia alkanivorans strain* 1B	Batch process with mechanical agitation (30 °C, pH– 7.5, 150 rpm, 168 h, water/oil ratio 10:1), Initial DBT concn: 100 ppm	63%	Alves et al. 2008
n–tridecane	*Bacillus subtitlis* WU–S2B	Batch process with mechanical agitation (50°C, 140 rpm, 12 h), Initial DBT concn: 100 ppm	50%	Kirimura et al. 2001
n–tridecane	*Mycobacterium phlei* WU–F1	Batch process with mechanical agitation (50°C, 180 rpm, 3 days), Initial DBT concn: 150 ppm	99%	Furuya et al. 2001
Decane	*Rhodococcus erythropolis* (ATCC 53968)	Agar plate interface bioreactor (30°C, 40 rpm, 5 days), Initial DBT concn: 184 ppm	90%	Oda and Ohta 2002
n–Hexadecane	*Bacterium*, strain RIPI–22	Batch process with mechanical agitation (30°C, 100 rpm), Initial DBT concn: 100 ppm	77%	Rashtchi et al. 2006
Methenol	*Lysinibacillus sphaericus* DMT–7	Batch process with mechanical agitation (150 rpm, 37oC, 15 days), Initial DBT concn: 100 ppm	60%	Bahuguna et al., 2011

* All of these microorganisms follow 4S pathway of biodesulfurization. # The model sulfur compound used in all studies in DBT

1.8 BASIC CONCEPTS AND PRINCIPLES OF ULTRASOUND AND CAVITATION

Ultrasound essentially refers to the sound waves having frequency beyond the upper limit of human hearing range (16 Hz – 16 kHz), or typically in the range of 20 kHz up to approximately 500 MHz.. Sound waves pass through an elastic medium in the form of longitudinal wave, i.e. in series of alternating compressions and rarefactions regions generated due to small amplitude oscillatory motion of fluid elements in the direction of propagation of the wave. The amplitude of displacement of fluid elements depends the pressure amplitude of the ultrasound wave, which in turn depends on the energy of the wave. The frequency (f) and the acoustic amplitude ($P_{A,max}$) are the most important properties that characterize a sound wave. The bulk pressure in the liquid medium undergoes periodic (usually sinusoidal) variation during propagation of the ultrasound wave. In simple form, the pressure amplitude of the ultrasound wave (P_A) and the bulk pressure in the medium (P_t) at any instance (time, t) for frequency f by the following equation:

$$P_A = P_{A,\max} \sin\left(2\pi ft\right)$$

$$P_t = P_o - P_{A,\max} \sin\left(2\pi ft\right)$$

where $P_{A,max}$ is the pressure amplitude of the ultrasound wave and P_o is the static pressure in the bulk liquid medium. Ultrasound waves can be generated in the medium using a transducer, which essentially converts one form of energy (electrical) into another form (mechanical). The piezo–electric crystal undergoes volume oscillations under influence of alternating voltage (or potential) applied across it. These mechanical oscillations can be converted into sound energy, once the piezo–electric element is coupled to a fluid medium such as water.

Cavitation is a secondary effect of ultrasound. The basic definition of cavitation phenomenon can be given as nucleation, growth and implosive transient collapse of gas or vapour bubbles in the medium driven by pressure variation in the bulk liquid

due to ultrasound propagation. Occurrence of cavitation phenomenon induced by the propagation of the ultrasound wave can be explained as follows: In oscillatory motion during propagation of the wave, the fluid elements in the bulk medium are pulled apart from each other. If the amplitude of the ultrasound wave is strong enough to overcome the Laplace pressure ($2\sigma/r$) of the liquid medium, the bond between the two fluid elements can break with creation of a void or cavity between them. In the subsequent compression cycle, this cavity is annihilated, giving rise to extreme concentration of energy. Theoretically, for creation of a "cavity", the acoustic pressure has to overcome the van der Waal's distance between the two molecules. This would require enormous pressure amplitude (> 10,000 bar) of the ultrasound wave. However, in practical situation, cavitation occurs at very low pressure amplitude as 1.2 bar. This is due to presence of nuclei or weak spots in the liquid that assist occurrence of cavitation phenomenon. These nuclei or weak spots could be small bubbles or particles already present in the liquid or these could also be gas pockets trapped in the crevices in the solid boundaries of the processor or ultrasound probe. Under the influence of pressure variation due to ultrasound, these gas pockets or bubbles expand in the rarefaction cycle giving rise to cavitation event. The cavitation bubbles in this case are filled with non-condensable gas, usually air. If the temperature of the bulk liquid is sufficiently high, local vaporization of the liquid may also occur resulting in formation of vapor bubble.

1.8.1 Cavitation Bubble Dynamics

As noted earlier, the word cavitation essentially refers to the phenomenon of formation or nucleation, growth and transient collapse of gas or vapour bubbles under the influence of pressure variation in the system. The principal cause leading to

occurrence of cavitation in the medium is variation in the bulk pressure of the medium. On the basis of this criterion, various types of cavitation can be categorized as follows:

Acoustic Cavitation: Acoustic cavitation is caused by the pressure variation in the liquid due to passage of an acoustic wave. It generally occurs in the acoustic frequency range of 20 kHz – 1 MHz.

Hydrodynamic Cavitation: Hydrodynamic cavitation occurs due to pressure variation in the liquid flow velocity generated by the changing flow geometry. This pressure variation generally occurs at low frequencies (100 Hz – 10 kHz).

Optical Cavitation: Optical cavitation is a result of local evaporation of liquid due to intense local energy dissipation caused due to sources such as high–intensity laser.

Particle Cavitation: Particle cavitation is produced by any elementary particle (such as proton) rupturing the liquid.

The phenomenon of cavitation is influenced by many physical factors related to ultrasound itself and the physical properties of the liquid medium. Given below is a brief description of the effect of each of this factor / property. Fig. 1.10 lists some of these factors and properties that affect the radial motion of cavitation bubbles.

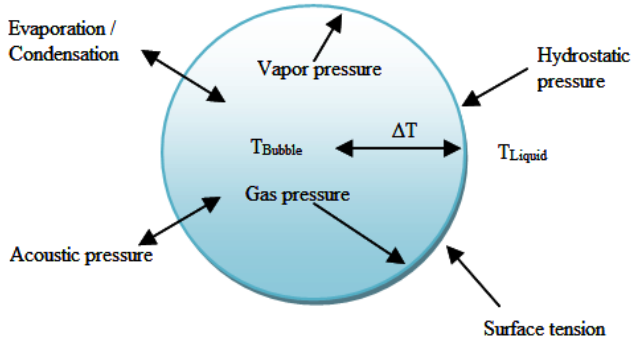

Figure 1.10: Physical factors (or parameters) and properties influencing cavitation phenomenon

Ultrasound Frequency: The intensity of the transient collapse of the bubble in the compression half period of the ultrasound wave depends on the expansion of the bubble, which occurs in the rarefaction half period. As the frequency of the ultrasound wave increases, the period of the wave and the duration of both rarefaction and compression half cycles decrease. For a given pressure amplitude of the ultrasound wave (higher than transient cavitation threshold), expansion of the bubble reduces with increasing frequency; and hence, the intensity of the subsequent transient collapse as well. Thus, the cavitation effect tends to be lower at higher frequencies. For power ultrasound used for sonochemical application, frequencies in the range of 20–30 kHz are normally used. In oxidation reactions, however, higher frequencies could be employed so as to enhance the reaction rate due to higher rate of hydroxyl radical formation at these frequencies. The acoustic pressure amplitude (and hence the net power input) required to cause transient cavitation at higher frequencies (in the range of 100-500 kHz) is significantly higher than that for 20 kHz.

Ambient or Static Pressure in the Medium: Ambient or static pressure in the medium is an important factor governing the expansion of the cavitation bubble in the rarefaction half cycle of ultrasound. The bubble expands to size higher than its original (or equilibrium) size, only when the instantaneous pressure in the medium falls below the ambient pressure. This means that higher acoustic pressure amplitude (and hence higher energy) is needed for generating cavitation at higher static pressure, or in other words, transient cavitation for a given acoustic pressure amplitude can be eliminated (and converted to stable, small amplitude oscillatory behavior) by raising the static pressure in the medium. For cavitation bubbles which are significantly smaller than the resonance size, the transient cavitation threshold is essentially equal to the static pressure in the medium.

Acoustic Intensity: Acoustic intensity or acoustic pressure amplitude has a profound effect on the characteristics of cavitation events occurring in the medium. To achieve transient motion of the cavitation bubble which would result in generation of high temperature and pressure peaks in the bubble during collapse would require certain minimum amplitude of the wave, called as "transient cavitation threshold". This requires expansion of the bubble to at least twice of its initial size. Below this threshold value, the amplitude of the wave would be too small to cause significant bubble growth. In such cases, the bubble undergoes small amplitude, stable, oscillatory motion, which is not energy intensive. As noted in previous sub-section, for cavitation bubbles which are much smaller than the resonance size corresponding to the applied frequency, the transient cavitation threshold is essentially equal to the static pressure in the medium. This for typical frequency range of 20-50 kHz used for power ultrasound used in sonochemical reactions, the transient cavitation threshold for atmospheric static pressure is about 1.2 to 1.5 bar. The size range of initial bubble radii that undergo transient motion and collapse for this range of frequency and pressure amplitude is 2 – 20 microns.

Physical Properties: Viscosity, Surface Tension and Vapor Pressure: Viscosity of the medium is result of the natural cohesive forces active in the liquid. It acts as a break on the radial motion of bubbles. Moreover, it is also responsible for the attenuation of the acoustic wave, with loss of the energy of the wave into thermal. Increase in liquid viscosity dampens the radial motion of the bubbles, thus limits the maximum size attained during radial motion. The cavitation intensity, as indicated by the temperature and pressure peak attained during collapse, decreases with increasing viscosity of the liquid.

Surface tension indicates the difficulty in creating cavitation in the liquid. An increase

in surface tension of the liquid increases the cavitation threshold, i.e. the minimum acoustic pressure amplitude for creation of cavitation in liquid. The intensity of the cavitation bubble collapse increases with increasing surface tension of the medium.

The vapor pressure of the bulk liquid medium depends on the temperature of the medium. During ultrasound irradiation, the temperature of the medium increases continuously due to viscous and thermal dissipation of the momentum of the ultrasound waves. Higher vapor pressure of the liquid medium causes evaporation of the solvent vapor in the bubble. This vapor can cushion the collapse of the bubble in the compression half cycle of the wave and reduce the intensity of the collapse. As explained in greater details in the next section, some of the vapor can also get entrapped in the bubble which results in generation of chemical and radical species during the collapse.

1.8.2 Chemical Effects of Cavitation

A description of the chemical effects induced by cavitation is given by Sivasankar et al., 2007; Krishnan et al., 2006. For convenience of the reader this description is reproduced here. The principal chemical effect of cavitation (known popularly as the sonochemical effect) is generation of highly reactive radicals such as $^{\bullet}O$, $^{\bullet}OH$, and $HO_2^{\bullet}$ during transient collapse of the cavitation bubbles. These radicals are mainly produced through the thermal dissociation of the vapor molecules entrapped in the cavitation bubbles at the instance of transient collapse, when the temperature inside the bubble reached extreme. Thus, two factors are mainly responsible for the radical generation by cavitation bubbles, i.e. the composition of the bubble interior (i.e. the number of gas and vapor molecules) and the temperature of the bubble interior reached during collapse. During radial motion, the composition inside the bubble

varies continuously due to several phenomena such as gas diffusion, gas rectification, water vapor condensation / evaporation and the chemical reactions.

Several authors have addressed the problem of water vapor entrapment in the bubble and its consequences (i.e. chemical reactions, alteration of heat transfer across bubble) with different approaches (Kamath et al. 1993; Prasad Naidu et al. 1994; Sochard et al. 1997; Yasui 1997, 1997a; Gong and Hart 1998; Colussi et al. 1998; Colussi and Hoffmann 1999; Moss et al. 1999; Storey and Szeri 2000, 2001; Toegel et al. 2000).

In a landmark paper published in 2000, Storey and Szeri (2000) presented a general treatment of the problem of vapor transport across bubble interface relaxing several assumptions made in earlier studies. The Navier–Stokes equations for the gas mixture in the bubble were coupled to the reaction mechanism. The transport properties (thermal and mass diffusion, viscosity) were calculated from the equations based on Chapman–Enskog theory and the equation of state was of Redlich–Kwong–Soave type. The rate of transport of water molecules was proportional to the difference between partial pressure of water in the bubble and the saturation pressure at interface. However, not all the water molecules that approach the surface stick to it, giving rise to non–equilibrium phase change. The fraction of water molecules that stick to the surface is the accommodation coefficient (σ_a). In other words, σ_a is a representative of the resistance to condensation at the interface during bubble collapse. The lower the value of σ_a, the greater this resistance and higher the amount of water vapor entrapped. Storey and Szeri (2000) used value of $\sigma_a = 0.4$, following Yasui (1997). The principal result of paper by Storey and Szeri (2000) was that water vapor transport in the bubble is a two–step process: diffusion to bubble wall and condensation. Thus, it is influenced by two time scales, viz. time scale of diffusion

(t_{dif}) and time scale of condensation (t_{cond}), and their magnitudes relative to bubble dynamics (or oscillations) time scale, t_{osc}. In the earlier phases of bubble collapse, $t_{osc} >> t_{dif}$, t_{cond}, which results in uniform bubble composition. As the bubble wall acceleration increases during collapse, the time scales for bubble dynamics and diffusion become equal. At this stage, rate of reduction of water vapor in the central region of bubble is lesser than at the bubble wall. With further acceleration of bubble wall, $t_{osc} << t_{dif}$, and the water vapor has insufficient time to diffuse to bubble wall, which results in nearly fixed distribution of water vapor in the bubble. Another mechanism, which traps water vapor in bubble during collapse, is the non–equilibrium phase change at bubble wall, as mentioned above. The time scale for the condensation varies inversely with σ_a. Qualitatively, when $t_{osc} >> t_{cond}$, the condensation is in equilibrium with respect to the bubble motion. On the other hand, when $t_{cond} >> t_{osc}$, no water vapor can escape bubble during collapse. Thus, the amount of water vapor trapped is sensitive to the value of σ_a. There is some disagreement about the value of σ_a, which affects the overall physics of water vapor entrapment, as discussed later in this section.

The exact mechanism by which water vapor is trapped in the bubble is determined by the relative magnitudes of t_{osc}, t_{dif} and t_{cond}. When the bubble dynamics time scale is smaller than either the diffusion or condensation time scale, water vapor entrapment occurs. However, both mechanisms can contribute to the water vapor entrapment. Storey and Szeri showed that the condition $t_{osc} << t_{dif}$ is reached well before $t_{osc} << t_{cond}$. Thus, the water vapor trapping is diffusion limited. Parallel studies conducted by Hoffmann & co–workers (Colussi *et al.* 1998; Colussi and Hoffmann 1999) clearly show the effect of condensation time scale that varies inversely with the accommodation coefficient, as mentioned earlier. In their first paper, Hoffmann & co–

workers (Colussi et al., 1998) used a very low value of $\sigma_a = 0.001$, without accounting for the finite rate of mass diffusion. With such unrealistically low value of σ_a, the condition $t_{osc} << t_{cond}$ reaches well before $t_{osc} << t_{dif}$. This makes the water vapor trapping condensation, rather than diffusion limited. In another study, Colussi & Hoffmann (1999) used a value of $\sigma_a = 0.3$, taking into account diffusive resistance generated in the bubble. With this value, the simulation results of Colussi and Hoffmann (1999) are in accordance with those of Storey and Szeri (2000) that the water vapor trapping is diffusion limited.

In view of the results of Storey and Szeri (2000) with full numerical simulations, Toegel *et al.* (2000) developed a simple diffusion limited model using boundary layer approximation. For the validation of the simple model, Toegel *et al.* (2000) have compared their results with those of Storey & Szeri (2000), finding an excellent qualitative and quantitative agreement. This is another confirmation that the water vapor transport is diffusion, rather than condensation, limited. In this thesis, we have extensively used the model of Toegel et al. (2000) for discernment of the physical mechanism of sono-hybrid techniques for oxidative desulfurization. The main equations and databases of this model have been described in detail in subsequent chapters.

1.9 AIM, APPROACH AND SCOPE OF THE PRESENT THESIS

As noted in previous sections, development of competent and commercially viable technologies for deep desulfurization of liquid transportation fuels is an urgent need of the hour. Two new technologies that have emerged in recent past (in addition to the conventional technologies of hydrodesulfurization) are microbial or biodesulfurization and oxidative desulfurization. Sonolysis has also been attempted as

an alternative for desulfurization. Some recent studies have attempted combination of these alternative technologies for deep desulfurization with encouraging results. Basically, both oxidative desulfurization and biodesulfurization systems are liquid-liquid heterogeneous systems, which are limited by mass transfer. Ultrasound irradiation or sonication is a well-known technique for enhancement and intensification of heterogeneous chemical systems. Moreover, ultrasound and its secondary effect, cavitation, can also lead to independent oxidation of the sulfur compounds through the sonochemical effect of generation of oxidizing radicals. The literature on these "sono-hybrid" techniques of desulfurization is rather limited and is mainly focused on the results than rationale. The exact mechanistic interactions between either oxidative desulfurization or biodesulfurization with ultrasound and cavitation have not been fully explored and established. Some other techniques for the intensification of biphasic reactions by enhancing interphase transport have also been reported in literature. Two common techniques in this category are: (1) addition of a phase transfer agent that would enhance transport of oxidizing species in aqueous phase to organic phase, or (2) addition of a surfactant that would form a temporary complex with the sulfur compound and would increase its solubility in the aqueous phase. These techniques may also be combined with sonication so as to give further intensification in desulfurization kinetics and yield.

The present thesis is aimed at discernment of the physical mechanism of the sono-hybrid processes for desulfurization. Mainly two sono-hybrid techniques, viz. the combinations of oxidative desulfurization (with different oxidants)/ultrasound and biodesulfurization (either microbial or enzymatic)/ultrasound, have been treated. These sono-hybrid systems have also been combined with the phase transfer agent and surfactant systems mentioned earlier. The main approach adopted in analysis of

these systems is coupling of experimental results with simulations of cavitation bubble dynamics at the experimental conditions using a mathematical model that takes into account essential physics and chemistry of the cavitation bubbles. Concurrent analysis of experimental and simulations results gives an insight into the physical mechanism of the sono-hybrid process for desulfurization. In addition, kinetic and Arrhenius analysis of the experimental data also gives an insight into the physical mechanism of the process.

In some cases, we have used the approach of fitting the experimental data of desulfurization to known deterministic models through Genetic Algorithm based optimization. These models contain several parameters that represent kinetics or physiology of the system. Fitting of the experimental data under different conditions that vary the characteristics of the ultrasound and cavitation phenomena in the system gives values of the model parameters. Comparison of values of these parameters in different experimental categories gives an insight into the physical mechanism of process.

The results and analysis presented in this thesis have brought forth some crucial links and interactions between the individual mechanisms of different techniques that eventually result in enhancement of the process. These mechanistic insights not only give important input for further research in this area but also forms important guidelines for optimization and scale-up of the process. The thesis comprises of 7 chapters (including the present one) and brief content of each chapter is described herewith:

- Chapter 1 presents the general introduction to the subject of desulfurization with description of basic aspects of conventional as well as new techniques of desulfurization. A brief review of literature in various areas of desulfurization has

been presented followed by description of aim and approach of the thesis.

- Chapter 2 presents investigations in ultrasound assisted oxidative desulfurization using the hybrid Fenton-peracetic acid system. Combination of Fenton chemistry with oxidation chemistry of peracetic acid has resulted several competing pathways and reactions of overall oxidative desulfurization process. An attempt is also made in distinguishing between contributions of ultrasound and cavitation to the process.
- Chapter 3 describes investigations in ultrasonic enhancement of phase transfer agent assisted oxidative desulfurization system. Two oxidant systems, viz. peracetic acid and performic acid have been coupled with a phase transfer agent. Synergistic links between the mechanisms of phase transfer agent and physical/chemical effects of ultrasound and cavitation have been identified.
- Chapter 4 presents further research on mechanistic links between ultrasound/cavitation and phase transfer agent. With performic acid as the oxidant system, experiments have been performed with variation of conditions that alter the nature of cavitation phenomena in the system. Kinetic and Arrhenius analysis of the experimental data has been coupled with simulations of cavitation bubble dynamics to get physical insight into the combined effect of PTA and ultrasound on oxidative desulfurization system.
- Chapter 5 presents investigations in microbial desulfurization using immobilized cells of Rhodococcus rhodocorus MTCC 3552. The approach has been to fit Haldane kinetics model to dibenzothiophene metabolism and analyze trends in model parameters concurrently with simulations of cavitation bubble dynamics to gain mechanistic insight into synergy between sonication and biodesulfurization.
- Chapter 6 presents studies in ultrasound-assisted enzymatic desulfurization

using system comprising Horseradish peroxidase enzyme and dibenzothiophene. This study involves identification of metabolic pathway of enzymatic degradation as well as study of conformational changes in the enzyme structure induced by ultrasound and cavitation. Concurrent analysis of desulfurization profiles, Arrhenius and thermodynamic parameters, and simulations of cavitation bubble dynamics reveal interesting mechanistic links between biochemistry of enzymatic oxidation and physics/chemistry of ultrasound and cavitation.

- Chapter 7 presents an overview of the mechanistic investigations in various sono-hybrid techniques. Despite significantly different chemistry, several physical aspects of the four sono-hybrid techniques for oxidative desulfurization, viz. sono-Fenton-peracetic acid, sono-PTA-peracetic/performic acid, sono-microbial and sono-enzymatic, have been revealed to be strikingly similar. These physical aspects have been identified and discussed in this chapter. These aspects also present general guidelines for optimization and scale-up of the process. Some suggestions have been made for further work on sono-hybrid techniques for oxidative desulfurization.

REFERENCES

Abdel–Wahab AMA, Gaber AEAM. TiO_2–photocatalytic oxidation of selected heterocyclic sulfur compounds. *J. Photochem. Photobiol. A* 1998; 114: 213–218.

Al–Dolama K, Stanislaus A. A comparative study of the influence of chelating agents on the hydrodesulfurization (HDS) activity of alumina and silica–alumina–supported CoMo catalysts. *Energ. Fuel* 2006; 20: 1777–1783.

Ali SH, Hamad DM, Albusairi BH, Fahim MA. Removal of dibenzothiophenes from fuel by oxy–desulfurization. *Energ. Fuel* 2009; 23: 5986–5994.

Alves L, Marque S, Matos J, Tenreiro R, Grio FM. Dibenzothiophene desulfurization

by *Gordonia alkanivorans* strain 1B using recycled paper sludge hydrolyzate. *Chemosphere* 2008; 70: 967–973.

Andari MK, Behbehani H, Stanislaus A. Sulfur compounds type distribution in naphtha and gas oil fractions of Kuwait oil. *Fuel Sci Technol Int.* 1996; 14: 939–961.

Babich VI, Moulijn JA. Science and technology of novel processes for deep desulfurization of oil refinery streams: A review. *Fuel* 2003;82: 607–631.

Bahuguna A, Lily MK, Munjal A, Singh RN, Dangwal K. Desulfurization of dibenzothiophene (DBT) by a novel strain *Lysinibacillus sphaericus* DMT–7 isolated from diesel contaminated soil. *J. Environ. Sci*. 2011; 23(6): 975–982.

Boikov E, Vakhrushin P, Vishnetskaya M. Oxidative desulfurization of hydrocarbon feedstock." *Chem. Technol. Fuel Oil* 2008; 44: 271 – 274.

Bunthid D, Prasassarakich P, Hinchiranan N. Oxidative desulfurization of tire pyrolysis naphtha in formic acid/H_2O_2/pyrolysis char system. *Fuel* 2010; 89: 2617–2622.

Campos–Martin J, Capel–Sanchez M, Fierro J. Highly efficient deep desulfurization of fuels by chemical oxidation. *Green Chem.* 2004; 6: 557–562.

Caro A, Letón P, García–Calvo E, Setti L. Enhancement of dibenzothiophene biodesulfurization using β–cyclodextrins in oil–to–water media. *Fuel* 2007; 86: 2632–2636.

Chen H, Zhang WJ, Cai YB, Zhang Y, Li W. Elucidation of 2–hydroxybiphenyl effect on dibenzothiophene desulfurization by *Microbacterium* sp. strain ZD–M2. *Bioresour. Technol*. 2008; 99: 6928–6933.

Chianelli RR, Berhault G, Torres B. Unsupported transition metal sulfide catalysts: 100 years of science and application. *Catal. Today* 2009; 147: 275–286

Colussi AJ, Hoffmann MR. Vapor supersaturation in collapsing bubbles: relevance to mechanisms of sonochemistry and sonoluminescence. *J. Phys. Chem. A* 1999;103: 11336– 11339.

Colussi AJ, Weavers LK, Hoffmann MR. Chemical bubble dynamics and quantitative sonochemistry. *J. Phys. Chem. A* 1998; 102(35): 6927–6934.

Constanti M, Giralt J, Bordons A. Desulfurization of dibenzothiophene by bacteria. *World J. Microbiol. Biotechnol.* 1994; 10: 510–516.

Corma A, Grande MS, Gonzalez–Alfaro V, Orchilles AV. Cracking activity and hydrothermal stability of MCM–41 and its comparison with amorphous silica–alumina and a USY zeolite. *J. Catal*. 1996; 159: 375–382.

Corma A, Martinez A, Martinez–Soria V, Monton JB. Hydrocracking of vacuum gasoil on the novel mesoporous MCM–41 aluminosilicate catalyst. *J. Catal*. 1995; 153: 25–31.

Costa P, Manoli J–M, Potvin C, Djega–Mariadassou G. Deep HDS on doped molybdenum carbides: From probe molecules to real feedstocks. *Catal. Today* 2005; 107–108: 520–530.

Costa V, Marchand K, Digne M, Geantet C. New insights into the role of glycol–based additives in the improvement of hydrotreatment catalyst performances, *Catal. Today* 2008;130: 69–74.

Dai Y, Qi Y, Zhao D, Zhang H. An oxidative desulfurization method using ultrasound/Fenton's reagent for obtaining low and/or ultra low sulfur diesel fuel. *Fuel Process Technol*. 2008; 89:927–932.

Dastanian M, Seyedeyn–Azad F. desulfurization of gasoline over nanoporous nickel–loaded y–type zeolite at ambient conditions. *Ind. Eng. Chem. Res.* 2010; 49: 11254–11259.

Dehkordi A, Kiaei Z, Sobati M. Oxidative desulfurization of simulated light fuel oil and untreated kerosene. *Fuel Process. Technol.*2009; 90: 435–445.

Dehkordi A, Kiaei Z, Sobati M. Oxidative desulfurization of simulated light fuel oil and untreated kerosene. *Fuel Proces. Technol.* 2009; **90**(3): 435 – 445.

Di L, Chenguang L. Deep hydrodesulfurization of diesel fuel over diatomite–dispersed NiMoW sulfide catalyst. *China Petrol. Process. Petrochem. Technol*. 2013; 15: 38–43.

Etemadi O, Yen TF. Selective adsorption in ultrasound–assisted oxidative desulfurization process for fuel cell reformer application. *Energ. Fuel* 2007; 21: 2250–2257.

Filippis P, Scarsella M. Oxidative desulfurization: oxidation reactivity of sulfur compounds in different organic matrixes. *Energ. Fuel* 2003; 17: 1452–1455.

Flego C, Arrigoni V, Ferrari M, Riva R, Zanibelli L. Mixed oxides as a support for new CoMo catalysts. *Catal. Today* 2001 ;65: 265–270.

Fuel Regulations, www.dieselnet.com/standards/fuels.html

Fuentes GA, Bartholomew CH, Catalyst Deactivation. Elsevier; 1997.

Fujikawa T. Highly active HDS catalyst for producing ultra–low sulfur diesel fuels, *Top. Catal.* 2009; 52: 872–879.

Furuya T, Kirimura K, Kino K, Usami S. Thermophilic biodesulfurization of dibenzothiophene and its derivatives by *Mycobacterium pheli* WU–F1. *FEMS Microbiol. Lett*. 2001; 204: 129–133.

Furuya T, Kirimura K, Kino K, Usami S. Thermophilic biodesulfurization of dibenzothiophene and its derivatives by *Mycobacterium phlei* WU–F1. *FEMS Microbiol. Lett.* 2001; 204: 129–133.

Gallagher JR, Olson ES, Stanley DC. Microbial desulphurization of dibenzothiophene: a sulfur–specific pathway. *FEMS Microbiol. Lett.* 1993 107: 31–36.

Girgis MJ, Gates BC. Reactivities, reaction networks and kinetics in high pressure catalytic hydroprocessing. *Ind. Eng. Chem. Res.* 1991; 30: 2021–2058.

Gong C, Hart, DP, Ultrasound induced cavitation and sonochemical yields. *J. Acoust. Soc. Am.* 1998; 104: 2675–2682

Grossman MJ, Lee MK, Prince RC, Garrett KK, George GN, Pickering IJ. Microbial desulfurization of a crude oil middle–distillate fraction: analysis of the extent of sulfur removal and the effect of removal on remaining sulfur. *Appl. Environ. Microbiol*. 1999; 65: 181–188.

Gutierrez OY, Perez F, Fuentes GA, Bokhimi X, Klimova T. Deep HDS over NiMo/Zr–SBA 15 catalysts with varying MoO_3 loading deep HDS over NiMo/Zr–SBA–15 catalysts with varying MoO_3 loading. *Catal. Today* 2008; 130: 292–301.

Hermann N, Brorson M, Topsoe H. Activities of unsupported second transition series metal sulfides for hydrodesulfurization of sterically hindered 4,6–dimethyldibenzothiophene and of unsubstituted dibenzothiophene. *Catal. Lett*. 2000; 65: 169–174.

Hernandez–Maldonado AJ, Yang RT, Desulfurization of transportation fuels by adsorption. *Catal. Rev.* 2004; 46: 111–150.

Hirai T, Ogawa K, Komasawa I. Desulfurization process for dibenzothiophenes from light oil by photochemical reaction and liquid– liquid extraction. *Ind. Eng. Chem. Res.* 1996; 35: 586–589.

Hirai T, Shiraishi Y, Ogawa K, Komasawa I. Effect of photosensitizer and hydrogen peroxide on desulfurization of light oil by photochemical reaction and liquid–liquid extraction. *Ind. Eng. Chem. Res.*1997; 36: 530–533.

Ho TC. Hydroprocessing catalysis on metal sulfides prepared from molecular complexes, *Catal. Today* 2008; 130: 206–220.

Ho TC. Inhibiting effects in hydrodesulphurization of 4,6–diethyl dibenzothiophenes. *J. Catal*. 2003; 219: 442–451.

Hubaut R, Altafulla J, Rives A, Scott C. Characterization and HDS activities of mixed Fe–Mo sulphides supported on alumina and carbon. *Fuel* 2007; 86: 743–749.

Irvine RL, Varraveto DM. Adsorption process for removal of nitrogen and sulphur. *PTQ Summer*, 1999; 37–44.

Izumi Y, Ohshiro T, Ogino H, Hine Y, Shimao M. Selective desulfurization of dibenzothiophene by *R. erythropolis* D–1. *Appl. Environ. Microbiol*. 1994; 60: 223–226.

Juan Z, Dishun Z, Liyan Y, Yongbo L. Photocatalytic oxidation dibenzothiophene using TS–1. *Chem. Eng. J.* 2010; 156: 528–531.

Kagami N, Vogelaar BM, van Langeveld AD, Moulijn JA. Reaction pathways on NiMo/Al2O3 catalysts for hydrodesulfurization of diesel fuel. *Appl. Catal. A: Gen*. 2005; 293: 11–23.

Kamath V., Prosperetti A., Egolfopoulos FN. A theoretical study of sonoluminescence. *J. Acoust. Soc. Am.*1993; 94: 248–260.

Kanda Y, Temma C, Nakata K, Kobayashi T, Sugioka M, Uemichi Y. Preparation and performance of noble metal phosphides supported on silica as new hydrodesulfurization catalysts. *Appl. Catal. A: Gen*. 2010; 386: 171–178.

Kayser KJ, Cleveland L, Park HS, Kwak JH, Kolhathar, Kilbane JJ II. Isolation and characterization of a moderate thermophile *Mycobacterium pheli* GTIS10, capable of dibenzothiophene desulfurization. *Appl. Microbiol. Biotechnol.* 2002; 59: 737–745.

Kilbane II J. Microbial biocatalyst developments to upgrade fossil fuels. *Curr. Opin. Biotechnol*. 2006; 17: 305–314.

Kilbane JJ III, Jackowski K. Biodesulphurisation of watersoluble coal–derived material by Rhodococcus rhodochrous IGTS8. *Biotechnol. Bioeng.* 1992; 40: 1107–1114.

Kirimura K, Furuya T, Nishii Y, Ishii Y, Kino K, Usami S. Biodesulfurization of dibenzothiophene and its derivatives through the selective cleavage of C–S bonds by a moderately thermophilic bacterium *Bacillus subtilis* WU–S2B. *J. Biosci. Bioeng.* 2001; 91: 262–266.

Kirimura K, Furuya T, Nishii Y, Ishii Y, Kino K, Usami S. Biodesulfurization of dibenzothiophene and its derivatives through the selective cleavage of carbon–sulfur bonds by a moderately thermophilic bacterium *Bacillus subtilis* WU–S2B. *J. Biosci. Bioeng.* 2001; 91(3): 262–266.

Klimova T, Ramirez J, Calderon M, Dominguez JM. New Mo and NiMo catalysts supported on MCM–41/alumina for thiophene hydrodesulfurization. *Stud. Surf. Sci. Catal*. 1998; 117: 493–500.

Knudsen KG, Cooper BH, Topsoe H. Catalyst and process technologies for ultra low

sulfur diesel. *Appl. Catal. A: Gen*. 1999; 189: 205–215.

Kodama K, Nakatini S, Umehara K, Shimizu K, Minoda Y, Yamada K. Microbial conversion of petro–sulfur compounds. Part III. Isolation and identification of products from dibenzothiophene. *Agric Biol Chem.* 1970; 34: 1320–1324.

Kodama K, Umehara K, Shimizu K, Nakatani S, Minoda Y, Yamada K. Identification of microbial products from dibenzothiophene and its proposed oxidation pathway. *Agric. Biol. Chem.*1973; 37: 45–50.

Kodama K. Induction of dibenzothiophene oxidation by *Pseudomonas jianni*. *Agric. Biol. Chem.* 1977; 41: 1193–1196.

Konishi J, Ishii Y, Onaka T, Okumura K, Suzuki M. Thermophilic carbon–sulfur–bond targeted biodesulfurization. *Appl. Environ. Microbiol*. 1997; 63:3164–3169.

Konishi J, Ishii Y, Onaka T, Okumura K, Suzuki M. Thermophilic carbon–sulfur–bond targeted biodesulfurization. *Appl. Environ. Microbiol*. 1997; 63: 3164–3169.

Kouzu M, Kuriki Y, Hamdy F, Sakanishi K, Sugimoto Y, Saito I. Catalytic potential of carbon–supported NiMo–sulfide for ultra–deep hydrodesulfurization of diesel fuel. *Appl. Catal. A: Gen*. 2004; 265: 61–67.

Krishnan SJ, Dwivedi P, Moholkar VS. Numerical Investigation into the Chemistry Induced by Hydrodynamic Cavitation. *Ind. Eng. Chem. Res*. 2006; 45: 1493-1504.

Kubota T, Rinaldi N, Okumura K, Honma T, Hirayama S, Okamoto Y. In situ XAFS study of the sulfidation of Co–Mo/B_2O_3/Al_2O_3 hydrodesulfurization catalysts prepared by using citric acid as a chelating agent. *Appl. Catal. A: Gen*. 2010; 373: 214–221.

Larrubia MA, Gutierrez–Alejandre A, Ramirez J, Busca G. A FT–IR study of the adsorption of indole, carbazole, benzothiophene, dibenzothiophene and 4,6–dibenzothiophene over solid adsorbents and catalysts. *Appl. Catal. A: Gen* 2002; 224: 167–178.

Li FL, Xu P, Ma CQ, Luo LL, Wang XS. Deep desulfurization of hydrodesulfurization–treated diesel oil by a facultative thermophilic bacterium *Mycobacterium sp*. X7B. *FEMS Microbiol. Lett*. 2003; 142: 65–70.

Li FT, Liu Y, Sun ZM, Zhao Y, Liu RH, Chen LJ, Zhao DS. Photocatalytic oxidative desulfurization of dibenzothiophene under simulated sunlight irradiation with mixed–phase Fe_2O_3 prepared by solution combustion. *Catal. Sci. Technol.* 2012; 2: 1455–1462.

Li W, Dhandapani B, Oyama, ST. Molybdenum phosphide: a novel catalyst for hydrodenitrogenation. *Chem. Lett*. 1998; 3: 207–208

Lin L, Zhanga Y, Kong Y. Recent advances in sulfur removal from gasoline by pervaporation. *Fuel* 2009; 80: 1799–1809.

Lu ZF, Zhan FT, Li L. Desulfurization of catalytic diesel oil by hydroperoxide–organic acid oxidation system. *J Univ. Petrol.* 2001; 25(3): 26–30.

Lu ZF, Zhan FT, Wang P. Oxidative desulfurization of straight–run diesel oil by hydrogen–peroxide /acetic anhydride. *J.Chem. Eng. oil gas* 2006, 35(2): 114–117.

Majid Dastanian and Fakhry Seyedeyn–Azad. Desulfurization of Gasoline over Nanoporous Nickel–Loaded Y–Type Zeolite at Ambient Conditions. *Ind. Eng. Chem. Res*. 2010; 49: 11254–11259

Mamaghani AH, Fatemi S, Asgari M. Investigation of influential parameters in deep oxidative desulfurization of dibenzothiophene with hydrogen peroxide and formic acid. *Int. J. Chem. Eng*. 2013; doi.org/10.1155/2013/951045.

Mei H, Mei BW, Yen TF. A new method for obtaining ultra–low sulfur dieselfuel via ultrasound assisted oxidative desulfurization. *Fuel*, 2003; 82(4): 405–414.

Mei H, Mei BW, Yen TF.A new method for obtaining ultra–low sulfur diesel fuel via ultrasound assisted oxidative desulfurization. *Fuel* 2003; 82:405–414.

Mogica–Betancourt JC, Lopez–Benitez A, Montiel–Lopez JR, Massin L, Aouine M, Vrinat M, Berhault G, Guevara–Lara A. Interaction effects of nickel polyoxotungstate with the Al_2O_3–MgO support for application in

dibenzothiophene hydrodesulfurization. *J. Catal*. 2014; 313: 9–23.

Mohebali G, Ball AS, Rasekh B, Kaytash A. Biodesulfurization potential of a newly isolated bacterium, *Gordonia alkanivorans* RIPI90A. *Enzyme Microb. Tech*. 2007;40: 578–584.

Monticello D. Biodesulfurization and the upgrading of petroleum distillates. *Curr. Opin. Biotechnol*. 2000; 11: 540–546.

Moss WC, Young DA, Harte JA, Levalin JL, Rozsnyai BF, Zimmerman GB, Zimmerman IH. Computed optical emissions from sonoluminescing bubbles. *Phys. Rev. E* 1999;59: 2986–2992.

Muralidhar G, Massoth FE, Shabtai J. Catalytic functionalities of supported sulfides. I. Effect of support and additives on the CoMo catalyst. *J. Catal*. 1984 ;85: 44–52.

Muralidhar G, Srinivas BN, Rana MS, Kumar M, Maity SK. Mixed oxide supported hydrosulfurization catalysts— a review. *Catal. Today* 2003; 86: 45–60.

Nozaki F, Kitoh T, Sodesawa T. Promoting effect of oxygen for hydrogenation of butadiene over Ni_2P catalysts. *J. Catal*. 1980; 62: 286–293.

Oda S, Ohta H. Biodesulfurization of dibenzothiophene with *Rhodococcus erythropolis* ATCC 53968 and its mutant in an interface bioreactor. *J. Biosci. Bioeng*. 2002: 94(5): 474–477.

Ohshiro T, Hine Y, Izumi Y. Enzymatic desulfurization of dibenzothiophene by a cell free system of *Rhodococcus erythropolis* D–1. *FEMS Microbiol. Lett*. 1994; 118: 341–344.

Okamoto Y. A novel preparation–characterization technique of hydrodesulfurization catalysts for cleaner fuels. *Catal. Today* 2008; 132: 9–17;

Otsuki S, Nonaka T, Takashima N. Oxidative desulfurization of light gas oil and vacuum gas oil by oxidation and solvent extraction. *Energ. Fuel* 2000; 14(6): 1232–1239.

Otsuki, S, Nonaka T, Takashima N, Qian W, Ishihara A, Imai T, Kabe T. Oxidative

desulfurization of middle distillate using ozone. *J. Jap. Pet. Ins.* 1999; 42: 315–320.

Oyama ST, Gott T, Zhao H, Lee YK. Transition metal phosphide hydroprocessing catalysts: a review. *Catal. Today* 2009;143: 94–107.

Pafko W, Petroleum, Modern Refining, Case Study: 2000; http:// www. pafko. com/ history/ h_refine.html

Pawelec B, Navarro RM, Campos–Martin JM. Towards near zero–sulfur liquid fuels: a perspective review. *Catal. Sci. Technol*. 2011; 1: 23–42.

Paybarah A, Bone RL, Corcoran WH. Selective oxidation of dibenzothiophene by peroxybenzoic acid formed in situ. *Ind. Eng. Chem. Process Des. Dev*. 1982; 21: 426–431.

Perot G. Hydrotreating catalysts containing zeolites and related materialsmechanism aspects related to deep desulfurization. *Catal. Today* 2003; 86: 111–128.

Plantenga FL, Cefortain R, Eijsbouts S, van Houtert F, Soled SL, Miseo S, Krycak R, Anderson G, Fujita K. NEBULA: a hydroprocessing catalysts with breakthrough activity. *Stud. Surf. Sci. Catal*. 2003;145: 407–410.

Prasad Naidu DV, Rajan R, Kumar R, Gandhi KS, Arakeri VH, Chandrasekaran S. Modeling of a batch sonochemical reactor. *Chem. Eng. Sci.* 1994; 49(6): 877–888.

Ramirez–Erduzco LF, Torres EG. Desulfurization of diesel by oxidation/extraction scheme: influence of the extraction solvent. *Catal. Today* 2004; 98: 289–294.

Rana MS, Huidobro ML, Ancheyta J, Gomez MT. Effect of support composition on hydrogenolysis of thiophene and Maya crude. *Catal. Today* 2005; 107–108: 346–354.

Rashidi F, Sasaki T, Rashidi AM, Kharat AN, Jozani KJ. Ultradeep hydrodesulfurization of diesel fuels using highly efficient nanoalumina–supported catalysts: Impact of support, phosphorus, and/or boron on the structure and catalytic activity. *J. Catal*. 2013; 299: 321–335.

Rashtchi M, Mohebali, G.H, Akbarnejad M.M, Towfighi J, Rasekh B, Keytash A. Analysis of biodesulfurization of model oil system by the bacterium, strain RIPI–22. *Biochem. Eng. J*. 2006; 29: 169–173.

Rayo P, Ramirez J, Rana MS, Ancheyta J, Aguilar–Elguezabal A. Effect of the incorporation of Al, Ti, and Zr on the cracking and hydrodesulfurization activity of NiMo/SBA–15 catalysts. *Ind. Eng. Chem. Res.* 2009; 48: 1242–1248.

Ren J, Wang A, Li X, Chen Y, Liu H, Hu Y. Hydrodesulfurization of dibenzothiophene catalyzed by Ni–Mo sulfides supported on amixture of MCM–41 and HY zeolite. *Appl. Catal. A: Gen*. 2008; 344: 175–182.

Rhee SK, Chang JH, Chan YK, Chang HN. Desulfurization of dibenzothiophene and diesel oils by a newly isolated Gordona strain, CYKS1. *Appl. Environ. Microbiol*. 1998; 64: 2327–2331.

Richard F, Boita T, Perot G. Reaction mechanism of 4,6–dimethyldibenzothiophene desulfurization over sulfided NiMoP/Al_2O_3–zeolite catalysts. *Appl. Catal. A: Gen* . 2007; 320: 69–79.

Robertson J, Bandosz TJ. Photooxidation of dibenzothiophene on TiO2/hectorite thin films layered catalyst. *J. Colloid. Interface Sci.* 2006; 299: 125–135.

Samokhvalov A, Tatarchuk BJ. Review of experimental characterization of active sites and determination of molecular mechanisms of adsorption, desorption and regeneration of the deep and ultradeep desulfurization sorbents for liquid fuels. *Catal. Rev. Sci. Eng.* 2010; 52: 381–410.

Sano Y, Sugahara K, Choi KH, Korai Y, Mochida I. Two–step adsorption process for deep desulfurization of diesel oil. *Fuel* 2005; 84: 903–910.

Selvavathi V, Chidambaram V, Meenakshisundaram A, Sairam B, Sivasankar B. Adsorptive desulfurization of diesel on activated carbon and nickel supported systems. *Catal. Today* 2009; 141: 99–102.

Shafi R, Hutchings GJ. Hydrodesulfurization of hindered dibenzothiophenes: an overview. *Catal. Today* 2000; 59: 423–442.

Shi Y, Zhang X, Liu G. Adsorptive desulfurization performances of ordered mesoporous carbons with tailored textural and surface properties. *Fuel* 2015; 158: 565–571.

Shiraishi Y, Hirai T, Komasawa I. A deep desulfurization process for light oil by photochemical reaction in an organic two–phase liquid–liquid extraction system. *Ind. Eng. Chem. Res.* 1998; 37: 203–211.

Shiraishi Y, Hirai T, Komasawa I. Photochemical desulfurization and denitrogenation process for vacuum gas oil using an organic two–phase extraction system. *Ind. Eng. Chem. Res.* 2001; 40: 293–303.

Shiraishi Y, Taehibana K, Hirai T, Komasawa I. Desulfurization and denitrogenation process for light oils based on chemical oxidation followed by liquid–liquid extraction. *Ind. Eng. Chem. Res*. 2002; 41(17): 4362–4375.

Sintarako P, Praserthdama P, Thammongkol V, Pokacharoenwatjana B, Yuanglamyai W, Inthiwong C. The suppression of a basic nitrogen compound influence on hydrodesulfurization activity of dibenzothiophene in treated diesel over Al_2O_3 supported CoMo catalysts by ZrO_2 as a secondary support. *Catal. Commun.* 2015; 62: 89–94.

SivasankarT, Paunikar AW, Moholkar VS. Mechanistic Approach to Enhancement of the Yield of a Sonochemical Reaction. *AIChE J*. 2007; 53: 1132-1143.

Sochard S, Wilhelm AM, Delmas H. Modeling of free radicals production in a collapsing gas–vapor bubble. *Ultrason. Sonochem.* 1997; 4: 77–84.

Soled SL, Miseo S, Krycak R, Vroman H, Ho TC, Riley K. Nickel molybodtungstate hydrotreating catalysts, US Patent 6299760; 2000.

Soled SL, Miseo S, Zhiguo H. Bulk Ni–Mo–W catalysts made from precursors containing an organic agent, US Patent 7544632; 2005.

Song C, Reddy KM. Mesoporous molecular sieve MCM–41 supported Co–Mo catalyst for hydrodesulfurization of dibenzothiophene in distillate fuels. *Appl. Catal. A: Gen*. 1999; 176: 1–10.

Song CS, Uday T, Ma XL. Desulfurization. In: Encyclopedia of Chemical processing,

doi: 10.1081/E–ECHP–120007732, Taylor and Francis, 2006.

Srivastava VC. An evaluation of desulfurization technologies for sulfur removal from liquid fuels. *RSC Adv.* 2012; 2: 759–783.

Storey BD, Szeri AJ. Water vapor, sonoluminescence and sonochemistry. *Proc. R. Soc. Lond. Ser. A* 2000; 456: 1685–1709.

Sun MZ, Zhao DZ, Sun WW. Study on the oxidative desulfurization of diesel fuel with power ultrasound. *Chem. Adhesion* 2008; 30(2): 65–68.

Tam PS, Kittrell JR, Eldridge JW. Desulfurization of fuel oil by oxidation and extraction. 1. Enhancement of extraction oil yield. *Ind. Eng. Chem. Res.* 1990; 29: 324–329.

Tang H, Li WL, Liu QF, Guan LL, Song JQ, Xing JM, Liu HZ. Adsorptive desulfurization of diesel with mesoporous aluminosilicates. *Sci. China Ser B–Chem.* 2009; 52: 276–281.

Tang K, Song LJ, Duan L, Li X, Gui J, Sun Z. Deep desulfurization by selective adsorption on a heteroatoms zeolite prepared by secondary synthesis. *Fuel Process Technol.* 2008; 89: 1 – 6.

Tao H, Nakazato T, Sato S. Energy–efficient ultra–deep desulfurization of kerosene based on selective photooxidation and adsorption. *Fuel* 2009; 88: 1961–1969.

Tetsuo A, Yamamoto D. Oxidative desulfurization of liquid fuels. *ACS Div. Fuel Chem.*1994; 39: 623 – 626.

Toegel R, Gompf B, Pecha R, Lohse D. Does water vapor prevent upscaling sonoluminescence? *Phys. Rev. Lett.* 2000;85: 3165–3168.

Topsoe H, Hinnemann B, Norskov JK, Lauritsen JV, Besenbacher F, Hansen PL, Hytoft G, Egeberg RG, Knudsen KG. The role of reaction pathways and support interactions in the development of high activity hydrotreating catalysts. *Catal. Today* 2005; 12: 107–108.

Torrisi S, Gunter M. Key Fundamentals of ultra–low sulfur diesel production: the four C's. In: *NPRA Annual Meeting, San Antonio, TX*, 2004.

TuragaUT, Song U. MCM–41–supported Co–Mo catalysts for deep hydrodesulfurization of light cycle oil. *Catal. Today* 2003; 86: 129–140.

Velu S, Watanabe S, Ma X, Song C. Regenerable adsorbents for the adsorptive desulfurization of transportation fuels for fuel cell applications. *Prepr. Pap. Am. Chem. Soc. Div. Fuel Chem.* 2003; 48: 526–528.

Wan G, Duan A, Zhang Y, Zhao Z, Jiang G, Zhang D, Gao Z, Liu J, Chung KH. Hydrodesulfurization of fluidized catalytic cracking diesel oil over NiW/AMB catalysts containing H–type beta–zeolite in situ synthesized from kaolin material. *Energ. Fuel* 2009; 23: 3846–3852.

Wan G, Duan A, Zhao Z, Jiang G, Zhang D, Li R, Dou T, Chung KH. Al_2O_3–TiO_2/Al_2O_3–TiO_2–SiO_2 composite–supported bimetallic Pt–Pd catalysts for the hydrodearomatization and hydrodesulfurization of diesel fuel. *Energ. Fuel* 2009; 23: 81–85.

Wan MW, Biel LC, Lu MC, de Leon R, Arco S. Ultrasound–assisted oxidative desulfurization (UAOD) using phosphotungstic acid: effect of process parameters on sulfur removal. *Desalin. Water Treat.* 2012; 47: 96–104.

Wan MW, Yen TF. Enhance efficiency of tetraoctyl ammonium fluoride applied to ultrasound assisted oxidative desulphurization (UAOD) process. *Appl. Catal. A* 2007; 319: 237–245.

Wang L, Shen BX, Li SZ. Model of fluidized catalytically cracked (fcc) gasoline photochemical desulfurization reactor. *Energ. Fuel* 2006; 20: 1287–1293.

Wang P, Krawiee S. Desulfurization of dibenzothiophene to 2–hydroxybiphenyl by some newly isolated bacterial strains. *Arch. Microbiol.* 1994; 161: 266–271.

Wang T, Fan Y, Wang X, Chou L, Lin H. Selectivity enhancement of CoMoS catalysts supported on tri–modal porous Al2O3 for the hydrodesulfurization of fluid catalytic cracking gasoline. *Fuel* 2015; 157: 171–176.

Whitehurst DD, Isoda I, Mochida I. Present state of the art and future challenges in the hydrodesulfurization of polyaromatic sulfur compounds**.** *Adv. Catal.*1998; 42:345–357.

Wu Z, Ondruschka B. Ultrasound–assisted oxidative desulphurization of liquid fuels and its industrial application. *Ultrason. Sonochem*. 2010; 17: 1027–1032.

Xiaoliang M, Schobert HH. Molecular simulation on hydrodesulfurization of thiophenic compounds over MoS_2 using ZINDO. *J. Mol. Catal. A– Chem.* 2000; 16: 409–427.

Yao XQ, Wang SJ, Ling FX. Oxidative desulfurization of simulated light oil. *J. Fuel Chem. Tech.* 2004; 32(3): 3318–3322.

Yasui, K. Chemical reactions in a sonoluminescing bubble. *J. Phys. Soc. Jpn*. 1997a; 66: 2911–2920.

Yoosuk B, Kim J.H, Song C, Ngamcharussrivichai C, Prasassarakich P. Highly active MoS_2, $CoMoS_2$ and $NiMoS_2$ unsupported catalysts prepared by hydrothermal synthesis for hydrodesulfurization of 4,6–dimethyldibenzothiophene. *Catal. Today* 2008; 130: 14–23.

Zannikos F, Lois E, Stournas S. Desulfurization of petroleum fractions of oxidation and solvent extraction. *J. Fuel Process. Technol*. 1995; 42(1): 35–45.

Zhao Y, Shen B, Zhang W, Tian R, Zhang Z, Gao J. Hydrodesulfurization and hydrodearomatization activities of catalyst containing ETS–10 and $AlPO_4$–5 on Daqing FCC diesel. *Fuel* 2008; 87: 2343–2346.

Zhong H, Wang X. Hydrodeoxygenation of model compounds and catalytic systems for pyrolysis bio–oils upgrading. *Catal. Sustain. Energ*. 2012; 1: 28–52.

Chapter 2

Mechanistic Features of Oxidative Desulfurization Using Sono-Fenton-Peracetic Acid System

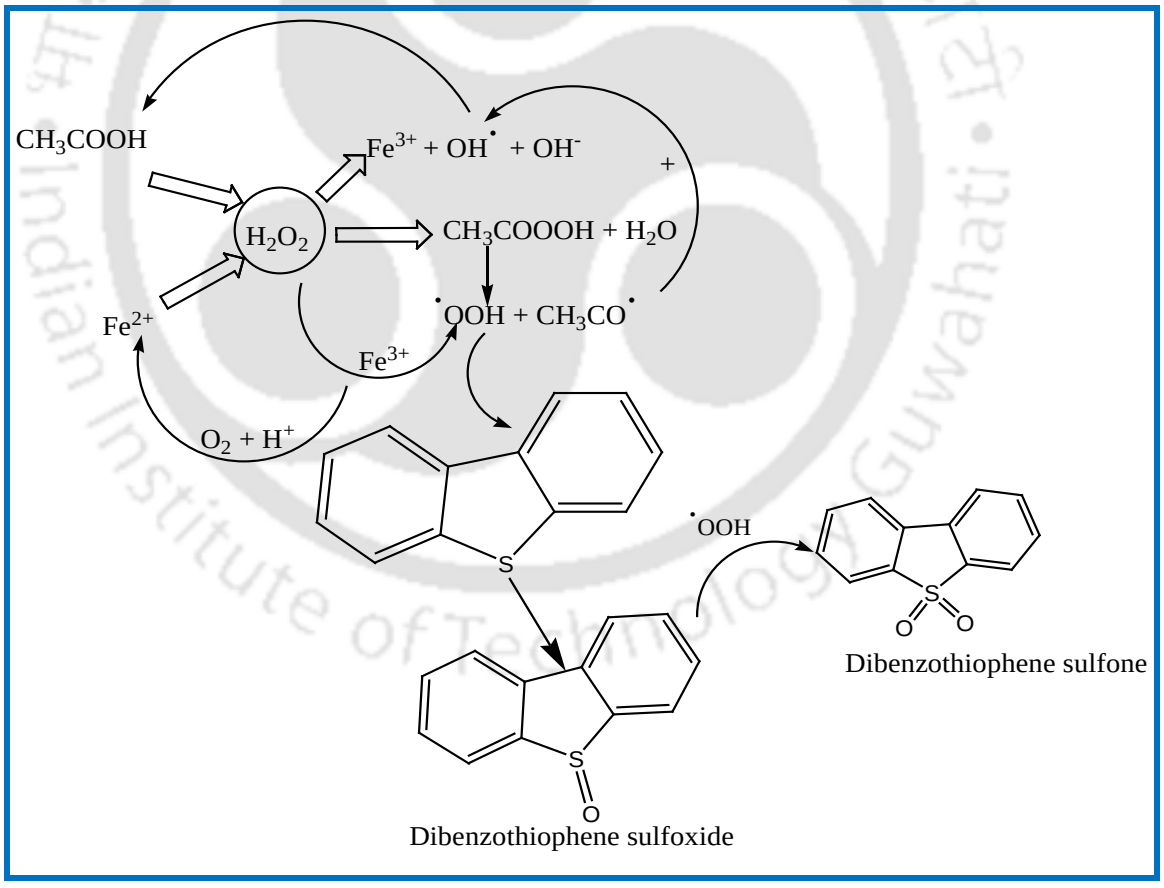

Mechanistic Features of Oxidative Desulfurization Using Sono-Fenton-Peracetic Acid System

2.1 INTRODUCTION

The new technology of oxidative desulfurization overcomes demerits of hydrodesulfurization process as stated in previous chapter. Oxidation of sulfur compounds is achieved through common oxidants like peroxy-organic acids (which give better results than peroxy-inorganic acids), hydroperoxides, nitrogen oxides, peroxy salts and ozone. The reaction mixture of oxidative desulfurization is essentially a liquid-liquid heterogeneous system limited by mass transfer. Ultrasound irradiation or sonication is a well known technique for enhancing the mass transfer in heterogeneous systems leading to improvement in their kinetics (Shah et al., 1999). Both ultrasound and its secondary effect, cavitation (which is nucleation, growth and transient collapse of tiny gas bubbles driven by ultrasound) induce physical and chemical effects in the reaction system that assist enhancement of the kinetics and yield of the process.

In this chapter, we have attempted to identify roles of different components of oxidants in the overall process of ultrasound-assisted oxidative desulfurization and its

links with transient cavitation. We have used toluene as model diesel or gasoline and dibenzothiophene (DBT) has been the model sulfur compound. Either peracetic acid ($CH_3COOH + H_2O_2$) or peracetic acid-Fenton ($CH_3COOH + H_2O_2 + Fe^{2+}$) system has been used as model oxidant. The overall methodology is similar to our earlier study, however in addition to establishing physical mechanism of oxidative desulfurization; we have also attempted to optimize the process.

2.2 MATERIALS, METHODS AND MATHEMATICAL MODEL

2.2.1 Materials

Following chemicals have been used in experiments: Dibenzothiophene (98%, Sigma Aldrich); Dibenzothiophene sulfone (97%, Sigma Aldrich); Toluene (Merck, Synthesis grade); 30% v/v H_2O_2 (Merck, AR Grade), Acetic acid (Merck, 99-100%, AR Grade), $FeSO_4 \cdot 7H_2O$ (Merck. Grade: AR) Acetonitrile (Spectrochem, HPLC grade) was used as a mobile phase for HPLC analysis process. All chemicals were used as a received without any pre-treatment or purification.

2.2.2 Experimental Setup

A schematic diagram of experimental setup is shown in Fig. 2.1. An ultrasonic bath (Make: Jeio-Tech, Model: UC02, Capacity: 2 L) was used for sonication of the reaction mixture. This bath had transducers attached to the bottom of the bath that operated at frequency 35 kHz with maximum theoretical power dissipation of 70 W. The bath was filled with water that acted as media for propagation of ultrasound waves. The actual power dissipated in the bath was determined calorimetrically (Sivasankar et al., 2007) and on that basis, the acoustic pressure amplitude generated in the bath was calculated as 150 kPa. Oxidative desulfurization reactions were carried out in a test tube (Vol: 38 mL, Dimensions: length = 100 mm, diameter = 25

mm) made of borosilicate glass. The test tube was placed in the center of the bath. As the ultrasound intensity in the bath shows significant spatial variations (Moholkar et al., 2000) the position of the test tube inside bath was carefully maintained the same in all experiments. The experiments were carried out at two different static pressures: (a) atmospheric pressure (101.3 kPa), and (b) elevated pressure of 162 kPa. For raising the static pressure in the reaction test tube, the mouth of the test tube was air sealed using rubber cork with a metal tube pierced at the center. The outer end of the tube was connected to a nitrogen cylinder with double-stage pressure regulator. The pressure inside the test tube was raised carefully to 162 kPa using the regulator.

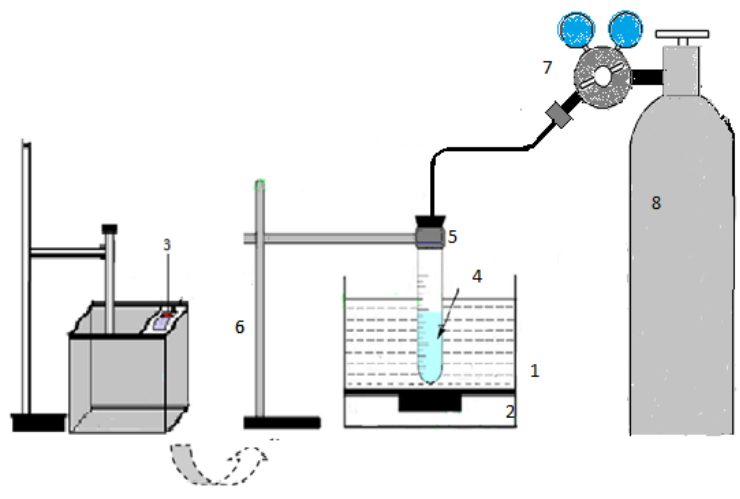

Figure 2.1 : Schematic of the experimental setup
(Legends: 1. Ultrasound bath; 2. Transducer; 3. Controller or regulator; 4. Reaction mixture; 5. Test tube with rubber cork; 6. Burette stand; 7. Pressure regulator; 8. N_2 gas cylinder)

2.2.3 Method

Dibenzothiophene (DBT) was used as a model sulfur compound and toluene as model fuel. The oxidants employed were H_2O_2, peracetic acid (CH_3COOH + H_2O_2), and peracetic acid-Fenton system (CH_3COOH + H_2O_2 + Fe^{2+}) coupled with either mechanical stirring or ultrasonication. The initial concentration of DBT in toluene was 100 ppm, with total volume of toluene being 20 mL in all experiments. To this,

appropriate volume of acetic acid (99%) and H_2O_2 (30% v/v) were added as per reaction mixture composition described in Table 2.1 for peracetic acid system. For peracetic acid-Fenton system, Ferrous sulfate heptahydrate ($FeSO_4 \cdot 7H_2O$) as a source of Fe^{2+} ions was added to the reaction mixture, and the pH of the aqueous solution was adjusted to 2 ± 0.1 before initializing the reaction (Dai et al., 2008). Initial temperature of water in the bath and also the reaction mixture inside the test tube was 298 K. The temperature of water in the bath increased during sonication. In order to avoid significant rise in temperature, some water in the bath was replaced after every 15 min. With this, the temperature variation was controlled within ± 3 K. The total sonication time was fixed as 90 min based on preliminary assessments. 1 mL aliquots of reaction mixture were withdrawn in every 15 min and analyzed for the concentration of DBT. In case of peracetic acid-Fenton process, pH of the aliquot was adjusted to 7.0 to stop the Fenton reaction. Moreover, aliquot was filtered to separate the Fe(III) floc using 0.22 μm filter (Millipore). In each category, experiments were done in triplicate to assess reproducibility of results. The mean value of DBT reduction in three experimental runs was considered for analysis along with the standard deviation.

2.2.4 Analysis

The aliquots of reaction mixtures in different experimental categories were analyzed using HPLC (Shimadzu, Model: UFLC SPD-20A) equipped with reverse phase C-18 column (5 μm, 4.6 mm × 250 mm) to quantify the concentration of DBT at λ_{max} = 287 nm. The mobile phase was mixture of acetonitrile and water (80:20 v/v) with a flow rate of 1.8 mL/min. The product of desulfurization was sulfone. The dibenzothiophene sulfone in the aliquot was also detected using same C-18 column at

UV wavelength of λ = 280 nm. The mobile phase in this case was mixture of acetonitrile and water (70:30 v/v) with a flow rate of 1 mL/min. The confirmation of formation of DBT sulfone was also done using FTIR (Shimadzu, Model: IRAffiniti1).

2.2.5 Experimental Categories

Experimental work in this study was carried out in two phases, preliminary experiments followed by main experiments. Main experiments were carried out in 4 categories, viz. A, B, C and D as described below.

Category A: These are the basic experiments with either ultrasound alone, ultrasound + acetic acid or ultrasound + H_2O_2

Category B: Experiments with peracetic acid (with either ultrasound or stirring) at optimum ratio of CH_3COOH/H_2O_2 as determined from preliminary experiments

Category C: Experiments with peracetic acid-Fenton system (with either ultrasound or stirring) at optimum ratio of CH_3COOH/H_2O_2 and Fe^{2+} loading as determined from preliminary experiments. The static pressure of the system is either atmospheric or elevated.

Category D: Experiments with peracetic acid-Fenton system (with either ultrasound or stirring) at optimum Fe^{2+} loading for excess H_2O_2 and as determined from preliminary experiments. The static pressure of the system is either atmospheric or elevated.

Prior to the main experiments, initial or preliminary experiments were carried out to assess effect of following parameters and fix the optimum value of these parameters: (1) effect of acetic acid to H_2O_2 ($CH_3COOH:H_2O_2$) molar ratio, (2) effect of volume ratio of the organic and aqueous phases, (3) effect of iron catalyst loading, (4) effect of iron catalyst in presence of excess H_2O_2.

The exact composition of the reaction mixture in different categories along with ratios

of CH_3COOH/H_2O_2 and H_2O_2/Fe^{2+} is given in Table 2.1. Rise in the static pressure of the medium causes significant changes to the characteristics of cavitation bubble dynamics, as explained in results and discussion section.

2.3 SIMULATIONS OF CAVITATION BUBBLE DYNAMICS

As mentioned earlier, ultrasound as well as cavitation induces physical and chemical effects in the bulk liquid medium. In the present case, the reaction system is a two-phase mixture, viz. organic phase (toluene) and aqueous phase (peracetic acid). Passage of ultrasound through the reaction mixture induces micro-streaming in both phases, but the magnitudes are slightly different.

The micro-streaming velocity is calculated as: $u = P_A/\rho_L c$, where P_A is the pressure amplitude of ultrasound wave, while ρ_L and c are the density of and sonic velocity in the liquid medium, respectively. As stated previously, the amplitude of the ultrasound wave in the medium was determined as 150 kPa using calorimetric measurements. For toluene, ρ_L = 867 kg/m^3 and c = 1275 m/s, and thus, u = 0.137 m/s. For peracetic acid, ρ_L = 1216 kg/m^3 and c = 1584 m/s, and thus, u = 0.078 m/s. For estimation of the physical and chemical effects produced by cavitation bubbles, we have resorted to simulations of cavitation bubble dynamics.

2.3.1 Cavitation Bubble Model for Toluene

For modeling of bubble dynamics in toluene we have used the diffusion limited ODE model proposed by Toegel et al., 2000 that uses boundary layer approximation. This model is based on the comprehensive PDE model of Storey and Szeri (2000), who showed that vapor entrapment in the cavitation bubble, leading to formation of radicals is essentially a diffusion limited process. This model has been extensively described in our previous work (Sivasankar et al., 2000; Krishnan et al., 2006). The

essential equations and thermodynamic data of this model have been summarized in the Table 2.2 and Table 2.3 respectively (Reid et al., 1987; Hirschfelder et al., 1954; Condon and Odishaw, 1958; Zhou et al., 2000; Zhu et al., 2000).

Table 2.1: Experimental categories with composition of reaction mixture

Experimental Category (Oxidant composition)	Molar Ratio $\frac{CH_3COOH}{H_2O_2}$	Molar Ratio $\frac{H_2O_2}{Fe^{2+}}$
A1. Ultrasound alone	N.A.	N.A.
A2. Ultrasound + CH_3COOH	N.A.	N.A.
A3. Ultrasound + H_2O_2	N.A.	N.A.
B1. Stirring + CH_3COOH + H_2O_2	2.0	N.A.
B2. Ultrasound + CH_3COOH + H_2O_2	2.0	N.A.
C1. Stirring + CH_3COOH + H_2O_2 + Fe^{2+}	2.0	0.017
C2. Ultrasound + CH_3COOH + H_2O_2 + Fe^{2+}	2.0	0.017
C3. Ultrasound + CH_3COOH + H_2O_2 + Fe^{2+} Static Pressure = 162 kPa	2.0	0.017
D1. Stirring + H_2O_2 + CH_3COOH + Fe^{2+}	0.5	0.05
D2. Ultrasound + CH_3COOH + H_2O_2 + Fe^{2+}	0.5	0.05
D3. Ultrasound + CH_3COOH + H_2O_2 + Fe^{2+}; Static pressure = 162 kPa	0.5	0.05

N.A. – Not applicable. The static pressure during the experiments was atmospheric, unless otherwise stated.

The model is essentially a set of 4 ordinary differential equations: (1) Keller–Miksis equation for the radial motion of the bubble, (2) equation for the diffusive flux of water vapor and heat conduction through bubble wall, and (3) overall energy balance. Thermal conductivity of the bubble contents and diffusion coefficient of

water vapor inside the bubble are determined using Chapman–Enskog theory using Lennard–Jones 12–6 potential. Diffusion of gas across bubble interface is ignored in the present model as the time scale for the diffusion of gases is much higher than the time scale for the radial motion of bubble. The model equations have been solved using Runge–Kutta adaptive step size method (Press et al., 1992). An air bubble has been considered for simulations. The condition for bubble collapse is taken as the first compression after an initial expansion. Various parameters used in the simulation of bubble dynamics equation and their numerical values are as follows: Ultrasound frequency (f) = 35 kHz; Ultrasound pressure amplitude (P_A) = 150 kPa; Equilibrium bubble radius (R_o) = 5 μm; Vapor pressure of toluene was calculated using Antoine type correlation. Various physical properties of toluene are as follows: ρ_L = 867 kg/m^3, kinematic viscosity (ν) = 6.8 × 10^{-7} Pa–s, surface tension (σ) = 0.0285 N/m and c = 1275 m/s, static pressure (P_0) = 101.3 kPa (for experiments at atmospheric static pressure) or 162 kPa (for experiments with elevated static pressure).

2.3.2 Model for Peracetic Acid

The diffusion limited model of Toegel et al., (2000) requires Lennard-Jones parameters, which were not available to us for peracetic acid. Therefore, we have done simulations of cavitation bubble dynamics in peracetic with the approach of Prasad Naidu et al., 1994. The salient features of this approach are as follows: (1) Assumption of ideal behavior for the bubble contents, i.e. mixture of air and solvent vapor; (2) Isothermal expansion of the bubble followed by isothermal / adiabatic collapse; (2) The bubble content is assumed to be at the solvent temperature and saturated with solvent vapor initially; (4) The transition from isothermal to adiabatic behavior in the collapse phase is assumed to occur when partial pressures of gas and vapour in the bubble equalize (Flynn, 1975). Thereafter, the cavitation bubble is a

closed system, on which work is done by surrounding fluid; (5) The temperature and pressure peak reached in the bubble at the point of minimum radius (or maximum compression) calculated using polytropic law. For the radial motion of the bubble, Prasad Naidu et al., 1994 have used the Rayleigh-Plesset equation (Plesset, 1949) that does not take into account liquid compressibility.

Table 2.2: Model for the Radial Motion of Cavitation Bubble

Model Component	Equation	Initial Value
1. Radial motion of the cavitation bubble	$\left(1-\frac{dR/dt}{c}\right)R\frac{d^2R}{dt^2}+\frac{3}{2}\left(1-\frac{dR/dt}{3c}\right)\left(\frac{dR}{dt}\right)^2=\frac{1}{\rho_L}\left(1+\frac{dR/dt}{c}\right)(P_i-P_t)+\frac{R}{\rho_L c}\frac{dP_i}{dt}-4\nu\frac{dR/dt}{R}-\frac{2\sigma}{\rho_L R}$ Internal pressure in the bubble: $P_i=\frac{N_{tot}(t)\,kT}{\left[4\pi\left(R^3(t)-h^3\right)/3\right]}$ Pressure in bulk liquid medium: $P_t=P_0-P_A\sin(2\pi ft)$	At t = 0, $R = R_o$ = 5 μm dR/dt = 0
2. Diffusive flux of toluene molecules	$\frac{dN_{TOL}}{dt}=4\pi R^2 D_{TOL}\left.\frac{\partial C_{TOL}}{\partial r}\right\|_{r=R}\approx 4\pi R^2 D_{TOL}\left(\frac{C_{TOL,R}-C_{TOL}}{l_{diff}}\right)$ Instantaneous diffusive penetration depth: $l_{diff}=\min\left(\sqrt{\frac{RD_{TOL}}{\lvert dR/dt\rvert}},\frac{R}{\pi}\right)$	At t = 0, N_{TOL} = 0
3. Heat conduction across bubble wall	$\frac{dQ}{dt}=4\pi R^2\lambda\left.\frac{\partial T}{\partial r}\right\|_{r=R}\approx 4\pi R^2\lambda\left(\frac{T_0-T}{l_{th}}\right)$ Thermal diffusion length: $l_{th}=\min\left(\sqrt{\frac{R\kappa}{\lvert dR/dt\rvert}},\frac{R}{\pi}\right)$	At t = 0, Q = 0
4. Overall energy balance	$C_{V,mix}dT/dt=dQ/dt-P_i dV/dt+\left(h_{TOL}-U_{TOL}\right)dN_{TOL}/dt$ Mixture heat capacity: $C_{V,mix}=\sum C_{V,i}N_i$ (i = N_2/O_2/toluene) Molecular properties of toluene: Enthalpy: $h_{TOL} = 4kT_o$ Internal energy: $U_{TOL}=N_{TOL}kT\left(3+\sum_{i=1}^{3}\frac{\theta_i/T}{\exp(\theta_i/T)-1}\right)$ Heat capacity of various species (i = N_2/O_2/toluene): $C_{V,i}=N_i k\left(f_i/2+\sum\left((\theta_i/T)^2\exp(\theta_i/T)\Big/\left(\exp(\theta_i/T)-1\right)^2\right)\right)$	At t = 0, $T = T_o$ = 25°C

Table 2.3: Thermodynamic Properties of Various Species

Species	Degrees of freedom (translational + rotational) (f_i)	Lennard–Jones force constants		Characteristic vibrational temperatures θ (K)	
		σ (10^{-10} m)	ε/k (K)		
N_2	5	3.68	92	3350	
O_2	5	3.43	113	2273	
Toluene	6	5.822	450.7	1004.131, 2111.628, 2325.744, 4375.023	1055.813, 2163.311, 4224.076,

Notations for Table 2.2 and 2.3: R – radius of the bubble; dR/dt – bubble wall velocity; c – velocity of sound in bulk liquid medium; ρ_L – density of the liquid; ν – kinematic viscosity of liquid; σ – surface tension of liquid; λ – thermal conductivity of bubble contents; κ – thermal diffusivity of bubble contents; θ – characteristic vibrational temperature(s) of the species; N_{TOL} – number of toluene molecules in the bubble; N_{N2} – number of nitrogen molecules in the bubble; N_{O2} – number of oxygen molecules in the bubble; t – time, D_{TOL} – diffusion coefficient of toluene vapor; C_{TOL} – concentration of toluene molecules in the bubble; $C_{TOL,R}$ – concentration of toluene molecules at the bubble wall or gas–liquid interface; Q – heat conducted across bubble wall; T – temperature of the bubble contents; T_o – ambient (or bulk liquid medium) temperature; k – Bolzmann constant; h_{TOL} – molecular enthalpy of toluene; U_{TOL} – internal energy of toluene molecules; f_i – translational and rotational degrees of freedom; $C_{V,i}$ – heat capacity at constant volume for species i; N_{tot} – total number of 'molecules (gas + vapor) in the bubble; h – van der Waal's hard core radius; P_o – ambient (bulk) pressure in liquid; P_A – pressure amplitude of ultrasound wave; f – frequency of ultrasound wave; V_b – volume of the bubble; r – distance from bubble center at which microturbulence velocity is estimated (representative value taken as 1 mm); V_{turb} – velocity of microturbulence; P_{AW} – pressure amplitude of the acoustic (or shock waves) emitted by the bubble.

In the present case, we have chosen a modified form of the original Rayleigh-Plesset equation with inclusion of the compressibility effect (Prosperetti and Lezzi, 1986; Keller and Miksis, 1980; Lofstedt et al., 1995; Hilgenfeldt et al., 1996; Barber et al., 1997).

$$R\frac{d^2R}{dt^2}+\frac{3}{2}\left(\frac{dR}{dt}\right)^2=\frac{1}{\rho_L}\left(p(R,t)-P_0-P(t)\right)+\frac{R}{\rho_L c}\frac{d}{dt}\left[p(R,t)-P(t)\right]-\frac{4\mu}{\rho_L R}\frac{dR}{dt}-\frac{2\sigma}{\rho_L R} \quad (1)$$

Various notations are as follows: R = radius of the bubble at any time; dR/dt = velocity of bubble wall; μ = viscosity of the bulk liquid. $p(R,t)$ and $P(t)$ are the

pressures inside the cavitation bubble and the time variant pressure of the acoustic wave, respectively; and are written as:

$$p(R,t) = \left(P_0 + \frac{2\sigma}{R_0} - P_v \right) \left(\frac{R_0^{\,3} - h^3}{R^3 - h^3} \right)^{\gamma} + P_v \qquad (2)$$

$$P(t) = P_A \cos(2\pi ft) \qquad (3)$$

Various notations are as follows: P_v = vapor pressure of bulk liquid; h = van der Waal's hard core radius; γ = polytropic constant of bubble content. Values of simulation parameters for peracetic acid are: f = 35 kHz; P_A = 150 kPa; R_o = 5 μm; P_v = 1933 Pa (at 298 K), ρ_L = 1216 kg/m^3, ν = 2.697 × 10^{-6} Pa–s, σ = 0.036 N/m, and c = 1584 m/s, P_o = 101.3 kPa or 162 kPa (for experiments with elevated static pressure). The peak temperature and pressure conditions reached in the bubble at the point of maximum compression (or minimum radius) are determined as: (1) $T_{max} = T_o \left(R_2 / R_{min} \right)^{3(\gamma-1)}$, (2) $P_{max} = P_2 \left(R_2 / R_{min} \right)^{3\gamma}$, where R_2 is the radius of the cavitation bubble during the collapse phase at which the partial pressure of gas inside the bubble becomes equal to the vapor pressure of the solvent.

2.4 ESTIMATION OF PHYSICAL AND CHEMICAL EFFECT OF THE CAVITATION BUBBLES

As noted earlier, the physical effect of cavitation bubbles is the generation of convection in the medium through phenomena of micro-turbulence and acoustic waves; while the chemical effect is generation of radical species through thermal dissociation of gas and solvent vapor at peak temperature and pressure conditions reached during transient collapse.

2.4.1 Sonophysical Effect

The magnitude of the convective effects, viz. velocity of the microturbulence (V_{turb}) and pressure amplitude of the acoustic waves (P_{AW}) are a function of distance from center of the bubble and can be calculated as follows (Grossmann et al., 1997; Moholkar and Warmoeskerken, 2003):

$$V_{turb} = \frac{R^2}{r^2}\left(\frac{dR}{dt}\right) \tag{4}$$

$$P_{AW}(r,t) = \rho_L \frac{R}{r}\left[2\left(\frac{dR}{dt}\right)^2 + R\frac{d^2R}{dt^2}\right] \tag{5}$$

where r is the distance from bubble center. A representative value of this parameter is taken as 0.1 mm.

2.4.2 Sonochemical Effect

Using the numerical solution of bubble dynamics models described above, one can estimate the composition of the bubble contents at the collapse. While calculating the composition of the bubble at the time of collapse, we assume that thermodynamic equilibrium is attained (Krishnan et al., 2006). The equilibrium mole fraction of the various species in the bubble at the conditions of temperature and pressure at first the compression of the bubble can be calculated using Gibbs free–energy minimization technique (Eriksson, 1975).

2.5 RESULTS OF PRELIMINARY EXPERIMENTS

2.5.1 Effect of Acetic Acid to H_2O_2 (CH_3COOH:H_2O_2) Molar Ratio

The effect of molar ratio of Acetic acid (CH_3COOH) to H_2O_2 (CH_3COOH: H_2O_2) on the kinetics and yield of oxidation of DBT to DBT sulfone was investigated to identify the optimum value for the highest results. The initial concentration of DBT

in the reaction mixture was 100 ppm. In the oxidant mixture forming peracetic acid, the volume of CH_3COOH (99%) was varied in the range of 0.5–5 mL, keeping the volume of H_2O_2 (30% v/v) fixed at 2 mL (0.025 M). With mixtures of different volumetric composition, the molar ratio of CH_3COOH: H_2O_2 varied in the range of 0.67–3.36. The percentage reduction of DBT obtained for different molar ratios of CH_3COOH:H_2O_2 is depicted in Fig. 2.2. The highest reduction in DBT was obtained for molar ratio of 2.01 (corresponding to 2:1 v/v ratio). The main experiments on oxidative desulfurization with peracetic acid were carried out using this optimum value of mixture of acetic acid (4 mL) and H_2O_2 (2 mL).

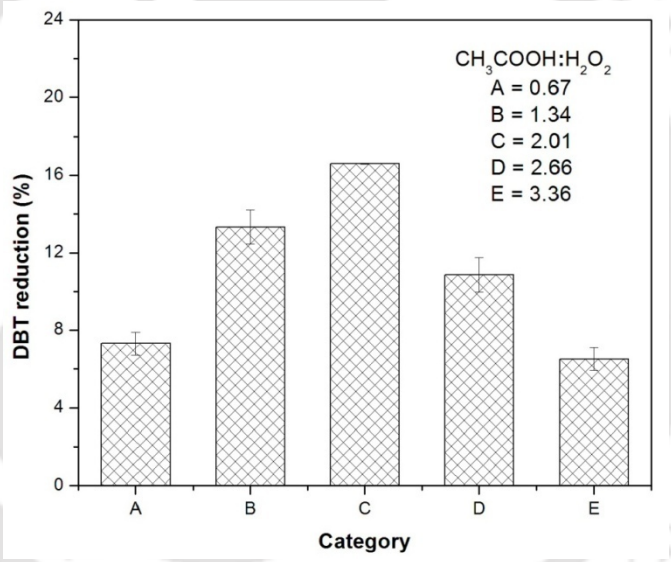

Figure 2.2: Effect of acetic acid to H_2O_2 molar ratio on oxidation of DBT

2.5.2 Effect of Volume Ratio of Phases

In the present study, toluene has been used as the model solvent representing gasoline and diesel. The reaction mixture is biphasic in that sulfur compounds are present in solvent (representing organic phase), while oxidizing species ($HO_2^{\bullet}$ radicals) are generated in the oxidant (i.e. peracetic acid representing aqueous phase). The transfer of the oxidizing $HO_2^{\bullet}$ species from aqueous phase to solvent occurs at the interface between the phases. Formation of emulsion is, thus, a critical factor, which

in turn is a strong function of volume ratio of aqueous to organic phase. To optimize volume ratio of phases, experiments were carried out with varying quantities of toluene (with 100 ppm of DBT, as in previous section) and peracetic acid. The volume ratio of two components of peracetic acid, viz. acetic acid and H_2O_2, however was maintained as 2:1, in accordance with the results of previous section. The trends in percentage oxidation of DBT for different volume ratios of toluene to H_2O_2 are shown in Fig. 2.3. The highest DBT oxidation was obtained for volume ratio of 10:1 (with H_2O_2 volume being 2 mL). On the basis of this result, the total toluene volume in main experiments was fixed as 20 mL.

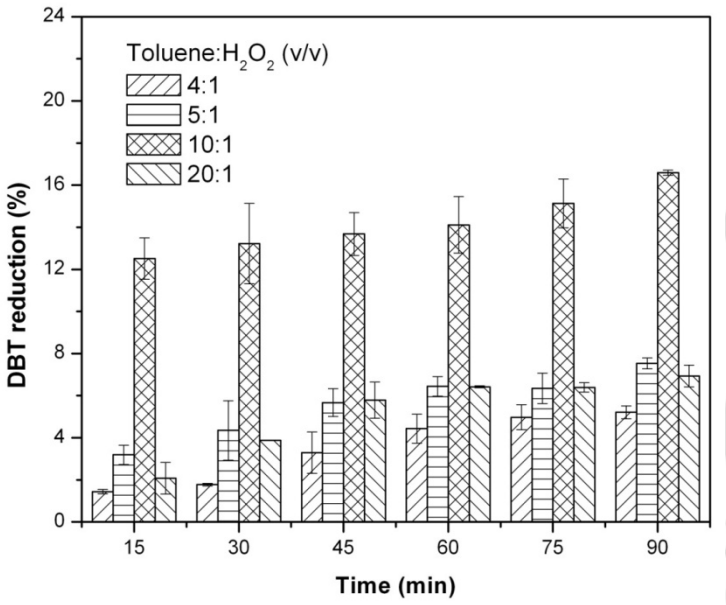

Figure 2.3: Effect of Toluene to H_2O_2 ratio on oxidation of DBT

2.5.3 Effect of Iron Catalyst Loading

The main oxidant for desulfurization used in the present study was peracetic acid. Addition of Fenton reagent to peracetic acid helps in augmentation of oxidation potential, as the $^{\bullet}OH$ radicals generated by the Fenton reactions combine with the $CH_3CO^{\bullet}$ radicals formed during dissociation of peracetic acid to regenerate acetic

acid. In view of the beneficial action of Fenton reagent, we have also assessed peracetic acid-Fenton oxidant assisted by sonication for desulfurization process in this present study. Fenton reagent was synthesized in-situ by addition of Fe^{2+} (in the form of Ferrous sulfate heptahydrate in solid form) to peracetic acid (with optimum CH_3COOH/H_2O_2 volume ratio of 2:1, as obtained in previous section). The volume ratio of toluene to hydrogen peroxide (as component of peracetic acid) was kept at 10:1, in accordance with results of previous section. Fig. 2.4 shows the results of the experiments in which addition of Fe^{2+} to peracetic acid was varied in range of 0.5-2 M. It could be inferred that percentage DBT reduction passes through a maxima at Fe^{2+} concentration of 1.5 M. As the loading of iron catalyst increases, the rate of desulfurization also increases, but after a certain value of iron catalyst loading the process shows lesser rate of desulfurization. On the basis of experimental result, the addition of Fe^{2+} to peracetic acid (with volume ratio of acetic acid to H_2O_2 as 2:1) was fixed at 1.5 M.

In the above process, the Fenton reagent was generated in-situ by addition of Fe^{2+} to peracetic acid. Fe^{2+} competitively consumes H_2O_2 in the peracetic acid mixture. Thus, the combination of CH_3COOH and H_2O_2 is hampered. In order to obviate this limitation, we have also conducted experiments with excess addition of H_2O_2 to peracetic acid. The volume ratio of CH_3COOH and H_2O_2 in peracetic acid is fixed as 1:1 (corresponding to molar ratio of 1.01, instead of 2:1 in previous study), with conjecture that part of H_2O_2 will combine with CH_3COOH to yield peracetic acid and rest will react with Fe^{2+} to form $^{\bullet}OH$ radicals. The results of experiments are shown in Fig. 2.5. The Fe^{2+} addition to peracetic acid in this case was varied between 0.5-1.5 M. It could be inferred that the maxima for DBT reduction with Fe^{2+} concentration occurs at 1 M. This value has been used in the main experiments with

excess addition of H_2O_2.

As per the results of these experiments, the optimum values or ratios of different components of peracetic acid-Fenton system (within the range of values or ratios assessed as per published literature) are: molar ratio of CH_3COOH/H_2O_2 = 2, volume ratio of toluene/H_2O_2 = 10, Fe^{2+} loading = 1.5 M, and Fe^{2+} loading under excess H_2O_2 = 1 M.

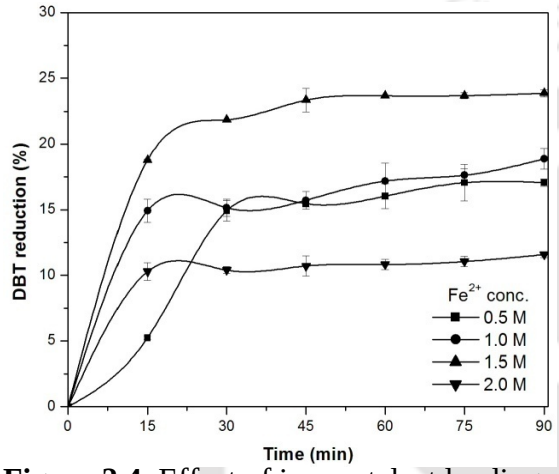

Figure 2.4: Effect of iron catalyst loading on oxidation of DBT

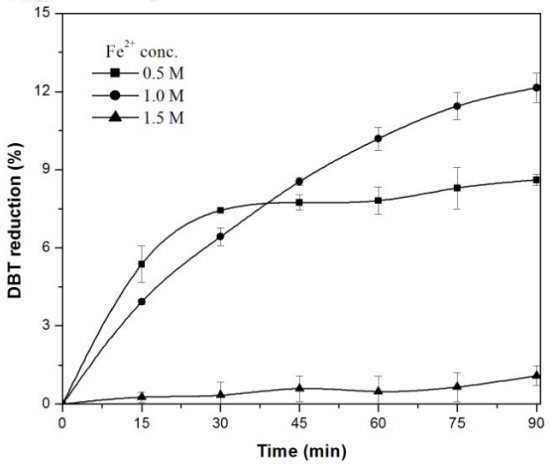

Figure 2.5: Effect of iron catalyst on DBT reduction in presence of excess H_2O_2

2.6 RESULTS AND DISCUSSION

The oxidation of DBT and DBT sulfone occurs through a series of reactions, which have been given in Fig. 2.6. Acetic acid and H_2O_2 react to form peracetic acid, which then decomposes to hydroperoxy ($HO_2^{\bullet}$) radicals, and $CH_3CO^{\bullet}$. Fe^{2+} reacts with H_2O_2 to yield $^{\bullet}OH$ radical that combine with $CH_3CO^{\bullet}$ to regenerate acetic acid. $HO^{\bullet}_2$ radicals attack sulfur in the DBT ring and convert it to sulfone in two step process: first to DBT sulfoxide and further to DBT sulfone. An alternate source of $HO^{\bullet}_2$ radicals is reaction between $^{\bullet}OH$ and H_2O_2. A competing pathway for $HO^{\bullet}_2$ radical is the regeneration of Fe^{2+} from Fe^{3+} (during Fenton reaction). These reactions

are highly interlinked, and H_2O_2 is the major component of reaction mixture that plays crucial role of balancing between various series/parallel pathways.

Before proceeding to main results and discussion section, we present the IR analysis of the reaction mixture that confirms formation of sulfone. Fig. 2.7 shows the IR spectra of DBT (pure), DBT sulfone (pure) and the aliquot of reaction mixture drawn at end of 90 min. The characteristic peaks at 918 cm^{-1}, 1038 cm^{-1} (S = O stretch) and 2253 cm^{-1} in the IR spectrum of reaction mixture confirm formation of sulfone (Castillo et al., 2009; Olson et al., 1993). A small peak at 729 cm^{-1} also confirms presence of un-reacted DBT in the reaction mixture.

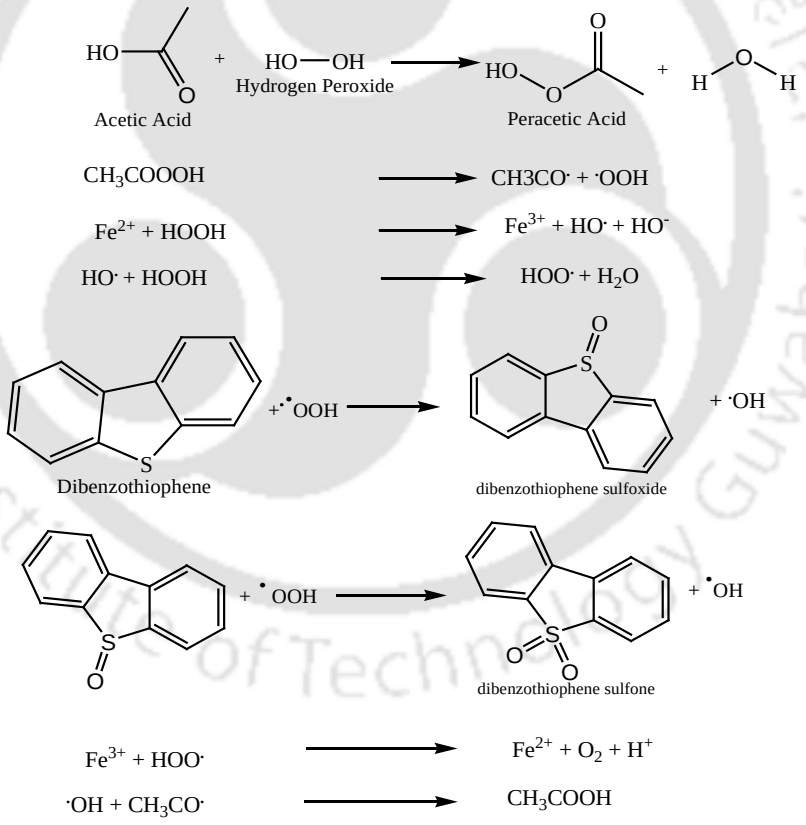

Figure 2.6: Reaction scheme for oxidative desulfurization

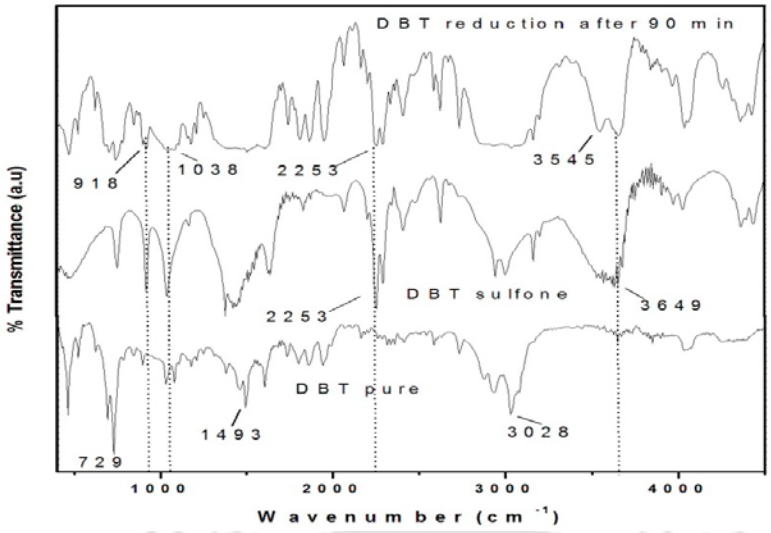

Figure 2.7: FTIR spectra of DBT (pure), DBT sulfone (pure) and aliquot with withdrawn from reaction mixture after 90 min of sonication (category C)

2.6.1 Results of Preliminary Experiments

Preliminary experiments were carried out to access influence of 4 parameters. It is interesting that the optimum value of molar ratio of CH_3COOH/H_2O_2 is not 1, as the stoichiometry of peracetic acid formation would predict, but more than 1 (i.e., 2). This means that H_2O_2 is a limiting agent and not all of CH_3COOH gets converted to peracetic acid at any time. Thus, the extent of formation of peracetic acid, and its consequent decomposition into $CH_3CO^{\bullet}$ and $HO^{\bullet}_2$ radicals is also less as compared to stoichiometric CH_3COOH/H_2O_2 molar ratio of 1. We explain this anomaly on the basis of scavenging of $HO^{\bullet}_2$ radicals by H_2O_2 (Vardanyan et al., 1974):

$$H_2O_2 + HO_2^{\bullet} \longrightarrow {}^{\bullet}OH + H_2O + O_2 \qquad \text{(R 1)}$$

If acetic acid and H_2O_2 are added in stoichiometric ratio, $HO^{\bullet}_2$ radicals generated are scavenged by H_2O_2 itself, before they are transferred to organic phase at interface between phases. At lower quantities of H_2O_2 (or larger quantities of acetic acid) competitive consumption of H_2O_2 towards peracetic acid formation expected to be high, which limits the scavenging action. Although the extent of $HO^{\bullet}_2$ formation is

less, the scavenging is also negligible, which facilitates transfer of these radicals to organic phase. The net utilization of these radicals towards oxidation is high that results in greater oxidation of DBT. In addition greater formation of peracetic acid results in higher evaporation of it into cavitation bubbles that results in $^{\bullet}OH$ radicals generation (as explained in the next section of simulations results), which can also scavenge $HO^{\bullet}_2$ radicals through reaction.

$$^{\bullet}OH + H_2O_2 \longrightarrow H_2O + HO^{\bullet}_2 \qquad \text{(R.2)}$$

With CH_3COOH:H_2O_2 molar ratio of 2:1, the quantity of Fe^{2+} required for maximum DBT oxidation is high (1.5 M), as compared to just 1 M required at excess addition of H_2O_2 (i.e. 1:1 molar ratio). This is a consequence of competitive consumption of H_2O_2 by CH_3COOH and Fe^{2+}. Larger amount of Fe^{2+} is required to consume fraction of H_2O_2 added to reaction mixture for generation $^{\bullet}OH$ radicals through Fenton reactions, which in turn assist regeneration of CH_3COOH, due to combination of $CH_3CO^{\bullet}$ and $^{\bullet}OH$ radicals. Quite interestingly, the product of Fenton reaction, Fe^{3+} ions, react with $HO^{\bullet}_2$ generated from decomposition of peracetic acid to regenerate Fe^{2+}. The above discussion clearly establishes that H_2O_2 is the species that plays central role in the overall chemistry of DBT oxidation. This essentially shows that chemistry of oxidative desulfurization is complex and highly interlinked, which is depicted in Fig. 2.8.

2.6.2 Results of Main Experiments

The results of the experiments in different categories are given in Table 2.4 as mean DBT reduction in each category, along with standard deviation of the results of triplicate experimental runs. The time history of DBT reduction in experimental categories A and B is given in Fig. 2.9, while that for categories C and D is given in

Fig. 2.10. The time data of DBT reduction in each category was fitted to a pseudo 1st order kinetic model, and the kinetic constant for different experimental categories is also listed in Table 2.4. The salient features of trends in DBT reduction in different experimental categories can be identified as follows:

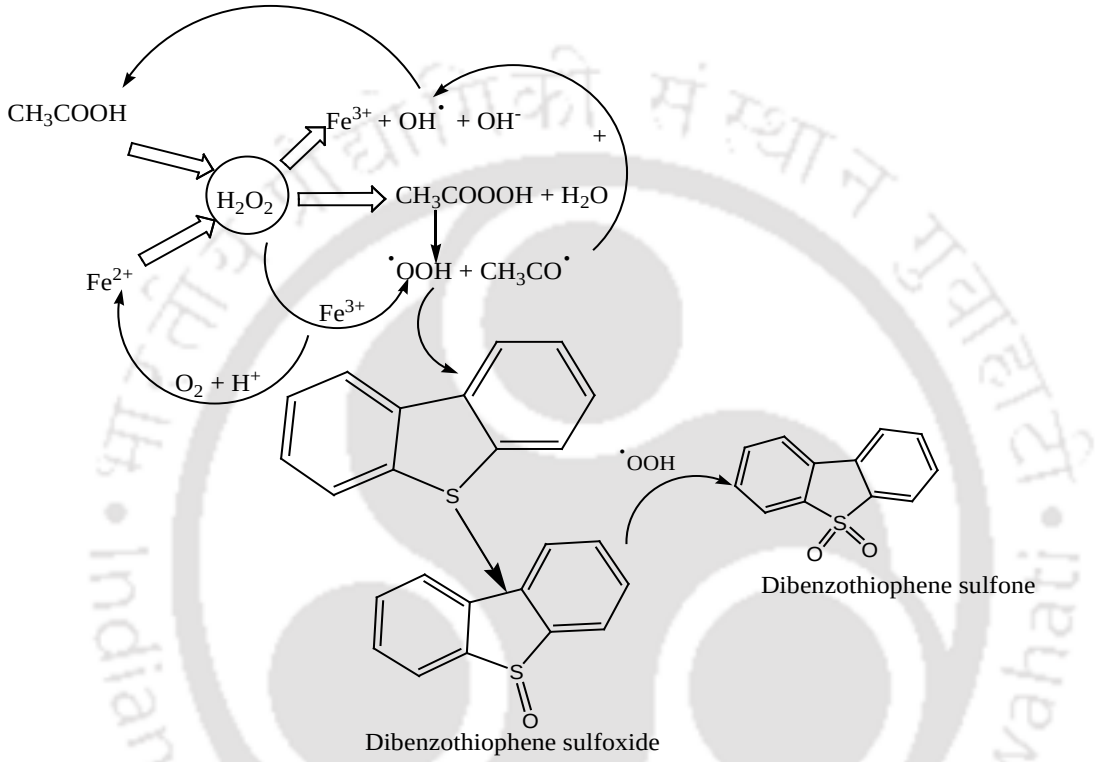

Figure 2.8: Links or interactions between different chemical species in peracetic acid – Fenton process for oxidative desulfurization

1. In Category A experiments, ultrasound alone gives a low DBT reduction of 8.69% in 90 min. Addition of CH_3COOH (which is completely miscible with toluene) results in ~ 50% rise in DBT reduction, while addition of H_2O_2 (which is immiscible with toluene and forms second phase) results decrease of DBT reduction.

2. Category B experiments employed peracetic acid as the oxidant. Replacement of stirring with sonication gives the marked boost (~ 3 fold) to the extent of DBT reduction.

3. Addition of Fe^{2+} to peracetic acid also shows a marked rise in the DBT reduction in category C experiments. The DBT reduction with stirring rises almost 3 fold (as compared to category B) while that with sonication shows ~ 50% increase. Application of high static pressure to reaction system takes DBT reduction further up by ~ 50%.

Table 2.4: Summary of Experimental Results

Experimental Category	% DBT oxidation in 90 min	Pseudo 1st Order Kinetic Constant (min^{-1})	Regression Coefficient (R^2)
A1	8.69 ± 0.03	1.59×10^{-3}	0.84
A2	12.22 ± 1.06	1.87×10^{-3}	0.97
A3	3.92 ± 0.98	5.80×10^{-4}	0.90
B1	6.40 ± 0.29	8.89×10^{-4}	0.80
B2	16.59 ± 0.97	2.81×10^{-3}	0.91
C1	17.44 ± 0.44	2.04×10^{-3}	0.99
C2	24.74 ± 0.27	3.62×10^{-3}	0.99
C3	32.56 ± 0.78	8.01×10^{-3}	0.63
D1	13.19 ± 1.42	1.13×10^{-3}	0.97
D2	12.15 ± 0.55	1.87×10^{-3}	0.96
D3	29.86 ± 0.38	7.72×10^{-3}	0.65

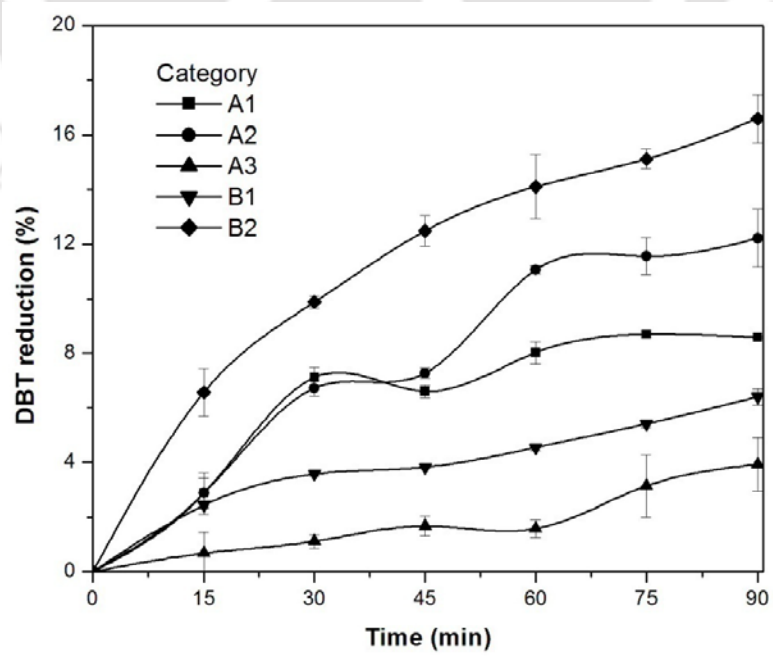

Figure 2.9: Time history of DBT reduction experimental categories A and B (please refer to Table 1 for details).

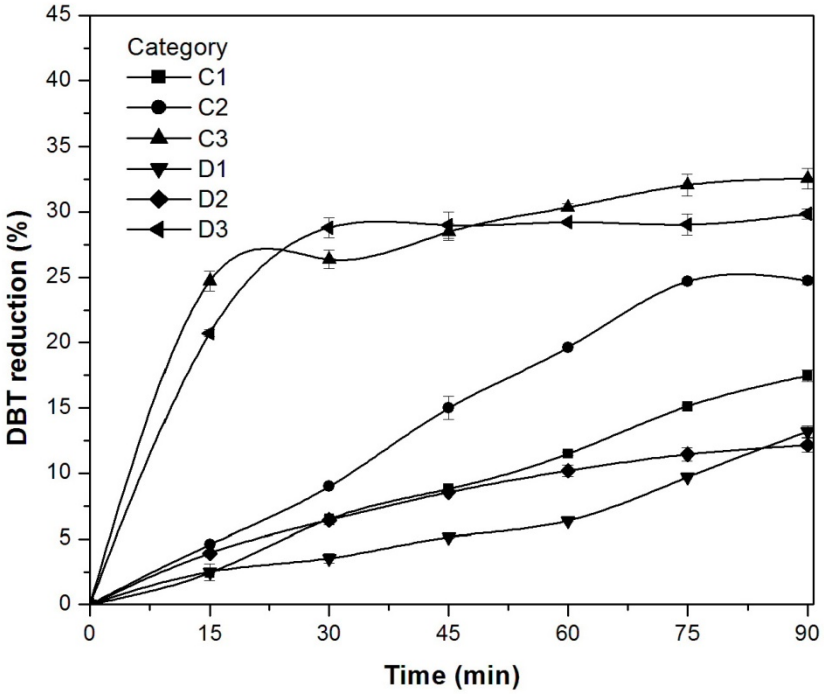

Figure 2.10: Time history of DBT reduction experimental categories C and D

4. Addition of excess H_2O_2 in category D experiments lowers the DBT reduction, in contradiction of our conjecture of synergism between OH radical productions, acetic acid regeneration and peracetic acid dissociation that eventually results in augmentation of HO_2 radical production. Comparing between categories D1 & C1 and D2 & C2, we observed significant reduction of DBT oxidation in presence of excess H_2O_2 (for both mechanically stirred as well as sonicated reaction systems). At high static pressure, however, reduction is less marked as seen from comparison of results in categories C3 & D3.

2.6.3 Simulation Results

Representative simulations of 5 micron air bubble at atmospheric static pressure in toluene and peracetic acid are shown in Figs. 2.11 and 2.12, respectively. It should be noted that due to high viscosity of peracetic acid, the cavitation bubble does not expand much during the rarefaction half period of ultrasound wave. The

expansion of the bubble at atmospheric static pressure, as predicted by the bubble dynamics model, is only 3.6 times the original volume. As a result, the minimum gas pressure attained in the bubble at the point of maximum radius is 2713 Pa, which is higher than the vapor pressure of peracetic acid (1933 Pa) at the bulk temperature (298 K) of the medium. Thus, as per Flynn's hypothesis stated in simulations section, the bubble in the present situation always remains a closed system during the radial motion. The mole fractions of nitrogen, oxygen and peracetic acid inside the bubble can be easily calculated as x_{N2} = 0.788, x_{O2} = 0.197 and x_{PAA} = 0.015. Representative simulations of 5 micron air bubble at elevated static pressure in toluene and peracetic acid are shown in Figs. 2.13 and 2.14, respectively. At elevated static pressure, the expansion of cavitation bubble is even lesser, just 2 times the initial radius, and thus, in this case as well the initial mole fractions of nitrogen, oxygen and peracetic acid in the bubble do not change during radial motion. The summary of the simulations results is given in Table 2.5. Some peculiar features of the cavitation bubble dynamics in both toluene and peracetic acid can be identified as follows: (1) At atmospheric static pressure, the temperature and pressure peaks reached in the cavitation bubble for both toluene and peracetic acid are very high, resulting in generation wide spectrum of species. (2) For peracetic acid, most of the species generated from dissociation of N_2, O_2 and peracetic acid vapor are of molecular nature (for example N_2, O_2, CO_2 H_2O, NO, NO_2). Formation of radical species like $^{\bullet}O$ and $^{\bullet}OH$ is seen, but in relatively small quantities (with mole fraction ~ 10^{-4} or lesser). (3) For toluene, the evaporation of vapor molecules in the bubble is very small (with mole fractions ~ 10^{-6} or 10^{-7}) due to low vapor pressure of toluene. However, the temperature peak reached at collapse is high (4835 K). As such, most of the species generated at transient collapse are from dissociation of N_2 and O_2. Among these, the predominant oxidative

radical species is O• and some traces of •OH (with mole fraction ~ 10^{-6}) are also seen. (4) Radial bubble motion in both toluene and peracetic acid generates strong convection due to microturbulence as well as acoustic waves. (5) With application of high static pressure, the intensity of the bubble motion reduces sharply. The temperature and pressure peak reached in bubble at transient collapse fall, and no formation of any radical species is seen. For peracetic acid, formation of CO_2 and H_2O are seen, while for toluene some traces of nitrogen oxides (NO, NO_2) are observed. (6) Magnitude of turbulence velocity and acoustic waves generated from bubble also reduce drastically with elevated static pressure.

(7) It should be noted that the total convection in the system has contribution of micro-steaming generated by ultrasound as well. The magnitude of micro-streaming velocity is 0.137 m/s and 0.078 m/s for toluene and peracetic acid, respectively. This component of convection does not change with rise static pressure. Moreover, comparing these magnitudes with the velocity of micro-turbulence generated by cavitation bubbles at two levels of static pressure, we can deduce that at elevated static pressure, the convection in the reaction mixture is mostly contributed by micro-streaming, with negligible contribution from cavitation bubbles.

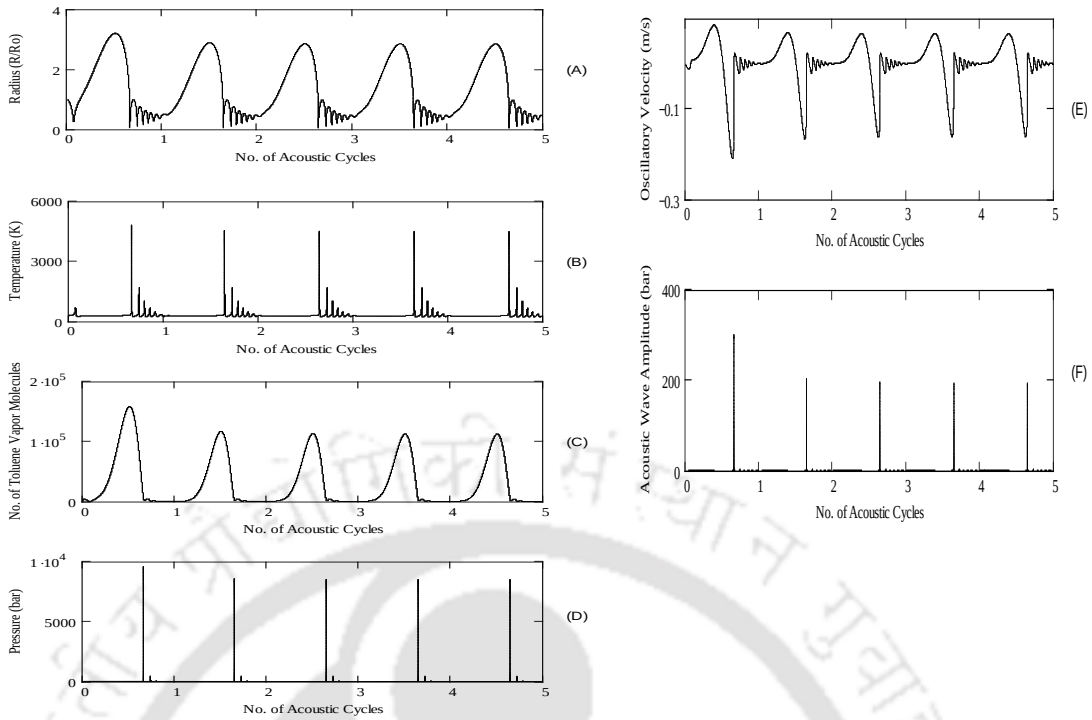

Figure 2.11. Simulations of radial motion of a 5 micron air bubble in toluene at atmospheric static pressure. Time history of (A) radius of the bubble; (B) temperature inside the bubble; (C) toluene vapor evaporation in the bubble; (D) pressure inside the bubble; (E) microturbulence generated by the bubble; (F) acoustic waves emitted by the bubble

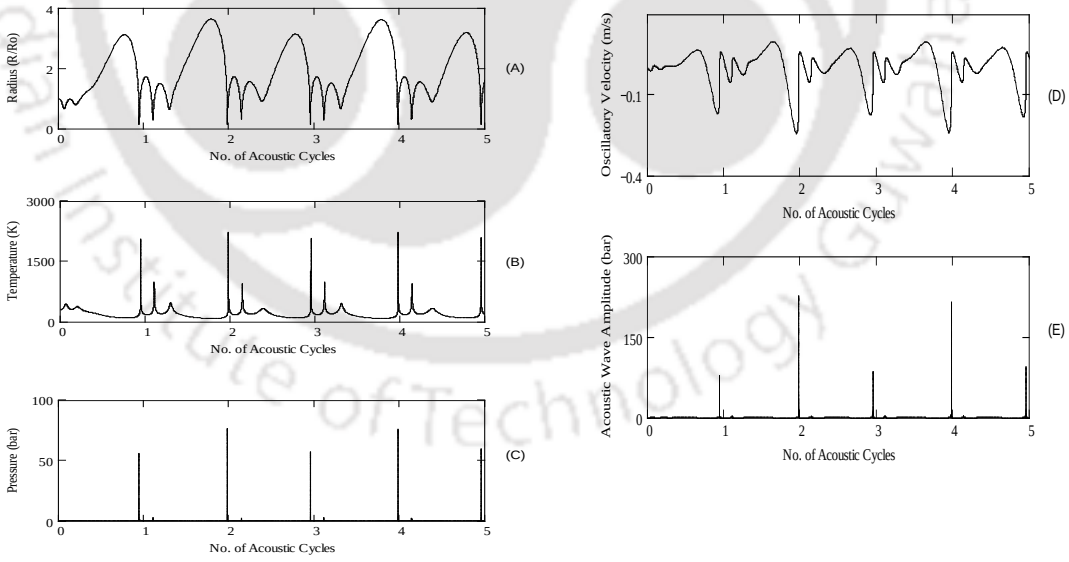

Figure 2.12: Simulations of radial motion of a 5 micron air bubble in peracetic acid at atmospheric static pressure. Time history of (A) radius of the bubble; (B) temperature inside the bubble; (C) pressure inside the bubble; (D) microturbulence generated by the bubble; (E) acoustic waves emitted by the bubble.

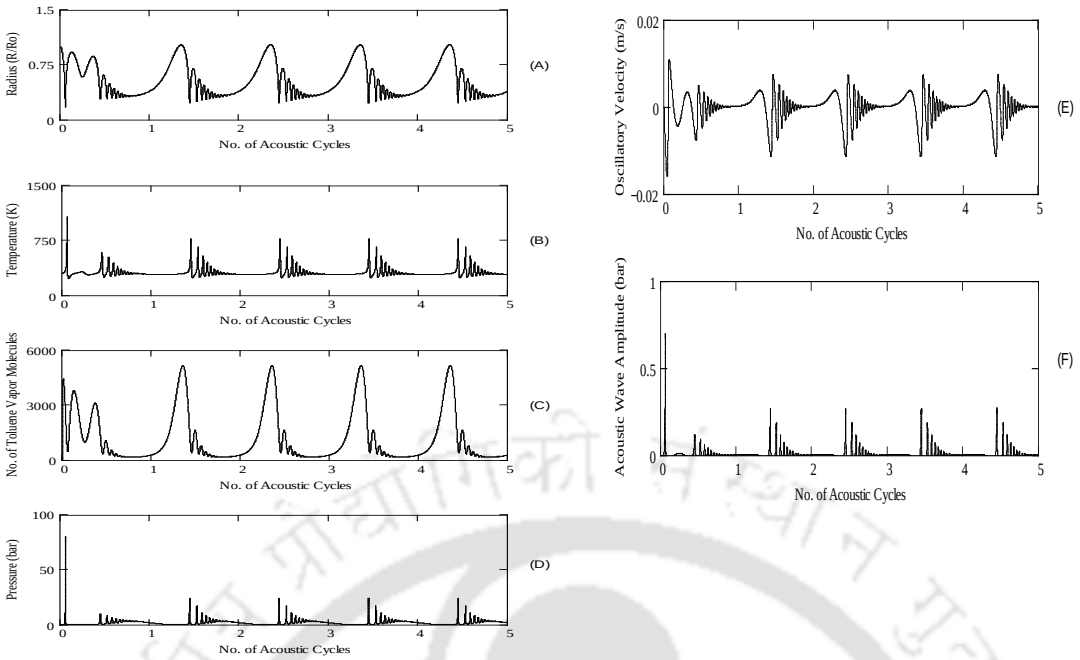

Figure 2.13: Simulations of radial motion of a 5 micron air bubble in toluene at elevated static pressure (162 kPa). Time history of (A) radius of the bubble; (B) temperature inside the bubble; (C) toluene vapor evaporation in the bubble; (D) pressure inside the bubble; (E) microturbulence generated by the bubble; (F) acoustic waves emitted by the bubble.

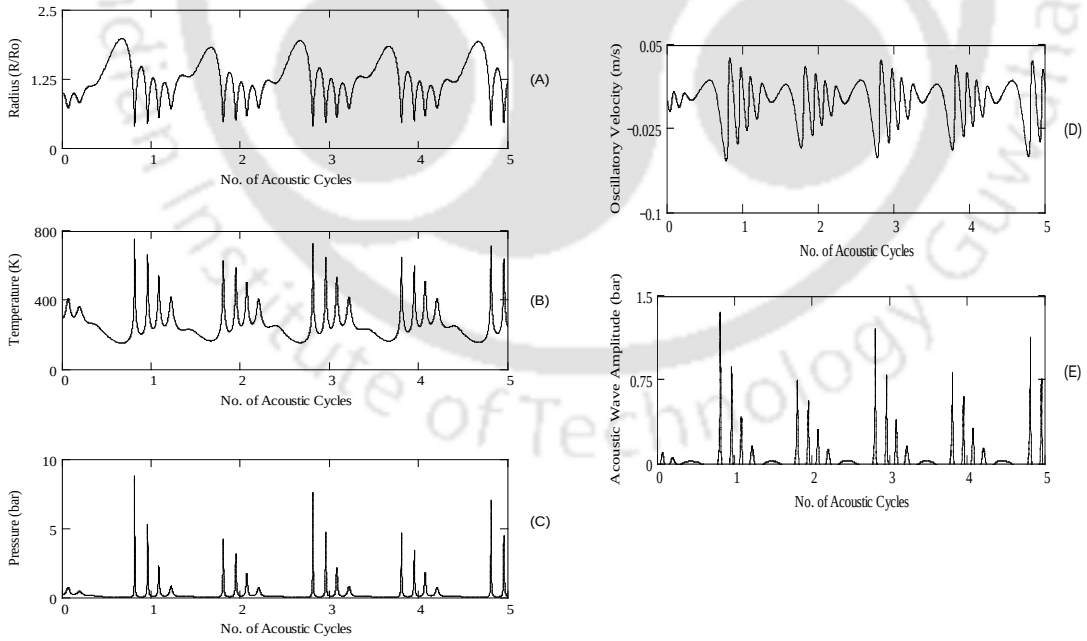

Figure 2.14: Simulations of radial motion of a 5 micron air bubble in peracetic acid at elevated static pressure of 162 kPa. Time history of (A) radius of the bubble; (B) temperature inside the bubble; (C) pressure inside the bubble; (D) microturbulence generated by the bubble; (E) acoustic waves emitted by the bubble.

Table 2.5: Summary of the simulation results

Species	Parameters for simulations			
	Peroxyacetic Acid		Toluene	
	Air bubble R_o = 5 μm P_o = 101.3 kPa	Air bubble R_o = 5 μm P_o = 162 kPa	Air bubble R_o = 5 μm P_o = 101.3 kPa	Air bubble R_o = 5 μm P_o = 162 kPa
	Conditions at the first collapse of the bubble			
	T_{max} = 2050 K P_{max} = 7.7 MPa V_{turb} = 0.17 m/s P_{AW} = 7.8 MPa	T_{max} = 754.3 K P_{max} = 0.88 MPa V_{turb} = 0.046 m/s P_{AW} = 0.13 MPa	T_{max} = 4835 K P_{max} = 961 MPa V_{turb} = 0.147 m/s P_{AW} = 30.2 MPa	T_{max} = 1076 K P_{max} = 80.25 bar V_{turb} = 0.014 m/s P_{AW} = 0.696 bar
	x_{N2} = 0.788 x_{O2} = 0.197 x_{PAA} = 0.015	x_{N2} = 0.788 x_{O2} = 0.197 x_{PAA} = 0.015	x_{N2} = 0.79 x_{O2} = 0.21 x_{TOL} = 2.77E–6	x_{N2} = 0.79 x_{O2} = 0.21 x_{TOL} = 4.91E–7
	Equilibrium composition of radical and other oxidizing species in the bubble at collapse			
N_2	7.66E–1	7.71E–1	7.11E–1	7.90E–1
O_2	1.66E–1	1.71E–1	1.25E–1	2.10E–1
O	7.67E–6	–	2.05E–2	–
O_3	–	–	3.80E–5	–
N	–	–	1.91E–4	–
N_3	–	–	3.82E–6	–
NO	8.14E–3	–	1.41E–1	7.60E–5
NO_2	5.51E–4	3.53E–6	2.27E–3	2.18E–5
NO_3	–	–	1.64E–6	–
N_2O_3	–	–	1.14E–6	–
N_2O	2.08E–5	–	7.41E–4	–
CO	2.72E–6	–	1.23E–6	–
CO_2	2.93E–2	2.93E–2	2.18E–6	–
OH	1.88E–4	–	3.37E–6	–
H_2O	2.92E–2	2.93E–2	–	–
HO_2	2.09E–5	–	–	–
H_2O_2	1.35E–6	–	–	–
HNO_2	3.16E–5	–	–	–

Notation for Table 2.5: P_o – static pressure in the liquid medium; R_o – initial radius of the cavitation bubble; V_{turb} – average velocity of the micro–turbulence in the medium generated by ultrasound and cavitation in the medium (estimated at 1 mm distance from bubble center); P_{AW} – pressure amplitude of the acoustic wave generated by the cavitation bubble; T_{max} – temperature peak reached in the bubble at the time of first collapse; P_{max} – pressure peak reached in the bubble at the time of first collapse; x_{PAA} – mole fraction of peroxyacetic acid in the bubble; x_{N2} – mole fraction of N_2 in the bubble; x_{O2} – mole fraction of oxygen in the bubble; x_{TOL} – mole fraction of toluene in the bubble

2.7 ANALYSIS

Concurrent analysis of experimental and simulation results help us to identify the physical and mechanistic features of oxidative desulfurization with sono-Fenton-peracetic acid system. It should be noted that there are three sources of radicals in the present system, viz. (1) $^{\bullet}OH$ radicals generated from Fenton process, (2) $HO^{\bullet}_2$ radicals generated from peracetic acid and, (3) $O^{\bullet}$, $^{\bullet}OH$, $HO^{\bullet}_2$ radicals generated from cavitation bubble. Interaction of these radicals among themselves as well as H_2O_2 in the medium plays a crucial role in overall chemistry of the process. We have already stated reactions R.1 and R.2, in addition to these following reactions occur:

$$O^{\bullet} + H_2O_2 \longrightarrow {}^{\bullet}OH + HO^{\bullet}_2 \qquad \text{(R.3)}$$

$$^{\bullet}OH + HO^{\bullet}_2 \longrightarrow O_2 + H_2O \qquad \text{(R.4)}$$

$$O^{\bullet} + HO^{\bullet}_2 \longrightarrow {}^{\bullet}OH + O_2 \qquad \text{(R.5)}$$

We present following analysis for the trends in experimental results: (1) Small DBT oxidation with ultrasound alone is attributed to generation of $HO^{\bullet}_2$ radicals in insignificant quantities in toluene. Addition of acetic acid to toluene can increase generation of radical species, as acetic acid has a higher vapor pressure than toluene, and can evaporate into the bubble. Reduction in DBT oxidation with H_2O_2 is attributed to scavenging of radicals generated in toluene by H_2O_2. A side reaction of toluene itself getting oxidized by H_2O_2 to benzoic acid may also occur. (2) Marked enhancement in DBT oxidation with sonication is a consequence of formation of the fine emulsion between aqueous and organic phase. (3) Addition of Fe^{2+} shows more marked enhancement for mechanically stirred system than sonication system. This essentially means that the mass transfer characteristics of the system have more influence on DBT oxidation than the oxidation chemistry. $^{\bullet}OH$ radical production by Fe^{2+} assists regeneration of acetic acid that further enhances $HO^{\bullet}_2$ production in

aqueous phase. However, the above result clearly point out that effective transfer of $HO^{\bullet}_2$ radicals from aqueous to organic phase is more significant than mere generation of these radicals for effective DBT oxidation. (4) Addition of excess H_2O_2 in category D experiments was expected to increase production of $^{\bullet}OH$ radicals, which could combine with $CH_3CO^{\bullet}$ for regeneration of acetic acid. This process was expected to enhance $HO^{\bullet}_2$ production from dissociation of peracetic acid. However, contrary to this conjecture, a sharp production in DBT oxidation is seen. We attribute this effect to scavenging of $HO^{\bullet}_2$ radicals by $^{\bullet}OH$ radicals as well as H_2O_2 through reactions R.1 and R.4. (5) Application of high static pressure to the system eliminates transient cavitation and the physical/chemical effects associated with it. Despite this, significant rise in extent of DBT oxidation is seen in C3 and D3 category experiments with elevated static pressure. We explain this anomaly in terms of reduction in the scavenging of radicals, without much affecting the mass transfer characteristics of the system. It should be noted that ultrasound wave phenomenon is not affected by rise in static pressure (by a very moderate extent to only 162 kPa, as in present study). Thus, the micro-streaming generated by ultrasound remains unaltered even at high static pressure. Elimination of transient cavitation also eliminates the major source of $^{\bullet}OH$ and $O^{\bullet}$ radicals that scavenge the $HO^{\bullet}_2$ radicals. As a result, there is more effective transfer of $HO^{\bullet}_2$ radicals from aqueous to organic phase, and also utilization of DBT oxidation to sulfone. Moderate reduction of DBT oxidation from C3 to D3 category experiments is attributed to higher concentration of H_2O_2 in D3 leading to relatively higher scavenging of $HO^{\bullet}_2$ radicals.

2.8 CONCLUSION

In this chapter, we have attempted to establish links between oxidation chemistry and cavitation physics for the ultrasound-assisted oxidative desulfurization process using peracetic acid – Fenton oxidant system. The results of this study have not only demonstrated relative role of each component of the oxidant system in the process, but have also highlighted the mechanistic or physical features of the process. H_2O_2 is revealed to be the crucial component of the oxidant system that balances between different competing reaction pathways of the process. Addition of Fe^{2+} to peracetic acid helps in augmentation of oxidative desulfurization due to regeneration of acetic acid, while addition of excess gives an adverse effect due to scavenging of $HO_2^{\bullet}$ radicals by itself and also through generation $^{\bullet}OH$ radicals. These results clearly point out that smaller scavenging and effective interfacial transfer of the $HO_2^{\bullet}$ radical is crucial to oxidation of sulfur compounds than mere generation of these radicals. Most interesting result of this study is that cavitation is found to play a negative role in the process. Radicals generated from transient cavitation scavenge the $HO_2^{\bullet}$ radicals that hamper their utilization for oxidation. Elimination of cavitation with application of elevated static pressure results in significant augmentation of oxidative desulfurization due to elimination of cavitation. Micro-streaming produced by ultrasound has a beneficial effect in that it generates fine emulsion between oxidant and toluene and increases the interfacial area that assists effective transfer of HO_2 radicals. We believe that the results of this paper would give important inputs for further research in the area of oxidative desulfurization.

REFERENCES

Barber BP, Hiller RA, Lofstedt R, Putterman SJ, Weninger KR. Defining the Unknowns of Sonoluminescence. *Phys. Rep.* 1997; 281: 65-143.

Castillo K, Parsons JG, Chavez D, Chianelli RR. Oxidation of Dibenzothiophene to Dibenzothiophene-sulfone using Silica Gel. *J. Catal.* 2009; 268: 329-334.

Condon EU, Odishaw H. *Handbook of Physics*; McGraw− Hill: New York, 1958.

Dai Y, Qi Y, Zhao D, Zhang H. An Oxidative Desulphurization Method Using Ultrasound/ Fenton's Reagent for Obtaining Low and/or Ultra–low Sulfur Diesel Fuel. *Fuel Process. Technol.* 2008; *89*: 927-932.

Eriksson G. Thermodynamic Studies of High Temperature Equilibria XII: SOLGAMIX, A Computer Program for Calculation of Equilibrium Composition in Multiphase Systems. *Chem. Scr*. 1975; 8: 100-103.

Flynn HG. Cavitation dynamics I. A Mathematical Formulation. *J. Acoust. Soc. Am.* 1975; 57: 1379-1396.

Grossmann S, Hilgenfeldt S, Zomack M, Lohse D. Sound Radiation of 3 MHz Driven Gas Bubbles. *J. Acoust. Soc. Am.* 1997; 102: 1223-1230.

Hilgenfeldt S, Lohse D, Brenner MP. Phase Diagrams for Sonoluminescing Bubbles. *Phys. Fluids* 1996; 8: 2808-2826.

Hirschfelder JO, Curtiss CF, Bird RB. Molecular Theory of Gases and Liquids; Wiley: New York, 1954.

Keller JB, Miksis MJ. Bubble Oscillations of Large Amplitude. *J. Acoust. Soc. Am.* 1980; 68: 628-633.

Krishnan SJ, Dwivedi P, Moholkar VS. Numerical Investigation into the Chemistry Induced by Hydrodynamic Cavitation. *Ind. Eng. Chem. Res*. 2006; 45: 1493-1504.

Lofstedt R, Weninger K, Puttermann SJ, Barber BP. Sonoluminescing Bubbles and Mass Diffusion. *Phys. Rev. E*. 1995; 51: 4400-4410.

Moholkar VS, Sable SP, Pandit AB. Mapping the Cavitation Intensity in an Ultrasonic Bath Using the Acoustic Emission. *AIChE J*. 2000; 46: 684-694.

Moholkar VS, Warmoeskerken MMCG. Integrated Approach to Optimization of an Ultrasonic Processor. *AIChE J*. 2003; 49: 2918-2932.

Olson ES, Stanley DC, Gallagher JR. Characterization of Intermediates in the Microbial Desulfurization of Dibenzothiophene. *Energ. Fuel* 1993; 7: 159-164.

Plesset M. The Dynamics of Cavitation Bubbles. *J. Appl. Mech. (Trans. ASME)* 1949; 16: 277-282.

Prasad Naidu DV, Rajan R, Kumar R, Gandhi KS, Arakeri VH, Chandrasekaran S. Modeling of a Batch Sonochemical Reactor. *Chem. Eng. Sci.* 1994; 49: 877-888.

Press WH, Teukolsky SA, Flannery BP, Vetterling WT. Numerical Recipes; Cambridge University Press*:* New York, 1992.

Prosperetti A, Lezzi A. Bubble Dynamics in a Compressible Liquid. Part 1. First Order Theory. *J. Fluid Mech.* 1986; 168: 457-478.

Reid RC, Prausnitz JM, Poling BE. Properties of Gases and Liquids. McGraw−Hill: New York, 1987.

Shah YT, Pandit AB, Moholkar VS. Cavitation Reaction Engineering. Plenum Press / Kluwer Academic: New York, 1999.

Sivasankar T, Paunikar AW, Moholkar VS. Mechanistic Approach to Enhancement of the Yield of a Sonochemical Reaction. *AIChE J*. 2007; 53: 1132-1143.

Storey BD, Szeri AJ. Water Vapor, Sonoluminescence and Sonochemistry. *Proc. R. Soc. London, Ser. A* 2000; 456: 1685-1692.

Toegel R, Gompf B, Pecha R, Lohse D. Does Water Vapor Prevent Upscaling Sonoluminescence? *Phys. Rev. Lett*. 2000; 85: 3165-3168.

Vardanyan IA, Sachyan GA, Philiposyan AG, Nalbandyan AB. Kinetics and Mechanism of Formaldehyde Oxidation-II. *Combust Flame.* 1974; 22: 153-

159.

Zhou J, Lu X, Wang Y, Shi J. Molecular Dynamics Investigation on the Finite Dilute Diffusion Coefficients of Organic Compounds in Supercritical Carbon Dioxide. *Fluid Phase Equilib*. 2000; 172: 279-291.

Zhu Y, Lu X, Zhou J, Wang Y, Shi J. Prediction of Diffusion Coefficients for Gas, Liquid and Supercritical Fluid: Application to Pure Real Fluids and Infinite Dilute Binary Solutions Based on the Simulations of Lennards-Jones Fluid. *Fluid Phase Equilib*. 2000; 194−197: 1141-1159.

CHAPTER 3

OXIDATIVE DESULFURIZATION PROCESS ASSISTED SIMULTANEOUSLY BY PHASE TRANSFER AGENT AND ULTRASOUND

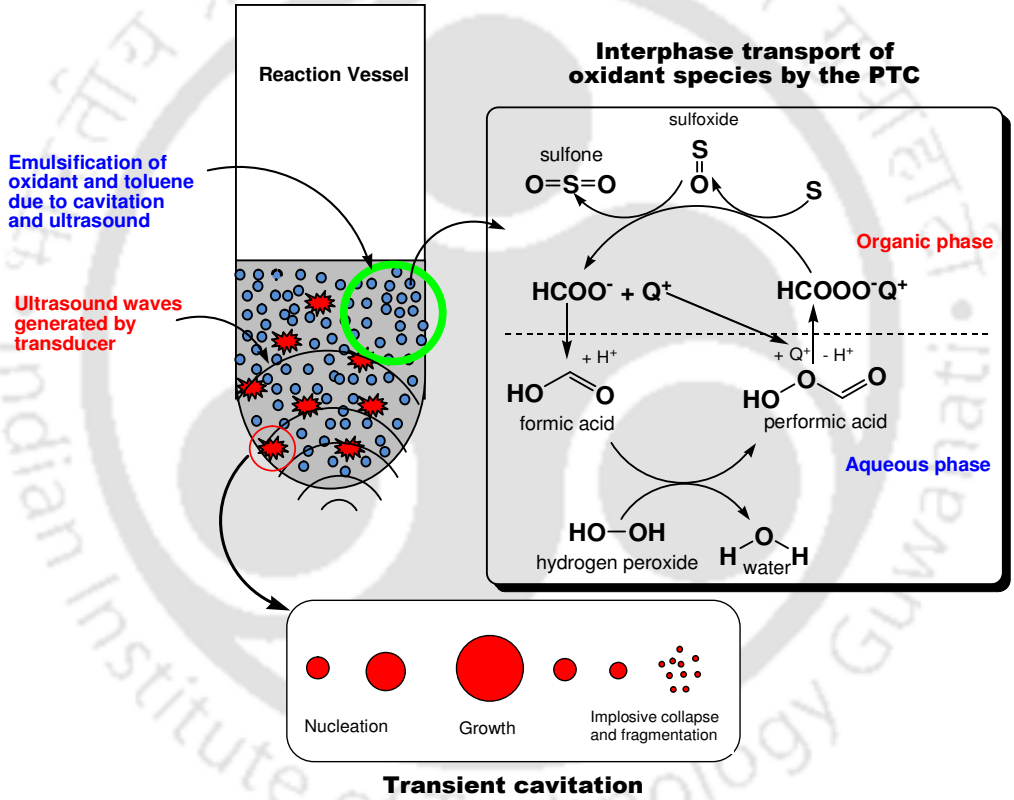

Oxidative Desulfurization Process Assisted Simultaneously by Phase Transfer Agent and Ultrasound

3.1 INTRODUCTION

The oxidative desulfurization reaction system is essentially a liquid–liquid heterogeneous system, i.e. the oxidant is in aqueous phase, while the substrate or sulfur compounds on which it acts is in organic phase. These systems are well known to be limited by mass transfer, as the rate of reaction is determined by the interfacial area between the two phases, and the rate of transfer of reactants across this interface. The emulsification of the reaction mixture, which governs the interfacial area generated between phases, therefore plays a crucial role in determination of overall kinetics of oxidative desulfurization. The emulsification itself, in turn, is a function of the convection present in the system.

This chapter attempts to discern the physical mechanism of the oxidative desulfurization process simultaneously assisted by ultrasound and phase transfer agent

(PTA). With different experimental protocols, an attempt is made to deduce individual beneficial effects of PTA and ultrasound on the oxidative desulfurization system, and also the synergy between the effects of PTA and ultrasound.

3.2 MATERIALS AND METHODS

3.2.1 Chemicals

Following chemicals have been used in the experiments: dibenzothiophene (DBT, 98%, Sigma Aldrich) as model sulfur compound; toluene (synthesis grade, Merck) as the model liquid fuel; 30% v/v H_2O_2 (AR Grade, Merck), acetic acid (99–100%, AR Grade, Merck), formic acid (86%, AR Grade, Loba Chemi), tetraoctylammonium bromide (TOAB, Sigma Aldrich) used as a phase transfer agent (PTA), acetonitrile (HPLC grade, Merck) was used as a mobile phase for HPLC analysis. All chemicals were used as received without any pre–treatment.

3.2.2 Experimental Setup

The schematic diagram of experimental setup and procedure was similar as discussed in chapter 2. The experiments were carried out at two different static pressures: (a) atmospheric pressure (101.3 kPa), and (b) elevated pressure of 162 kPa. For raising the static pressure in the reaction test tube, the mouth of the test tube was air sealed using rubber cork with a metal tube pierced at the center. The outer end of the tube was connected to a nitrogen cylinder with double-stage pressure regulator. The pressure inside the test tube was raised carefully to 162 kPa using the regulator.

3.2.3 Experimental Protocols

In present study, Toluene (20 mL) with an initial DBT concentration of 100 ppm has been used in all experiments. The main oxidant used in the reaction is H_2O_2 promoted by either acetic acid (CH_3COOH) or formic acid (HCOOH), which combine

to form peracetic acid or performic acid. The total volume of oxidant solution was either 6 or 8 mL shown in Table 3.1. The volume ratio of oil to oxidant was decided on the basis of results of previous chapter 2. The amount of PTA added to reaction solution was varied in the range of 0.01–0.1 g. With this, the molar ratio of PTA to DBT varied in the range of 1.67–16.67. The experiments employed two oxidants, viz. performic acid and peracetic acid along with phase transfer agent TOAB. Either mechanical stirring at 600 rpm or ultrasound irradiation was applied for mixing of the reaction solution. In some experiments, the static pressure on the reaction solution was raised to 1.8 bar using nitrogen atmosphere. The rationale underlying this technique will be explained subsequently. With permutation–combination of the oxidant system and static pressure, 3 groups of experimental protocols were devised as A, B, C, which have been listed in Table 3.1. The initial temperature of reaction solution was 298 K. The temperature variation of reaction solution during sonication was controlled (within ±2 K) by changing the water in the ultrasound bath every 15 min. The total reaction time was 90 min. During the reaction, the test tube was placed at the center of the bath to avoid the significant spatial variations (Gogate et al., 2002). The actual acoustic energy dissipation and the amplitude of the ultrasound wave generated in the bath was determined using calorimetric method as 1.5 bar (Chakma and Moholkar, 2014). During the reaction, small aliquots of reaction mixture were withdrawn every 15 min and were analysed for the residual DBT concentration. All experiments were done in triplicate to assess reproducibility of results. Since this study is aimed at investigation of the physical mechanism of desulfurization process, we have not followed the conventional post–reaction protocol of extraction of sulfones from the reaction solution and analysis of the raffinate and extract (Wan et al., 2007; Mei et al., 2003), and our analysis is based on average DBT

reduction in different experimental protocols.

3.2.4 Analysis

The residual concentration of DBT in the aliquots of reaction mixture was analyzed using Shimadzu Ultra High Performance Liquid Chromatography (UHPLC, Model: SPD–20A) equipped with a reverse phase C–18 column (5 µm, 4.6 mm × 250 mm) and UV detector at 287 nm. The mobile phase was a mixture of acetonitrile and water (80:20 v/v) with a flow rate of 1.8 mL/min. The formation of sulfone in oxidative desulfurization was confirmed using FTIR analysis of aliquots of reaction mixture in category B.2 (as a representative of all experimental protocols listed in Table 3.1 after completion of sonication. To identify the intermediates during DBT oxidation, GC–MS analysis of the same reaction sample was performed using Varian 240–GC equipped with VF–5ms column (30 m × 0.25 m ID DF = 0.25). 1 µL of sample was injected with a split ratio of 100:1. The temperature program was as follows: injection temperature – 250^{o}C, column temperature – 100^{o}C for zero min and increased to 300^{o}C at a ramping rate of 7^{o}C/min. The scanned mass range was from 50 – 1000 m/z and helium gas was used as a carrier gas.

3.3 RESULTS AND DISCUSSION

Before presentation of the experimental results and their analysis, we give herewith a brief discussion about the individual mechanisms of effect of ultrasound and PTA on oxidative desulfurization reaction system. The mechanism of action of PTA is explained in Fig. 3.2 (Wan et al., 2007; Mei et al., 2003). Either formic acid or acetic acid reacts with H_2O_2 to form peracids, which then dissociate to form an anion species (either $HCOOO^-$ or CH_3COOO^-) and a proton. PTA forms a complex with the anion oxidant species and transports it to the organic phase, where it can induce the

oxidation reaction of sulfur compound to sulfone.

Table 3.1: Summary of DBT reduction in different experimental categories

Experimental Category	**% DBT oxidation**	***k* (min^{-1})**	***R*^{2}**
A.1 STR + AA (4 mL) + H_2O_2 + TOAB	18.89 ± 0.33	2.82×10^{-3}	0.70
A.2 US + AA (4 mL) + H_2O_2 (2 mL) + TOAB	28.25 ± 0.26	4.03×10^{-3}	0.98
A.3 STR + AA (4 mL) + H_2O_2 (4 mL) + TOAB	12.41 ± 0.14	1.82×10^{-3}	0.86
A.4 US + AA (4 mL) + H_2O_2 (4 mL) + TOAB	24.26 ± 0.17	3.89×10^{-3}	0.87
B.1 STR + FA (4 mL) + H_2O_2 (2 mL) + TOAB	26.94 ± 0.55	3.86×10^{-3}	0.93
B.2 US + FA (4 mL) + H_2O_2 (2 mL) + TOAB	42.00 ± 0.96	7.50×10^{-3}	0.93
B.3 STR + FA (4 mL) + H_2O_2(4 mL) + TOAB	20.30 ± 0.67	3.23×10^{-3}	0.82
B.4 US + FA (4 mL) + H_2O_2 (4 mL) + TOAB	28.48 ± 0.63	4.79×10^{-3}	0.86
C.1 US + AA (4 mL) + H_2O_2 (2 mL) + TOAB + ESP (1.8 bar)	32.31 ± 0.47	1.39×10^{-2}	0.82
C.2 US + FA (4 mL) + H_2O_2 (2 mL) + TOAB + ESP (1.8 bar)	47.05 ± 0.59	2.11×10^{-2}	0.89

Notations: US – ultrasound, STR – stirring, TOAB – tetraoctyl ammonium bromide, AA –acetic acid, FA – formic acid, ESP – elevated static pressure (1.8 bar), η – DBT reduction in (%), k – pseudo 1st order kinetic constant in (s^{-1}), R^2 – regression coefficient, Reaction solution: All experiments were conducted using [TOAB] = 0.05 g (0.091 mmol)

This transport is, of course, dependent on the interfacial area between the organic and aqueous phase, which in turn depends on the convection present the system. After oxidation reaction both species, i.e. the anion of acid ($HCOO^-$ or CH_3COO^-) and the cation of PTA (Q^+) return to aqueous phase, and the cycle continues. PTA thus assists

faster transport of oxidant species across interface and helps overcome the mass transfer limitations of the process that result in enhancement of kinetics of oxidation.

The selectivity of sulfur hydrocarbon compounds towards oxidation in comparison of other hydrocarbons in the reaction mixture is an important issue. Chen et al. (2010) have stated that organic sulfur compounds have higher oxidative reactivity than their analogue pure hydrocarbons in fossil fuels. In another publication, Chen et al.(2012) have assessed the relative reactivities of different sulfur compounds, *viz*. thiophene, benzothiophene and dibenzothiophene towards oxidation to corresponding sulfones. Essentially, the electron density on the sulfur atom of these compounds and their oxidative rate constants were examined. This chapter revealed that oxidative reactivity of sulfur compounds increased with electron density on sulfur atoms. The least oxidative reactivity of thiophene among the compounds mentioned above is attributed to low electron density of sulfur atom and low boiling point. On the other hand, the highest oxidative reactivity was observed for dibenzothiophene, which is also the model sulfur hydrocarbon species in the present study.

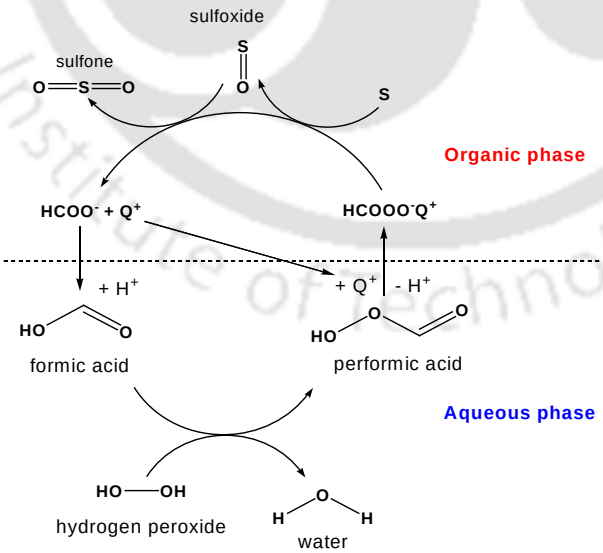

Figure 3.1: The cyclic mechanism of phase transfer agent (PTA) during oxidative desulfurization with perorganic acid (e.g. performic acid).

Ultrasound and cavitation induce the physical effects of intense micro–mixing

and emulsification that enhance the mass transfer in the system through different mechanisms, viz. micro–streaming, micro–convection, shock (or acoustic) waves and micro jet. Greater description of these mechanisms is given elsewhere (Kuppa and Moholkar, 2010; Shah et al., 1999). Moreover, the organic solvent can get evaporated into the cavitation bubbles during the expansion phase of the bubble. Some of this vapor gets entrapped into the bubble at the instance of transient collapse. The temperature and pressure inside the bubble reach extreme at which the solvent vapor undergoes thermal cleavage that results in formation of reducing species such as CO, H_2 and CH_4. These species can competitively consume the oxidant species that are transferred from aqueous to organic medium, and hamper their utilization for oxidation of sulfur species. Thus, the physical effect of ultrasound and cavitation is beneficial towards enhancement of oxidation kinetics, while the sonochemical effect has an adverse effect. In our earlier studies (Chakma and Moholkar, 2013; Morya et al., 2008; Sivasankar et al., 2008), we have reported simulations of cavitation bubble dynamics that give quantitative estimates of the physical and chemical effects of cavitation bubbles in different reaction systems.

3.3.1 FTIR and GC–MS Analysis of Reaction Mixture

Fig.3.2 compares the IR spectra of pure DBT sulfone and that of the aliquot of reaction mixture of experimental category B.2 (after 90 min of sonication). Fig. 3.2 shows two different characteristic peaks of sulfone compound at 1288 cm^{-1} and 1166 cm^{-1}, which confirms the oxidation of DBT during sonication. The FTIR spectrum of reaction mixture also shows peaks at 692 cm^{-1} and 732 cm^{-1}, which correspond the unreacted DBT in the reaction mixture.

The GC–MS results of the DBT after oxidation of 90 min is shown in Fig. 3.3. The peaks obtained at 20.11 min, 20.156 min and 25.322 min are shown in Fig.

3.3(a)–(c). The major ions obtained at different m/z (% intensity, proposed derivation from molecular ion, M) values are 200 (9, [M]+), 184 (100, [M–O]+), 171 (15, [M–CHO]+), 152 (5, [M–O–S]+), 139 (12, [M–COH–S]+), 216 (100, [M]+), 187 (40, [M–COH]+), 168 (23, [M–O–S]+), 160(30, [M–CO–CO]+),150 (10, [M–OH–OH–S]+).

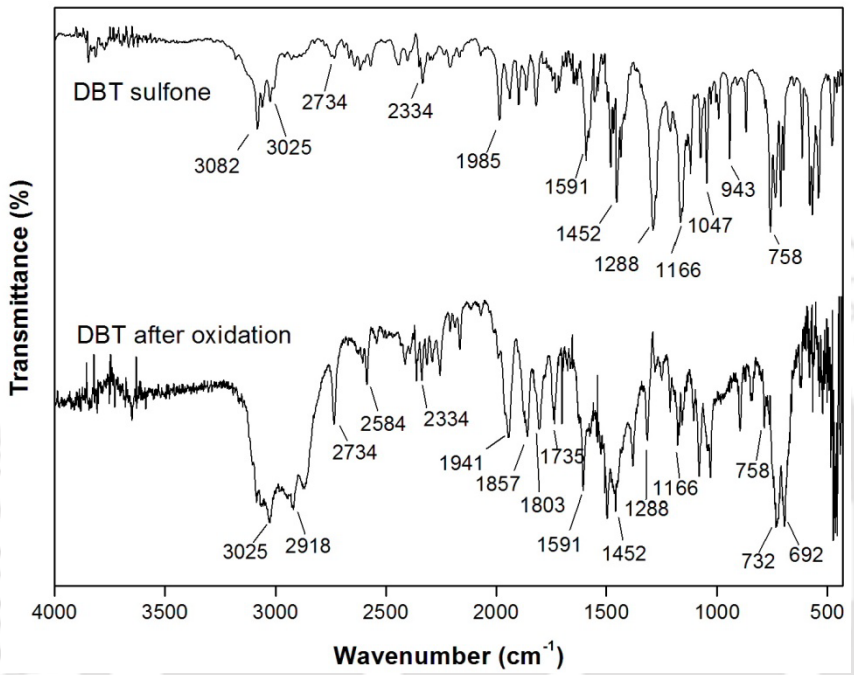

Figure 3.2: Comparison of the FTIR spectra of pure DBT sulfone and the aliquot of reaction mixture in experimental category B.2

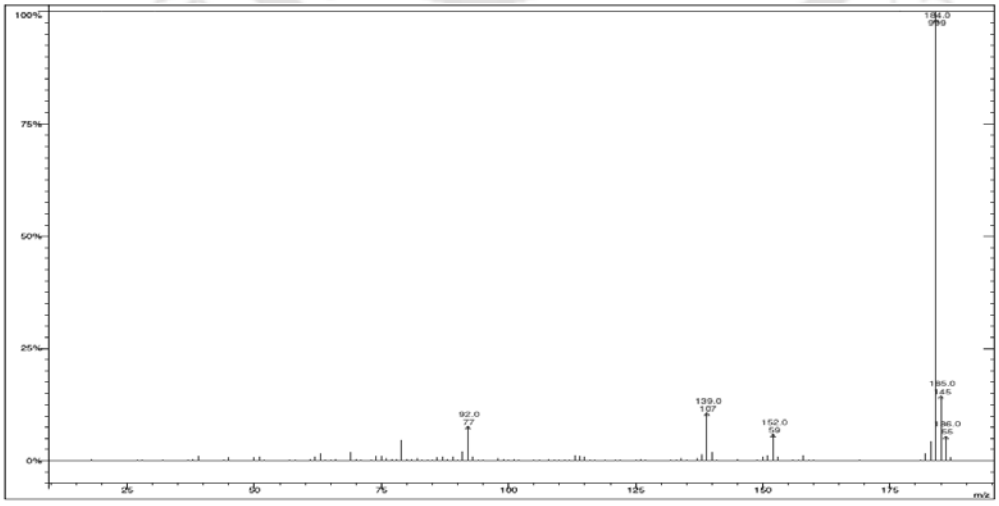

(a)

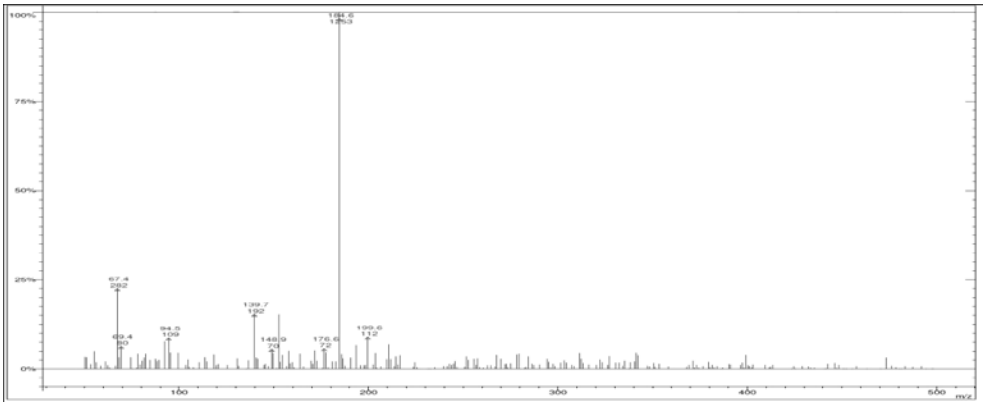

(b)

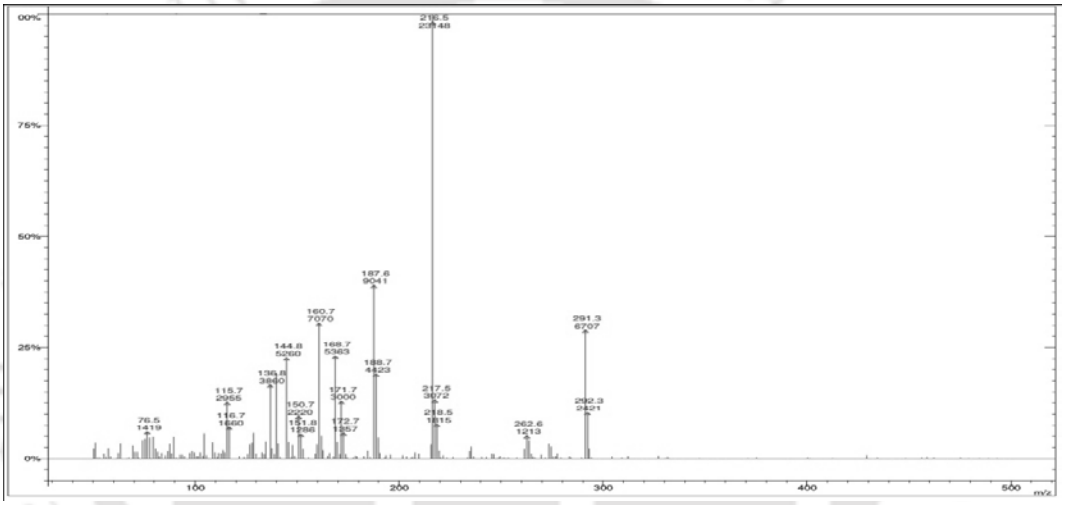

(c)

Figure 3.3: Gas chromatography mass spectra of DBT after 90 min oxidation. Peaks obtained at (a) 20.11 min, (b) 20.156 min, and (c) 25.322 min.

3.3.2 Experimental Results and Analysis

The results of the experiments are depicted in Figs. 3.4–3.7. Fig. 3.4 shows the results of optimization study for the dosage of PTA under mechanical stirring and sonication. Figs. 3.5–3.7 depict the time histories of reduction of DBT in experimental categories, viz. A, B, C. Table 3.1 gives the summary of the results on DBT reduction in all experiments, along with the first order kinetic constant fitted to experimental data. We justify fitting of 1st order kinetic model to the time data of DBT oxidation on

the basis of simple mathematical model proposed by Zhao et al. (2007). The typical trends in experimental results in categories A, B and C can be identified as follows:

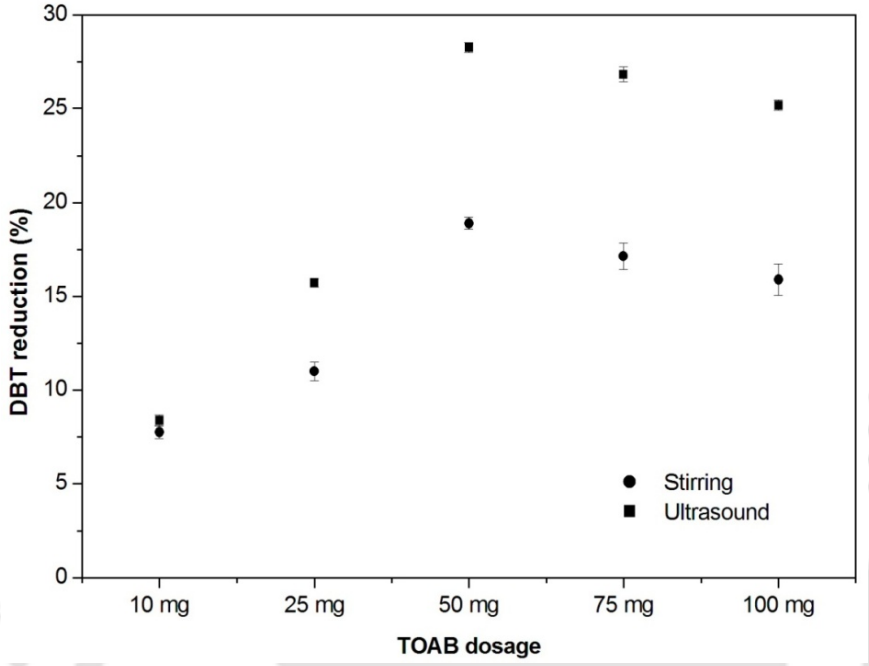

Figure 3.4: DBT reduction in presence of peracetic acid ($CH_3COOH + H_2O_2$) with different dosage of tetraoctyl ammonium bromide (TOAB) phase transfer agent

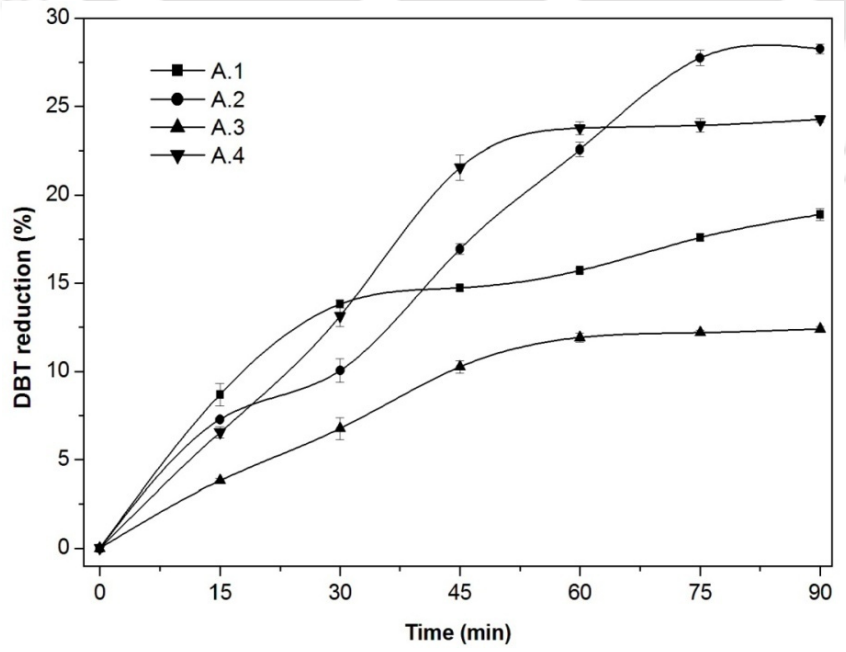

Figure 3.5: DBT reduction under experimental category A

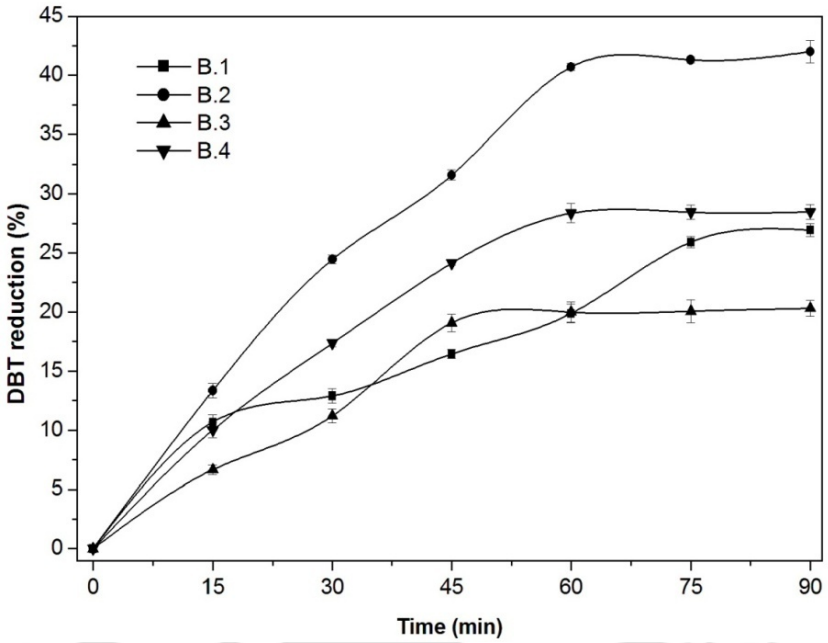

Figure 3.6: DBT reduction under experimental category B

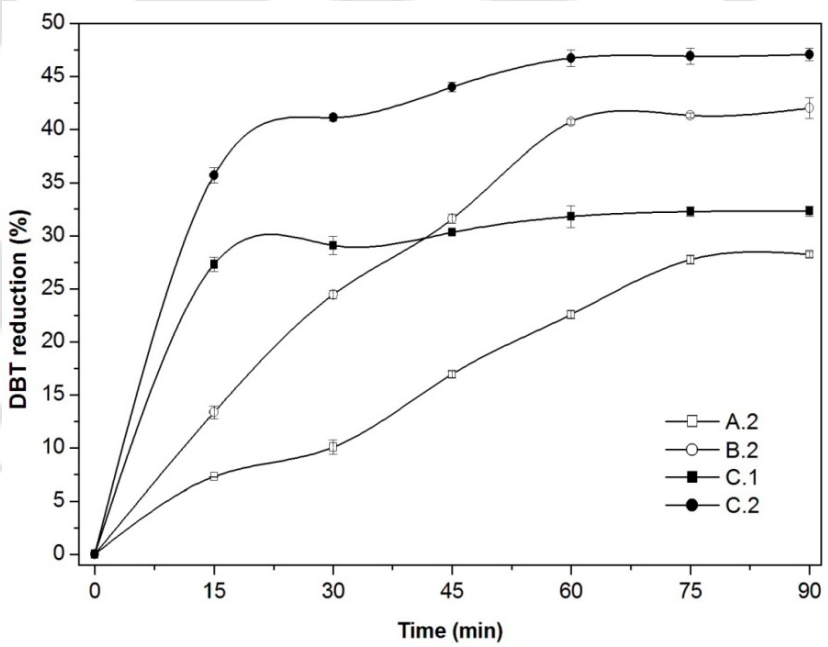

Figure 3.7: Influence of static pressure on DBT reduction in presence of ultrasound

(1) The category A used peracetic acid (CH_3COOH + H_2O_2) as the oxidant, with either mechanical stirring (A.1 and A.3) or ultrasound irradiation (A.2 and A.4) used for mixing of reaction system. In sub–category A.1 and A.2, stoichiometric quantities of acetic acid and H_2O_2 have been mixed, while, in sub–categories A.3 and A.4, an

excess of H_2O_2 is used. Comparing between categories A.1 and A.2, and also within them, the relative influences of ultrasound and PTA on enhancement of oxidation are evident. Replacement of stirring (category A.1) with ultrasound (category A.2) causes about 56% enhancement. In our previous chapter, we have studied the oxidative desulfurization of DBT without PTA. In this study, we had obtained 6.4% of DBT reduction for mechanically stirred system, while for ultrasound assisted system, the percentage DBT reduction was 16.6%. Comparing these values with the results of present study reveals interesting facets of effect of PTA on the oxidative desulfurization. For mechanically stirred system, addition of PTA boosts the DBT reduction to 18.89%, which is more than 3-fold enhancement. On the contrary, beneficial effect of PTA addition is less marked for ultrasound irradiated system – in that the DBT reduction increases from 16.6% to 28.25%, which is relativity much lesser enhancement of ~ 70%. An explanation for these results can be given as follows: Enhancement in interfacial area by strong micro–convection generated sonication causes more effective interfacial transport of oxidant, and hence, further addition of PTA to reaction mixture does not significantly augment this transport, which is manifested in enhancement of DBT reduction. On the other hand, the interfacial area generated by mechanical stirring is expected to be much lesser due to lower intensity of convection. Thus, the role of PTA in augmentation of transport of oxidant is more marked in case of mechanical stirring.

(2) Sub–categories A.3 and A.4, in which an excess quantity of H_2O_2 was used, revealed reduction in extent of oxidation as compared to sub–categories A.1 and A.2. For mechanically stirring (A.3), reduction is ~ 35%, while for ultrasound irradiation (A.4), the reduction is relatively smaller ~ 14%.

The physical explanation for this result can be given as follows: Since H_2O_2

added to the reaction system is in excess, some H_2O_2 will be left unreacted in the oxidant medium after formation of peracetic acid. Mei et al. (2003) have postulated several possible reactions that excess H_2O_2 may undergo in the reaction mixture. These are: (1) thermal decomposition into molecular oxygen and water, (2) homolytic cleavage due to ultrasound irradiation to form hydroxyl radicals, and (3) direct transfer by PTA to the organic phase. The amount of PTA added to the oxidant is same as that for the stoichiometric quantities of H_2O_2 (category A.1 and A.2), there would be competition between peracetic acid and unreacted H_2O_2 for the formation of complex with PTA. The total oxidation of DBT achieved will be the total of individual contributions of H_2O_2 and peracetic acid. The oxidation potentials of H_2O_2 (1.8 eV) and peracetic acid (1.7 eV) are very similar. However, the H_2O_2–PTA complex is expected to have more polar character than CH_3COOO^-–PTA. The polar nature of the H_2O_2–PTA complex adversely affects the transfer of H_2O_2–PTA complex to the organic medium, which in turn reduces the total oxidation of DBT as compared to the oxidation achieved with peracetic acid alone. Moreover, this effect is more marked for mechanically stirred system, where the interfacial area is limited and the role of PTA in transport of oxidant to organic phase is more prominent. For sonicated system (A.4), higher interfacial area can overcome the limitation of transfer of H_2O_2–PTA complex, and thus, the total oxidation achieved is higher than category A.3. However, the extent of oxidation for category A.4 is still lower than that for A.2.

(3) The results of experimental category B, in which formic acid was used instead of acetic acid show essentially same trend as category A, however with significantly higher extent of oxidation as compared to acetic acid. The enhancements are: 42% (A.1 vs. B.1), 49% (A.2 vs. B.2), 63% (A.3 vs. B.3) and 17% (A.4 vs. B.4). The explanation for trends in category B experiments can be given essentially along same

lines as for category A. The major reason underlying enhancement of oxidation with formic acid (as compared to acetic acid) is probably higher intrinsic diffusivity of the formic acid–PTA complex due to smaller size. Moreover, several earlier literatures in the area of disinfectants have asserted higher oxidation potential and reactivity of performic acid as compared to peracetic or perpropionic acid (Huss et al., 1999; Merka et al., 1965; Aksela and Renvall, 2009).

(4) In category C experiments, an elevated static pressure was applied during sonication of the reaction mixture. The major effect of elevated static pressure is elimination of transient cavitation in the system, which leads to generation of radicals. In addition, contribution of transient cavitation to overall convection in the system also reduces drastically. However, the ultrasound wave phenomenon remains practically uninfluenced by elevated static pressure. For greater discussion on the effect of elevated static pressure on cavitation bubble dynamics with quantitative details (numerical simulations of cavitation bubble dynamics) shown in our previous chapter. Propagation of ultrasound wave through liquid medium causes small amplitude oscillatory motion of fluid elements at very high frequency, which is called "micro–streaming". This is responsible for mixing and fine emulsification of the reaction mixture. Thus, application of elevated static pressure essentially renders effect of sonication purely physical. Comparison of results of categories A.2 vs. C.1 and B.2 vs. C.2 gives an account of influence of elevated static pressure. In both cases, argumentation in oxidation is seen. However, this augmentation is rather moderate, ~ 14% for peracetic acid, and ~ 12% for performic acid.

In previous chapter, we have explained the influence of application of elevated static pressure on oxidative desulfurization reaction system with help of simulation of cavitation bubble dynamics, which is briefly summarized as follows: At atmospheric

static pressure, transient cavitation occurs in both organic and aqueous medium during sonication of the reaction mixture. Occurrence of transient cavitation events in the organic medium generate reducing species such as H_2 and CO through thermal dissociation of organic solvent vapor entrapped in the cavitation bubble. These species competitively consume the oxidant species generated from dissociation of perorganic acids, and thus, hamper their utilization for effective oxidative desulfurization. On the other hand, transient cavitation in the aqueous medium can generate oxidizing radical species such $^{\bullet}OH$, $O^{\bullet}$ and $HO^{\bullet}_2$ due to dissociation of H_2O_2. These radicals are extremely unstable and do not diffuse in the medium, and hence, their contribution to the oxidation of DBT is likely to be small. However, if the transient cavitation occurs near the interface between organic and aqueous medium, these radicals can further enhance the oxidation of DBT. Application of high static pressure eliminates transient cavitation in the organic medium, and also generation of reducing species, and help effective utilization of oxidant species towards oxidation of sulfur compounds.

In the present situation, the effect of high static pressure is not marked as in our previous studies. We attribute this result to the difference in interfacial transport of the oxidant species in presence and absence of PTA. In the present case, the oxidant transport is in the form of a complex between PTA and oxidant, which reduces the adverse effect of consumption of the oxidant by the reducing species generated during transient cavitation in the organic phase. This promotes effective utilization of the oxidants for desulfurization.

3.4 CONCLUSION

This chapter has attempted to deduce the physical or mechanistic features of the

oxidative desulfurization process simultaneous assisted by ultrasound and PTA. The relative role of ultrasound and PTA in enhancement of oxidation has been verified with different experimental protocols. The results have been compared on the basis of oxidative desulfurization achieved with mechanical stirring. The results of this study have highlighted several interesting facets of the oxidative desulfurization process as follows:

(1) Both ultrasound and PTA influence each other's individual beneficial effects on the reaction system. Effect of PTA is more marked for mechanically stirred system due to mass transfer limitations as a consequence of smaller interfacial area. Intense emulsification with generation of high interfacial area due to ultrasound helps overcome the mass transfer limitations and reduces the extent of enhancement of oxidation by PTA.

(2) Despite assistance of the oxidative desulfurization process by PTA and ultrasound, the intrinsic factors and properties such as polarity (and hence partition coefficient) and diffusivity have a crucial effect on the extent of oxidation. The intrinsic reactivity of the oxidant also plays a vital role, as seen from the extent of oxidation achieved with performic acid and peracetic acid.

(3) Complexing of the oxidant with PTA reduces the undesired consumption of oxidant by the reducing species formed during transient cavitation in organic medium.

REFERENCES

Aksela R, Renvall I. Process for preparation of peroxy acids. US Patent 12/066, 686, Sep 2009.

Chakma S, Moholkar VS. Investigations in synergism of hybrid advanced oxidation processes with combinations of sonolysis + fenton process + UV for

degradation of bisphenol–A. *Ind. Eng. Chem. Res*. 2014; 53: 6855–6865.

Chakma S, Moholkar VS. Physical mechanism of sono–Fenton process. *AIChE J*. 2013; 59: 4303–4313.

Chen TC, Shen YH, Lee WJ, Lin CC, Wan MW. Optimization of thiophene removal by an ultrasound–assisted oxidative desulfurization process. *Environ. Eng. Sci*. 2012; 29: 623–629.

Chen TC, Shen YH, Lee WJ, Lin CC, Wan MW. The study of ultrasound–assisted oxidative desulfurization process applied to the utilization of pyrolysis oil from waste tires. *J. Clean. Prod.* 2010; 18: 1850–1858.

Gogate PR, Tatake PA, Kanthale PM, Pandit AB. Mapping of sonochemical reactors: review, analysis, and experimental verification. *AIChE J*.2002; 48: 1542–1560.

Huss M, Schneider R, Preuss A, Fuchs R. Aqueous disinfecting agent containing performic acid and peracetic acid. Canadian Patent CA 2266523, May 1999.

Kuppa R, Moholkar VS. Physical features of ultrasound enhanced heterogeneous permanganate oxidation. *Ultrason. Sonochem*. 2010; 17: 123–131.

Mei H, Mei BW, Yen TF. A new method for obtaining ultra–low sulphur diesel fuel via ultrasound assisted oxidative desulphurization. *Fuel* 2003; 82: 405–414.

Merka V, Sita F, Zikes V. Performic and perpropionic acids as disinfectants in comparison with peracetic acid. *J. Hyg. Epidemiol. Microbiol. Immunol*.1965; 9: 220–226.

Morya NK, Iyer PK, Moholkar VS. A physical insight into sonochemical emulsion polymerization with cavitation bubble dynamics. *Polymer* 2008; 49: 1910–1925.

Shah YT, Pandit AB, Moholkar VS. Cavitation Reaction Engineering. Plenum Press / Kluwer Academic: New York; 1999.

Sivasankar T, Paunikar AW, Moholkar VS. Mechanistic features of the sonochemical degradation of organic pollutants. *AIChE J*.2008; 54: 2206–2219.

Wan MW, Yen TF. Enhance efficiency of tetraoctyl ammonium fluoride applied to ultrasound assisted oxidative desulphurization (UAOD) process. *Appl. Catal. A* 2007; 319: 237–245.

Zhao D, Ren H, Wang J, Yung Y, Zhao Y. Kinetics and mechanism of quaternary ammonium salts as phase–transfer catalysts in the liquid–liquid phase for oxidation of thiophene. *Energ. Fuel* 2007; 21: 2543–2547.

Chapter 4

Mechanistic Insight in Phase Transfer Agent Assisted Ultrasonic Oxidative Desulfurization

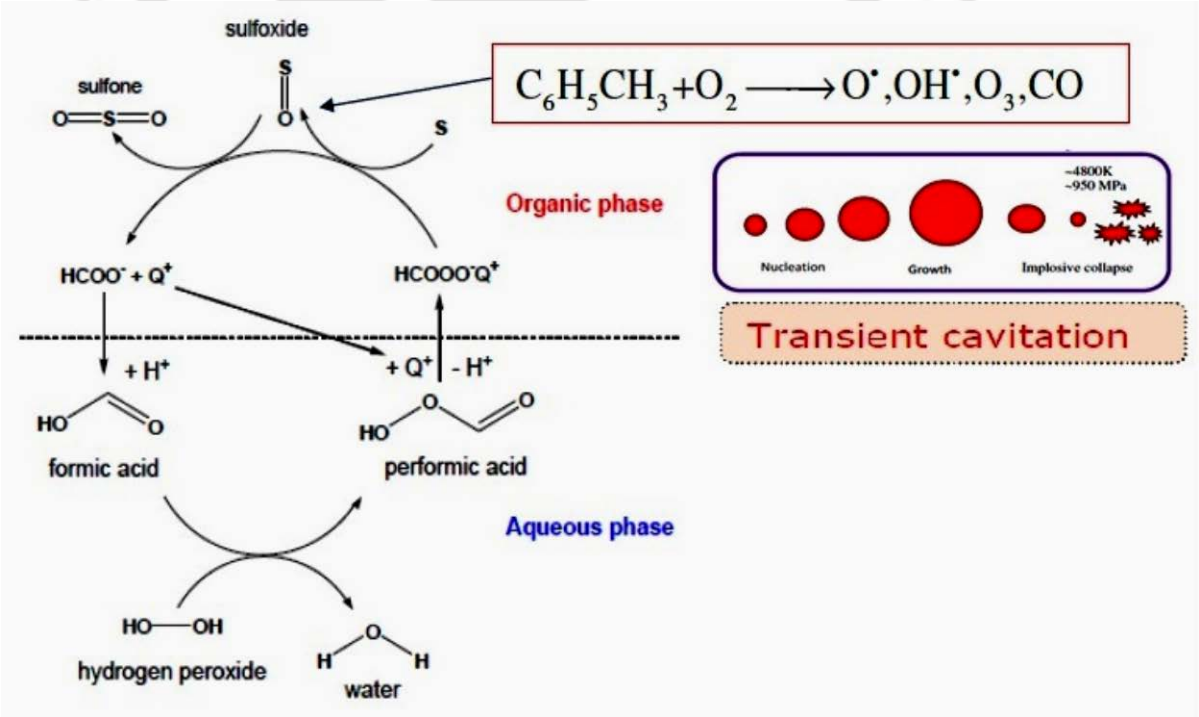

Mechanistic Insight in Phase Transfer Agent Assisted Ultrasonic Oxidative Desulfurization

4.1 INTRODUCTION

Oxidative desulfurization system is essentially a liquid-liquid heterogeneous system limited by mass transfer. Ultrasound irradiation (or sonication) is a well–known technique for enhancing the interphase mass transfer through generation of strong micro–convection. Another means of enhancing the interfacial mass transfer in a liquid–liquid heterogeneous system is the use of phase transfer catalyst or phase transfer agent (PTA) (Doraiswamy, 2001). PTA enhances interphase mass transfer by formation of complex with the nucleophilic reagent in aqueous phase (or the oxidant in context of present study), and transport of the complex to the organic phase. Simultaneous application of ultrasound and PTA for oxidation desulfurization has been attempted by several authors (Mei et al., 2003; Etemadi et al., 2007; Wan and Yen, 2007). Hagenson et al. (1994) and Hagenson and Doraiswamy (1998) have analyzed the effect of ultrasound, phase transfer agent and microphase in enhancement of synthesis of benzyl sulfide from benzyl chloride and sodium sulfide.

Ultrasound was revealed to enhance intrinsic mass transfer as well as effective diffusivity of the organic reactant through the product layer. Ultrasound was revealed to boost the effects of microphase and PTA on enhancement of reaction kinetics. In the previous chapter we showed that interfacial transport of oxidant in the form of oxidant–PTA complex reduces the undesirable consumption of oxidant by reducing species.

This chapter attempts to gain physical insight into the phase transfer agent (PTA) assisted ultrasonic oxidative desulfurization process. Essentially, the synergistic links between mechanisms of PTA and ultrasound / cavitation have been identified by coupling experimental results with simulations of cavitation bubble dynamics and Arrhenius & thermodynamic analysis of reaction kinetics.

4.2 MATERIALS AND METHODS

4.2.1 Chemicals

The following chemicals have been used in the experiments: Dibenzothiophene (98%, Sigma Aldrich), toluene (Synthesis grade, Merck), 30% v/v H_2O_2 (AR Grade, Merck), formic acid (~ 86%, AR Grade, Lobachem), tetrabutyl ammonium bromide (TBAB, Sigma Aldrich), acetonitrile (HPLC grade, Merck). All chemicals were used as received without any pretreatment.

4.2.2 Experimental Setup

Experiments were conducted in an ultrasound bath (Make: Jeio–Tech, Model: UC02, Capacity: 2 L, Frequency: 35 kHz, Power: 70 W). The actual power dissipated in the bath was determined calorimetrically, and the acoustic pressure amplitude generated in the bath was calculated as 150 kPa (Chakma and Moholkar, 2014).

Oxidative desulfurization reactions were carried out in 38 mL test tube, which was placed at the center of the bath. Due to spatial variations of ultrasound intensity in the bath, the position of the test tube inside bath was carefully kept constant in all experiments (Gogate et al., 2002). For determination of activation energy, experiments were carried out at four temperatures (viz. 303, 313, 323 and 333 K) using a temperature controlled water bath (Make: International Commercial Traders, Model: B/CH). Similar procedure was followed for mechanically stirred system, in which a hot metal plate stirrer was used. A schematic of the experimental setup used in the experiments is shown in Figs. 4.1a & 4.1b.

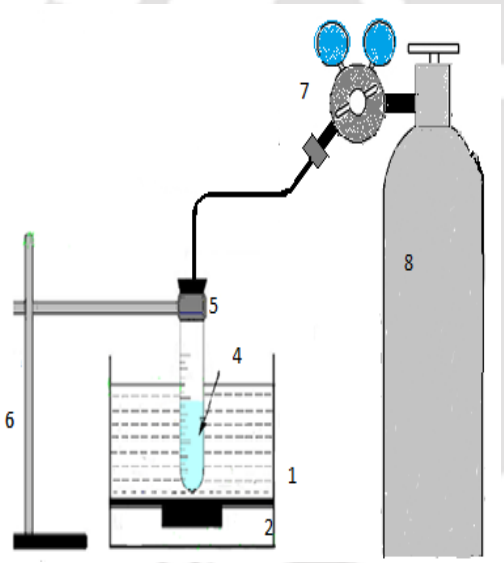

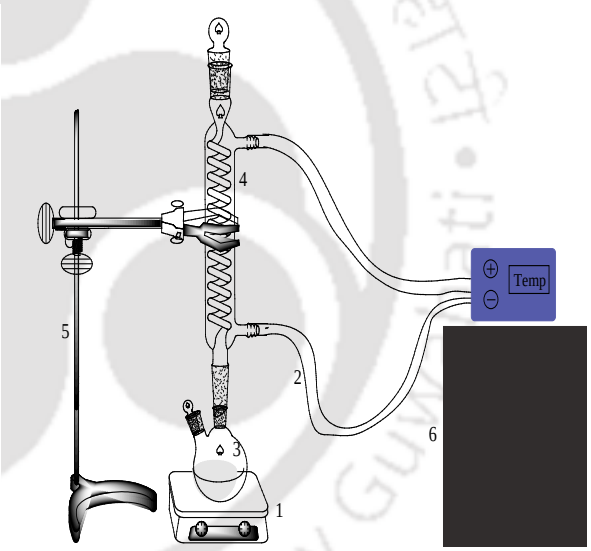

Figure 4.1a: Experimental setup for ultrasound system

Figure 4.1b: Experimental setup for mechanical stirring

Legends (Figure 4.1a): 1. Ultrasound bath; 2. Transducer; 3. Controller or regulator; 4. Reaction mixture; 5. Test tube with rubber cork; 6. Burette stand; 7. Pressure regulator; 8. N_2 gas cylinder

Legends (Figure 4.1b): 1 – Magnetic stirrer, 2 – Silicon pipe, 3 – Round bottom flask containing reaction mixture, 4 – Condenser, 5 – Holding stand, 6 – Temperature controllers

4.2.3 Experimental Protocols

Toluene (20 mL) with an initial DBT concentration of 100 ppm has been used as model fuel. The oxidant system employed for oxidative desulfurization was H_2O_2 promoted by formic acid, which formed performic acid (HCOOOH) *in–situ* in the reaction system. The experiments were planned in three categories, which have been depicted in Table 4.1. The exact composition of the reaction mixture in each experimental protocol is given in Table 4.2. Composition of reaction mixture was decided on the basis of preliminary experiments, which have been described in subsequent section. TBAB was used as phase transfer agent (PTA). The amount of PTA added to reaction mixture was varied in the range of 0.25 – 0.1 g. In some experiments, the static pressure on the reaction solution was raised to 1.6 bar using a nitrogen cylinder with two–stage regulator. During the reaction, aliquots of reaction mixture (0.5 mL) were withdrawn every 15 min and were analyzed for the residual DBT concentration. All experiments were done in triplicate to assess reproducibility of results.

4.2.4 Analysis

The residual concentration of DBT in the aliquots of reaction mixture was analyzed using Shimadzu High Performance Liquid Chromatography (HPLC, Model: SPD–20A) equipped with a reverse phase C–18 column (5 μm, 4.6 mm × 250 mm) and UV detector at 287 nm. The mobile phase was a mixture of acetonitrile and water (80:20 v/v). The formation of sulfone in oxidative desulfurization was confirmed using FTIR analysis after completion of reaction. To identify the intermediates during DBT oxidation, GC–MS analysis of the same reaction sample was performed using Varian 240– GC equipped with VF–5ms column (30 m × 0.25 m ID, DF = 0.25). The temperature program was as follows: injection temperature – 250^{o}C, column

temperature – 100°C at zero time and increased to 300°C at a ramping rate of 7°C/min.

4.2.5 Characterization of Oxidized Product

***HPLC chromatograph*:** Representative HPLC chromatographs of the aliquots of reaction mixture are shown in Fig. 4.2. Peaks corresponding to DBT and DBT sulfone were obtained at retention times of 9.1 and 3.9 min, respectively.

Table 4.1: Summary of DBT oxidation in four experimental categories

Experimental Category	Solvent: Toluene		
	DBT oxidation (%)	k (min^{-1})*	R^2
A1. MS +PFA	28.30 ± 1.12	4.13×10^{-3}	0.97
A2. US + PFA	31.22 ± 0.98	4.43×10^{-3}	0.95
B1. MS +PFA + TBAB	63.50 ± 0.92	1.22×10^{-2}	0.96
B2. US +PFA + TBAB	96.65 ± 1.06	4.26×10^{-2}	0.97
C.1 US + PFA+ TBAB + ESP (1.8 bar)	77.63 ± 1.30	1.52×10^{-2}	0.85

* – pseudo 1st order kinetic constant, *k*, obtained at reaction temperature of 313 K for ultrasound assisted desulfurization experiments, and 333 K for experiments using mechanical stirring.

Table 4.2: Experimental categories with exact composition of reaction mixture

Experimental Category	Molar Ratio $\frac{H_2O_2}{HCOOH}$	Molar Ratio $\frac{H_2O_2}{PTA}$	Volume Ratio $\frac{Solvent}{Oxidant}$
A.1 US + H_2O_2 + HCOOH (4 mL) [PFA]	0.6	16.11	3.33
A.2 MS+ H_2O_2 + HCOOH (4 mL)	0.6	16.11	3.33
B.1 US +PFA + TBAB (50 mg)	0.6	16.11	3.33
B.2 MS +PFA + TBAB (50 mg)	0.6	16.11	3.33
C. US + PFA+ TBAB + ESP (1.8 bar)	0.6	16.11	3.33

Note: In each of the experimental categories A, B, and C, the total volume of solvent (or model fuel) used is 20 mL.

***FTIR analysis*:** Fig. 4.3 compares the IR spectra of reaction mixture before and after DBT oxidation reaction. Fig. 4.3 shows two different characteristic peaks of sulfone compound at 1370 cm^{-1} and 1035 cm^{-1}, while characteristic peak at 917 cm^{-1} represents the sulfoxide compound confirming the oxidation of DBT during treatment.

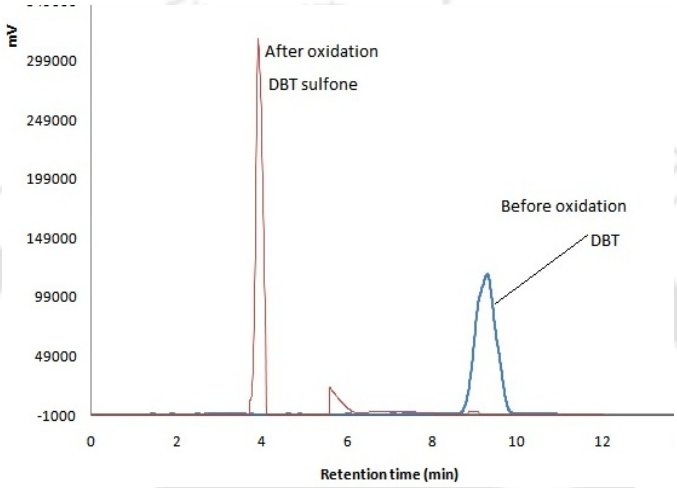

Figure 4.2: HPLC Chromatograph of reaction mixture before and after treatment for oxidant system: Performic acid + TBAB as phase transfer agent

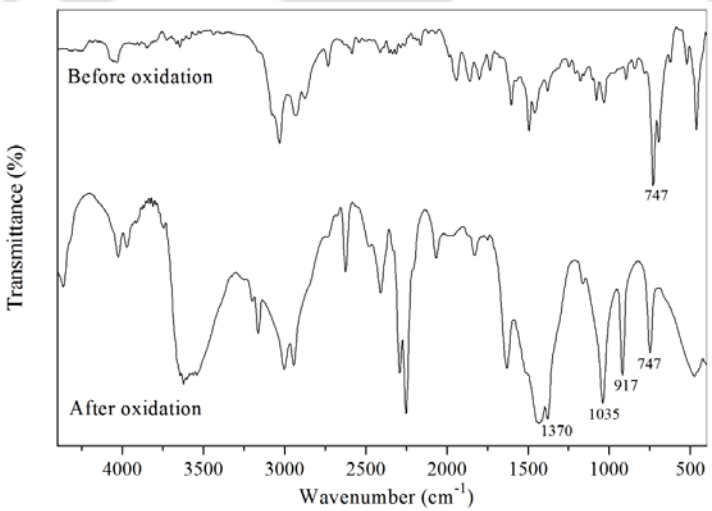

Figure 4.3: Comparison of the FTIR spectra of before and after oxidation reaction (protocol: experimental category B, i.e. ultrasound treatment with oxidant performic acid in presence of TBAB as phase transfer agent)

GC–MS analysis: The high resolution GC–MS total ion chromatograms of reaction mixture (initial and after completion of the reaction) are shown in Figs. 4.4A and 4.4.B, respectively. The molecular mass of DBT was determined to be 184.3, which is close to the calculated value of 184.26. The oxidized products were found to have a mass of 199.6 and 216.03 giving a mass difference of 16 and 32 units with respect to DBT, respectively. These additional units correspond to the mass of 1 and 2 oxygen atoms. The peaks obtained at 20.08, 22.1 and 25.3 min correspond to DBT, DBT sulfoxide and DBT sulfone, respectively. The major ions obtained at different m/z (% intensity, proposed derivation from molecular ion, M) values are 200 (10, [M]+), 184 (100, [M–O]+), 171 (12.5, [M–CHO]+), 139 (20, [M–COH–S]+), 216 (100, [M]+), 187 (37.5, [M–COH]+), 168 (23, [M–O–S]+), 160(10, [M–CO–CO]+), and 150 (7.5, [M–OH–OH–S]+). The mass spectra of DBT, DBT sulfone and DBT sulfoxide are shown in Figures 4.5A – 4.5C.

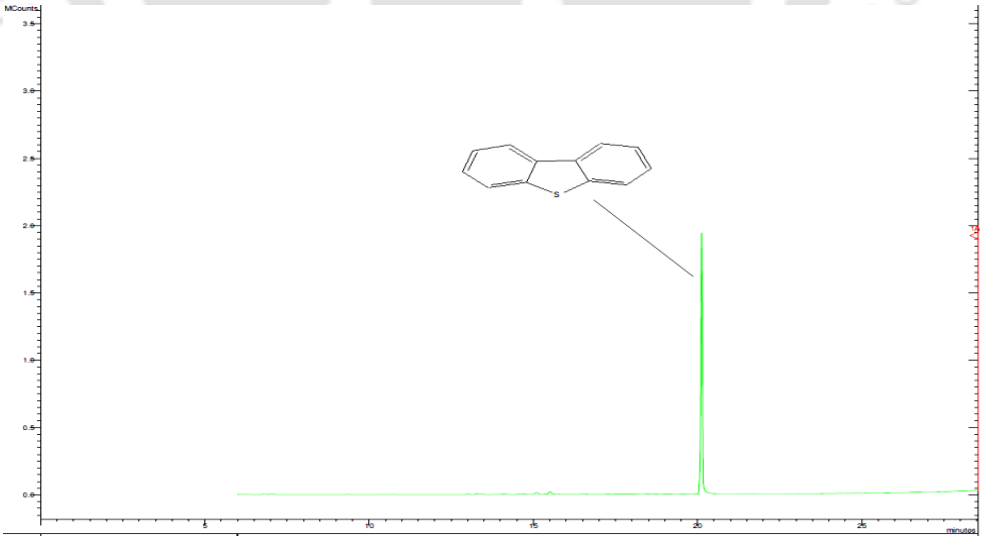

(A)

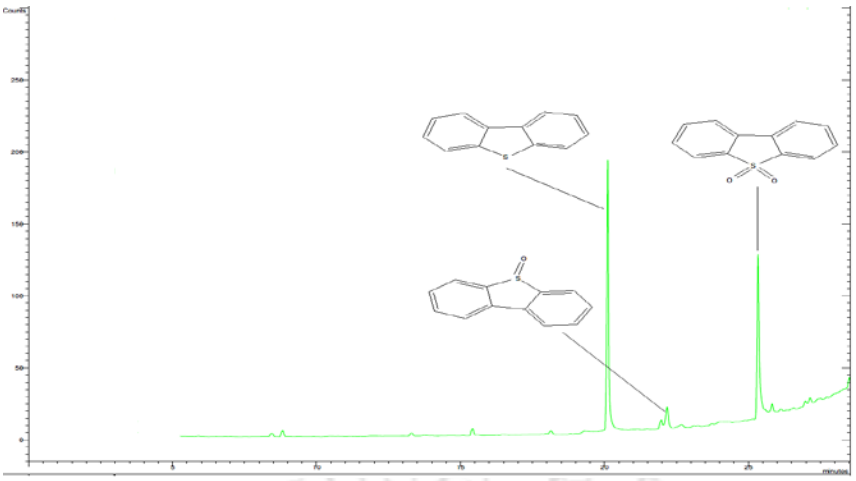

(B)

Figure 4.4: Total ion chromatogram of the reaction mixture in experimental category B (protocol: ultrasound treatment with oxidant performic acid in presence of TBAB as phase transfer agent). (A) Initial (before reaction) chromatogram; (B) Final (after oxidation reaction) chromatogram

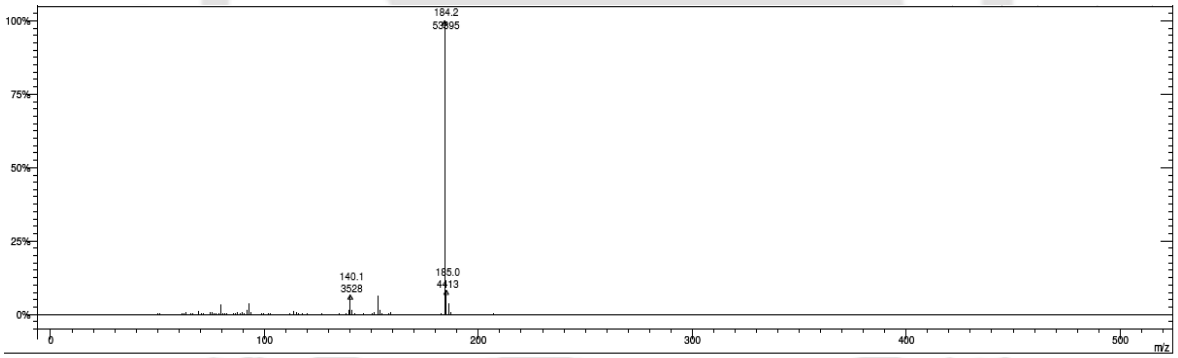

(A)

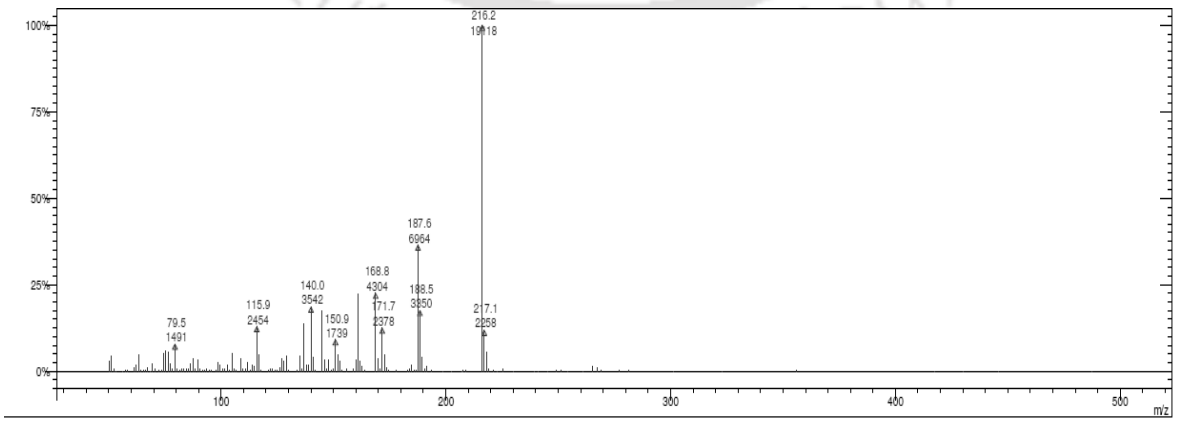

(B)

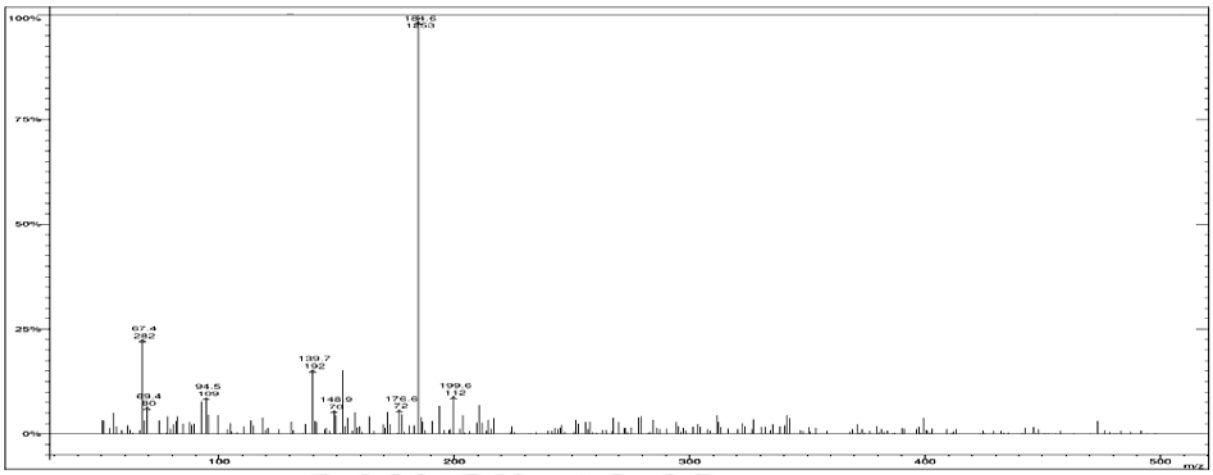

(C)

Figure 4.5: Mass spectrum of reaction mixture after treatment in experimental category B (protocol: ultrasound treatment with oxidant performic acid in presence of TBAB as phase transfer agent). **(A)** Mass spectrum of DBT; **(B)**: Mass spectrum of DBT sulfone; **(C)** Mass spectrum of DBT sulfoxide.

4.3 MATHEMATICAL MODELS

In the analysis of the physical mechanism of PTA–assisted ultrasonic oxidative desulfurization, we have used two models, viz. kinetic model for PTA–assisted oxidative desulfurization system and model for cavitation bubble dynamics, as described below:

4.3.1 Kinetic Model for PTA–Assisted Oxidative Desulfurization

In the classic review on science and engineering of phase transfer catalysis, Naik and Doraiswamy[15] have described the general considerations in modeling of PTA assisted reactions. PTA enhances slow (or kinetically controlled) reactions as well as fast reactions, which occur – either partially or completely – in diffusion film at the interphase. Therefore, Naik and Doraiswamy (1998) have recommended that a model for PTA–assisted reaction must consider all individual steps in the PTA cycle, i.e. interphase mass transfer, ion exchange and the organic phase reactions. The active

catalyst concentration (or the concentration of the PTA–anion complex) in the organic phase is an important parameter. However, the concentration of PTA–anion complex in organic phase remains constant in presence of large excess of nucleophilic reagent (performic acid in the context of present study). Enhanced mass transfer rate in presence of ultrasound also contributes to achieving constant concentration of PTA–anion complex in organic phase. The ion exchange rate has also been revealed to be much faster (~ 10×) than the rate of reaction in organic phase (Wang and Yang, 1990). Under these circumstances, the organic reaction is the rate controlling step, and is usually modeled using pseudo–1st order kinetics. Several studies on modeling of phase transfer catalyzed liquid–liquid heterogeneous reaction have confirmed suitability of pseudo–1st order kinetics for the overall reaction (Wang and Yang, 1991a, 1991b). Bhattacharya (1996) has presented a general kinetic model for liquid–liquid phase transfer catalyzed reactions, in which he has pointed out that assumption of constant concentration of PTA–anion complex is valid only when the rate of transfer of nucleophile to organic phase equals its consumption through organic reaction.

As stated earlier, we have determined the kinetic constants of PTA–assisted oxidative desulfurization in different experimental protocols using the model proposed by Zhao et al. (2007). This model is based on the model of Wang and Chen (2009) for PTA–assisted synthesis of formaldehyde acetals from alcohols and dibromomethane in an alkaline solution of KOH and organic solvent. This model has been developed for mechanically agitated system. We have used this model for ultrasonic desulfurization in view of the predominant influence of micro–convection generated by ultrasound on the reaction system. Zhao et al. (2007) have also proposed that complexation of the anion of oxidant ($HCOOO^-$) with cation of the PTA reduces

its polarity, which enable faster transport to the organic phase. Although this hypothesis is perceivable, it should be noted that the PTA–anion still has ionic character– as the net charge is not neutralized after complexation. For the convenience of the reader, we have reproduced below this model.

The oxidant in present study, viz. performic acid, forms by reaction between formic acid and H_2O_2 as follows:

$$HCOOH + H_2O_2 \longrightarrow HCOOOH + H_2O$$

Performic acid undergoes dissociation to yield nucleophilic anionic oxidant species $HCOOO^-$ as follows:

$$HCOOOH \rightleftarrows HCOOO^- + H^+$$

The nucleophile anion $HCOOO^-$ forms a complex with cation of PTA (quaternary ammonium salt), represented as Q^+Br^- as:

$$HCOOO^- + Q^+Br^- \longrightarrow [HCOOO--Q--Br] \qquad (1)$$

Desulfurization reaction occurs in the organic phase in two steps: (1) formation of PTA–oxidant complex in the aqueous phase (represented by subscript aq), and (2) transfer of the complex across interphase to organic phase (represented by subscript org). This process is reversible and is characterized by two rate constants (k_1 and k_{-1}). Usually, the intrinsic reaction between PTA and the oxidant is very fast. Hence, the overall rate constants k_1 and k_{-1} are essentially the functions of rate of mass transfer (which can be called as rate limiting step). In a liquid–liquid heterogeneous system, the rate of mass transfer across interphase is a function of the interfacial area. The second step (reaction 3) is the irreversible oxidation of sulfur compound in the organic phase and this is characterized by rate constant k_2.

$$(Q^+Br^-)_{aq} + (HCOOO^-)_{aq} \underset{k_{-1}}{\overset{k_1}{\rightleftarrows}} (Br^-)_{aq} + (Q^+CHOOO^-)_{org} \qquad (2)$$

$$(Q^+CHOOO^-)_{org} + (C_{12}H_8S)_{org} \xrightarrow{k_2} (C_{12}H_8SO)_{org} + (Q^+)_{org} + (HCOO^-)_{org} \quad (3)$$

The rate of oxidation of DBT in organic phase (or formation of product DBT sulfone $[C_{12}H_8SO]_{org}$) is written as:

$$\frac{d[C_{12}H_8SO]_{org}}{dt} = k_2[Q^+HCOOO^-]_{org}[C_{12}H_8S]_{org} \quad (4)$$

In order to determine the rate of reaction in organic phase, we need to know the concentration of PTA–anion complex in organic phase. The formation of PTA–oxidant complex $(Q^+HCOOO^-)_{org}$ can be described by following rate expression as per equations 2 and 3 given above:

$$\frac{d[Q^+HCOOO^-]_{org}}{dt} = k_1[Q^+Br^-]_{org}[HCOOO^-]_{aq} - k_{-1}[Q^+HCOOO^-]_{org}[Br^-]_{aq} - k_2[Q^+HCOOO^-]_{org}[C_{12}H_8S]_{org} \quad (5)$$

At steady–state, the net concentration of the PTA–oxidant complex in the organic phase stays constant and this gives the condition: $\frac{d[Q^+HCOOO^-]_{org}}{dt} = 0$ (6)

Other factors that also contribute to constant concentration of PTA–oxidant complex in organic phase are fast ion exchange and mass transfer across interphase, and large excess of the oxidant and PTA, as compared to the concentration of sulfur compound in organic phase (Naik and Doraiswamy, 1998). It follows therefore that:

$$k_1[Q^+Br^-]_{org}[HCOOO^-]_{aq} = k_{-1}[Q^+HCOOO^-]_{org}[Br^-]_{aq} + k_2[Q^+HCOOO^-]_{org}[C_{12}H_8S]_{org} \quad (7)$$

The PTA exists in the organic phase of the reaction system in pure form Q^+Br^- as well as in the form of the complex. Hence, the total concentration of PTA cation $[Q^+]_{org}$, which forms complex with nucleophilic oxidant is written as:

$$\left[Q^+\right]_{org} = [Q^+Br^-]_{aq} + [Q^+HCOOO^-]_{org} \quad (8)$$

Substituting for $[Q^+Br^-]_{aq}$ as $[Q^+]_{org} - [Q^+HCOOO^-]_{org}$ in equation 7, we get:

$$[Q^+HCOOO^-]_{org} = \frac{k_1[Q^+]_{org}[HCOOO^-]_{aq}}{k_1[HCOOO^-]_{aq} + k_{-1}[Br^-]_{aq} + k_2[C_{12}H_8S]_{org}} \quad (9)$$

Now substituting eqn. (9) in eqn. (4), the rate of reaction of DBT oxidation in organic phase is:

$$\frac{d[C_{12}H_8SO]_{org}}{dt} = \frac{k_1k_2[Q^+]_{org}[HCOOO^-]_{aq}[C_{12}H_8S]_{org}}{k_1[HCOOO^-]_{aq} + k_{-1}[Br^-]_{aq} + k_2[C_{12}H_8S]_{org}} \quad (10)$$

Due to convection present in the system (either in the form of mechanical agitation or ultrasound irradiation), the rate of interphase mass transfer of $(HCOOO^-)_{aq}$ can be assumed to be very fast. This results in rapid accumulation of $(HCOOO^-)_{aq}$ and $(Q^+)_{org}$ in the organic phase. This favors the forward reaction of eq. (2). Moreover, the intrinsic kinetics of the DBT oxidation reaction in the organic phase is also likely to be much slower than the dissociation of performic acid. Under these conditions, the following inequality holds true:

$$k_1[HCOOO^-]_{aq} >> k_{-1}[Br^-]_{aq} + k_2[C_{12}H_8S]_{org} \quad (11)$$

With this, the rate expression for product formation gets transformed as:

$$\frac{d[C_{12}H_8SO]_{org}}{dt} = k_2[Q^+]_{org}[C_{12}H_8S]_{org} \quad (12)$$

The stoichiometry of reaction between DBT (reactant) and DBT–sulfone (product) is essentially one. Hence, one can easily substitute rate of formation of product in terms of rate of disappearance of reactant (DBT):

$$-\frac{d[C_{12}H_8S]_{org}}{dt} = \frac{d[C_{12}H_8SO]_{org}}{dt} \quad (13)$$

Therefore, equation 12 becomes:

$$\frac{d[C_{12}H_8S]_{org}}{dt} = -k_2[Q^+]_{org}[C_{12}H_8S]_{org} \quad (14)$$

Since the PTA concentration is usually in large excess, and that mass transfer rate

across interphase is also fast, its total concentration of quaternary cation (in free and complex form) in organic phase stays constant. Hence, we can club together the rate constant k_2 and the concentration of PTC, $[Q^+]_{org}$ to give a new constant, k_3.

$$\frac{d[C_{12}H_8S]_{org}}{dt} = -k_3[C_{12}H_8S]_{org}, \text{ where } k_3 = k_2[Q^+]_{org} \quad (15)$$

Integrating the above equation between limits, at $t = 0$, $[C_{12}H_8S]_{org} = [C_{12}H_8S]_{org,0}$, and at $t = t$, $[C_{12}H_8S]_{org} = [C_{12}H_8S]_{org,t}$, we get:

$$\ln\frac{[C_{12}H_8S]_{org,0}}{[C_{12}H_8S]_{org,t}} = kt \quad (16)$$

where, k is overall or gross pseudo 1st order rate constant for oxidative desulfurization process. Thus, analysis of Zhao et al. (2007) essentially proves that with excess of oxidant as well as PTA employed during oxidative desulfurization (as is the case in present study), the overall oxidative desulfurization reaction follows pseudo 1st order kinetics.

4.3.2 Simulations of Cavitation Bubble Dynamics

In the present case, the reaction system is a two–phase mixture, viz. organic phase (toluene) and aqueous phase (performic acid). Passage of ultrasound through the reaction mixture induces micro–streaming (i.e. oscillatory motion of fluid elements) in both phases, but due to larger volume fraction in reaction mixture, the micro–streaming in toluene contributes mostly to the emulsification of organic and aqueous phases. The micro–streaming velocity is calculated as: $u = P_A/\rho_L c$. The acoustic pressure amplitude (P_A) in the medium was determined as 150 kPa using calorimetric measurements. For toluene, ρ_L (density) = 867 kg/m^3 and c (sonic velocity) = 1275 m/s, and thus, u = 0.137 m/s.

The magnitudes of physical and chemical effects of cavitation bubbles have been determined using diffusion limited ordinary differential equation model proposed by

Toegel et al., (2000) It should be noted that cavitation phenomena occurs in both organic medium (toluene) and aqueous medium (performic acid). However, since the DBT oxidation reaction occurs in organic phase, we have considered the cavitation bubble dynamics phenomena in toluene only in our model. Cavitation phenomenon occurring in aqueous medium mainly contributes to emulsification of the two phases, due to the convection induced by radial motion of transient cavitation bubbles. The diffusion limited model of Toegel et al., (2000) is based on the comprehensive partial differential equation model of Storey and Szeri, (2000) who showed that solvent vapor transport and entrapment in the cavitation bubble, leading to formation of radicals, is essentially a diffusion limited process. This model has been extensively described in previous papers (Sivasankar et al., 2007; Moholkar et al., 2000; Krishnan et al., 2006). More recently, Kumar et al., (2012) have coupled the diffusion limited model with the continuum mixture model of van Wijngaarden (1968) for hydrodynamic cavitation. Capocelli et al., (2014) have been used the model of Kumar et al., (2012) for describing the chemical effects of hydrodynamic cavitation.

The essential equations and thermodynamic data of this model have been summarized in chapter 2. The model is essentially a set of 4 ordinary differential equations: (1) Keller–Miksis equation for the radial motion of the bubble, (2) equation for the diffusive flux of water vapor and heat conduction through bubble wall, and (3) overall energy balance. Thermal conductivity of the bubble contents and diffusion coefficient of water vapor inside the bubble are determined using Chapman–Enskog theory using Lennard–Jones 12–6 potential. Diffusion of non–condensable gas across bubble interface during radial motion is ignored in the present model as the time scale for the diffusion of gases is much higher than the time scale for the radial motion of bubble. The model equations have been solved using Runge–Kutta adaptive step size

method. An air bubble has been considered for simulations. The condition for bubble collapse is taken as the first compression after an initial expansion. Various parameters used in the simulation of bubble dynamics equation and their numerical values are as follows: Ultrasound frequency (f) = 35 kHz; Ultrasound (or acoustic) pressure amplitude (P_A) = 150 kPa; Equilibrium bubble radius (R_o) = 5 μm; Vapor pressure of toluene was calculated using Antoine type correlation at the temperature of the reaction (298 K). Various physical properties of toluene are as follows: density (ρ_L) = 867 kg/m^3, kinematic viscosity (ν) = 6.8 × 10^{-7} Pa–s, surface tension (σ) = 0.0285 N/m, and sonic speed (c) = 1275 m/s, static pressure (P_o) = 101.3 kPa (for experiments at atmospheric static pressure) or 162 kPa (for experiments with elevated static pressure).

***Estimation of physical and chemical effects of cavitation*:** The chemical effect of cavitation bubble dynamics (or the sonochemical effect) is generation of small chemical species (including some radical species) from thermal dissociation of gas and solvent vapor molecules entrapped in the bubble at the moment of transient collapse – when the temperature and pressure conditions in the bubble reach extreme. Numerical solution of the diffusion–limited cavitation bubble dynamics model gives the number of solvent (toluene) vapor molecules present in the bubble at the point of minimum radius during radial motion along with the temperature and pressure peak reached in the bubble. Due to extreme temperature and pressure in the bubble, and also very high concentrations of chemical species due to extremely small volume of the bubble, the rates of different chemical reactions occurring in the bubble are extremely fast, and thermal equilibrium is likely to prevail all through the radial motion of the bubble (Brenner et al., 2002). In view of this hypothesis of Brenner et al. (2002) the equilibrium mole fraction of various species in the bubble (at the

conditions of temperature and pressure at first the compression of the bubble) resulting from thermal dissociation of air (oxygen and nitrogen) and toluene molecules have been calculated using Gibbs free–energy minimization technique (Chemical Equilibrium Calculation, 2013).

The principal physical effect of cavitation is generation of strong micro–convection in the bulk medium through two phenomena, viz. micro–turbulence, and shock or acoustic waves. The magnitudes of these two parameters can be calculated using bubble dynamics model as follows (Leighton, 1994; Grossmann et al., 1997; Moholkar and Warmoeskerken 2003):

Velocity of micro–turbulence: $V_{\text{turb}} = \frac{R^2}{r^2}\left(\frac{dR}{dt}\right)$ (17)

Pressure amplitude of shock waves: $P_{AW} = \rho_L \frac{R}{r}\left[2\left(\frac{dR}{dt}\right)^2 + R\frac{d^2R}{dt^2}\right]$ (18)

r is the distance from bubble center. A representative value of r is taken as 1 mm.

4.3.3 Arrhenius (Kinetic) and Thermodynamic Analysis

Arrhenius analysis was done using pseudo–1st order kinetic constants (at various temperatures) obtained from the model of Zhao et al. (2007) in different experimental categories. The activation energy (E_a) and frequency factor (A) of desulfurization in different experimental categories were estimated using plots of ln k vs $1/T$. The basic thermodynamic properties of the reaction system could be determined using Eyring equation as follows:

$$\ln\frac{k}{T} = -\frac{\Delta H}{R}\frac{1}{T} + \ln\frac{k_b}{h} + \frac{\Delta S}{R} \quad (19)$$

$$\Delta H = E_a - RT \quad (20)$$

$$\Delta G = \Delta H - T\Delta S \quad (21)$$

k_b and h are Boltzmann and Planck's constants, respectively. The results of Arrhenius

analysis can be used to determine the thermodynamic parameters of ΔH, ΔS and ΔG.

4.4 RESULT AND DISCUSSION

4.4.1 Preliminary Experiments

Preliminary experiments were carried out to identify the optimum quantities of phase transfer agent (PTA), TBAB. Another optimization parameter was the temperatures of the reaction mixture, which play an important role in DBT oxidation reaction. As far as other experimental parameters such as volume ratio of organic to aqueous phase and optimum composition of peracetic acid (quantities of acetic acid and H_2O_2) and performic acid (quantities of formic acid and H_2O_2) are concerned, we have used the results of chapter 2.

***Optimization of Quantity of Phase Transfer Agent*:** The results of effect of quantity of phase transfer agent, tetrabutyl ammonium bromide (TBAB), on DBT reduction (or desulfurization efficiency) are shown in Fig. 4.6. The other experimental parameters have been given in the figure caption. The amount of PTA (TBAB) added to reaction solution was varied in the range of 0.25–1.0 g. Extent of DBT oxidation showed sharp proportionate rise with amount of PTA in the reaction mixture increasing from 0 to 0.5 g. However, increase of PTA quantity from 0.5 to 0.75 g did not show any marked increase in the oxidation efficiency. Further rise in PTA quantity (from 0.75 to 1.0 g) reduced the extent of oxidation. On the basis of these results, we have taken as a 0.5 g phase transfer agent optimum dose for further experiments.

***Effect of temperature*:** The effect of temperature on extent of oxidative desulfurization in ultrasound system and mechanical stirred system is shown in Fig. 4.7. The range of temperature for optimization of oxidative desulfurization was 30°–

60°C for ultrasound and mechanical stirring. The oxidant used in all experiments was performic acid with TBAB as a phase transfer agent. The DBT removal rate increase with increasing in temperature. Sufficiently high removal rates are obtained upto 40°C in ultrasound system because of the intense emulsification with generation of high interfacial area due to ultrasound. This effect helps overcome the mass transfer limitations due to which the reaction kinetics increases. For temperature higher than 40°C, the intensity of transient cavitation is reduced due to large evaporation of solvent vapor in the cavitation bubble which later on cushions its collapse. In case of mechanical stirring, the oxidation efficiency shows marked rise for temperature range of 30°-40°C, and relatively lesser rise till 60°C. Another factor that contributes to this effect is decomposition of H_2O_2 to H_2O and O_2 at higher temperature. On the basis of these results, we have considered 40°C as the optimum temperature for ultrasound treatment while 60°C as the optimum temperature for mechanical stirring.

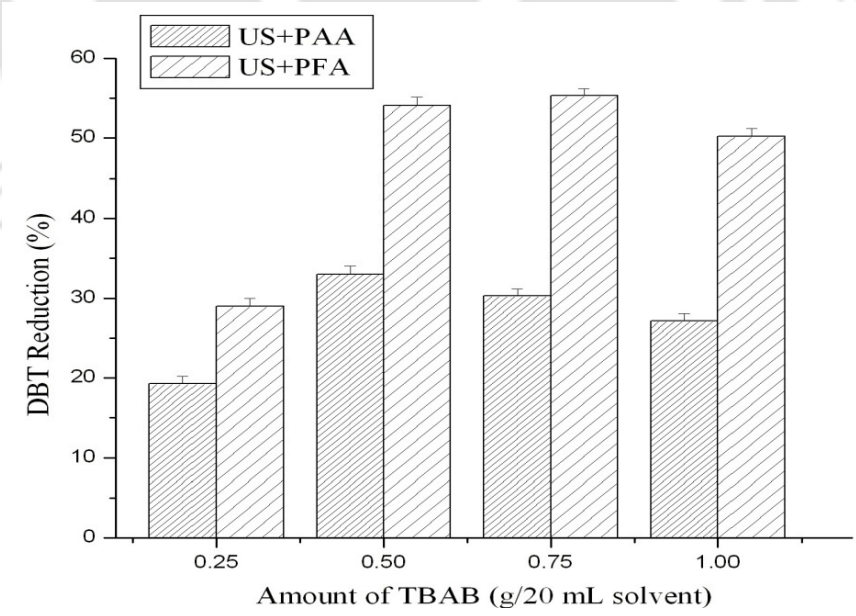

Figure 4.6: Effect of PTA dose on DBT reduction

Other parameters for experiment: solvent: toluene = 20 mL, oxidant: PFA - Performic acid (formic acid = 4 mL, H_2O_2 = 2 mL) = 6 mL; PAA - Peracetic acid (acetic acid = 4 mL, H_2O_2 = 2mL) = 6 mL; Temperature = 303 K

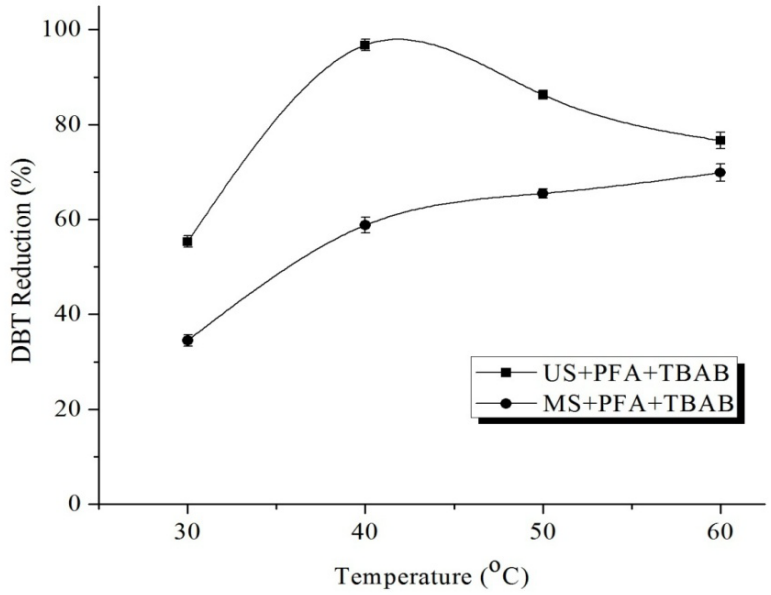

Figure 4.7: Temperature effect on DBT reduction for US and MS system

Other parameter: Solvent – toluene, Oxidant: performic acid + TBAB as PTA

4.4.2 Trends in DBT Oxidation

The time histories of DBT oxidation in different experimental categories are depicted in Figs. 4.8A and B. Results of DBT oxidation in different experimental categories are summarized in Table 4.1 and reveal following distinct features:

(1) Comparing the extent of DBT oxidation for categories A.2 and B.2, 3.1× (or 3.1–fold) rise in oxidation is seen when PTA is used in presence of ultrasound. On the other hand, comparing the results for categories A.1 and B.1, relatively lesser rise of 2.25× (or 2.25–fold) in oxidation is seen for PTA applied in mechanically stirred systems. Thus, the enhancement in DBT oxidation in presence of PTA is more pronounced for ultrasonic systems than mechanically stirred systems. This result is in complete concurrence with conclusion of Hagenson et al. (1994) that enhancement effect of PTA on reaction kinetics acquires higher significance in presence of ultrasound.

(2) Comparison of results of categories B.1 and B.2 reveals that effect of PTA is more pronounced for ultrasound–assisted system than mechanically agitated one. This is yet another proof of the synergism between mechanism of ultrasound and PTA – which is corroborated by conclusions of Hagenson et al. (1994).

(3) Reduction in DBT oxidation at elevated static pressure, as evident from comparison of the results of the categories B.2 and C.1, is attributed to suppression of the transient cavitation phenomenon at elevated static pressure, as explained in greater detail subsequently.

4.4.3 Arrhenius and Thermodynamic Analysis

The kinetic analysis of the DBT oxidation reactions at different temperatures (viz. 303, 313, 323, and 333 K) in various experimental categories using pseudo–1st order model (eq. 16) is presented in Figs. 4.9.A.1–D.1. The corresponding Arrhenius plots are given in Figs. 4.9.A.2–D.2. Arrhenius and thermodynamic parameters of the oxidative desulfurization in different experimental categories are summarized in Table 4.3A and B, respectively. The characteristic variations in Arrhenius parameters evident from results presented in Table 4A are as follows:

(1) Use of PTA in mechanically stirred system reduces the activation energy of oxidative desulfurization, as observed from comparison of the activation energies in categories A.1 and B.1. This result is in concurrence with observations of Zhao et al. (2007).

(2) The ultrasound–assisted systems (categories A.2 and B.2) have significantly lower activation energies as compared to mechanically stirred systems (categories A.1 and B.1, respectively). Moreover, it is interesting to note that the use of PTA in ultrasound assisted desulfurization systems leads to increase in activation energy, as seen from

the Arrhenius parameters for categories A.2 and B.2.

(3) The frequency factors for ultrasound assisted systems (categories A.2 and B.2) are one to two orders of magnitude smaller than the mechanically stirred system (categories A.1 and B.1). Use of PTA with ultrasound leads to rise in frequency factor, as evident from comparison of frequency factors for categories A.2 and B.2.

(4) Scatter of data points in Arrhenius plots and low regression coefficients in Figs. 4.9.B.2 and 4.9.D.2 (corresponding to the systems with ultrasound) are attributed to the inverse effect of temperature on intensity of transient cavitation. Both physical and chemical effects of cavitation diminish with increasing temperature. The reason underlying this effect is large evaporation of solvent vapor (due to high vapor pressure) and subsequent entrapment in the bubble at elevated temperature. The entrapped vapor "cushions" the transient collapse of the cavitation bubble. This causes reduction in the intensity of collapse (the peak temperature and pressure reached in the bubble) and also the physical/chemical effects associated with it. Consequently, the rate of reactions that are accelerated by physical/chemical effects of cavitation also reduce with temperature. This phenomenon violates the postulate of increase in rate of reaction with temperature in Arrhenius theory. Therefore, kinetic data of ultrasound–assisted reactions (in the present context experimental categories A.2 and B.2) shows a scatter when fitted to the Arrhenius model leading to low regression coefficients as seen in Figs. 4.9.B.2 and 4.9.D.2. However, despite this limitation, the trends in the Arrhenius parameters obtained for different experimental categories reveal a physically meaningful picture of the mechanism of PTA–assisted ultrasonic oxidative desulfurization.

The trends in thermodynamic parameters that can be identified from the results presented in Table 4.3B are as follows:

(1) Use of PTA in mechanically stirred system leads to reduction in ΔH and ΔG and increase in $-\Delta S$.

(2) Use of PTA in ultrasound assisted system shows rather opposite trend that ΔH increases, while $-\Delta S$ and ΔG reduce in presence of PTA.

(3) As compared to mechanically stirred systems, ΔH and ΔG values for ultrasound–assisted systems are significantly smaller, while $-\Delta S$ values are higher.

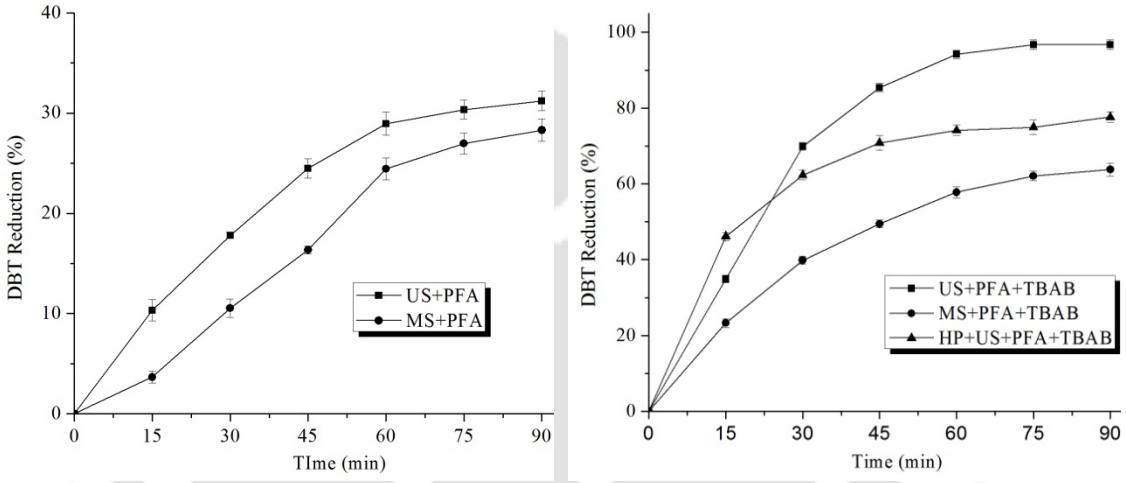

(A) (B)

Figure 4.8: (A) Time history of DBT oxidation in experimental category A. (B) Time history of DBT oxidation in experimental category B and C.

Table 4.3: (A) Arrhenius and thermodynamic analysis of PTA–assisted oxidative desulfurization.

Experimental Category	Parameter	Temperature (K)				E_a (kJ/mol)	A (min^{-1})
		303	313	323	333		
A. Kinetic and Arrhenius analysis							
MS + PFA	k (min^{-1})	1.15×10^{-3}	2.70×10^{-3}	3.45×10^{-3}	4.27×10^{-3}	39.35	6974.39
	R^2	0.92	0.97	0.94	0.95		
US + PFA	k (min^{-1})	4.43×10^{-3}	6.12×10^{-3}	5.84×10^{-3}	5.61×10^{-3}	5.84	0.051
	R^2	0.95	0.94	0.96	0.96		
MS +PFA + TBAB	k (min^{-1})	6.70×10^{-3}	9.80×10^{-3}	1.22×10^{-2}	2.02×10^{-2}	30.12	815.93
	R^2	0.95	0.96	0.97	0.97		
US + PFA + TBAB	k (min^{-1})	1.81×10^{-2}	4.25×10^{-2}	3.71×10^{-2}	3.58×10^{-2}	17.67	14.43
	R^2	0.92	0.97	0.98	0.95		

Experimental Category	(B) Thermodynamic Property											
	ΔH (kJ/mol)				$-\Delta S$ (kJ/mol K)				ΔG (kJ/mol)			
	Temperature											
B. Thermodynamic analysis	303 K	313 K	323 K	333 K	303 K	313 K	323 K	333 K	303 K	313 K	323 K	333 K
A1. MS + PFA	36.23	36.09	36.05	35.97	0.216	0.213	0.215	0.217	101.96	102.92	105.57	108.34
A2. US + PFA	3.49	3.41	3.36	3.91	0.313	0.311	0.312	0.313	98.23	100.72	104.14	107.55
B1. MS +PFA + TBAB	27.00	26.91	26.83	26.75	0.232	0.232	0.233	0.232	97.12	99.47	102.15	104.00
B2. US + PFA + TBAB	13.91	13.82	13.74	13.67	0.267	0.261	0.265	0.266	94.68	95.65	99.23	102.40

Notation: k – pseudo 1st order kinetic constant (min^{-1}), R^2 – regression coefficient, E_a – activation energy (kJ/ mol), A – frequency factor or pre–exponential factor (mol /L–min).

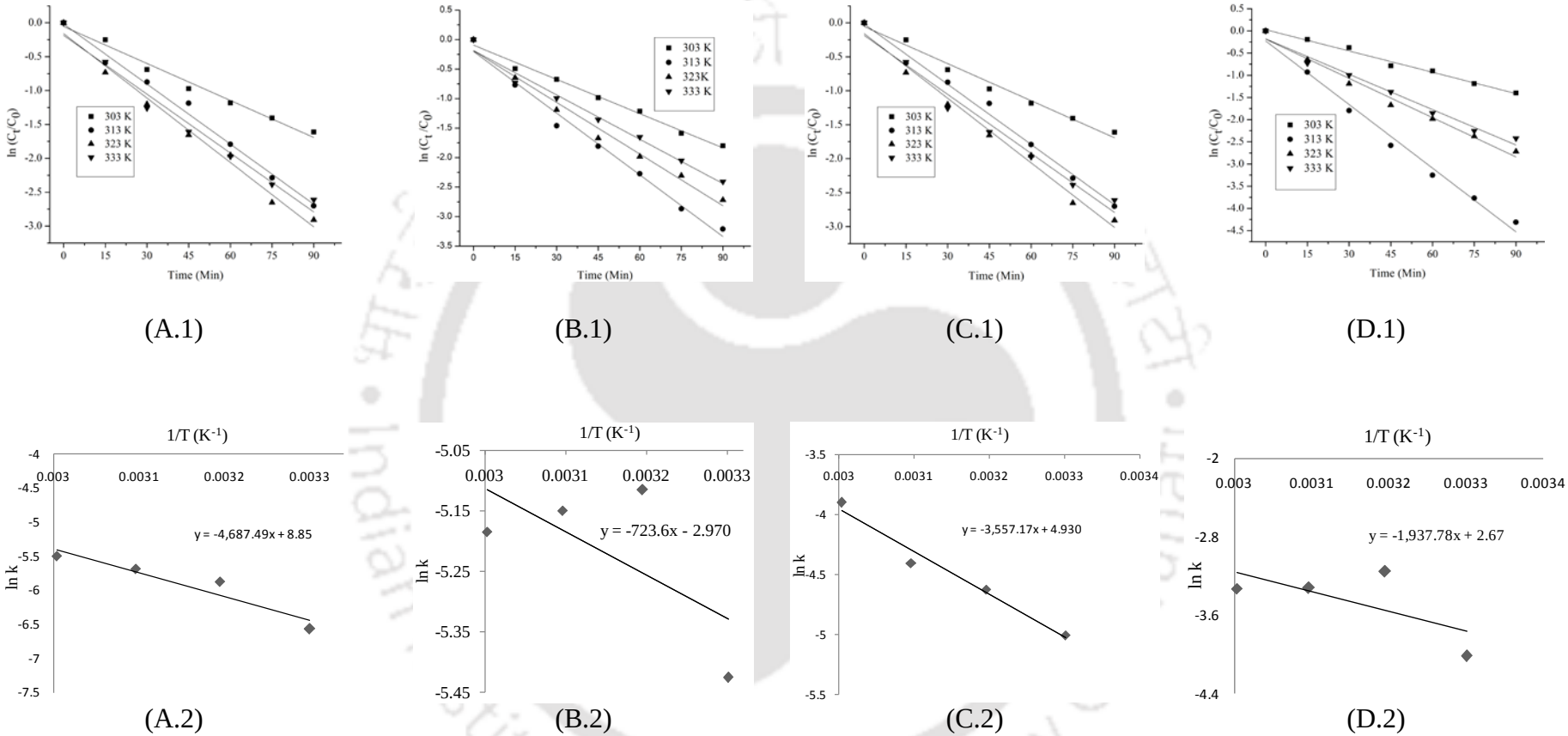

Figure 4.9: Kinetic analysis of oxidative desulfurization under ultrasound treatment and mechanical stirring using performic acid as oxidant coupled with TBAB as phase transfer agent. (A.1) 1st order fit of the experimental data for mechanical stirring + PFA treatment; (A.2) Arrhenius plot for the mechanical stirring + PFA treatment; (B.1) 1st order fit of the experimental data for ultrasound + PFA treatment; (B.2) Arrhenius plot for the ultrasound + PFA treatment, (C.1) 1st order fit of the experimental data for mechanical stirring + PFA + PTA; (C.2) Arrhenius plot for the mechanical stirring + PFA + PTA, (D.1) 1st order fit of the experimental data for only ultrasound treatment + PFA + PTA; (D.2) Arrhenius plot for the only ultrasound treatment + PFA + PTA.

4.4.4 Results of Cavitation Bubble Dynamics Simulations

The summary of results of cavitation bubble dynamics simulations for a 5 micron air bubble in toluene and representative graphical simulations of the radial motion of cavitation bubble are shown in chapter 2. It could be seen that the temperature and pressure conditions in the cavitation bubble reach extreme during transient collapse at atmospheric static pressure, which are sufficient to cause thermal dissociation of N_2, O_2 and toluene (C_6H_5–CH_3) molecules entrapped in the bubble into numerous chemical species – some of which are radical species. The predominant species generated during transient cavitation, which can contribute to DBT oxidation, is the $O^{\bullet}$ radical. Shock waves with high pressure amplitude emitted by cavitation bubble can create very fine emulsion of aqueous/organic phases with enormous interfacial area, which can boost the reaction kinetics.

Raising of the static pressure in reaction mixture results in drastic reduction of physical and chemical effects of transient cavitation. Not only the temperature and pressure peaks generated at transient bubble collapse drop sharply, but the magnitudes of shock waves (or acoustic pressure waves) and micro–turbulence generated by the bubble also shows marked reduction. Moreover, no formation of any radical species is seen from thermal dissociation of the bubble contents at the moments of transient collapse at elevated static pressure.

4.5 DISCUSSION

Concurrent analysis of the DBT oxidation in different experimental categories, simulations of cavitation bubble dynamics, and the trends in Arrhenius and thermodynamic parameters give an interesting mechanistic account of the PTA–assisted oxidative desulfurization as described below:

(1) Mechanical agitation of reaction mixture at 600 rpm generates limited interfacial area, which results in low (~ 28.3%) DBT oxidation. PTA cation forms a complex with oxidant anion, which is transported across the interphase. After completion of the oxidation reaction in organic phase, the PTA–cation returns to the aqueous phase. The chemical mechanism of PTA–assisted oxidative desulfurization with mechanical agitation is depicted in scheme 4.1. It could be perceived from scheme 4.1 that the process has purely ionic character. Addition of PTA to this system enhances DBT oxidation by more than 2× as a result of faster and effective transfer of oxidant across interface. This is reflected in reduction of activation energy of the oxidative desulfurization, as pointed out by Zhao et al. (2007). For same reason, the net enthalpy change (ΔH) for oxidative desulfurization also reduces with use of PTA.

(2) Despite very low activation energy and intense emulsification, the extent of DBT oxidation in ultrasound assisted system (category A.2) is almost same as that for mechanically agitated system (category A.1). This result is attributed to radical based mechanism of ultrasound–assisted oxidative desulfurization as shown in scheme 4.1. The oxidative radicals ($O^{\bullet}$) generated by transient bubble collapse are highly unstable and do not diffuse or penetrate much in the reaction medium from the point of bubble collapse. Hence, the probability of their interaction with DBT molecules is rather limited, which is reflected in low value of frequency factor (A) as compared to the mechanical agitated system (category A.1), and low DBT oxidation. Nonetheless, since $O^{\bullet}$ radicals are extremely energetic species (oxidation potential of 2.42 eV), the activation energy for the DBT oxidation induced by these species is quite small. For the same reasons, ΔH for category A.2 is much smaller than that for category A.1.

(3) With simultaneous use of PTA and ultrasound (as in categories B.2 and C.1), the chemical mechanism of the oxidative desulfurization has dual character, *viz*. ionic and

radical. The cation of PTA forms a complex with anion of oxidant. This reduces the polarity of the oxidant anion, which assists its effective transfer across interface to non–polar organic phase. It should however be noted that complexation of oxidant–anion with PTA–cation does neutralize latter's polarity, and hence, the overall mechanism of oxidative desulfurization has still ionic character. On a comparative basis, the process of complex formation between PTA–cation and oxidant–anion, the transfer of this complex across interface and the reaction between oxidant and DBT molecules, requires higher activation energy than the radical–induced DBT oxidation within organic phase. However, as the amount of oxidant and PTA present in the system is in large excess as compared to DBT (more specifically 1.24 mM of PTA, 25 mM of PFA oxidant, and 0.54 mM of DBT), the contribution of PTA–based oxidation to overall DBT oxidation is much higher than radical–induced oxidation. Thus, the chemical mechanism of PTA–assisted ultrasonic oxidative desulfurization is predominantly ionic, which is manifested in terms of higher activation energy as compared to ultrasonic oxidative desulfurization. Explanation for ~ 4× higher ΔH value for category B.2 as compared to category A.2 can also be given along similar lines. Due to contribution of radical–induced reactions to overall DBT oxidation in category B.2, the activation energy for this category is ~ 2× lesser than that for category B.1, in which PTA is applied with mechanical stirring. The role of ultrasound and cavitation in experimental categories B.2 and C.1 is more or less of physical nature, i.e. emulsification between organic and aqueous phase.

(4) Reduction in intensity of transient cavitation at elevated static pressure in category C.1, as indicated by results of simulation of cavitation bubble dynamics, is manifested in terms of lesser emulsification and interfacial area, as compared to the category B.2. The physical and chemical effects of transient cavitation are practically eliminated at

elevated static pressure. This causes significant reduction in intensity of micro–convection in the reaction system, which in turn, adversely affects emulsification and interfacial area. In this case, the ultrasonic system resembles a mechanical stirred system (as in category B.1). This essentially results in lesser DBT oxidation in category C.1. However, the micro–streaming induced by ultrasound (which remains unaffected by elevated static pressure) generates finer emulsion between phases, as compared to (macroscopic) mechanical stirring. Addition of PTA to the reaction system further boosts the extent of DBT oxidation. The beneficial effect of these two factors is manifested in significantly higher (> 2×) DBT oxidation, as compared to categories A.1 and A.2.

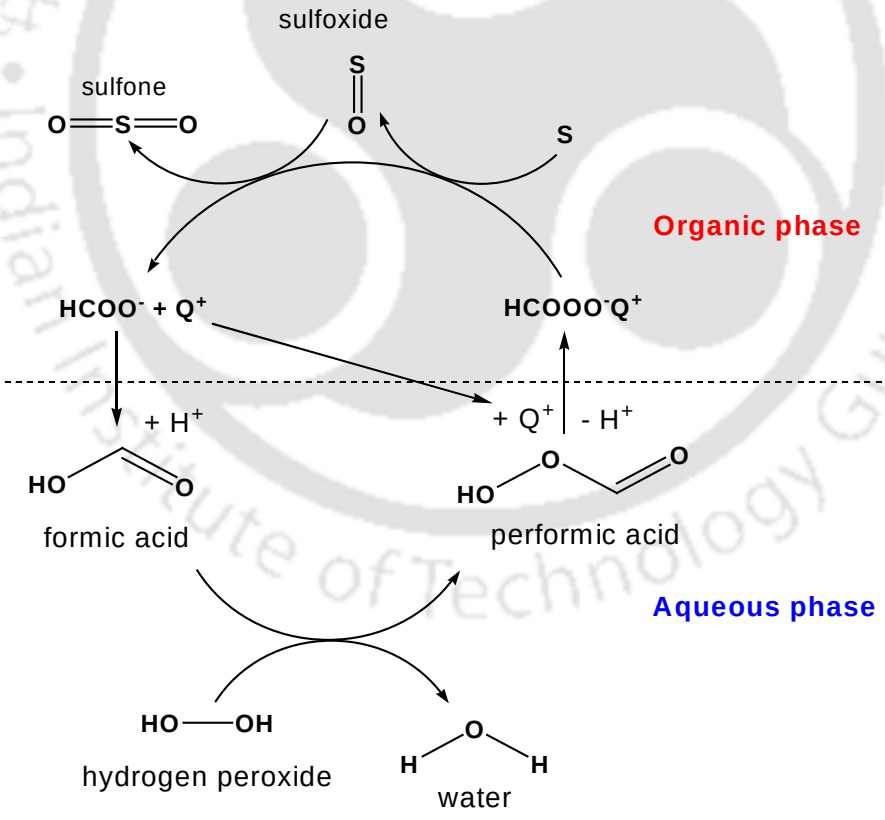

Scheme 4.1: The cyclic mechanism of phase transfer agent (PTA) during oxidative desulfurization with performic acid

$$HCOOH + H_2O_2 \longrightarrow HCOOOH + H_2O$$

$$HCOOOH \longrightarrow HCO^{\bullet} + HO_2^{\bullet}$$

$$C_{12}H_8S + HO_2^{\bullet} \longrightarrow C_{12}H_8SO + {}^{\bullet}OH$$

$$C_{12}H_8SO + HO_2^{\bullet} \longrightarrow C_{12}H_8SO_2 + {}^{\bullet}OH$$

Scheme 4.2: Reaction mechanism for performic acid induced oxidative desulfurization

(5) The entropy change values (–Δ*S*) in different experimental categories are again a manifestations of the predominant chemical mechanism of oxidative desulfurization. The highest (–Δ*S*) values are seen for category A.2, in which the chemical mechanism for oxidative desulfurization is purely radical–based and reactions occur almost instantly. The (–Δ*S*) values for mechanically stirred system increase with addition of PTA, indicating faster reactions. (–Δ*S*) values for category B.2 are intermediate between that of categories B.1 and A.2, indicating dual (ionic and radical induced) nature of the chemical mechanism of the PTA–assisted oxidative desulfurization. The dual nature of chemical mechanism in category B.2 also results in pseudo 1st order kinetic constants of intermediate value between the constants for categories A.2 and B.1.

(6) Despite significantly dissimilar chemical mechanisms that lead to dissimilar values of Δ*H* and (–Δ*S*), the Gibbs energy change (Δ*G*) is almost similar (±5%) for experimental categories B.1 and B.2, in which PTA was simultaneously applied with ultrasound. This essentially is an indication of the physical role played by ultrasound in PTA–assisted oxidative desulfurization. Moreover, lesser (Δ*G*) values for categories B.1 and B.2, as compared to categories A.1 and A.2, respectively, point out

supportive effect of the PTA in enhancement of the oxidative desulfurization by effective interphase transport of oxidant anion.

4.6 CONCLUSION

Concurrent analysis of extent of DBT oxidation and Arrhenius & thermodynamic parameters for different experimental conditions, and results of simulations of cavitation bubble dynamics presented in this study has revealed a cogent and coherent picture of the physical mechanism of the PTA–assisted ultrasonic oxidative desulfurization process. Essentially, this study has identified and established the links (or interactions) between the individual mechanisms of PTA and ultrasound/ cavitation in oxidative desulfurization process. Although ultrasonic oxidative desulfurization has the lowest activation energy and enthalpy change with the highest negative entropy change, the overall DBT oxidation achieved in this process is lesser due to low frequency factor, which is a consequence of high instability of the radicals generated by transient cavitation. Thus, contribution of chemical effect of transient cavitation to DBT oxidation is relatively small. The predominant mechanism of PTA–assisted oxidative desulfurization is ionic, which results in relatively higher activation energy and enthalpy change as compared to ultrasonic oxidative desulfurization. The synergistic effect of fine emulsification generated due to physical effect of micro–convection induced by transient cavitation and ultrasound, and PTA–assisted effective interphase transport of oxidant leads to almost complete conversion of DBT to DBT sulfone. It is thus established that prevalent role of ultrasound and cavitation in PTA–assisted ultrasonic oxidative desulfurization process is of physical nature that helps in boosting the beneficial effect of PTA for enhancement of DBT oxidation.

REFERENCES

1. Srivastava VC. An Evalution of desulfurization technologies for sulfur removal from liquid fuels. *RSC Adv*. 2012; 2: 759–783.

3. Doraiswamy LK. Organic synthesis engineering. New York; Oxford University Press:2001.

4. Mei H, Mei BW, Yen TF. A new method for obtaining ultra–low sulfur diesel fuel via ultrasound assisted oxidative desulfurization. *Fuel*. 2003;82:405–414.

5. Etemadi O, Yen TF. Selective adsorption in ultrasound–assisted oxidative desulfurization process for fuel cell reformer application. *Energ. Fuel.* 2007;21:2250–2257.

6. Wan MW, Yen TF. Enhance efficiency of tetraoctyl ammonium fluoride applied to ultrasound assisted oxidative desulphurization (UAOD) process. *Appl. Catal. A.* 2007;319:237–245.

7. Hagenson LC, Doraiswamy LK. Rate enhancement in a solid–liquid reaction using PTC, microphase, ultrasound and combination thereof. *Chem. Eng. Sci.* 1994;49:4787 – 4800

8. Hagenson, LC, Doraiswamy L.K. Comparison of the effects of ultrasound and mechanical agitation on a reacting solid–liquid system. *Chem. Eng. Sci.* 1998;53(1):131–148.

12. Zhao D, Ren H, Wang J, Yang Y, Zhao Y. Kinetics and mechanism of quaternary ammonium salts as phase–transfer catalysts in the liquid–liquid for oxidation of thiophene. *Energ. Fuel.* 2007;21:2543–2547.

13. Chakma S, Moholkar VS. Investigations in synergism of hybrid advanced oxidation processes with combinations of sonolysis + fenton process + UV for degradation of bisphenol–A. *Ind. Eng. Chem. Res.* 2014;53:6855–6865.

14. Gogate PR, Tatake PA, Kanthale PM, Pandit AB. Mapping of sonochemical reactors: review, analysis, and experimental verification. *AIChE J.* 2002;48:1542–1560.

15. Naik SD, Doraiswamy LK. Phase Transfer Catalysis: Chemistry and Engineering. *AIChE J.*1998;44:612–646.

16. Wang M–L, Yang H–M. Kinetic study of synthesizing 2,4,6–tribromophenol allyl ether by phase–transfer catalytic reaction. *Ind. Eng. Chem. Res.* 1990;29:522–526.

17. Wang M–L, Yang H–M. Simplified dynamic model for the allylation of 2,4,6–tribromophenol by phase transfer catalyst. *Ind. Eng. Chem. Res.* 1991;30:631–635.

18. Wang M–L, Yang H–M. Dynamic of phase transfer catalyzed reaction for the allylation of 2,4,6–tribromophenol. *Chem. Eng. Sci.*1991;46:619–627.

19. Bhattacharya A. General Kinetic Model for Liquid–Liquid Phase–Transfer Catalyzed Reactions. *Ind. Eng. Chem. Res.*1996;35:645–652.

20. Wang M–L, Chen W–H. Kinetic study of synthesizing dimethoxydiphenylmethane under phase–transfer catalysis and ultrasonic irradiation. *Ind. Eng. Chem. Res.* 2009;48:1376–1383.

21. Toegel R; Gompf B; Pecha R; Lohse D. Does Water Vapor Prevent Upscaling Sonoluminescence? *Phys. Rev. Lett*. 2000;85:3165–3168.

22. Storey BD, Szeri AJ. Water Vapor, Sonoluminescence and Sonochemistry. *Proc. R. Soc. London, Ser. A.*2000;456:1685–1709.

23. Sivasankar T, Paunikar AW, Moholkar VS. Mechanistic approach to enhancement of the yield of a sonochemical reaction. *AIChE J*. 2007;53:1132–1143.

24. Moholkar VS, Sable SP, Pandit AB. Mapping the cavitation intensity in an ultrasonic bath using the acoustic emission. *AIChE J*. 2000;46:684–694.

25. Krishnan SJ, Dwivedi P, Moholkar VS. Numerical investigation into the chemistry induced by hydrodynamic cavitation. *Ind. Eng. Chem. Res*. 2006;45:1493–1504.

26. Kumar P, Khanna S, Moholkar VS. Flow regime maps and optimization thereby of hydrodynamic cavitation reactors. *AIChE J*. 2012;58:3858–3866.

27. van Wijngaarden L. On the equations of motion for mixtures of liquid and gas bubbles. *J Fluid Mech*. 1968;33:465–474.

28. Capocelli M, Musmarra D, Prisciandaro M, Lancia A. Chemical effect of hydrodynamic cavitation: Simulation and experimental comparison. *AIChE J*. 2014;60:2566–2572.

29. Reid RC, Prausnitz JM, Poling BE. Properties of gases and liquids. New York: McGraw−Hill, 1987.

30. Hirschfelder JO, Curtiss CF, Bird RB. Molecular theory of gases and liquids. New York:Wiley, 1954.

31. Condon EU, Odishaw H. Handbook of physics. New York: McGraw− Hill, 1958.

32. Zhou J, Lu X, Wang Y, Shi J. Molecular dynamics investigation on the finite dilute diffusion coefficients of organic compounds in supercritical carbon dioxide. *Fluid Phase Equilib*. 2000;172:279–291.

33. Zhu Y, Lu X, Zhou J, Wang Y, Shi J. Prediction of diffusion coefficients for gas, liquid and supercritical fluid: Application to pure real fluids and infinite dilute binary solutions based on the simulations of Lennards–Jones fluid. *Fluid Phase Equilib*. 2000;194−197:1141–1159.

34. Press WH, Teukolsky SA; Flannery BP; Vetterling, WT. *Numerical recipes*. New York; Cambridge University Press:1992.

35. Keller JB, Miksis MJ. Bubble oscillations of large amplitude. *J. Acoust. Soc. Am.* 1980; 68: 628–633.

36. Brenner M, Hilgenfeldt S, Lohse D. Single–bubble sonoluminescence. *Rev. Mod. Phys.* 2002; 74: 425–484.

37. Chemical Equilibrium Calculation (Bioanalytical Microfluidics Program, Colorado State University), (accessed January 2013).

38. Leighton TG. The acoustic bubble. San Diego: Academic Press, 1994.

29. Grossmann S, Hilgenfeldt S, Zomack M, Lohse D. Sound radiation of 3 MHz driven gas bubbles. *J Acoust Soc Am.* 1997;102:1223–1227.

40. Moholkar VS, Warmoeskerken MMCG. Integrated approach to optimization of an ultrasonic processor. *AIChE J.* 2003;49:2918–2932.

भारतीय प्रौद्योगिकी संस्थान गुवाहाटी
Indian Institute of Technology Guwahati

CHAPTER 5

ULTRASOUND ASSISTED MICROBIAL DESULFURIZATION

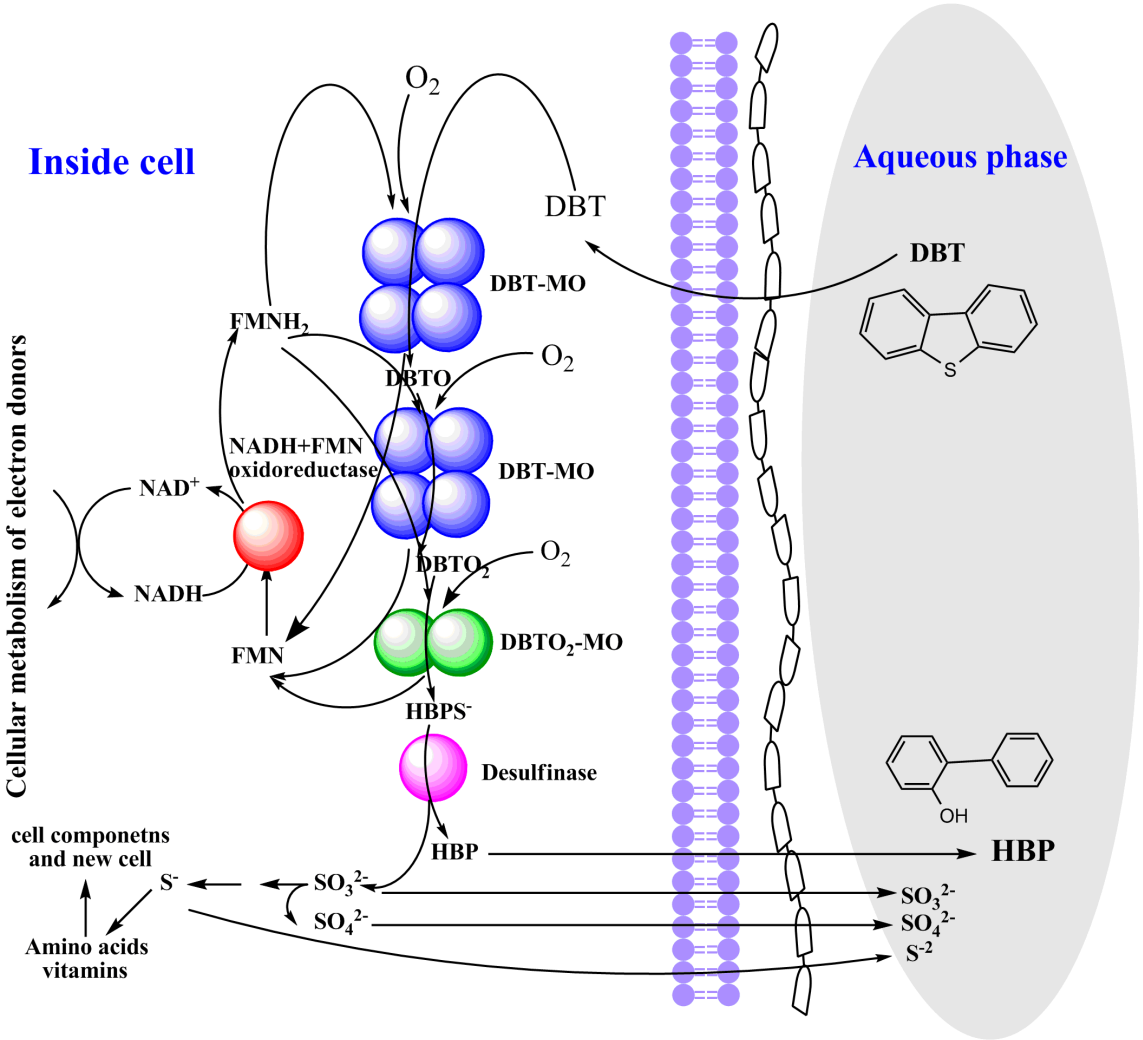

Ultrasound Assisted Microbial Desulfurization

5.1 INTRODUCTION

In the previous chapters, studies in oxidative desulfurization using chemical oxidant systems of peracids coupled with either Fenton system or phase transfer agent have been presented. These systems make use of strong and corrosive chemicals like acetic acid, formic acid and hydrogen peroxide. The alternate desulfurization technique, based on oxidation of the sulfur compounds, which has emerged in last few decades, is biodesulfurization (either microbial desulfurization or enzymatic desulfurization). Biodesulfurization has special merit of being eco–friendly and operation at mild conditions (Borgne et al., 2003). Numerous bacterial species such as *Arthrobacter*, *Pseudomonas* and *Rhodococcus* have been identified to be capable of metabolizing and biotransformation of DBT.

As mentioned in Chapter 1, three principal pathways have been identified for the metabolism of organo–sulfur compounds, viz. (1) reductive scission of C–S bond, (2) oxidative scission of C–S bond, and (3) oxidative scission of C–C bond. Among

these, the oxidative C–C bond scission mechanism, where the initial attack is directed against one of

the carbon atoms, is the destructive pathway (also known as Kodama pathway) (McFarland et al., 1998). This is rather undesired, as it leads to fragmentation of phenyl ring and loss of fuel value (Gupta et al., 2005). The other mechanism involving oxidative C–S bond scission is known as 4S pathway. This pathway involves successive oxidation of DBT to the final product of hydroxyl–biphenyl. The sulfur–containing intermediates of this pathway are: DBT–sulfoxide, DBT–sulfone and hydroxyl–phenyl benzene sulfinate. The first three conversion steps in 4–S pathway of DBT metabolism (DBT → DBTO → $DBTO_2$ → HPBS) are proposed to occur inside the cell (Monticello, 2000). The final product hydroxyphenyl benzene sulfinate (HPBS) is probably secreted in water. This product is soluble in water and is acted upon by the enzyme HPBS desulfinase to form 2-hydroxybiphenyl (2-HBP) and sulfate. 2-HBP, being hydrophobic, returns to the oil phase, thus conserving the fuel value. The exact biophysical mechanism of ultrasonic enhancement microbial biodesulfurization is not established yet.

In this chapter, we have attempted to deduce the biophysical mechanism of ultrasound assisted biodesulfurizarion. Experimental results on biodesulfurizarion have been coupled to simulations and cavitation bubble dynamics. Moreover, the kinetic data of the biodesulfurization has been fitted to the Haldane kinetics model. Analysis of variations in the numerical values of the parameters of Haldane kinetic model in different experimental categories vis-à-vis simulations of cavitation bubble dynamics has given an interesting mechanistic account of the influence of ultrasound on biodesulfurizarion process.

5.2 MATERIALS AND METHODS

5.2.1 Chemical and Reagents

The following chemicals have been used in the experiments: dibenzothiophene (98%, Sigma Aldrich) as model sulfur compound, β–cyclodextrin (β–CD, 95%, Himedia) as surfactant (or phase transfer agent), toluene (synthesis grade, Merck) as model liquid fuel, acetonitrile (HPLC grade, Merck) as mobile phase for HPLC analysis. HPLC was calibrated for product profile using 2–HBP (Sigma Aldrich). Reticulated polyurethane foam (density: 15 kg/m^3) was used as support for immobilization and was purchased from local market. All chemicals were used as received without any pre–treatment.

5.2.2 Microorganism Growth and Maintenance

Rhodococcus rhodochrous MTCC 3552 (ATCC 53968) was procured from Microbial Type Culture Collection (MTCC), Chandigarh. The cells were grown aerobically at 30°C for 24 h in 100 mL nutrient broth (NB) medium. The composition of NB medium was as follows: Beef extract 1.0 g, yeast extract 2.0 g, peptone 5.0 g, NaCl 5.0 g in 1 L distilled water. The pH was adjusted to 7.0 prior to autoclaving. The medium was placed into 250 mL Erlenmeyer flasks on a rotary shaker incubator (Make: Lab Companion; Model: SI–300R) at 150 rpm for 24 h. The cultures were used for streaking over agar plate having NB medium with 15 g/L of agar. This was kept at 4°C as stock culture and was sub–cultured every month.

5.2.3 Inoculum Preparation and Fermentation Media Composition

The cells from stock culture were grown in fresh NB medium prior to inoculation. 5% (v/v) of inoculum from mid–log phase of culture was used for

biodesulfurization (BDS) reaction. The BDS reaction was carried out in Basal Salt Medium (BSM). The BSM was a sulfur free medium prepared in deionised water with following composition (in g/L): 4 – $Na_2H_2PO_4$, 4 – K_2HPO_4, 2 – NH_4Cl, 0.2 – $MgCl_2$, 0.001 – $CaCl_2$, 0.001 – $FeCl_3$ and 2 – glycerol as a carbon source. The pH of the BSM adjusted to 7.0 (Kilbane, 1989; Kayser et al., 1993). DBT was used as a sulfur source. Experiments were carried out using three initial concentration of DBT in toluene as: 0.54 mM (100 ppm), 1.08 mM (200 ppm) and 1.62 mM (300 ppm). Toluene with dissolved DBT (with required initial concentration) was added to sterilized BSM. The volume ratio of organic to aqueous phase was maintained at 1.0 (v/v) as per the results of preliminary experiments for optimization of this parameter. Cultures were incubated on rotary shaker at 180 rpm at 30°C.

5.2.4 Immobilization and Cross Linking of Cells

The cells were immobilized on commercial grade polyurethane foam (cut into cubical pieces of dimensions 1 cm × 1 cm × 1 cm). These pieces were autoclaved prior to addition to the broth at the onset of log phase of the culture. The polyurethane pieces (or immobilization support) were incubated for 24 h in NB broth at 30°C with shaking at 180 rpm. After incubation, the polyurethane pieces were separated from the broth. The immobilization support was shaken with phosphate buffer (50 mM, pH 7.0) for 10 min. It was then washed twice with phosphate buffer and dried for 24 h at room temperature. The immobilized cells on the support were incubated with 0.1% (1 mM) glutaraldehyde solution for 1 h for cross–linking, followed by washing with phosphate buffer and subsequently drying at room temperature for 24 h. The extent of immobilization of the cells on the support was assessed by sonication of the support (in phosphate buffer as the medium) that would release all proteins inside immobilized cells. Lowry assay was carried out on the extract to determine presence

of proteins. A positive test confirmed the presence of proteins, which were released from the cells immobilized on the surface of the support. Moreover, immobilization and cross–linking of the cells on the support was also assessed with FE–SEM micrographs. These micrographs are given in Fig. 5.1.A, which clearly show proper immobilization of the cells on the surface of support in high density.

5.2.5 Experimental Setup for Sonication Experiments

A schematic diagram of experimental setup is shown in Fig. 5.1.B. An ultrasound bath (Make: Elma, Germany; Model: Transonic T–460; volume: 2 L; frequency: 35 kHz; power: 35 W) was used for sonication of the reaction mixture. The dimensions of this bath were (L × W × H: 25 cm × 15 cm × 10 cm) with transducers attached to the bottom of the bath. The bath was filled with water, which forms the medium for ultrasound propagation. BDS reactions were carried out in an Erlenmeyer flask (volume: 250 mL; dimensions: 85 mm × 140 mm) made of Borosilicate glass. The total volume of reaction mixture in all experiments was 100 mL. The flask was placed in the center of the bath. As the ultrasound intensity in the bath shows significant spatial variation (Moholkar et al., 2000), the position of the flask was carefully maintained the same in all experiments. The actual acoustic power dissipation was measured using calorimetric method. The corresponding pressure amplitude of the ultrasound waves generated in the bath was determined using calorimetric method as 150 kPa (Sivasankar et al., 2007). The temperature of water in the bath during sonication of reaction mixture was maintained at $30^{o}\pm2^{o}C$ by replacing water in the bath at regular interval. The sonication of the reaction mixture was carried out with duty cycle of 20% (i.e. 2 min ON and 8 min OFF in every 10 min of treatment), which was optimized in preliminary experiments on the basis of DBT reduction achieved for different values of duty cycles.

5.2.6 Experimental Categories

Experiments were carried out in two phases, viz. preliminary experiments and main experiments. The preliminary experiments were aimed at optimization of following parameters:

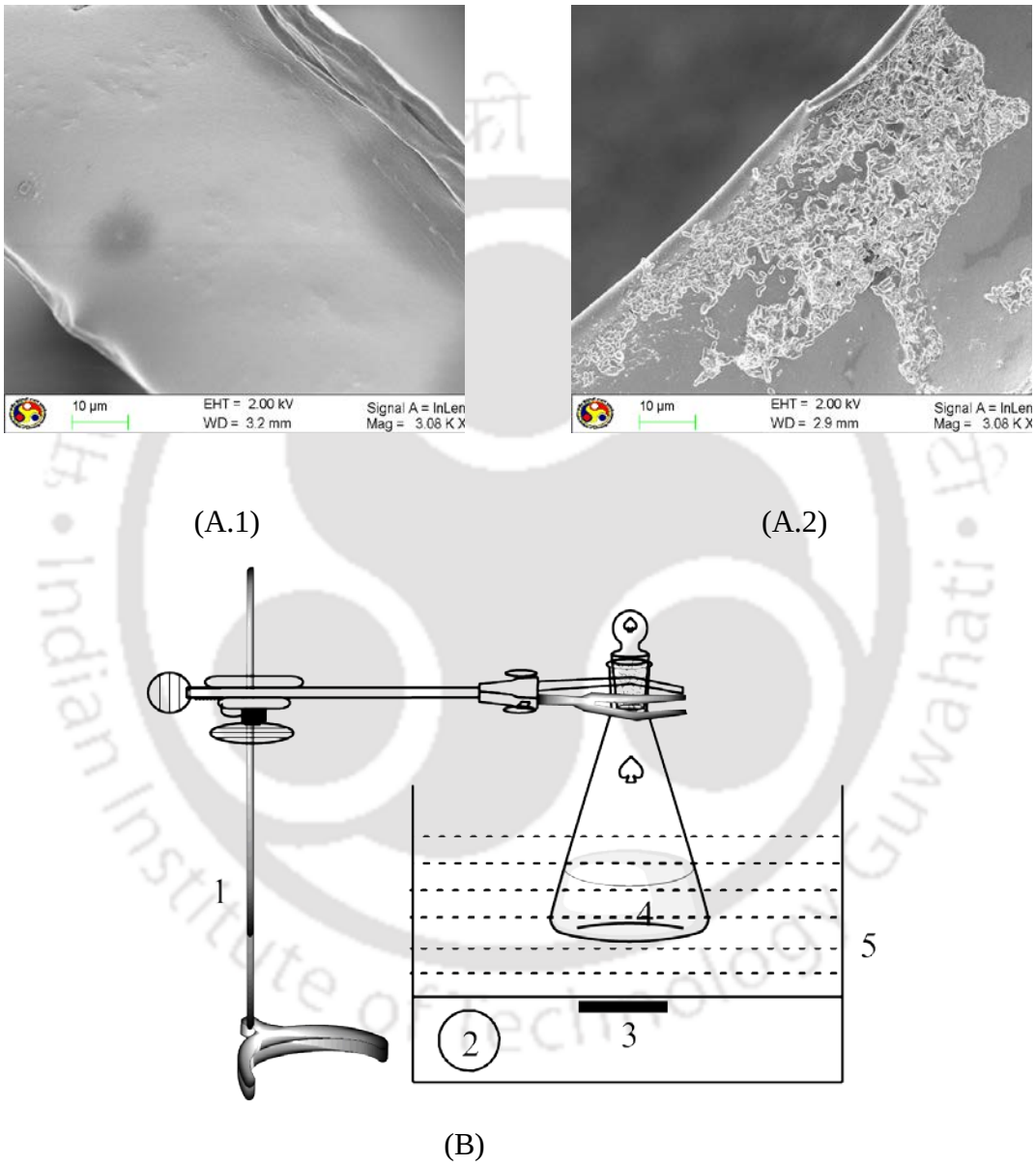

Figure 5.1: (A) FE-SEM micrographs of: (A.1) PU foam without cells, (A.2) *Rhodococcus rhodochrous* cells immobilized on PU foam. (B) Schematic of the experimental setup. Legends: 1. stand, 2. timer, 3. piezoelectric transducers, 4. reaction flask, 5. ultrasound bath.

(1) volume ratio of the aqueous and organic phases, (2) addition of surfactant (or phase transfer agent), and (3) amount of immobilization support. Main experiments were divided in 4 categories, viz. A, B, C and D as described in Table 5.2, employing different experimental conditions such as use of free or immobilized cells, mechanical agitation or sonication, and addition of surfactant that enhanced interphase DBT transport.

5.2.7 Analysis

The cell concentration in the reaction mixture was determined from the optical density at 660 nm (OD_{660}). Dry cell weight was determined after centrifugation of the culture broth at 10,000 rpm followed by drying the pellets at 100^{o}C till constant weight was achieved. Reduction of DBT and formation of the final product 2–hydroxybiphenyl (2–HBP) were quantified using High Performance Liquid Chromatography (HPLC) (Shimadzu, Model: UFLC SPD–20A) equipped with reverse phase C–18 column (5 µm, 4.6 mm × 250 mm) and UV detector (λ_{max} = 287 nm). The mobile phase was a mixture of acetonitrile and water (80:20 v/v) with flow rate 1 mL/min. The intermediates of microbial DBT oxidation were identified by GC–MS analysis (Varian 240, equipped with VF – 5 ms column, 30 m × 0.25 m ID, DF = 0.25) of the same reaction sample. 1 µL of sample was injected with a split ratio of 10:1. The temperature program was as follows: injection temperature – 250^{o}C, column temperature: initial – 100^{o}C, final – 300^{o} C, ramping rate – 7^{o}C/min. The mass detector worked in scan mode with m/z range of 50– 1000 and helium as carrier gas.

5.3. MATHEMATICAL MODELS

5.3.1 Cavitation Bubble Dynamics Model

The reaction mixture in the present study was liquid–liquid heterogeneous comprising organic (toluene) and aqueous (water) phase. Propagation of ultrasound wave through the reaction mixture in the form of compression/ rarefaction cycles induces microstreaming (or oscillatory motion of fluid elements) in both phases. The microstreaming velocity is given as: $u = P_A/\rho_L c$ (Pierce, 1989). Notation: P_A – pressure amplitude of ultrasound wave, ρ_L – density of liquid medium, c – sonic velocity in liquid medium. For ultrasound pressure amplitude of 150 kPa, the micro–streaming velocities in both phases are determined as follows: Toluene: ρ_L = 867 kg/m^3, c = 1275 m/s, and u = 0.137 m/s; Water – ρ_L = 1000 kg/m^3, c = 1481 m/s, and u = 0.101 m/s.

Physical and chemical effects induced by cavitation bubbles in aqueous and organic phases were estimated using simulations of the diffusion limited ordinary differential equation (ODE) model for cavitation bubble dynamics proposed by Toegel et al. (2000) that uses boundary layer approximation. This model is based on the conclusions of Storey and Szeri (2000) that solvent vapor transport and entrapment in the cavitation bubble is essentially a diffusion limited process. The model comprises of 4 ordinary differential equations: (1) Keller–Miksis equation for the radial motion of the bubble, (2) equation for the diffusive flux of water vapor, (3) equation for heat conduction through bubble wall, and (4) overall energy balance. Physical properties of the bubble contents (a mixture of air and vapor) such as thermal conductivity and diffusion coefficient of solvent vapor were determined using Chapman–Enskog theory using Lennard–Jones 12–6 potential. Diffusion of non–condensable gas (i.e. air) across bubble interface during radial motion is ignored in

this model, as the time scale of gas diffusion is much higher than the time scale of bubble dynamics. The set of 4 ODEs can be solved using Runge–Kutta adaptive step size method (Press et al., 1992). The condition for bubble collapse is taken as the first compression after an initial expansion. Numerical values of different parameters used in the model are: Ultrasound frequency (f) = 35 kHz; Ultrasound pressure amplitude (P_A) = 150 kPa; Equilibrium bubble radius (R_o) = 5 and 10 μm; Vapor pressure of water and toluene are calculated using Antoine type correlation. Various physical properties of toluene are as follows: ρ_L = 867 kg/m^3, kinematic viscosity (ν) = 6.8 × 10^{-7} Pa–s, surface tension (σ) = 0.0285 N/m and c = 1275 m/s. Various properties of water are as follows: ρ_L = 1000 kg/m^3,hh kinematic viscosity (ν) = 10^{-6} Pa–s, surface tension (σ) = 0.072 N/m and c = 1481 m/s.

Antoine correlations (in bar) (Chemistry Webbook, NIST 2014):

Toluene: $\log_{10} P_v = 4.08245 - \dfrac{1346.382}{T - 53.508}$

Water: $\log_{10} P_v = 3.55959 - \dfrac{643.748}{T - 198.043}$

5.3.2 Mathematical Model for Microbial Metabolism

The time profiles of product (HBP) formation and substrate consumption were fitted to Haldane kinetics model as suggested by Caro et al. (2007):

$$V_o = \frac{V_{max}[S_o]}{K_m + [S_o] + \dfrac{[S_o]^2}{K_I}}.$$

Various notations are: V_{max} – maximum reaction velocity or rate of product formation, K_m – Michaelis constant, K_I – inhibition constant, V_o – initial velocity of the reaction, S_o – initial substrate concentration. Haldane substrate inhibition kinetic model assumes that the enzyme has two binding sites for the substrate S. First site is a catalytic site that can produce a product, P; and the second is a non-catalytic site that

can produce a product at reduced rate or may not produce any product at all. Binding of substrate to catalytic site results in E·S complex formation ($E + S \rightleftarrows E \cdot S$), while binding of two substrate molecules to both catalytic and non-catalytic site results in formation of complex S·E·S ($E + S \rightleftarrows E \cdot S + S \rightleftarrows S \cdot E \cdot S$). Haldane kinetic model makes three assumptions: (1) binding of substrate to catalytic site precedes the binding to non-catalytic site, (2) no product forms through $S{\cdot}E{\cdot}S$ complex (or the kinetic constant of product formation through $S{\cdot}E{\cdot}S$ complex is zero), and (3) rapid equilibrium for the $E{\cdot}S$ complex formation in reaction: $E + S \rightleftarrows E \cdot S$.

K_I is the dissociation equilibrium for the reaction: $S \cdot E \cdot S \longleftrightarrow S + E \cdot S$. An inspection of the Haldane kinetic expression reveals that reaction velocity goes to zero for excess substrate concentration [S] for which the double binding of substrate to enzyme predominates resulting in non-productive $S{\cdot}E{\cdot}S$ complex. The parameters K_m, K_I and V_{max} in the Haldane kinetic expression have physical significance. Low value of K_m signifies greater affinity of enzyme towards substrate. High value of K_I signifies lesser tendency of enzyme towards substrate binding to non-catalytic site. Finally, high value of reaction velocity V_{max} indicates fast splitting of $E{\cdot}S$ complex into the products. Comparative evaluation of these parameters or constants for different experimental categories employing different experimental conditions gives a mechanistic account of the influence of ultrasound on biodesulfurization process. Numerical values of the three parameters of Haldane kinetics model can be determined by measuring initial reaction velocities of DBT oxidation for three initial substrate concentrations, and solving the Haldane kinetic equation with these values.

It should be noted that biodesulfurization of DBT occurs through four steps that involves four enzymes (DszA, DszB, DszC, Flavin reductase). The physiological

characteristics of each enzyme, and hence, their response to the different experimental conditions, could be distinct from other. The biodesulfurization rate calculated using time profiles reduction in concentration of DBT or increase in concentration of the final product HBP is a manifestation of the overall or gross kinetics of all enzymatic reactions in the metabolic pathway. The numerical values of parameters of Haldane kinetic model fitted to DBT reduction profile are, thus, representative of the "lumped" or "consolidated" physiology of all enzymes involved in the desulfurization metabolism.

5.4. RESULTS AND DISCUSSION

5.4.1 Preliminary Experiments

***Effect of organic (O)/aqueous (A) volume* ratio:** The effect of O/A volume ratio on reduction on DBT (for initial DBT concentration of 0.54 mM or 100 ppm) is depicted in Fig. 5.2.A. The maximum degradation of DBT occurs for volume ratio of 1:1 for both mechanical stirring and sonication. This result can be explained as follows: the extent of DBT reduction depends on two factors, viz. the cell density or population in the reaction mixture and the interfacial area between organic and aqueous phase. Microbial cell concentration (or population) in the reaction mixture reduces for higher O/A volume ratio (or lower fraction of water containing microbial cells in total reaction mixture). While for lower O/A ratio (or higher fraction of aqueous phase in reaction mixture), the extent of emulsification in reaction mixture is reduced. The cause leading to this effect could be high surface tension (and hence interfacial tension) of water due to which toluene does not get dispersed properly in the continuous aqueous phase. In case of sonication, another factor that also contributes to lower dispersion of toluene in aqueous phase is relatively lesser intensity of acoustic

(or shock) waves emitted by cavitation bubbles in water – as explained in greater detail in section on simulations results. The best combination of microbial cell population and interfacial area (or emulsification) is obtained for phase ratio of 1:1, which is reflected in the highest DBT oxidation.

***Optimization of amount of immobilized support*:** The optimum amount of immobilized support in the reaction mixture (for both mechanical agitation and sonication) was determined by varying the number of cubes of polyurethane foam added to reaction mixture. Results shown in Fig. 5.2.B reveal that the highest DBT oxidation was achieved for 2 cubes for both mechanical shaking and sonication system. Lesser cubes reduce the microbial cell population in the reaction medium. Large numbers of cubes in the reaction mixture hinder convection as well as emulsification in reaction mixture. Net result of both of these causes is reduction in DBT oxidation.

***Effect of surfactant*:** β–CD acts as a phase transfer agent for DBT as it forms complexes with DBT that have high solubility in the aqueous phase. The percentage reduction of DBT obtained for different concentration of β–CD is shown in Fig. 5.2.C. The highest DBT oxidation was observed for 20 ppm concentration of β–CD for both free and immobilized cells. At high concentration (> 30 ppm), the surfactant molecules can competitively adsorb on the water-toluene interface along with microbial cells. This effect can hinder access of microbial cells to the DBT molecules that are transported across the interface. This effect is more marked for free cells than the immobilized cells, which are already adsorbed on the polyurethane support and do not compete with surfactant for adsorption on interface.

5.4.2 Main Experiments and Simulations

***Microbial growth and metabolism of biodesulfurization*:** The typical microbial growth profile in experimental category A.1 (free cells with mechanical shaking) is shown in Fig. 5.2.D. It could be seen from Fig. 5.2.D that cell growth and DBT consumption occur simultaneously. This essentially points out that DBT reduction is a growth associated process. The metabolic pathway of DBT reduction was assessed by determination of the degradation intermediates.

The HPLC chromatogram of the reaction mixture (before and after reaction) for category D experiments is shown in Fig. 5.3. The peak corresponding to DBT diminishes significantly after the reaction, with appearance of the peak corresponding to the product 2-HBP. The representative GC–MS chromatogram of reaction mixture in category D1 is shown in Fig. 5.4.A. The mass spectra corresponding to peaks obtained at 15.69, 20.156, 24.01 and 25.31 min are shown in Figs. 5.4.B.1–5.4.B.4.

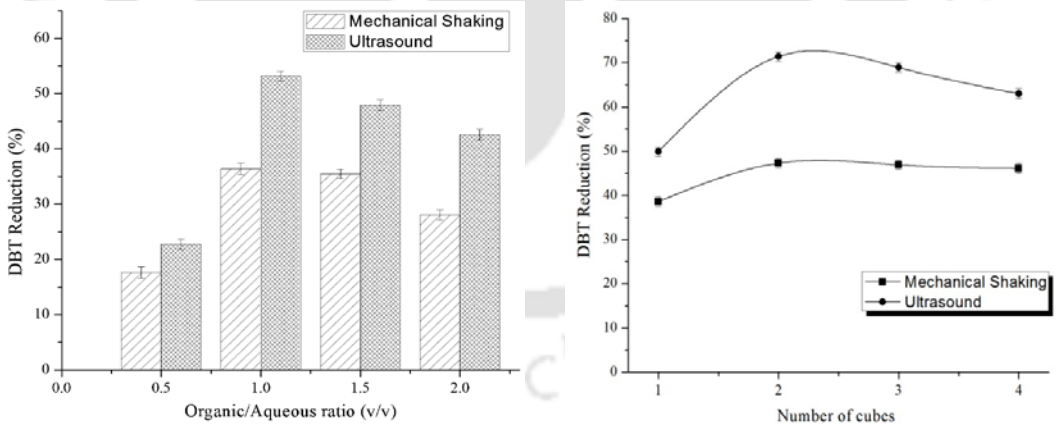

(A) (B)

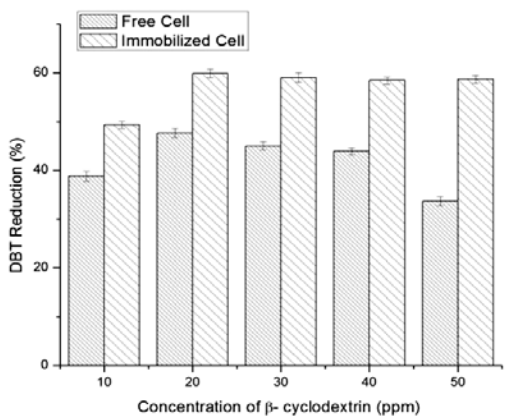

(C)

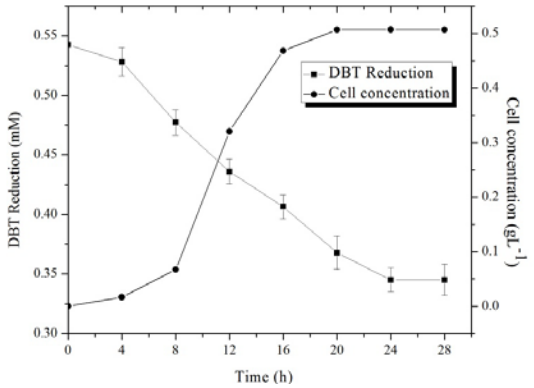

(D)

Figure 5.2: Results of preliminary experiments (influence of different experimental parameters on DBT oxidation). (A) Volume ratio of organic to aqueous phase in reaction mixture for free cells. (B) Amount of immobilized support added to reaction mixture. (C) Effect of addition of β–cyclodextrin (β–CD, a surfactant or phase transfer agent) to reaction mixture under mechanical shaking (volume ratio 1:1). (D) Representative profiles of microbial growth and the substrate (DBT) consumption in experimental category A.1.

The major ions obtained at different m/z (% intensity, proposed derivation from molecular ion, M) values were: 200 (9, [M]+), 184 (100, [M–O]+), 171 (15, [M–CHO]+), 152 (5, [M–O–S]+), 139 (12, [M–COH–S]+), 216 (100, [M]+), 187 (40, [M–COH]+), 168 (23, [M–O–S]+), 160(30, [M–CO–CO]+), 150 (10, [M–OH–OH–S]+), 170 (100, [M]+),142 (35, [M–CHO]+). Results of GC-MS analysis have confirmed formation of intermediates DBT sulfoxide, DBT sulfone and the final product 2-HBP. Similar results have also been obtained for GC-MS analysis of reaction mixture in other experimental categories. Presence of 2-HBP (the final product of 4S pathway) in the reaction mixture essentially confirms that biodesulfurization occurs via 4S pathway in case of both free and immobilized cells. It is noteworthy that although the bioconversion of DBT to the two intermediates, viz. DBT-sulfoxide and DBT-sulfone, occurs inside the microbial cell in the 4S pathway, these intermediates have been detected in the bulk liquid samples drawn from reaction mixture. The presence of these intermediates in bulk liquid are attributed to chemical effects of transient cavitation, as discussed in greater detail in subsequent sections.

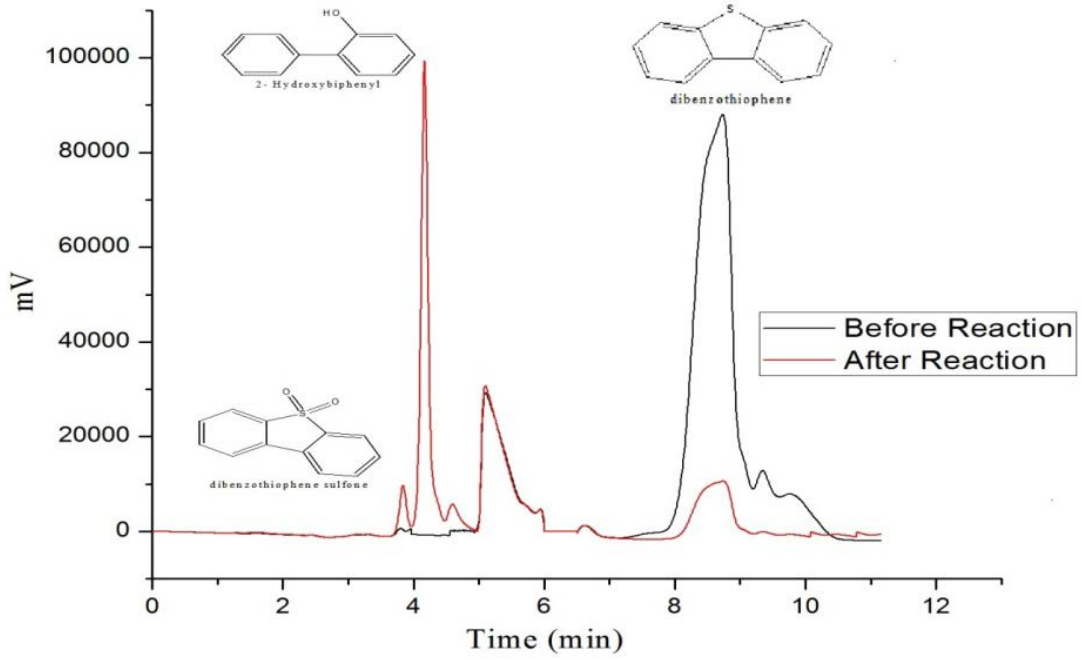

Figure 5.3: HPLC chromatogram for reaction mixture (Experimental category: D)

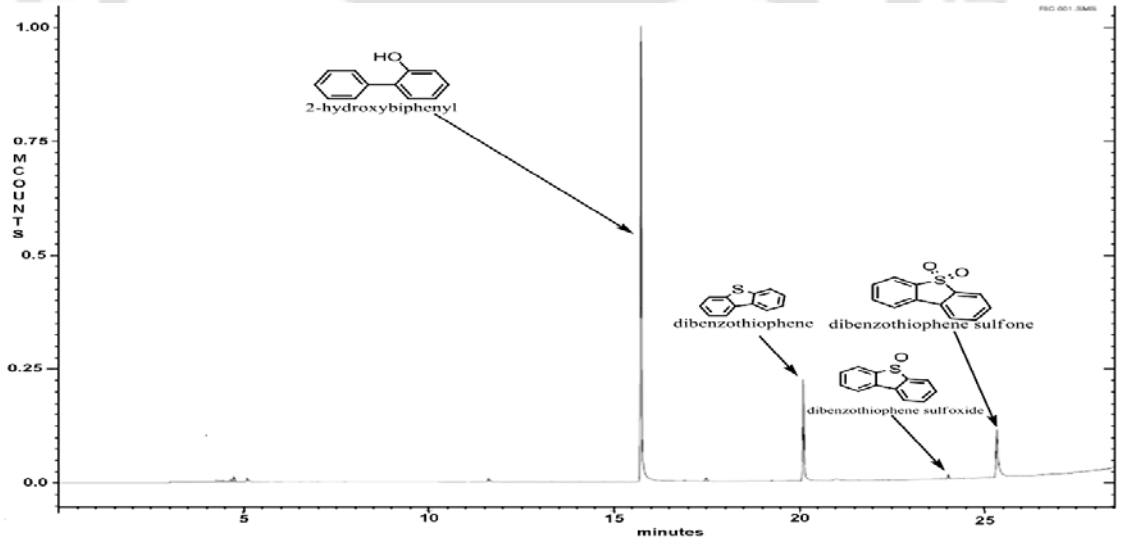

(A)

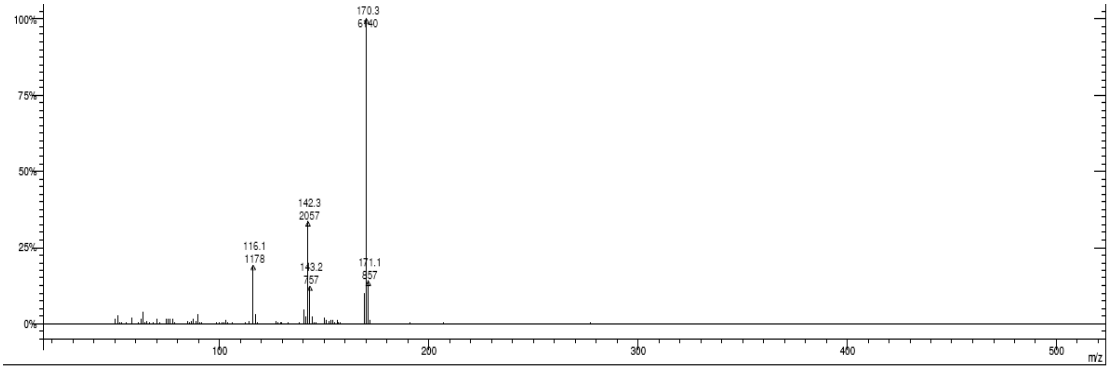
100%
75%
50%
25%
0%
170.3
6440
142.3
2057
116.1
1178
143.2
757
171.1
857
100
200
300
400
500
m/z

(B.1)

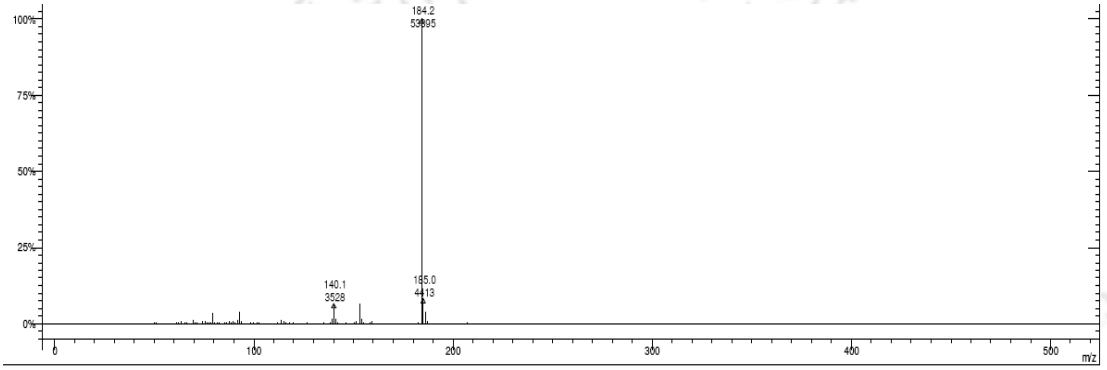
100%
75%
50%
25%
0%
184.2
5385
140.1
3528
185.0
4413
0
100
200
300
400
500
m/z

(B.2)

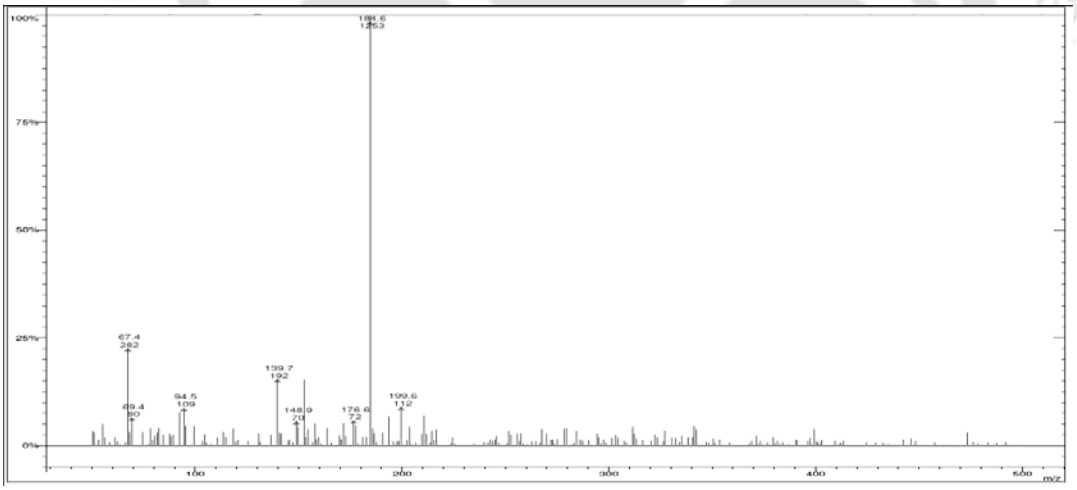
100%
75%
50%
25%
0%
67.4
282
69.4
80
94.5
109
139.7
192
148.9
24
176.6
72
193.6
112
100
200
300
400
500
m/z

(B.3)

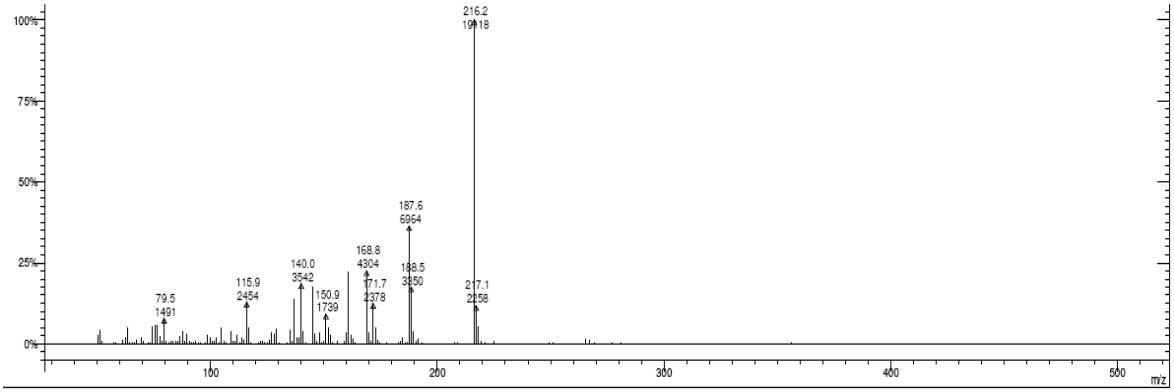

(B.4)

Figure 5.4: (A) GC-MS chromatogram of reaction mixture in experimental category D; (B) Mass spectra of reaction mixture in category D. Peaks obtained at (B.1) 15.69 min (HBP), (B.2) 20.11 min (DBT), (B.3) 20.156 min (DBT sulfoxide), (B.4) 25.322 min (DBT sulfone)

Biodesulfurization profiles and kinetics: Representative time histories of biodesulfurization of DBT and formation of 2-HBP are shown in Fig. 5.5 for initial DBT concentrations of 0.54 mM (100 ppm). The summary of the results for DBT oxidation for all three initial DBT concentrations (0.54, 1.08 and 1.62 mM) are given in Table 5.1 and Figs. 5.6 and 5.7. For all experimental categories, the immobilized cells resulted in higher DBT reduction. Comparative evaluation of DBT reduction in different experimental categories for either free or immobilized cells gives distinct trends of biodesulfurization. Given below are the features of DBT oxidation with initial concentration of 0.54 mM (or 100 ppm). Similar trends are also observed for DBT oxidation with other two initial DBT concentrations, viz. 1.08 mM (200 ppm) and 1.62 mM (300 ppm).

(1) For free cells, sonication of the broth results in marked increase (57.6%) in extent DBT reduction as compared to mechanical shaking. Addition of β-CD during mechanical shaking results in relatively lesser increment of 27.2% in DBT reduction. Combination of sonication and β-CD addition gives an increment of 77% in DBT

reduction.

(2) For immobilized cells, as compared to mechanical shaking, the increments obtained with sonication and β-CD are relatively smaller than free cells. The percentage increments in DBT oxidation obtained for sonication of the reaction mixture, addition of β-CD and sonication with β-CD addition are 51%, 23.8% and 59.8%, respectively.

Simulations results: Representative graphical results of simulations (time histories of radial motion of cavitation bubbles and associated effects such as evaporation of solvent vapor in the bubble, temperature & pressure reached in the bubble, and the microturbulence and acoustic waves generated by cavitation bubble) for an air bubble of 5 micron and 10 micron size in water using the diffusion limited cavitation bubble dynamics model are depicted in Figure 5.8 and 5.9 respectively, and for an air bubble of 5 micron and 10 micron size in toluene are depicted in Figure 5.10 and 5.11 respectively.

Table 5.1. Summary of the experimental results of DBT oxidation in different categories

Experimental Category		η_{DBT} (%) ($C_{f,DBT}$, mM)	η_{HBP} (%) ($C_{f,HBP}$, mM)	η_{DBT} (%) ($C_{f,DBT}$, mM)	η_{HBP} (%) ($C_{f,HBP}$, mM)	η_{DBT} (%) ($C_{f,DBT}$, mM)	η_{HBP} (%) ($C_{f,HBP}$, mM)
		$C_{o,DBT}$ = 0.54 mM (100 ppm)		$C_{o,DBT}$ = 1.08 mM (200 ppm)		$C_{o,DBT}$ = 1.62 mM (300 ppm)	
A.1	Mechanical shaking (FC)*	36.41 (0.34)	29.87 (0.176)	18.87 (0.88)	10.9 (0.063)	12.96 (1.41)	9.62 (0.052)
A.2	Mechanical shaking with sonication (FC)	57.4 (0.23)	40.83 (0.23)	52.78 (0.519)	37.61 (0.22)	32.71 (1.09)	18.91 (0.11)
B.1	Mechanical shaking (IMC)#	47.29 (0.27)	34. (0.2)	64.35 (0.385)	51.86 (0.304)	47.71 (0.84)	35.36 (0.207)
B.2	Mechanical shaking with sonication (IMC)	71.42 (0.155)	49.24 (0.29)	69.44 (0.33)	43.22 (0.253)	45.67 (0.88)	29.97 (0.176)
C.1	Mechanical shaking + β-CD (FC)	47.69 (0.284)	40.05 (0.23)	21.76 (0.845)	16.81 (0.098)	14.52 (1.4)	8.16 (0.048)
C.2	Mechanical shaking with sonication + β-CD (FC)	64.44 (0.192)	51.01 (0.3)	45.78 (0.585)	39.12 (0.229)	30.6 (1.13)	24.87 (0.1461)
D.1	Mechanical shaking + β-CD (IMC)	59.86 (0.216)	43.84 (0.26)	46.67 (0.576)	32.19 (0.1891)	37.86 (1.01)	24.76 (0.145)
D.2	Mechanical shaking with sonication + β-CD (IMC)	75.56 (0.133)	63.91 (0.376)	44.35 (0.601)	39.25 (0.23)	37.03 (1.02)	21.56 (0.126)

Notation: FC – free cells, IMC – immobilized cells, η_{DBT} – percentage DBT oxidation, η_{HBP} – percentage HBP formation, β-CD – experiments with addition of surfactant β-cyclodextrin, $C_{o,DBT}$ – initial concentration of DBT in the reaction mixture, $C_{f,DBT}$ – final concentration of DBT in the reaction mixture, $C_{f,HBP}$ – final concentration of HBP in the reaction mixture. * Category A.1 is considered as the base case for desulfurization with free cells. # Category B.1 is considered as the base case for desulfurization with immobilized cells.

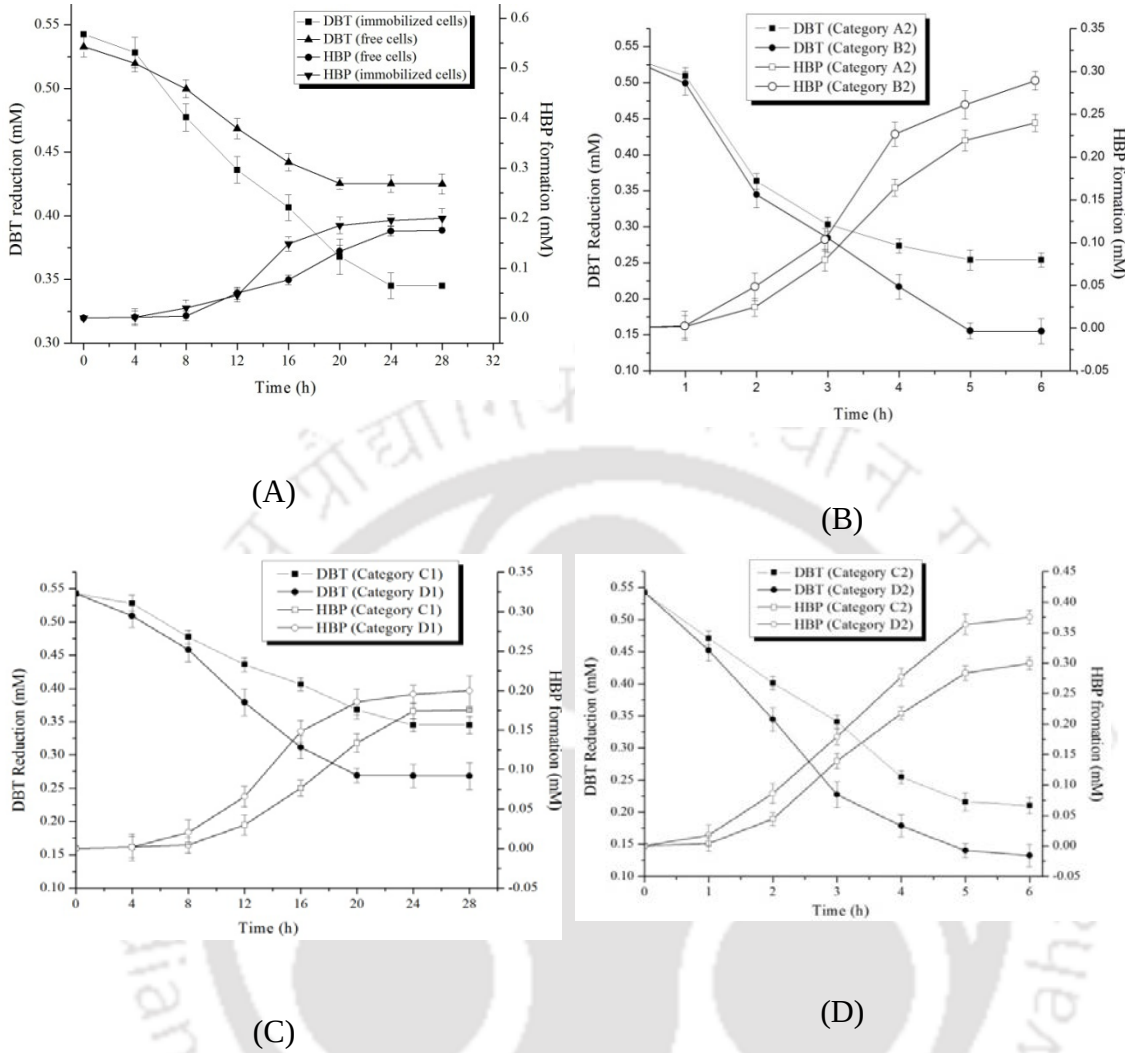

Figure 5.5: Time histories of DBT reduction and HBP formation in different experimental categories for initial DBT concentration of 0.54 mM or 100 ppm. (A) Category A1 and B1, (B) Category A2 and B2, (C) Category C1 and D1, (D) Category C2 and D2.

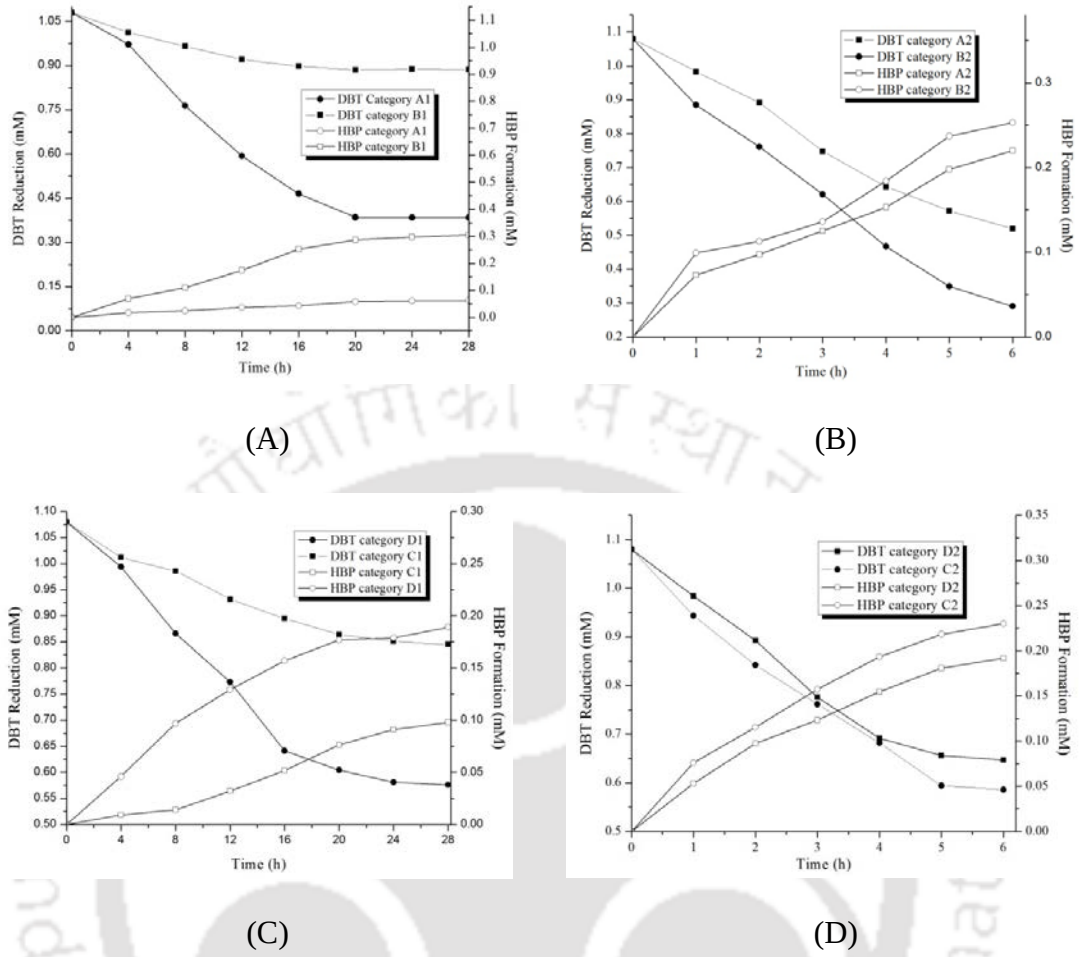

Figure 5.6: Time histories of DBT reduction and HBP formation in different experimental categories for initial DBT concentration of 1.08 mM or 200 ppm. (A) Category A1 and B1, (B) Category A2 and B2, (C) Category C1 and D1, (D) Category C2 and D2.

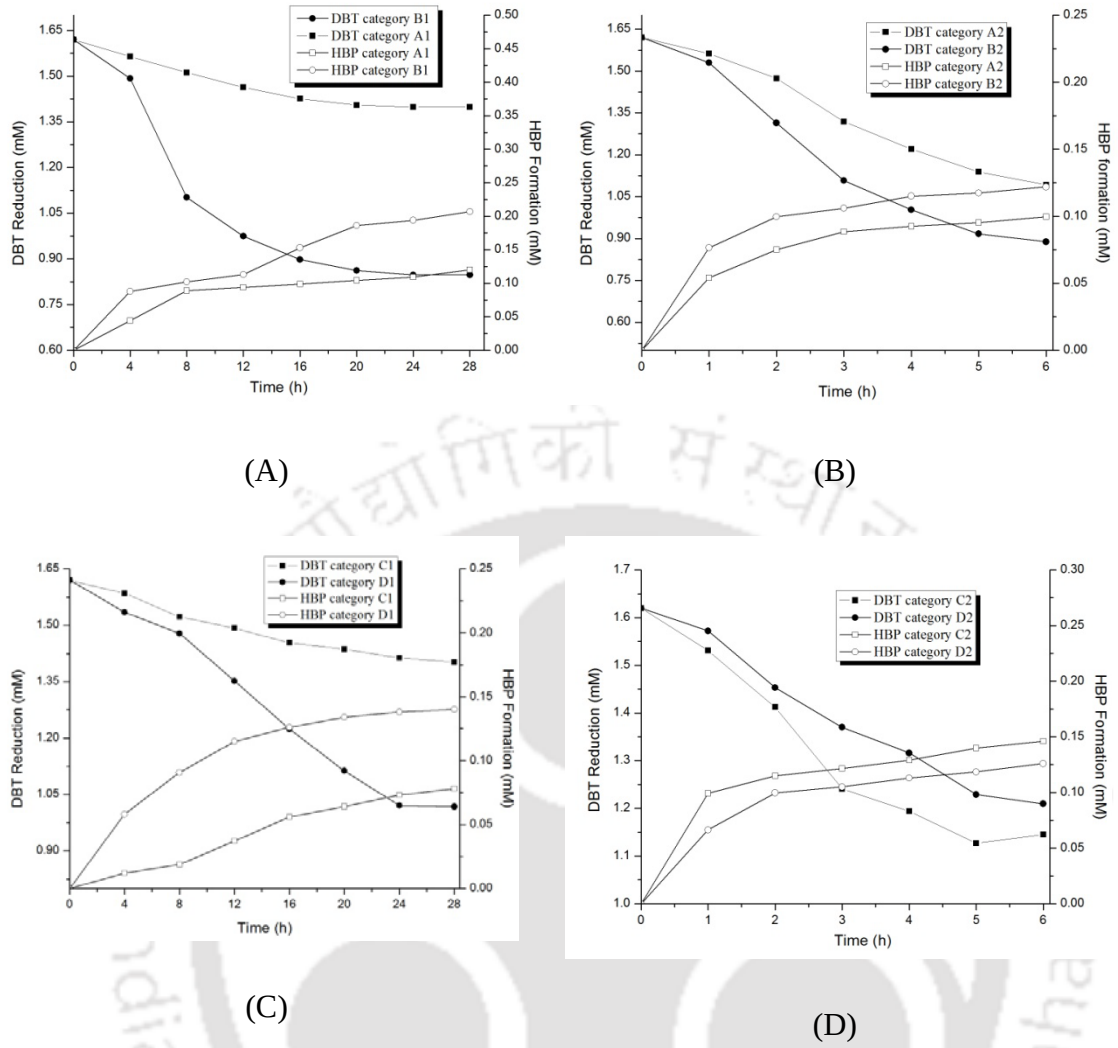

Figure 5.7: Time histories of DBT reduction and HBP formation in different experimental categories for initial DBT concentration of 1.62 mM or 300 ppm. (A) Category A1 and B1, (B) Category A2 and B2, (C) Category C1 and D1, (D) Category C2 and D2.

Summary of entire results of cavitation bubble dynamics simulation is given in Table 5.4. The following features of cavitation bubble dynamics are evident from simulations: (1) The extent of evaporation of water vapor into the bubble is much higher than toluene vapor due to lower vapor pressure of toluene. (2) Smaller bubble (5 micron) produces higher cavitation intensity than larger (10 micron) bubble in terms of temperature and pressure peak attained during collapse. (3) The predominant radical species produced during transient collapse are ˙OH and O˙. However, their

equilibrium mole fractions are quite low (~ 10^{-3} or lower). These radicals can get released into the bulk liquid as the fragments at the instance of minimum radius (or maximum compression) during radial motion. (4) The magnitudes of microturbulence velocities produced by the cavitation bubbles are far smaller than the microstreaming velocities generated by ultrasound (~ 0.1 m/s) for both toluene and water. Nonetheless, the acoustic (or shock) waves emitted by the bubbles also contribute to net convection and emulsification. The magnitude of these waves is much higher for toluene.

5.4.3 Analysis

A concurrent analysis of the values of Haldane kinetics parameters, which are characteristic of the metabolism of biodesulfurization, in different experimental categories along with the results of simulations of cavitation bubble dynamics give an insight into the physical mechanism of ultrasound assisted enhancement in biodesulfurization as discussed below. Before presentation of analysis, we outline the possible synergies between effects of ultrasound and cavitation and biodesulfurization metabolism.

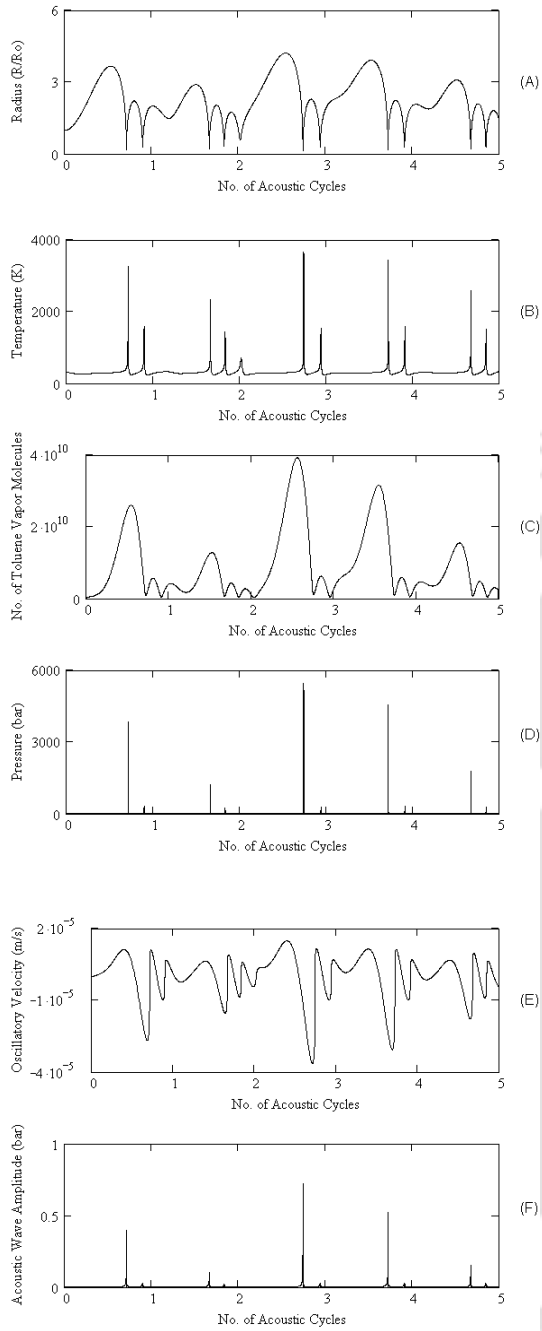

Figure 5.8: Simulation results for cavitation bubble dynamics (5 μm air bubble at 303 K in water)

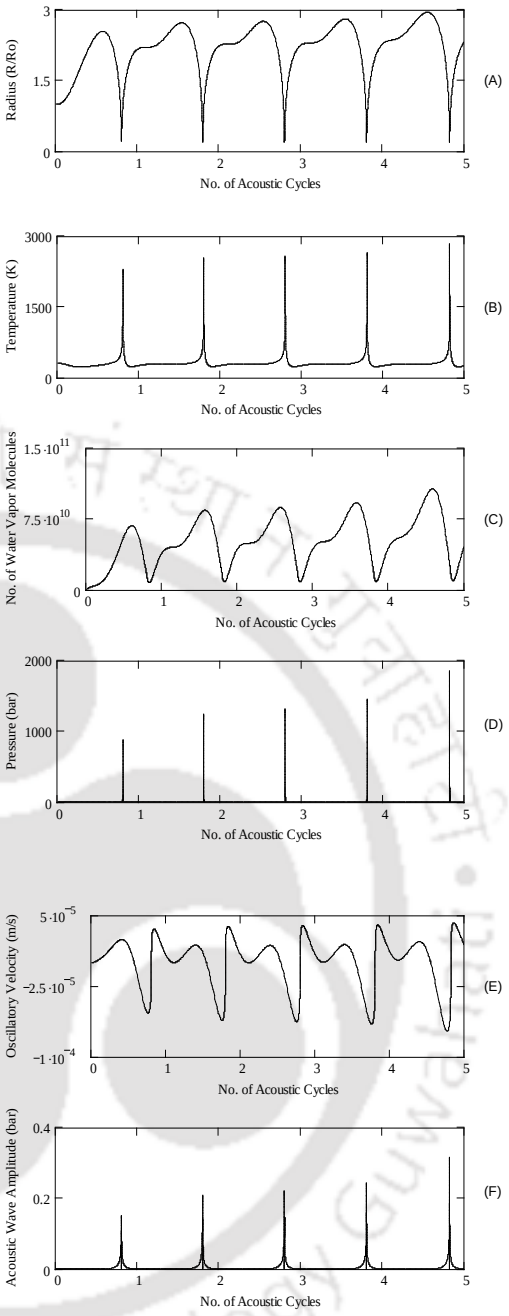

Figure 5.9: Simulation results for cavitation bubble dynamics (10 μm air bubble at 303 K in water)

(A) normalized bubble radius (R/R_o); (B) temperature in the bubble; (C) number of water molecules in the bubble; (D) pressure inside the bubble; (E) micro–turbulence generated by the cavitation bubble; (F) acoustic (or shock) waves emitted by the bubble.

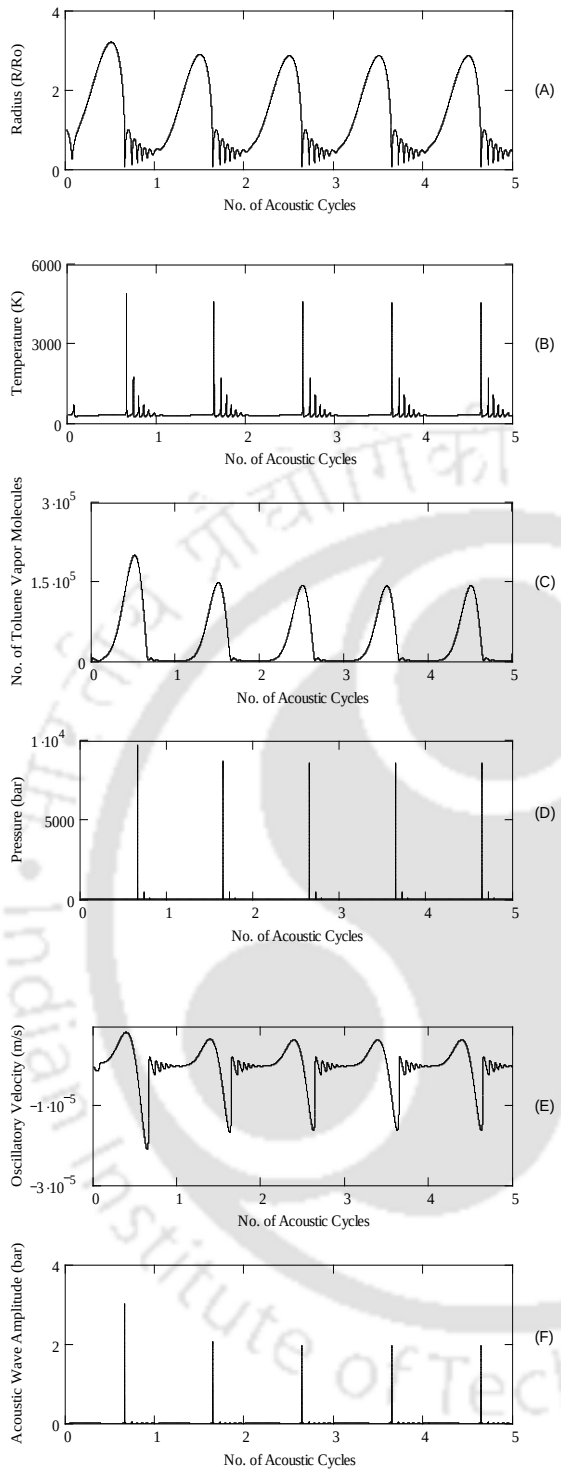

Figure 5.10: Simulation results for cavitation bubble dynamics (5 μm air bubble at 303 K in toluene)

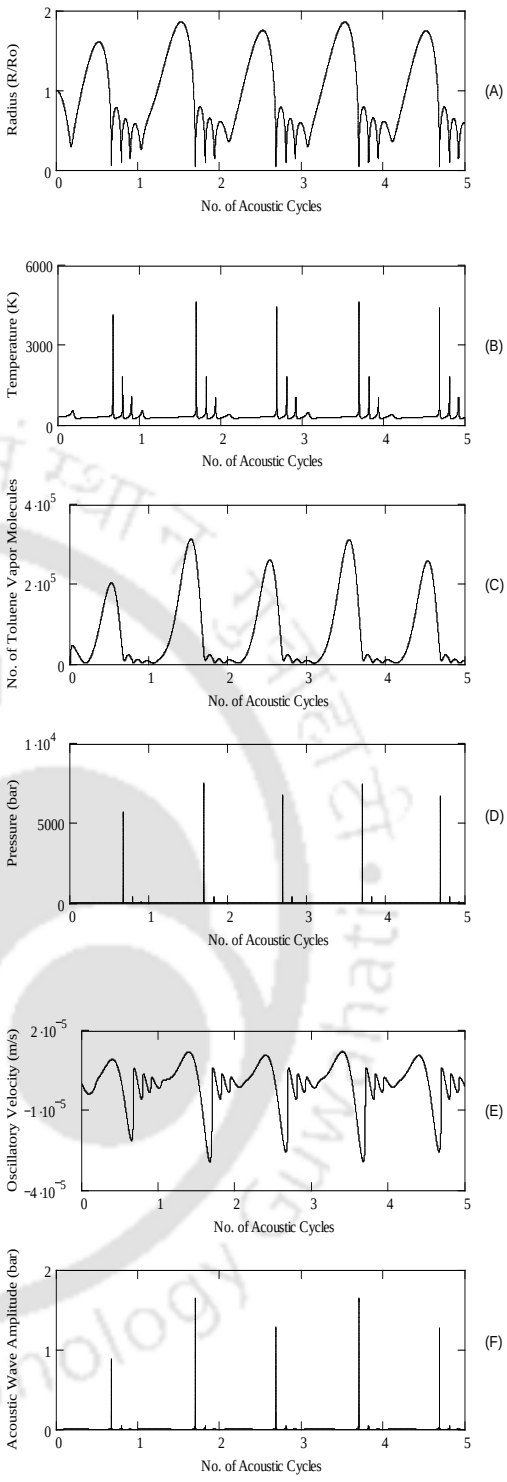

Figure 5.11: Simulation results for cavitation bubble dynamics (10 μm air bubble at 303 K in toluene)

(A) normalized bubble radius (R/R_o); (B) temperature in the bubble; (C) number of water molecules in the bubble; (D) pressure inside the bubble; (E) micro–turbulence generated by the cavitation bubble; (F) acoustic waves emitted by the bubble.

Table 5.2. Summary of simulations of cavitation bubble dynamics

Species	**Parameters for simulations**			
	Water		Toluene	
	Air bubble R_o = 5 μm	Air bubble R_o = 10 μm	Air bubble R_o = 5 μm	Air bubble R_o = 10 μm
	Conditions at the first collapse of the bubble			
	T_{max} = 3258 K P_{max} = 384 MPa V_{turb} = 0.03 mm/s P_{AW} = 72 kPa	T_{max} = 2304 K P_{max} = 88.4 MPa V_{turb} = 0.05 mm/s P_{AW} = 31.6 kPa	T_{max} = 4881 K P_{max} = 970 MPa V_{turb} = 0.01 mm/s P_{AW} = 300 kPa	T_{max} = 4141 K P_{max} = 573 MPa V_{turb} = 0.02 mm/s P_{AW} = 164.4 kPa
	x_{N2} = 0.72 x_{O2} = 0.19 x_W = 0.094	x_{N2} = 0.71 x_{O2} = 0.19 x_W = 0.1	x_{N2} = 0.79 x_{O2} = 0.21 x_{TOL} = 3.47E–06	x_{N2} = 0.79 x_{O2} = 0.21 x_{TOL} = 2.89E–06
	Equilibrium composition of radical and other oxidizing species in the bubble at collapse			
N_2	7.20E–01	7.01E–01	7.09E–01	7.32E–01
O_2	1.66E–01	1.81E–01	1.23E–01	1.48E–01
O	1.67E–03	7.22E–05	2.14E–02	9.8E–03
O_3	6.48E–06	–	3.91E–05	2.1E–05
H	7.18E–05	1.36E–06	1.92E–06	–
H2	1.86E–04	1.69E–05	–	–
N	–	–	2.11E–04	3.27E–05
N_3	–	–	4.27E–06	–
NO	5.62E–02	1.46E–02	1.43E–01	1.08E–01
NO_2	1.33E–03	4.12E–04	2.28E–03	1.88E–03
NO_3	–	–	1.68E–06	–
N_2O_3	–	–	1.19E–06	–
N_2O	1.72E–04	2.05E–05	7.61E–04	4.28E–04
CO	–	–	9.0E–06	3.63E–06
CO_2	–	–	1.51E–05	1.65E–05
OH	7.37E–03	1.34E–03	2.37E–05	2.07E–05
H_2O	4.68E–02	1.01E–01	–	–
HO_2	4.38E–04	7.06E–05	1.26E–06	1.08E–06
H_2O_2	2.68E–05	5.71E–06	–	–
HNO	2.25E–05	–	–	–
HNO_2	1.65E–04	3.70E–05	–	–

Notation: R_o – initial radius of the cavitation bubble; V_{turb} – average velocity of the micro–turbulence in the medium generated by ultrasound and cavitation in the medium (estimated at 1 mm distance from bubble center); P_{AW} – pressure amplitude of the acoustic wave generated by the cavitation bubble (estimated at 1 mm distance from bubble center); T_{max} – temperature peak reached in the bubble at the time of first collapse; P_{max} – pressure peak reached in the bubble at the time of first collapse; x_W – mole fraction of water vapor in the bubble; x_{N2} – mole fraction of N_2 in the bubble; x_{O2} – mole fraction of oxygen in the bubble; x_{TOL} – mole fraction of toluene vapor in the bubble

Physical synergy: Intense micro-convection generated by the cavitation bubbles results in fine emulsification of the reaction mixture with very high interfacial area for interphase transport of DBT from organic to aqueous phase. Moreover, the micro-turbulence can enhance diffusion of DBT and 2-hydroxy biphenyl sulfinate across cell membrane. It also enhances back diffusion of the final metabolite 2-HBP into the organic phase, thus avoiding its accumulation in the aqueous phase leading to inhibition (Caro et al. 2007). Intense micro-convection in the reaction mixture also causes rapid movement of microbial cells in the fermentation broth with inter-collisions and/or collisions with the walls of the reaction flask. Kinetic energy gained by the cells through such rapid motion can help accelerate the enzymatic reactions inside the cells.

***Chemical* synergy:** Another possible synergy between transient cavitation and microbial metabolism could be via sonochemical effect, i.e. reactions induced by radicals formed out of transient cavitation. The simulations result show formation of oxidizing radicals O$^{\bullet}$ and $^{\bullet}$OH. Attack of these radicals onto the DBT molecules can also lead to formation of the intermediates of cell metabolism, viz. DBT sulfoxide and DBT sulfone as discussed in chapter 2. Presence of these intermediates in the samples withdrawn from bulk reaction mixture as detected in the GC-MS analysis in section 5.4.2. It is clear evidence that supports chemical synergy. These intermediates can diffuse into the cells and undergo further transformation to final metabolite 2-HBP. Such synergy can not only help enhance rate of biodesulfurization of DBT but also reduction in the substrate inhibition.

***Discernment of physical mechanism of* biodesulfurization:** The values of parameters in the Haldane kinetic model obtained after fitting of the model to initial velocity of DBT reduction oxidation (V_o) and initial substrate concentration (S_o) are

given in Table 5.3. Comparison of the Haldane kinetic constants for different experimental categories can help deduce the physical mechanism of the ultrasonic enhancement of biodesulfurization. The peculiar trends in Haldane kinetic parameters as observed from Table 5.3 and the possible physical explanation for the same can be given as follows:

(1) Effect of ultrasound for both free and immobilized cells is mainly seen in terms of increase in velocity of reaction, and practically no effect is seen on K_m and K_I (as seen from Haldane kinetics parameters for categories A.1 & A.2 and B.1 & B.2). The substrate – enzyme affinity and inhibition characteristics of enzymes are intrinsic properties. Therefore, they remain unaffected by the physical effect of intense micro-convection generated by ultrasound and cavitation. The increase in reaction velocity is attributed to faster mass transport induced by the micro-convection generated by ultrasound and cavitation. The micro-convection also creates fine emulsification between phases that enhances the interfacial area for DBT and 2-HBP transport across organic and aqueous phases. Formation of the intermediates of DBT metabolism (DBTO and $DBTO_2$) due to reaction of radicals generated by transient cavitation in aqueous medium can also contribute to enhancement in DBT metabolism with application of ultrasound in categories A.2 and B.2.

(2) Immobilization results in reduction of exposed area of the cells and also activity of some enzymes. Therefore, value of K_m in category A.1 increases with immobilization in category B.1 indicating lesser substrate / enzyme affinity. Moreover, value of K_I also decreases in category B.1 indicating greater susceptibility of enzyme to inhibition.

(3) Cyclodextrins (β-CD) are essentially cyclic or ring compounds that are hydrophobic inside and hydrophilic outside. Hence, they can form complexes with hydrophobic DBT in organic phase, and can transport them to the aqueous phase. Thus, the solubility of DBT in aqueous phase enhances in with addition of β-CD. DBT concentration in aqueous phase is likely to increase with addition of β-CD to reaction medium. As per experimental conditions in different categories, the microbial cells react differently to this change – which is reflected in variations of the numerical values of parameters in Haldane kinetic model.

(4) The free cells are suspended in the medium, and hence, the entire cell surface is available for DBT uptake even at high concentrations in aqueous medium. Hence, an increase in DBT oxidation is seen in category C1 with addition of β-CD. An increase in V_{max} and K_I is seen with concurrent reduction in K_m, which are favorable variations for enhanced kinetics.

(5) An interesting observation is seen in kinetics of desulfurization for the category C2, where sonication is applied simultaneously with addition of β-CD. In this case, adverse effect is seen on values of K_m and K_I (in that K_m increases and K_I decreases, as compared to category A.2). We attribute this result to the adverse effect of strong micro-convection generated by ultrasound on formation of DBT-β-CD complex. Since this complex is formed out of relatively weak physical bonds, it is likely to undergo rupture due to high shear forces generated by micro-convection and shock (or acoustic) waves emitted by transient cavitation bubbles in reaction mixture, especially in the aqueous phase. This results in rise in K_m (indicating reduced affinity of substrate) as well as K_I. Another factor that could also contribute to this effect is the wetting of the cell surface, as explained later.

(6) In case of immobilized system (category D1), the cells are attached to the immobilization support, and hence, entire surface area is not available for cellular transport. Thus, it is likely that DBT uptake by the cells does not rise concurrently with the rise in DBT concentration in aqueous medium as a result of addition of β-CD. Thus, it is likely that there could be a surge in the DBT concentration in aqueous medium, which is reflected in rise in numerical value of K_m and K_I.

(7) For category D2, where ultrasound is applied concurrently with surfactant in presence of immobilized cells, an inverse trend in K_m and K_I (as compared to category C2 with free cells) is seen. In this case, K_m reduces while K_I increases, which are favorable variations for enhanced kinetics. This essentially means that adverse effect of strong micro-convection and shear force generated by ultrasound on the DBT-β-CD complex (seen for the free cells) disappears for immobilized cells. We attribute this result to hindrance created by the immobilization support to micro-convection, which reduces the intensity of shear force and also its adverse effect. Relatively milder convection can also assist uptake of DBT by immobilized cells, which is reflected in reduction in numerical value of K_m.

(8) Addition of β-CD to the reaction medium has adverse influence on the reaction velocity of DBT desulfurization, which is more profound for immobilized systems. Values of V_{max} for categories C1 and C2 employing free cells remain almost same as categories A1 and A2. For immobilized cells, the V_{max} values for categories D1 and D2 reduce as compared categories C1 and C2. This reduction could be consequences of reduction surface tension of the aqueous medium with β-CD addition, which can cause “wetting” of the hydrophobic surface of *Rhodococcus rhodochrous* cells. This

phenomenon can hinder the secretion of the product HBP and sulfite (SO_3^{2-}) out of the cells, which leads to reduction in velocity of the metabolic reactions.

(9) The adverse effect of ultrasound on the β-CD action is evident from comparative values of DBT oxidation in different experimental categories. Comparing DBT oxidation for categories A1 and C1 (free cells with mechanical shaking) increments of 30.9% is seen, while increment between categories A2 and C2 (mechanical shaking with ultrasound) is relatively much lesser, i.e. 12.26%. A similar trend is also seen for immobilized cells, in which an increment of 25.58% in DBT oxidation is seen comparing categories B1 and D1, while an increment of just 5.8% is seen comparing categories B2 and D2. Thus, adverse effect of ultrasound on enhancement of DBT oxidation by β-CD addition is more marked for the immobilized system, which is attributed to reduction in V_{max} for the reasons explained earlier.

Table 5.3. Haldane kinetic constants for different experimental categories

Experimental category	V_o (mM/h)			V_{max} (mM/h)	K_m (mM)	K_I (mM)
	$[S_o]$ = 0.54 mM	$[S_o]$ = 1.08 mM	$[S_o]$ = 1.62 mM			
A.1	0.0083	0.0098	0.0092	0.032	1.22	0.97
A.2	0.082	0.094	0.088	0.31	1.25	0.9
B.1	0.029	0.035	0.032	0.19	2.35	0.46
B.2	0.11	0.13	0.12	0.72	2.33	0.47
C.1	0.0089	0.0098	0.0091	0.022	0.59	1.57
C.2	0.066	0.082	0.079	0.41	2.3	0.59
D.1	0.013	0.021	0.025	0.11	3.73	1.7
D.2	0.068	0.072	0.068	0.12	0.33	2.78

5.5. CONCLUSIONS

This study has attempted to establish physical mechanism of sonication induced enhancement of biodesulfurization by concurrent analysis of Haldane kinetics model parameters and simulations of cavitation bubble dynamics. Both physical and chemical effects of sonication contribute to the enhancement. Strong microturbulence generated by sonication enhances interfacial mass transport and substrate/ product diffusion across cell. Oxidation of DBT to DBT-sulfoxide and DBT-sulfone (intermediates of DBT metabolism) by radicals generated by cavitation assists faster consumption of DBT by microbial cells. These effects result in enhancement in reaction velocity and enzyme-substrate affinity as well as reduction in substrate inhibition.

REFERENCES

Alves L, Marque S, Matos J, Tenreiro R, Grio FM. Dibenzothiophene desulfurization by *Gordonia alkanivorans* strain 1B using recycled paper sludge hydrolyzate. *Chemosphere*; 2008: 70, 967–973.

Babich VI, Moulijn JA. Science and technology of novel processes for deep desulfurization of oil refinery streams: A review. *Fuel* 2003; 82: 607–631.

Bahuguna A, Lily MK, Munjal A, Singh RN, Dangwal K. Desulfurization of dibenzothiophene (DBT) by a novel strain *Lysinibacillus sphaericus* DMT-7 isolated from diesel contaminated soil. *J. Environ. Sci*. 2011; 23(6): 975–982.

Borgne LS, Quintero R. Biotechnological processes for the refining of petroleum. *Fuel Process. Technol*. 2003; 81: 155–169.

Caro A, Letón P, García-Calvo E, Setti L. Enhancement of dibenzothiophene biodesulfurization using β-cyclodextrins in oil-to-water media. *Fuel* 2007; 86: 2632–2636.

Chen H, Zhang WJ, Cai Y.B, Zhang Y, Li W. Elucidation of 2-hydroxybiphenyl

effect on dibenzothiophene desulfurization by *Microbacterium* sp. strain ZD-M2. *Bioresour. Technol*. 2008; 99: 6928–6933.

Davoodi-Dehaghani F, Vosoughi M, Ziaee AA. Biodesulfurization of dibenzothiophene by a newly isolated *Rhodococcus erythropolis* strain. *Bioresour. Technol*. 2010; 101: 1102-1105.

Folsom BR, Schieche DR, DiGrazia PM, Werner J, Palmer S. Microbial desulfurization of alkylated dibenzothiophenes from a hydrodesulfurized middle distillate by *Rhodococcus erythropolis* I-19. *Appl. Environ. Microbiol*. 1999; 65: 4967–4972.

Furuya T, Kirimura K, Kino K, Usami S. Thermophilic biodesulfurization of dibenzothiophene and its derivatives by *Mycobacterium phlei* WU-F1. *FEMS Microbiol. Lett*. 2001; 204: 129–133.

Gray KA, Machkoyz GT, Squires CH. Biodesulfurization of fossil fuels. *Curr. Opin. Microbiol*. 2003; 6: 229–235.

Gupta NP, Roychoudhury K, Deb JK. Biotechnology of desulfurization of diesel: prospects and challenges. Appl. *Microbiol. Biotechnol*. 2005; 66: 356–366.

Kayser KJ, Bielaga-Jones BA, Jackowski K, Odusan O, Kilbane JJ. Utilization of organosulfur compounds by axenic and mixed cultures of *Rhodococcus rhodochrous* IGTS8. *J. Gen. Microbiol*. 1993; 139: 3123–3129.

Kilbane JJ. Desulfurization of coal: the microbial solution. *Trends Biotechnol*. 1989; 7: 97–101.

Kirimura K, Furuya T, Nishii Y, Ishii Y, Kino K, Usami S. Biodesulfurization of dibenzothiophene and its derivatives through the selective cleavage of carbon-sulfur bonds by a moderately thermophilic bacterium *Bacillus subtilis* WU-S2B. *J. Biosci. Bioeng*. 2001; 91(3): 262–266.

Konishi I, Yoshitaka I, Kouichi O, Suzuki M. High-temperature desulfurization by microorganisms. US Patent, 5925560, 1999.

McFarland BL, Boron DJ, Deever W, Meyer JA, Johnson AR, Atlas RM. Biocatalytic sulfur removal from fuels: applicability for producing low sulfur gasoline.

Crit. Rev. Microbiol. 1998; 24: 99–147.

Mohebali G, Ball AS, Rasekh B, Kaytash A. Biodesulfurization potential of a newly isolated bacterium, *Gordonia alkanivorans* RIPI90A. *Enzyme Microb. Technol*. 2007; 40: 578–584.

Mohebali G, Ball AS. Biocatalytic desulfurization (BDS) of petrodiesel fuels. *Microbiology* 2008; 154: 2169 – 2183.

Moholkar VS, Sable SP, Pandit AB. Mapping the cavitation intensity in an ultrasonic bath using the acoustic emission. *AIChE J*. 2000; 46(4): 684-694.

Monticello DJ. Biodesulfurization and the upgrading of petroleum distillates. *Curr Opin Biotechnol*. 2000; 11: 540–546.

NIST Data Gateway (Chemistry Webbook) Home Page. http://webbook.nist.gov/ chemistry (accessed January 2015).

Oda S, Ohta H. Biodesulfurization of dibenzothiophene with *Rhodococcus erythropolis* ATCC 53968 and its mutant in an interface bioreactor. *J. Biosci. Bioeng*. 2002; 94(5): 474–477.

Oldfield C, Pogrebinsky O, Simmonds J, Olson ES. Kulpa C F. Elucidation of the metabolic pathway for dibenzothiophene desulfurization by Rhodococcus sp. strain IGTS8 (ATCC 53968). *Microbiology* 1997; 143: 2961–2973.

Pierce AD. Acoustics: An introduction to its physical principles and applications. *Acoust. Soc. Am.* New York 1989.

Press WH, Teukolsky SA, Flannery BP, Vetterling WT. Numerical Recipes. Cambridge University Press, New York 1992.

Rashtchi, M., Mohebali, G.H., Akbarnejad, M.M., Towfighi, J., Rasekh, B., Keytash, A., 2006. Analysis of biodesulfurization of model oil system by the bacterium, strain RIPI-22. *Biochem. Eng. J.* 29, 169–173.

Srivastava VC. An evalution of desulfurization technologies for sulphur removal from liquid fuels. *RSC Adv*. 2012; 2: 759-783.

Sivasankar T, Paunikar AW, Moholkar VS. Mechanistic approach to enhancement of

the yield of a sonochemical reaction. *AIChE J*. 2007; 53: 1132–1143.

Song C, Ma X. New design approaches to ultra-clean diesel fuels by deep desulfurization and deep dearomatization. *Appl. Catal. B* 2003; 41: 207-238.

Storey BD, Szeri AJ. Water vapor, sonoluminescence and sonochemistry. *Proc. R. Soc. Lond. A Mat*. 2000; 456: 1685-1709.

Toegel R, Gompf B, Pecha R, Lohse D. Does water vapor prevent upscaling sonoluminescence? *Phys. Rev. Lett*. 2000; 85: 3165-3168.

Watkins LM, Rodriguez R, Schinder D, Broderick R, Cruz M, Chembers R, Ruckman E, Cody M, Mrachko GT. Purification and characterization of the aromatic desulfinase 2- (2'- hydeoxybiphenyl) benzene sulfinate desulfinase. *Arch. Biochem. Biophys*. 2003; 415: 14-23.

भारतीय प्रौद्योगिकी संस्थान गुवाहाटी
Indian Institute of Technology Guwahati

Chapter 6

Mechanistic Analysis of Ultrasound Assisted Enzymatic Desulfurization

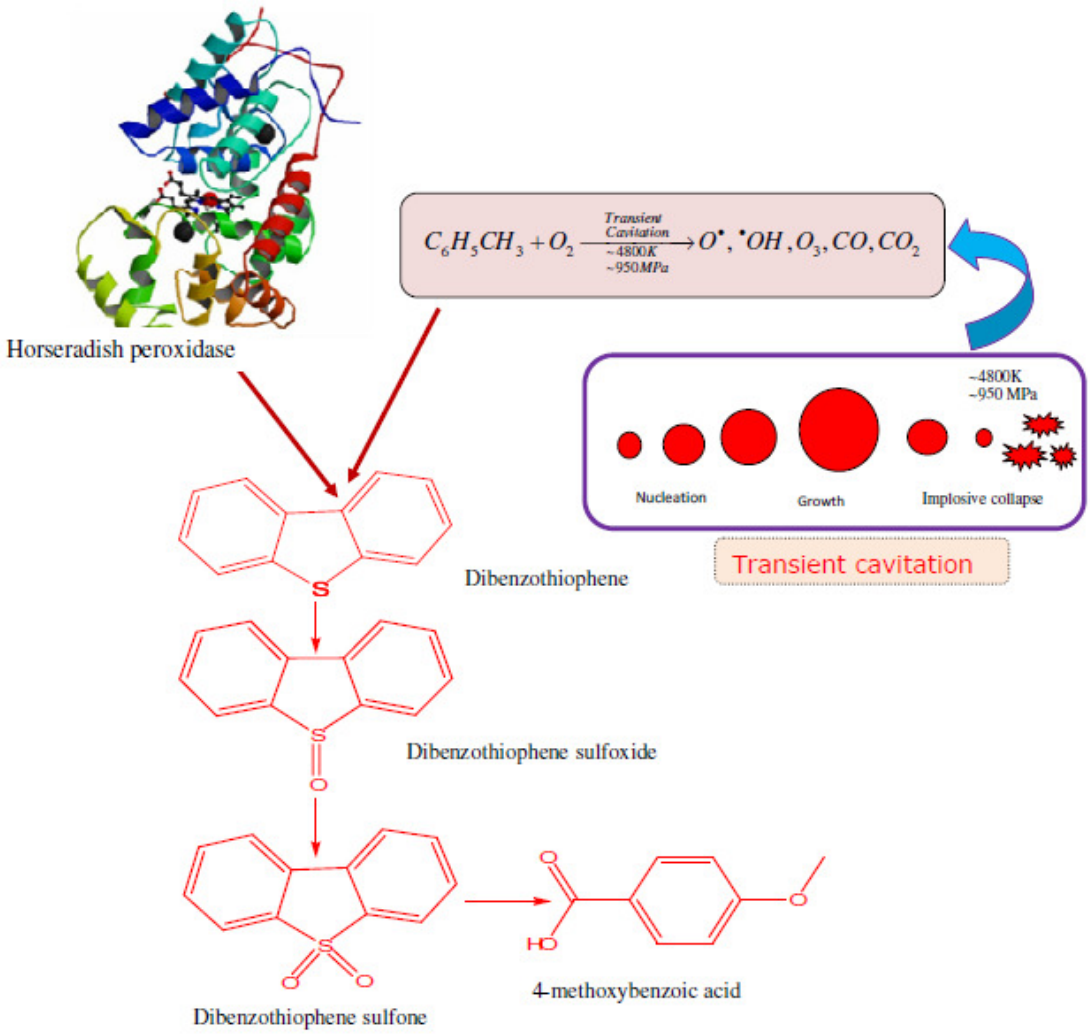

Mechanistic Analysis of Ultrasound Assisted Enzymatic Desulfurization

6.1 INTRODUCTION

Oxidative desulfurization can be carried out using three kinds of oxidants, *viz*. inorganic peracids, microbial route using strains such as *Rhodococcus* and *Psuedomonas*, and enzymatic route employing peroxidase enzymes (such as lacasse, manganese peroxidase or horseradish peroxidase containing heme proteins), which catalyze oxidation of variety of substrate utilizing H_2O_2 as an electron acceptor. Out of these three techniques, the enzymatic and microbial desulfurization has an additional merit of being eco–friendly and operation at mild conditions. In the previous chapter, we dealt with ultrasound-assisted microbial desulfurization of fuels using immobilized cultures of *Rhodococcus rhodochorous spp*. In this chapter, we take ahead the theme of ultrasound-assisted biodesulfurization with enzymatic treatment.

Enzymatic systems have been successfully applied for effective oxidation of a

variety of organic substrates such as, phenols, anilines, dyes and pesticides. However, literature on application of peroxidase enzymes for oxidative desulfurization of transportation fuel is quite limited. Villasenar et al. (2004) have reported enzymatic oxidation of dibenzothiophene (DBT) by lacasse in presence of ABTS (2,2'–azino–bis–(3ethylbenthiazoline–6–sulfonic acid)), and have compared the same with chemical oxidation with H_2O_2 catalyzed by phosphotungstic acid. The H_2O_2/ phosphotungstic acid system exhibited faster kinetics by 2–orders of magnitude. Villasenar et al. (2004) have concluded that slow kinetics could be a major hindrance for practical application of lacasse–based desulfurization process. da Silva Madeira et al. (2008) have studied DBT oxidation by horseradish peroxidase in monophasic organic media containing 25% (v/v) acetonitrile. Optimization of DBT/H_2O_2 ratio and mode of H_2O_2 addition was done. Best results were obtained for DBT/H_2O_2 molar ratio of 1:20 with stepwise addition of H_2O_2 at pH 8.0. The DBT oxidation rate with enzyme was 250–fold higher than microbial treatment. On the basis of these results, da Silva Madeira et al. (2008) have proposed a hybrid enzymatic–microbial treatment process for desulfurization. Eibes et al. (2006) have reported degradation of anthracene, dibenzothiophene and pyrene by manganese peroxidase using organic solvent with 30% (v/v) acetone. The major factor influencing kinetics and yield of degradation was concentration of enzymes. Although crude enzyme was able to degrade the pollutants, faster kinetics was seen only at high concentration of enzyme. The degradation rate for the three substrates was in the order: anthracene > dibenzothiophene > pyrene.

Literature published in the area of enzymatic oxidative desulfurization not only vividly demonstrates the efficacy of this technique over microbial desulfurization, but also calls for efforts towards intensification of the kinetics of this

process. More recently, enzymatic treatments have been combined with sonication, in which beneficial influence of physical and chemical effects of ultrasound and cavitation on enhancement of enzyme kinetics have been harnessed. A large number of studies have been published in recent past that combine sonication and enzyme treatment for a variety of physical/chemical processes (Jadhav et al., 2014; Malani et al., 2013; Malani et al., 2014; Patidar et al., 2012; Sangave et al., 2006; Singh et al., 2015). In this chapter, we have investigated the sono–enzymatic technique for oxidative desulfurization. The model system comprises toluene as fuel and dibenzothiophene (DBT) as sulfur compound. Our emphasis in this study is not only on optimization of parameters of sono–enzymatic process for which maximum DBT oxidation is achieved, but also attempt to establish the physical mechanism of ultrasound induced enhancement of enzyme kinetics. In this attempt, we have essentially tried to identify the links between the physics/chemistry of ultrasound and cavitation, and the biochemistry of enzymatic oxidative desulfurization. For this purpose, we have done kinetic (or Arrhenius) and thermodynamic analysis of the oxidative desulfurization profiles under different experimental conditions, and have correlated it with numerical simulations of cavitation bubble dynamics, which gives a quantitative estimate of the physical and chemical effects of ultrasound and transient cavitation mentioned earlier. Our study has revealed some important mechanistic features of sono–enzymatic oxidative desulfurization, as revealed in the subsequent sections.

6.2 MATERIALS, METHODS AND MATHEMATICAL MODEL

6.2.1 Materials

Following chemicals/ enzymes have been used in the present study:

dibenzothiophene (DBT, 98%, Sigma Aldrich), toluene (synthesis grade, Merck), acetonitrile (HPLC grade, Merck), horseradish peroxidase enzyme (HRP, EC 1.11.1.7, 140 U/mg, Sigma–Aldrich), pyrogallol (Sigma Aldrich), 30% v/v H_2O_2 (AR Grade, Merck). All chemicals/ enzymes were used as received without any pretreatment/purification. All solutions were prepared using ultrapure Milli–Q water.

6.2.2 Experimental Setup and Procedure

Experiments were carried out in three categories or protocols, *viz*. (1) enzymatic treatment with mechanical agitation at 150 rpm; (2) enzymatic treatment with sonication at atmospheric static pressure (P_o) = 101.3 kPa; (3) enzymatic treatment with sonication at elevated static pressure (P_o) = 162 kPa. The rationale underlying raising the static pressure of the reaction system will be explained subsequently. In each category, experiments have been conducted at three temperatures, i.e. 288, 298 and 308 K. 50 mL custom–built test tube of borosilicate glass was used for the experiments. The total reaction volume in each experiment was 20 mL with following composition: DBT= 100 ppm (or 0.54 mM), H_2O_2 = 8.14 mM, HRP = 0.078 U/mL, phosphate buffer (pH 7) = 10 mM. The pH of the reaction mixture was 7, which was optimum value for the enzyme activity, as reported by the supplier (Sigma–Aldrich). In first experimental category, mechanical agitation of the reaction mixture was done using a small magnetic bar. For sonication of reaction mixture in second and third experimental category, an ultrasound bath (Elma Transonic 460, Germany, frequency: 35 kHz, power: 35 W, dimensions: 25 × 15 × 10 cm) was used. Test tube with reaction mixture was placed at the center of the ultrasound bath. Due to spatial variation of acoustic intensity in the bath, the location of reaction tube was carefully maintained constant in all experiments (Gogate et al., 2002). The temperature of water in ultrasound bath was maintained constant within ±

2°C using a water circulator bath (Lab Companion, model: RW–0525G). Actual acoustic power input to the ultrasound bath was measured using calorimetric technique (Chakma and Moholkar, 2014; Bhasarkar et al., 2013) as 9.75 W. For piezoelectric transducer of diameter 40 mm, the acoustic intensity at the surface of the transducer was 7761.46 W/m^2. The pressure amplitude of the ultrasound waves corresponding to this intensity was calculated as 150 kPa (Bhasarkar et al., 2013). Ultrasound irradiation was applied in cycles of 15 min sonication and 5 min silent period. This was done in view of adverse effect of continuous sonication on enzyme activity (Patidar et al., 2012). Prolonged exposure to sonication (and transient cavitation) can cause degradation of the amino acid residues, which form important portion of substrate binding (or catalytic) domain of the enzyme molecules. For experiments at elevated static pressure (162 kPa), the reaction tube was connected to a N_2 gas cylinder with double stage regulator. Aliquots of reaction mixture (0.5 mL) were withdrawn every 15 min to monitor the residual concentration of DBT. The total reaction time in all experimental categories was 90 min.

6.2.3 Analysis

Residual concentration of DBT in the aliquots (200 µl) of reaction mixture was analyzed using Shimadzu Ultra High Performance Liquid Chromatography (UHPLC, Model: SPD–20A) equipped with a reverse phase C–18 column (5 µm, 4.6 mm × 250 mm) and UV detector at $\lambda_{287\ nm}$. The mobile phase was a mixture of acetonitrile and water (80:20 v/v). The intermediates of DBT oxidation were detected using GC–MS analysis (Varian 240–GC, VF–5ms column, carrier gas: Helium). The temperature program was as follows: injection temperature = 250°C, column temperature = 100°C for zero time and increased to 300°C at ramping rate of 7°C/min.

6.2.4 Determination of Effect of Sonication on HRP Enzyme Activity and Structure

***Activity*:** Activity of horseradish peroxidase (HRP) enzyme was determined as per standard protocol (Sigma–Aldrich, EC 1.11.1.7) using pyrogallol as substrate One unit of peroxidase will form 1 mg of purpurogallin from pyrogallol in 20 sec at 20°C. The procedure for determination of enzyme activity is as follows (Malani et al. 2014):

$$\text{Pyrogallol (donor)} + H_2O_2 \xrightarrow{\text{HRP}} 2\,H_2O + \text{Purpurogallin (oxidized donor)} \quad (1)$$

Composition: Ultrapure water 2.1 mL, phosphate buffer (pH 7, 100 mM) 0.32 mL, hydrogen peroxide (30% v/v) solution 0.16 mL, pyrogallol solution (5% w/v) 0.32 mL, enzyme (HRP) 0.1 mL. The absorbance of purpurogallin was recorded in every 20 sec at 420 nm using UV–visible spectrophotometer and the activity of the enzyme was calculated as follows:

$$\text{U/mL Enzyme} = \frac{\left(\Delta A_{420}/20\text{ s}\right)\times V_t \times D_f}{\varepsilon \times v_S} \quad (2)$$

Notation: V_t – total volume of reaction mixture (3 mL), D_f – dilution factor, ε – extinction coefficient (12 for purpurogallin at 420 nm), v_s– volume of sample (0.1 mL).

Bradford assay: The experiments were conducted to calculate the protein content of the HRP enzyme by Bradford assay. The composition of Bradford assay mixture was 3 ml of Bradford reagent and 0.1 ml HRP enzyme. The reaction mixture was incubated for 15 min and the absorbance of mixture was recorded at 595 nm. HRP had protein content of 0.0173 mg/mL

Sonication causes increase in the activity of the enzyme (Subhedar and Gogate, 2014) due to the conformational changes induced by strong micro–convection generated due to ultrasound and cavitation. Hence, the activity and protein

content of the HRP enzyme was checked after 20 min of ultrasound exposure time under atmospheric and elevate static pressure. Fig. 6.1 shows the time variation of the optical density of purpurogallin (the product of enzymatic oxidation of pyrogallol) for HRP enzyme before (native enzyme) and after sonication at both atmospheric (101.3 kPa) and elevated static pressure (162 kPa). Faster as well as higher oxidation of pyrogallol by HRP enzyme after exposure to sonication (at both atmospheric and elevated static pressure) clearly indicates an enhancement in the activity.

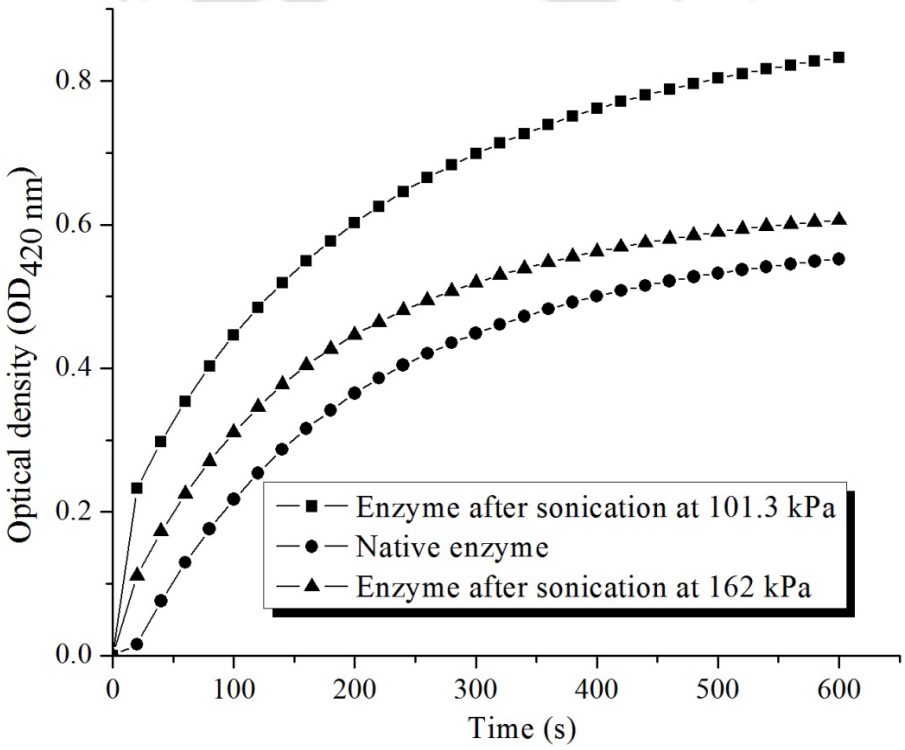

Figure 6.1: Effect of sonication on activity of the HRP enzyme

***Intrinsic fluorescence analysis*:** Three samples of HRP enzyme were used for measurement of intrinsic fluorescence, viz. (1) native enzyme (i.e. without exposure to ultrasound treatment), (2) enzyme with ultrasound treatment for 20 min at (101.3 kPa) static pressure, and (3) enzyme with ultrasound treatment for 20 min at elevated static pressure of 162 kPa. Intrinsic fluorescence spectra of all three enzyme samples

were measured at temperature of 25^{o} ± 1^{o}C with fluorescence spectrophotometer at 280 nm excitation wavelength (slit = 10 nm), 300–500 nm emission wavelength (slit = 10 nm) and 10 nm/s of scanning speed. Phosphate buffer used for dissolution of HRP enzyme was used as a blank solution for these measurements.

Circular dichroism (CD) analysis: Far UV Circular Dichroism (CD) spectra of the HRP enzyme were recorded from the difference in absorption of left and right–circularly polarized light in a Jasco J–815 spectro–polarimeter using a suprasil quartz cuvette of 1 mm optical path length at temperature (25^{o} ± 1^{o}C). The spectra were recorded between 240 – 190 nm with 3 replicates at a scan rate of 100 nm /min with 1nm bandwidth and a path length of the sample cell of 1mm. The CD data were expressed in terms of mean residue ellipticity [θ] based on the average molecular weight (44,000 Da) amino acid residues (308) and concentration (3.5 × 10^{-7} M) of HRP solution. The spectrum of phosphate buffer solution was used as blank and subtracted from the average of three spectra to obtain a corrected spectrum for each samples. The secondary structures of native enzyme and enzyme after sonication (under atmospheric and elevated static pressure) were analyzed using an online server DICHROWEB (Sreerama et al., 2000, Whitemore and Wallace 2004, 2008).

***Kinetic and thermodynamic analysis of experimental data*:** Enzymatic oxidation of DBT proceeds via several intermediates, and each step in the oxidation pathway has different kinetic behavior. Development of a comprehensive kinetic model that takes into accounts profiles of all intermediates would be a complicated and formidable task. Moreover, many of these intermediates have too short life span to be detected using HPLC. In view of this difficulty, we have fitted the time profiles of residual concentration of DBT in different experiments to pseudo–1st order kinetics. High regression coefficients (> 0.9) for the pseudo–1st order model indicate good fitness of

this model to experimental data. Results of Eibes et al. (2006) have also confirmed that oxidation of DBT with manganese peroxidase follows pseudo 1st order kinetic model.

Arrhenius parameters: The Arrhenius parameters of activation energy (E_a) and frequency factor (A) were estimated using slope and y–intercept of plots of ln k versus $1/T$, where k is the pseudo 1st order constant for DBT oxidation at temperature, T.

Thermodynamic parameters: Using the Arrhenius parameter of activation energy, the thermodynamic parameters of enthalpy change, entropy change and Gibbs energy change for DBT oxidation were calculated using Eyring equation (Malani et al., 2014). The relevant equations are given below:

$$\ln\left(\frac{k}{T}\right) = -\left(\frac{\Delta H}{R}\right)\left(\frac{1}{T}\right) + \ln\left(\frac{k_b}{h}\right) + \frac{\Delta S}{R} \tag{3}$$

$$\Delta H = E_a - R \cdot T \tag{4}$$

$$\Delta G = \Delta H - T \cdot \Delta S \tag{5}$$

Notation: k_b – Boltzmann constant and h – Planck's constant

6.2.5 Simulations of Cavitation Bubble Dynamics

The reaction system in the present study is biphasic, i.e. organic phase (toluene) and aqueous phase (enzyme solution). The magnitudes of the physical and chemical effects induced by ultrasound and transient cavitation depend on the properties of these phases. Passage of ultrasound in the form of a longitudinal wave through the reaction mixture induces micro–streaming, which is oscillatory motion of fluid elements. Micro–streaming velocity is given as: $u = P_A/\rho_L c$ (Notation: P_A = pressure amplitude of ultrasound wave; ρ_L = density of the liquid medium; c = sonic velocity in the liquid medium). In the present context, acoustic pressure amplitude in

the biphasic medium was 150 kPa. The corresponding micro–streaming velocity in aqueous (enzyme solution) and organic (toluene) phase is calculated as follows:

For toluene, ρ_L = 867 kg/m^3 and c = 1275 m/s, and thus, u = 0.137 m/s.

For enzyme solution, ρ_L = 1000 kg/m^3 and c = 1481 m/s, and thus, u = 0.1013 m/s.

***Model for cavitation bubble dynamics*:** The magnitude of the physical and chemical effects induced by cavitation bubble dynamics in toluene have been modeled using diffusion limited ODE model (Toegel et al., 2000). This model uses boundary layer approximation on the basis of the results of Storey and Szeri (2000) that vapor transport in the bubble is essentially a diffusion limited process. Transport of solvent vapor in the bubble during radial motion, and its entrapment in the bubble at the moment of transient collapse leads to formation of radicals through thermal dissociation of the vapor molecules. Greater details on this model can be found in our previous papers (Krishnan et al., 2007; Sivasankar et al., 2007), as well as in the original papers (Toegel et al., 2000; Toegel and Lohse, 2001). The diffusion limited bubble dynamics model comprises of 4 ordinary differential equations: (1) Equation for the radial motion of the bubble (Keller–Miksis, 1980), (2) Equation for the diffusive flux of water vapor through bubble interface, (3) Equation for the heat conduction through bubble interface, and (4) Overall energy balance assuming bubble as an open system. The transport parameters, viz. thermal conductivity of the bubble contents and diffusion coefficient of water vapor, are determined using Chapman–Enskog theory using Lennard–Jones 12–6 potential (Hirschfelder et al., 1954; Reid et al., 1987). Diffusion of non–condensable gas (dissolved in the liquid medium) across bubble interface is not accounted by the diffusion limited model, as the time scale for the diffusion of gases (of the order of milliseconds) is much higher than the time scale for the radial motion of bubble (of the order of microseconds). The set of 4

simultaneous ordinary differential equations in the model has been solved using Runge–Kutta 4th order – 5th order (or Cash–Karp method) adaptive step size method (Press et al., 1992). An air bubble has been considered for simulations. The condition for bubble collapse resulting in fragmentation of the bubble is taken as the first compression during radial motion. The numerical values of various parameters used in the simulation of bubble dynamics equation are: Ultrasound frequency (f) = 35 kHz; Acoustic pressure amplitude (P_A) = 150 kPa; Initial radius of cavitation bubble (R_o) = 5 μm; The physical properties of toluene are as follows: ρ_L = 867 kg/m^3, kinematic viscosity (ν) = 6.8 × 10^{-7} Pa–s, surface tension (σ) = 0.0285 N/m and c = 1275 m/s, static pressure (P_o) = 101.3 kPa (for experiments at atmospheric static pressure) or 162 kPa (for experiments with elevated static pressure). Vapor pressure of toluene was calculated using Antoine type correlation: $\log_{10} P_v\,(\text{bar}) = 4.08245 - \frac{1346.382}{T - 53.508}$ (NIST Data Gateway, 2014).

In the present context of enzymatic desulfurization, we have considered the cavitation bubble dynamics only in toluene. This is on the basis of predominant location of the desulfurization reactions. The substrate DBT is initially present in toluene (organic phase) and is practically insoluble in water. Hence, the interactions between enzyme and DBT occur only at the interface between aqueous and organic phase. Therefore, the DBT molecules remain predominantly in organic phase and are exposed only to the transient cavitation activity in this phase (and not in aqueous phase). This is in contrast to our earlier chapter of microbial desulfurization. In microbial desulfurization, the reactions occur inside the microbial cells, which are present in aqueous medium. This requires transfer of DBT molecules from organic to aqueous phase. For this purpose, the surfactant β–CD was used in earlier chapter of

microbial desulfurization, which forms a complex with DBT enhancing its solubility in aqueous phase. Thus, the DBT molecules are exposed to cavitation activity in both organic and aqueous phase, and hence taken into account simulations of cavitation bubble dynamics in both aqueous and organic phases.

***Physical and chemical effect of the cavitation bubbles*:** During radial motion driven by pressure variation due to ultrasound, the cavitation bubble induces microturbulence in the form of oscillatory motion of liquid in its close vicinity. At the point of maximum compression (or minimum radius) during radial motion, the bubble wall (or bubble interface) comes to a sudden halt. At this instance, the fluid elements in liquid converging towards bubble interface are reflected back at high velocity generating a shock wave. These waves can also create intense turbulence and mixing in localized zones in close vicinity of the bubble interface. Magnitudes of micro–turbulence velocity (V_{turb}) and shock waves (P_{AW}) generated by the bubble can be estimated using simulations of cavitation bubble dynamics using following equations (Grossmann et al., 1997; Moholkar and Warmoeskerken 2003):

$$V_{turb} = \frac{R^2}{r^2}\left(\frac{dR}{dt}\right) \tag{4}$$

$$P_{AW}(r,t) = \rho_L \frac{R}{r}\left[2\left(\frac{dR}{dt}\right)^2 + R\frac{d^2R}{dt^2}\right] \tag{5}$$

The chemical effect of transient cavitation is generation of radical species through thermal dissociation of gas and solvent vapor at extreme temperature and pressure conditions reached in the bubble during transient collapse. The numerical solution of bubble dynamics model gives the composition of the bubble contents (in terms of molecules of air and solvent vapor in the bubble) as well as magnitude of the peak temperature and pressure reached in the bubble at collapse. The equilibrium composition of the bubble at collapse is estimated using assumption that

thermodynamic equilibrium is attained in the bubble (Brenner et al., 2002; Krishnan et al., 2006). This assumption is based on extremely fast kinetics of various reactions occurring in the bubble (due to high temperature reached in the bubble, and high concentrations of chemical species due to very small volume of the bubble) Equilibrium mole fraction of different species resulting from thermal dissociation of gas and vapor molecules in the bubble at the conditions of temperature and pressure at first the compression of the bubble can be calculated using Gibbs free–energy minimization technique (Bale et al., 2002; Eriksson et al., 1975).

6.3 RESULTS AND DISCUSSION

6.3.1 Pathway of Enzymatic Desulfurization

The location of the desulfurization reaction in the present situation is the interface between aqueous (enzyme solution) and organic (toluene) media. Identification of the intermediates of the enzymatic desulfurization helps in establishing the biochemical pathway of desulfurization. The GC–MS spectra of reaction mixture for experimental protocol of sono–enzymatic treatment at atmospheric static pressure corresponding to the peaks obtained at 20.08, 22.1, 25.3 and 13.2 min are shown in Figs.6.2A–E. Retention data and major ions obtained at different m/z values for DBT oxidation have been listed in Table 6.1. The molecular mass of DBT was found to be 184.3, which is very close to the calculated value of 184.26. The oxidized products were found to have mass of 216.03, 199.6, and 152.2, corresponding to DBT sulfone, DBT sulfoxide and 4–methoxy benzoic acid, as the final product. On the basis of these intermediates, the pathway proposed for enzymatic desulfurization is depicted in Fig. 6.3. Eibes et al. (2006) have reported same pathway for degradation of dibenzothiophene with manganese peroxidase from

Bjerkandera sp.BOS55.

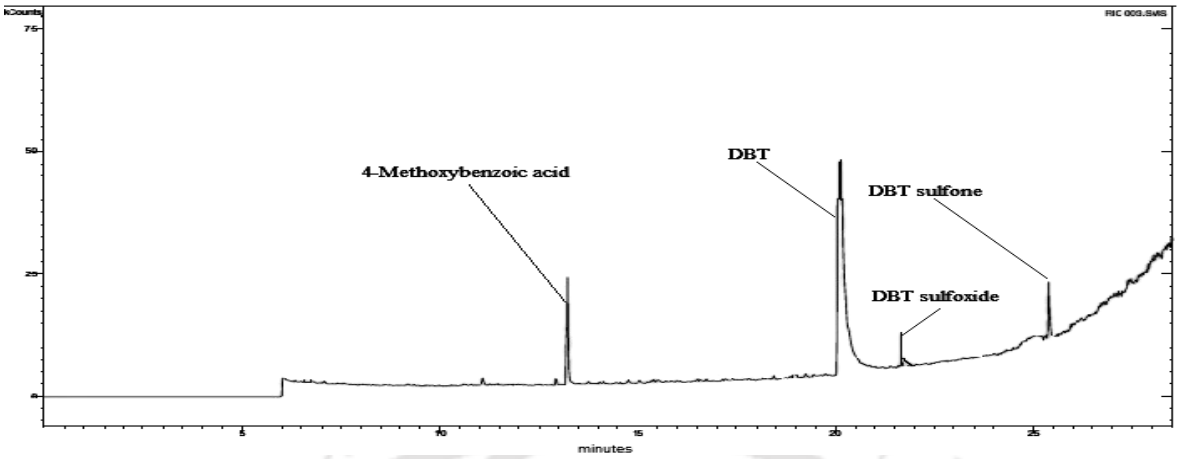

(A)

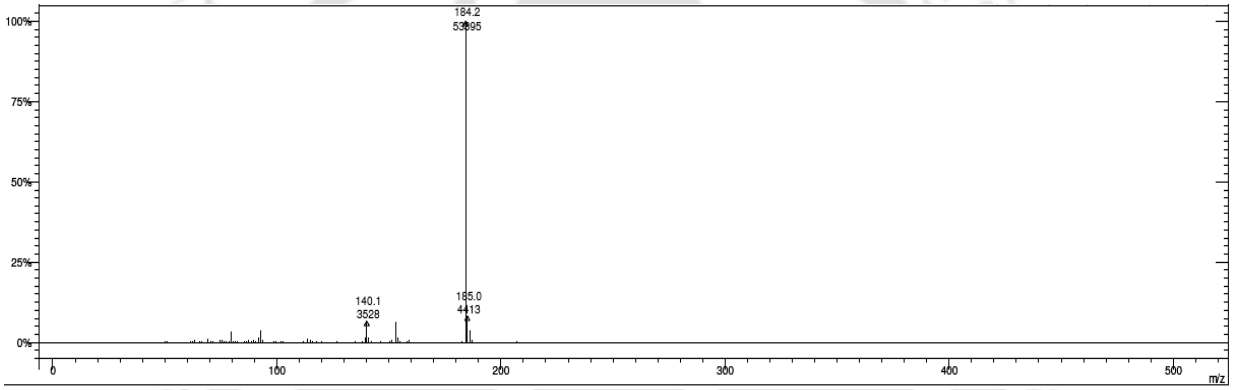

(B)

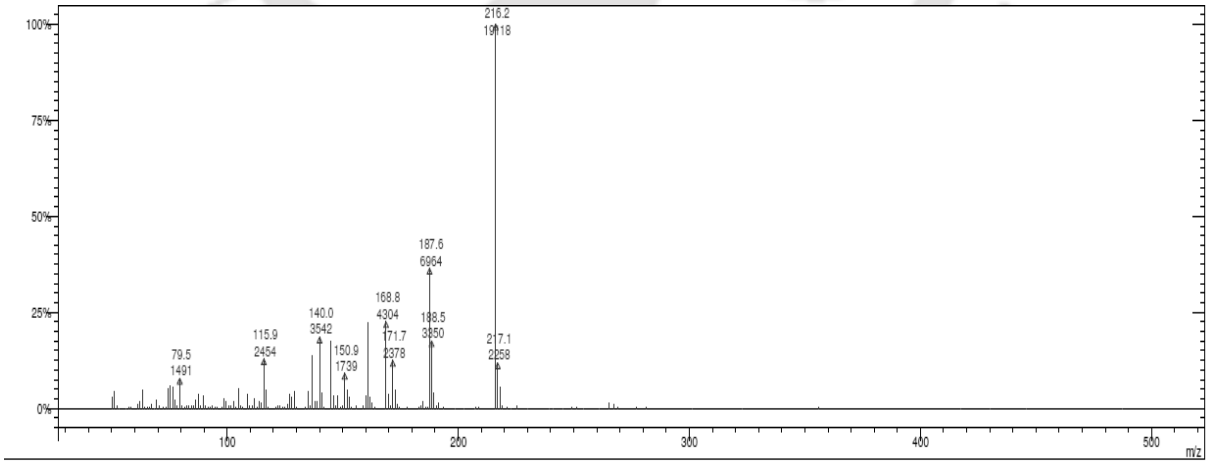

(C)

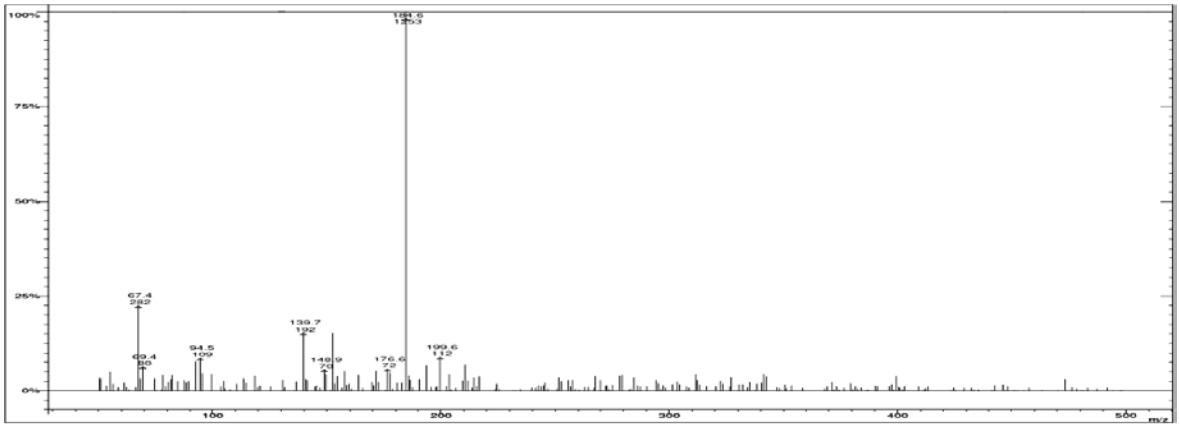

(D)

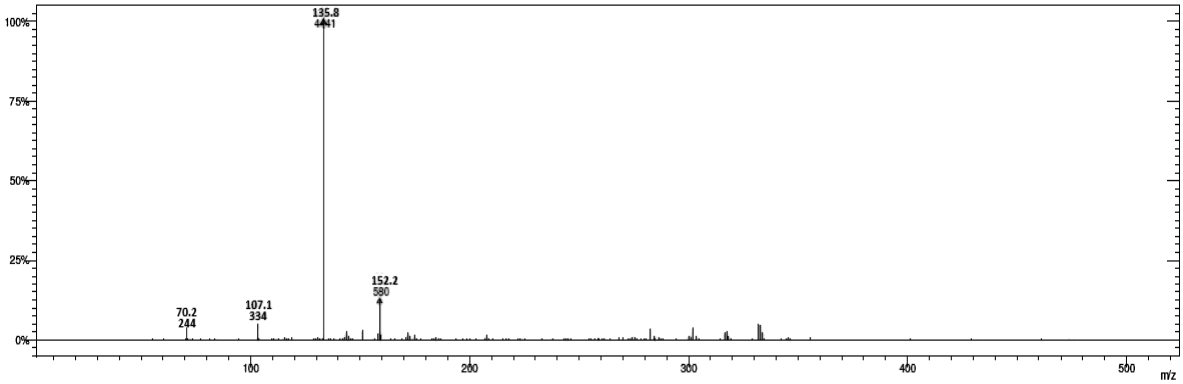

(E)

Figure 6.2: Mass spectrum of reaction mixture for DBT desulfurization for the experimental protocol of sono-enzymatic treatment at atmospheric pressure. (A) Total mass spectra chromatogram **(B)** Mass spectrum of DBT; **(C)**: Mass spectrum of DBT sulfone; **(D)** Mass spectrum of DBT sulfoxide; (E) Mass spectrum of 4-Methoxybenzoic acid.

6.3.2 Trends in Desulfurization Profile in Different Experimental Categories

The time histories of enzymatic DBT oxidation in three experimental protocols conducted at three temperatures of 288, 298 and 308 K have been shown in Fig. 6.4. The summary of the total DBT oxidation achieved in 90 min of treatment along with the pseudo 1st order kinetic constant in all protocols is given in Table 6.2A. The R^2 values (regression coefficient) for the pseudo 1st order kinetic model fitted to time profiles of DBT oxidation in all three experimental categories are > 0.9, indicating excellent fitness of the model. Comparative evaluation of the extent of

DBT oxidation in different experimental protocols shows following distinct features:

(1) Sono–enzymatic treatment (at both atmospheric and elevated static pressure) at all temperatures yields higher DBT oxidation than enzymatic treatment with mechanical agitation.

Table 6.1: Retention data and electron impact mass spectra for degradation of DBT

Retention time (min)	Molecular weight (g/mol)	Substrate	*m/z* of fragment ions	Compound suggestion
20.08	184.26	DBT	184 (100, [M–O]+), 140 (12.5, [M–S–O]+)	DBT
22.1	200	DBT	200 (10, [M]+), 139 (20, [M–COH–S]+), 150 (7.5, [M–OH–OH–S]+)	DBT sulfoxide
25.3	216	DBT	216 (100, [M]+), 187 (37.5, [M–COH]+), 168 (23, [M–O–S]+), 160(10, [M–CO–CO]+)	DBT sulfone
13.2	152.15	DBT	152 (23, [M]), 135(100, [M–O]+), 107 (12, [M–C–O–O])	4–Methoxy benzoic acid

For atmospheric static pressure, the percentage increment of in extent of desulfurization is in the range of 39.8% (at 308 K) to 48.7% (at 288 K). For elevated static pressure, the percentage increments in desulfurization are relatively smaller, i.e. in the range of 10.74% (at 308 K) to 32.5% (at 288 K). Sono–enzymatic treatment at atmospheric pressure is more effective than that at elevated static pressure for all temperatures. The extent of sono-biodegradation at atmospheric static pressure is higher than at elevated pressure in the range of 14.7% (at 298 K) to 32.5% (at 308 K).

(2) Highest pseudo 1st order kinetic constants are obtained for sono–enzymatic treatment at atmospheric static pressure. With rise in static pressure to 162 kPa, pseudo 1st order kinetic constant (k) for sono–enzymatic treatment fall by ~ 30% (for

example, at 298 K, k reduces from 1.65×10^{-4} s^{-1} to 1.25×10^{-4} s^{-1}, while at 308 K, k reduces from 1.83×10^{-4} s^{-1} to 1.31×10^{-4} s^{-1}). The pseudo 1st order kinetic constants for enzymatic treatment with mechanical stirring are approx. 30–60% lesser than those for sono–enzymatic treatments. For example, at 298 K, k increases from 9.83×10^{-5} s^{-1} (for mechanical agitation treatment) to 1.83×10^{-4} s^{-1} (for sono-enzymatic treatment at atmospheric static pressure).

6.3.3 Kinetic and Thermodynamic Analysis

The Arrhenius plots (ln k vs $1/T$) for the three experimental categories are shown in Fig. 6.5. The values of the activation energy and frequency factor calculated from these plots have been listed in Table 6.2A. Enzymatic treatment with mechanical agitation has the highest activation energy and frequency factor. With rise in static pressure, the activation energy of sono–enzymatic treatment increases by ~ 30%, while frequency factor shows 3× rise.

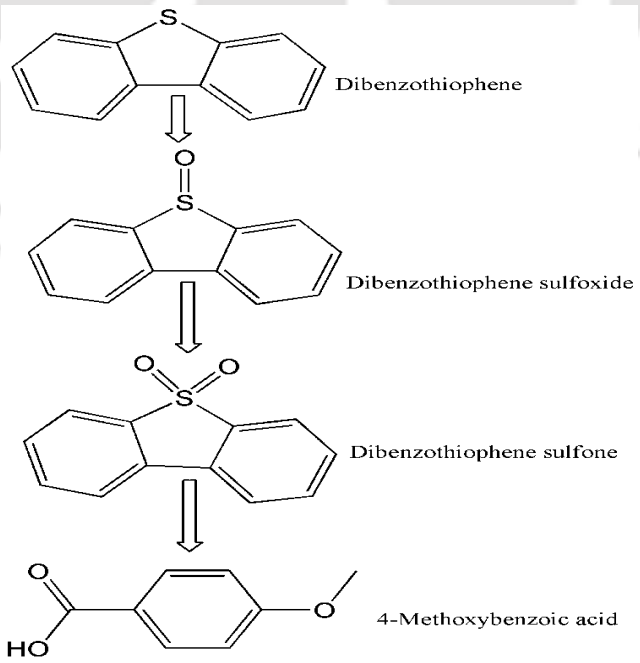

Figure 6.3: Enzymatic desulfurization of DBT pathway

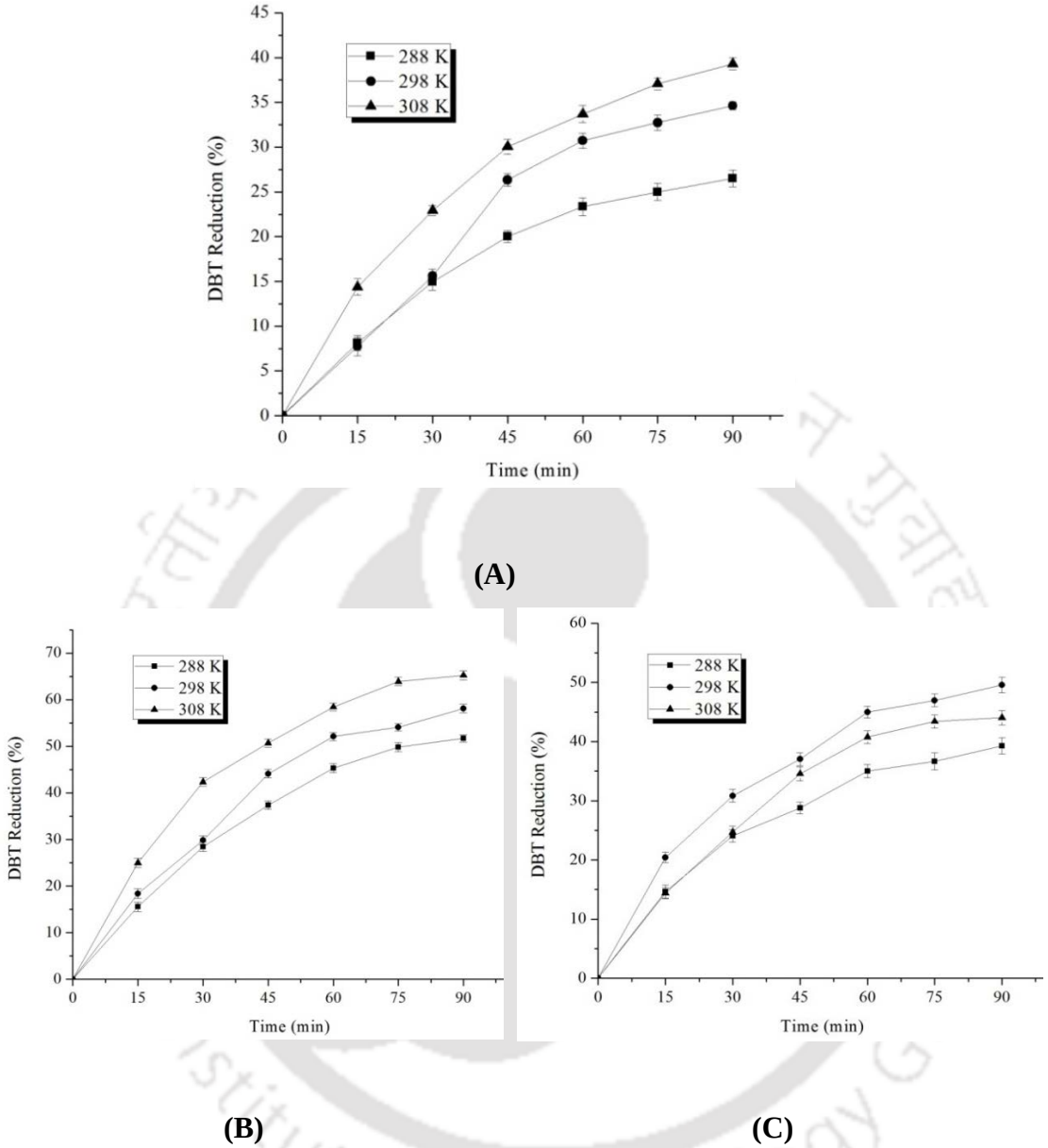

Figure 6.4: Time histories of DBT oxidation in different experimental categories. (A) Enzymatic treatment with mechanical agitation, (B) Sono-enzymatic treatment at atmospheric static pressure (101.3 kPa), (C) Sono-enzymatic treatment at elevated static pressure (162 kPa)

Table 6.2: (A) Summary of experimental results on enzymatic DBT oxidation in different experimental categories

Temperature	**288 K**		**298 K**		**308 K**		E_a (kJ mol^{-1})	A (s^{-1})
Experimental Category	η%	k (s^{-1})	η%	k (s^{-1})	η%	k (s^{-1})		
1. Enzymatic treatment with mechanical agitation	26.50 ± 1.31	5.76×10^{-5} ($R^2 = 0.94$)	34.62 ± 1.08	8.33×10^{-5} ($R^2 = 0.95$)	39.3 ± 0.98	9.83×10^{-5} ($R^2 = 0.94$)	20.36	0.29
2. Sono–enzymatic treatment (P_o = 101.3 kPa)	51.67 ± 1.26	1.38×10^{-4} ($R^2 = 0.97$)	58.12 ± 1.21	1.65×10^{-4} ($R^2 = 0.96$)	65.24 ± 1.1	1.83×10^{-4} ($R^2 = 0.96$)	10.4	1.08×10^{-2}
3. Sono–enzymatic treatment (P_o = 162 kPa)	39.28 ± 1.15	9.0×10^{-5} ($R^2 = 0.94$)	49.57 ± 1.18	1.25×10^{-4} ($R^2 = 0.95$)	44.03 ± 1.0	1.31×10^{-4} ($R^2 = 0.95$)	13.95	3.1×10^{-2}

(B) Thermodynamic parameters for different protocols of DBT oxidation

Experimental Protocols	**ΔH (kJ mol^{-1})**			**–ΔS (kJ mol^{-1} K^{-1})**			**ΔG (kJ mol^{-1})**		
	288 K	**298 K**	**308 K**	**288 K**	**298 K**	**308 K**	**288 K**	**298 K**	**308 K**
1. Enzymatic treatment with mechanical agitation	17.97	17.88	17.79	0.263	0.262	0.264	93.86	96.25	99.14
2. Sono–enzymatic treatment (P_o = 101.3 kPa)	8.00	7.92	7.83	0.29	0.29	0.291	91.73	94.56	97.55
3. Sono–enzymatic treatment (P_o = 162 kPa)	11.55	11.47	11.38	0.282	0.281	0.282	92.75	95.24	99.14

The thermodynamic parameters for the three experimental categories are listed in Table 6.2B. Enzymatic treatment with mechanical agitation has the highest ΔH. Rise in static pressure for sono–enzymatic treatment increases the ΔH value indicating requirement of more energy input for desulfurization reactions. Negative entropy change ($-\Delta S$) value are the highest for sono–enzymatic treatment at atmospheric static pressure, indicating the highest spontaneity of the reactions in this category. With increase in the static pressure, the spontaneity of the sono–enzymatic desulfurization reduces. Enzymatic treatment with mechanical agitation has the least spontaneity, as indicated by the lowest ($-\Delta S$) value. Despite significant variations in the values of ΔH and ($-\Delta S$), the Gibbs free energy change (ΔG) for all three experimental categories are almost similar.

6.3.4 Results of Cavitation Bubble Dynamics Simulations

Representative graphical simulations results for cavitation bubble dynamics for air bubble of 5 μm in toluene atmospheric (101.3 kPa) static pressure and 298 K are shown in Fig. 6.6. The summary of the magnitudes of the physical and chemical effects of cavitation bubbles (viz. temperature and pressure peaks reach in the bubble at transient collapse and equilibrium composition of the chemical species generated in the bubble, magnitudes of micro–turbulence velocity and pressure amplitude of shock waves generated by the bubble). It could be perceived from results depicted in Table 6.3 that, transient collapse of cavitation bubbles in toluene generates oxidizing $O^{\bullet}$ radicals, in addition to a relatively small fraction of $OH^{\bullet}$ radicals. These radicals can independently attack the DBT molecules converting them to sulfoxide and sulfones, which are the intermediates in the biodegradation pathway shown in Fig. 6.3. High micro–turbulence velocity and shock waves with pressure amplitude of ~ 30 MPa create intense micro–convection in the biphasic reaction system that causes fine

emulsification of reaction mixture and enhances interfacial area.

The static pressure in the reaction mixture has a strong influence on cavitation phenomenon. With rise in static pressure of medium to 162 kPa, the intensity of the transient cavitation drops drastically. The temperature and pressure peaks attained in the bubble at transient collapse reduce sharply. The magnitudes of the physical effects of micro–turbulence and shock waves also show sharp reduction. As a consequence, there is no generation of oxidizing radicals inside the bubble. Thus, the physical effect of emulsification and chemical effect of DBT oxidation are practically eliminated at elevated static pressure.

6.3.5 Fluorescence Spectra and Circular Dichroism (CD) Analysis

Enzymes are mostly protein macromolecules made up of α– amino acids linked together via amide (or peptide) bonds to form a linear chain, which is the primary structure. Formation of hydrogen bond between hydrogen in amide ($–NH_2$) group and oxygen in carboxyl (–COOH) group can cause folding of the protein chain to form two types of secondary structures, viz. α–helix and β–conformations (i.e. β–sheet and β–turns). Exposure of enzyme protein to ultrasound wave can induce conformational changes in the secondary structure of the protein, which in turn has an effect on its enzymatic activity (Gulseren et al., 2007; Subhedar and Gogate 2014; Wang et al., 2012). Mogharrab et al (2007) have given a description of the structure of aromatic substrate binding site in HRP enzyme. Oxidation of aromatic substrates (such as DBT in the present context) by HRP occurs at the exposed ‘heme’ edge. This region comprises of heme methyl C18 and heme meso C20 protons. Entrance to the exposed heme edge is guarded by a ring comprising peripheral Phe residues. The aromatic ‘binding pocket’ of HRP is formed of amino acid residues (Phe, Gly, Pro, Ala) flanking the substrate access channel together with heme C20- and heme C18-

methyl groups. The stability of the substrate-HRP complex depends mostly on the hydrophobic interactions, which characterize the peripheral region of the substrate channel of HRP.

Table 6.3. Summary of the cavitation bubble dynamics simulation for air bubble in toluene

Species	Parameters for simulations	
	R_o = 5 μm P_o = 101.3 kPa	R_o = 5 μm P_o = 162 kPa
	Conditions at the first collapse of the bubble	
	T_{max} = 4835 K P_{max} = 961 MPa V_{turb} = 0.147 m/s P_{AW} = 30.2 MPa	T_{max} = 1076 K P_{max} = 80.25 bar V_{turb} = 0.014 m/s P_{AW} = 0.696 bar
	x_{N2} = 0.79 x_{O2} = 0.21 x_{TOL} = 2.77E–6	x_{N2} = 0.79 x_{O2} = 0.21 x_{TOL} = 4.91E–7
	Equilibrium composition of the bubble at transient collapse	
N_2	7.11E–1	7.90E–1
O_2	1.25E–1	2.10E–1
O	2.05E–2	–
O_3	3.80E–5	–
N	1.91E–4	–
N_3	3.82E–6	–
NO	1.41E–1	7.60E–5
NO_2	2.27E–3	2.18E–5
NO_3	1.64E–6	–
N_2O_3	1.14E–6	–
N_2O	7.41E–4	–
CO	1.23E–6	–
CO_2	2.18E–6	–
OH	3.37E–6	–
H_2O	–	–
HO_2	–	–
H_2O_2	–	–
HNO_2	–	–

Notation for Table 6.3: P_o – static pressure in the liquid medium; R_o – initial radius of the cavitation bubble; V_{turb} – average velocity of the micro–turbulence in the medium generated by ultrasound and cavitation in the medium (estimated at 1 mm distance from bubble center); P_{AW} – pressure amplitude of the acoustic wave generated by the cavitation bubble; T_{max} – temperature peak reached in the bubble at the time of first collapse; P_{max} – pressure peak reached in the bubble at the time of first collapse; x_{N2} – mole fraction of N_2 in the bubble; x_{O2} – mole fraction of oxygen in the bubble; x_{TOL} – mole fraction of toluene in the bubble

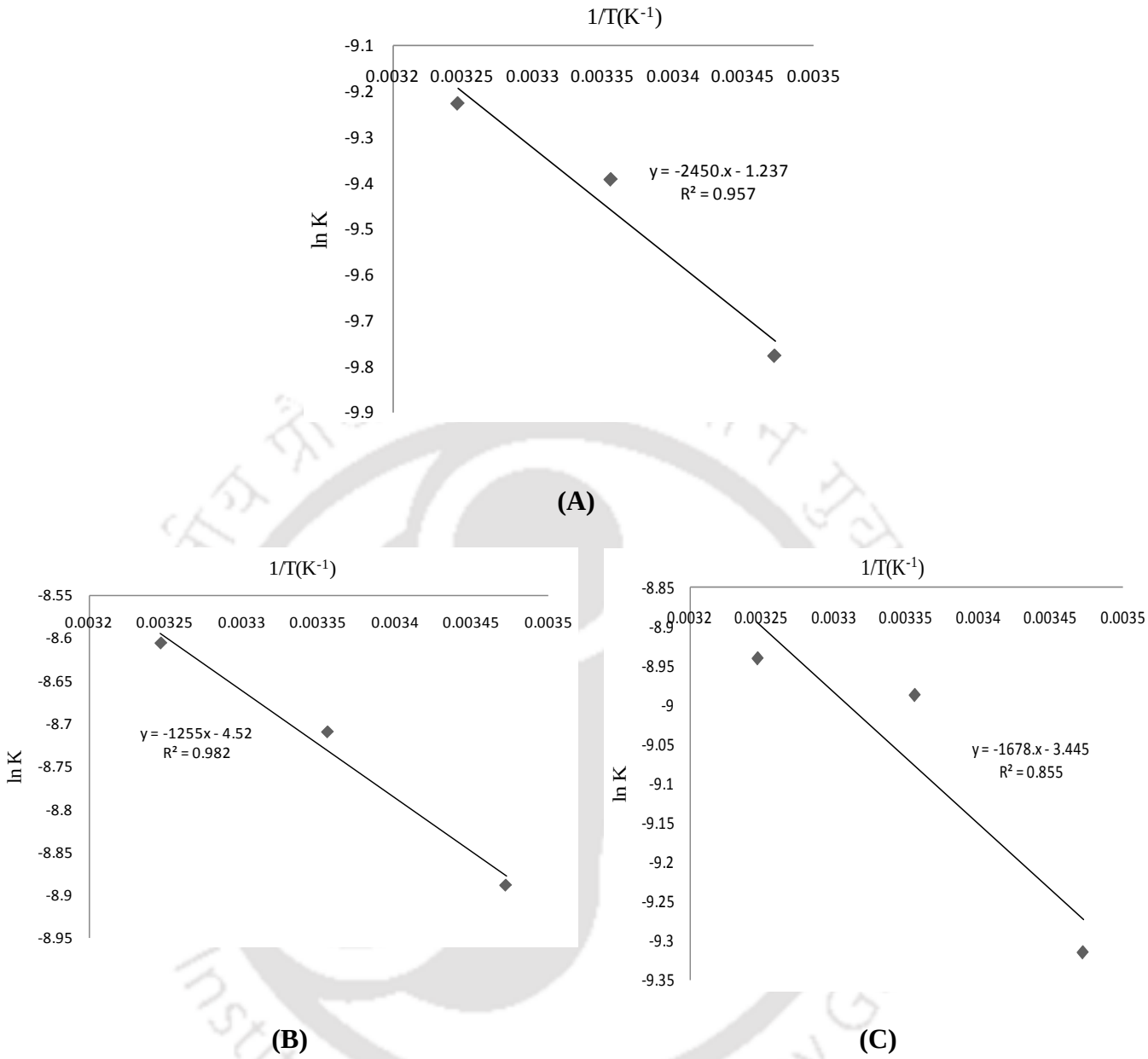

Figure 6.5: The Arrhenius plots for the different experimental categories. (A) Enzymatic treatment with mechanical agitation, (B) Sono-enzymatic treatment at atmospheric static pressure (101.3 kPa), (C) Sono-enzymatic treatment at elevated static pressure (162 kPa)

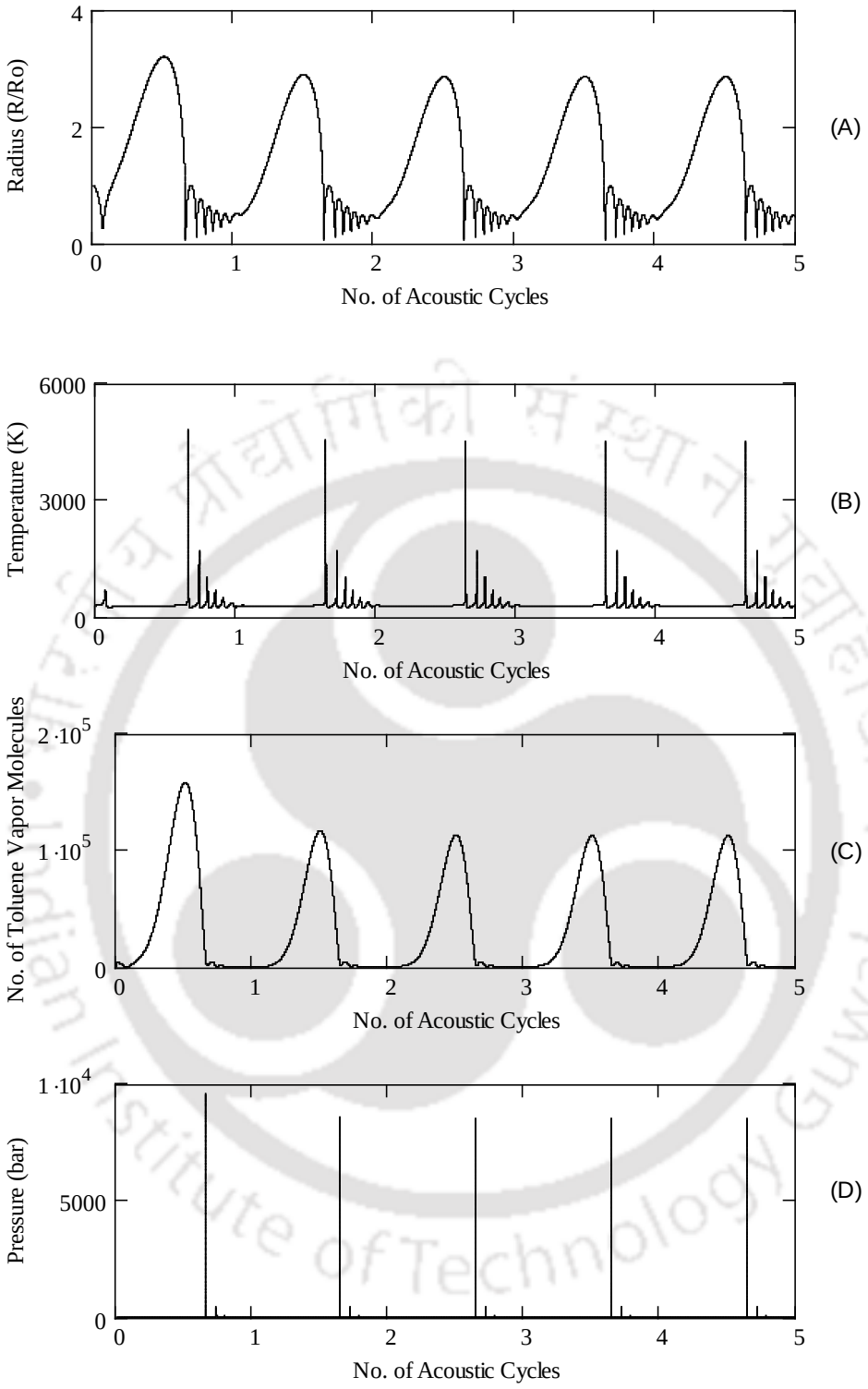

Figure 6.6: Simulations of radial motion of a 5 micron air bubble in toluene at atmospheric static pressure. Time history of (A) radius of the bubble; (B) temperature inside the bubble; (C) toluene vapor evaporation in the bubble; (D) pressure inside the bubble .

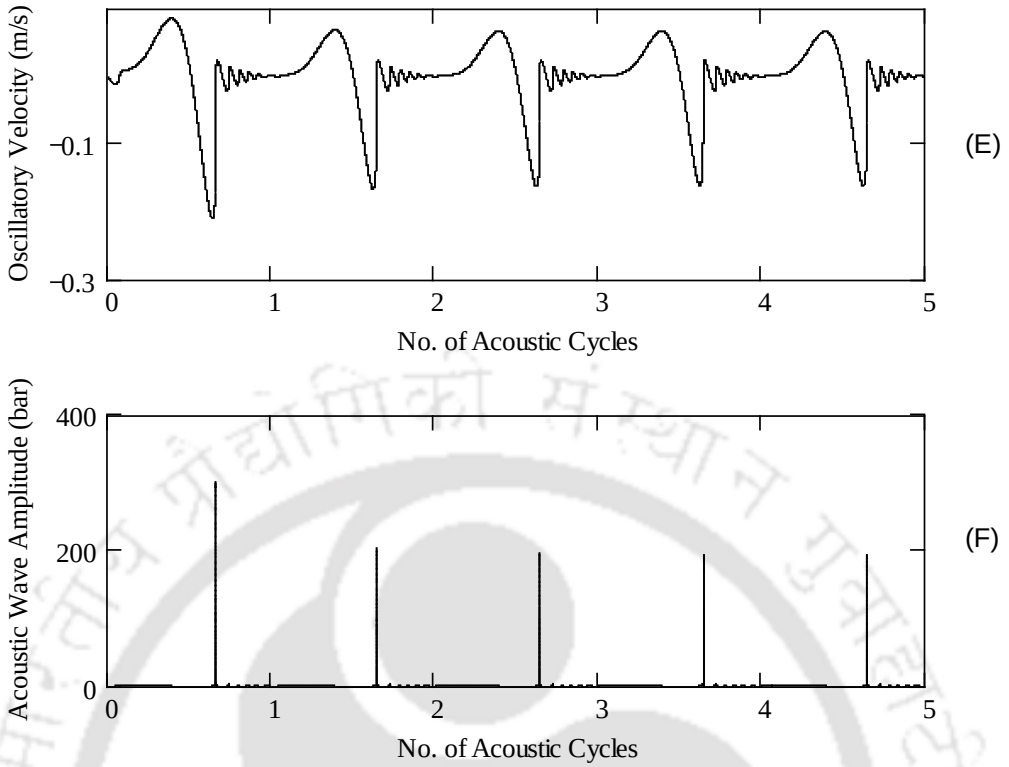

Figure 6.6(*continued*….). (E) microturbulence generated by the bubble; (F) acoustic waves emitted by the bubble.

The influence of sonication on secondary and tertiary structure of the HRP was assessed using the intrinsic fluorescence spectra and CD spectra. Fig. 6.7 shows the intrinsic fluorescence spectra of native enzyme, and the enzyme treated with ultrasound at atmospheric (101.3 kPa) and elevated (162 kPa) static pressure. The aromatics amino acid residues can change their state and structure depending on pH or the microenvironment. Fluorescence spectroscopy is a useful tool to map such structure alternations. The intrinsic fluorescence of the enzyme is mainly attributed to three amino acid residues, viz.Trp, Tyr and Phe (Subhedar and Gogate 2014; Wang et al. 2012). Fig. 6.7A shows the Trp fluorescence spectrum with maximum fluorescence emission wavelength at 348 nm. The spectra of native and ultrasound treated enzyme at atmospheric and elevated static pressure show interesting trends. The ultrasound treated HRP enzyme shows reduction in the fluorescence intensity,

however, the reduction is more marked for treatment at atmospheric static pressure. Moreover, Fig. 6.7A does not show any red or blue shift in optimum fluorescence emission wavelength. These results indicate rupture of hydrophobic interaction of protein molecules with molecular unfolding of proteins; which is induced by physical and chemical effect of ultrasound and cavitation. The reduction in fluorescence intensity is an evidence of decrease of population of exposed tryptophan residues on HRP surface, probably due to aggregation of the protein after exposure. These conformational changes in enzyme essentially lead to exposure of hydrophobic amino acid groups and structures inside the enzyme molecules (Gulseren et al., 2007; Jambrek et al. 2008; Subhedar and Gogate 2014; Wang et al. 2012), as further confirmed by the CD analysis described below.

The conformational changes in protein structure of the enzyme have also been evaluated using CD spectra of native and ultrasound treated enzyme. Fig. 6.7B shows the CD spectra of the native and ultrasound treated enzyme at atmospheric and elevated static pressure. The analysis of the spectra in terms of the contents of secondary structure components, viz. α–helix, β–sheet, β–turn and random coil calculated using the online software of DICHROWEB is given in Table 6.4. Table 6.4 also lists the activity of the native and ultrasound treated enzyme. The α–helix and β–conformations content of HRP enzyme reduces significantly after ultrasound treatment at atmospheric static pressure. Percentage reduction in α–helix, β–sheet and β–turn content of enzyme structure are 7.73, 26.14 and 9.3%, respectively. The random coil content of HRP enzyme showed almost ~50% rise after ultrasound treatment at atmospheric pressure. On the other hand, ultrasound treatment at elevated static pressure induces only negligible changes in enzyme structure. α–helix and β–turn content shows slight reduction, while random coil content shows ~10% increase

after ultrasound treatment at elevated static pressure. The analysis of CD spectra shows that hydrophobic residues forming 'substrate binding pocket' in HRP are more exposed after ultrasound treatment (Mogharrab et al., 2007). The ultrasound treated enzyme possesses an extended hydrophobic patch, which functions as binding site or a 'trap' for DBT molecules. This augments the affinity of the DBT molecules for the enzyme active site. The net manifestation of these conformational changes is an increase in turnover number and catalytic efficiency of the HRP enzyme. Concurrent with these observations, the activity of the HRP enzyme showed 26% and 11% rise after ultrasound treatment at atmospheric and elevated static pressure, respectively. Similar results of structural transformations in the cellulase enzyme induced by ultrasound have been reported by Subhedar and Gogate (2014) and Wang et al. (2012). Wang et al. (2012) have reported a reduction of 8.85 % in α–helix content with 29.5 % increase in random coil content in the cellulase structure after sonication. Subhedar and Gogate (2014) have reported 12.4 % decrease in α–helix content with 29.6 % increase in random coil content in cellulase structure after sonication.

Table 6.4: Contents of secondary structure of untreated and ultrasound treated enzyme

Treatment	α–Helix (%)	β–Sheet (%)	β–Turn (%)	Random coil (%)	Enzyme Activity (U/mL)
1. Native enzyme	37.5	15.3	25.8	20.8	0.073 ± 0.0018
2. Ultrasound treated enzyme at atmospheric static pressure (101.3 kPa)	34.6	11.3	23.4	31.6	0.092 ± 0.0022
3. Ultrasound treated enzyme at elevated static pressure (162 kPa)	37.2	15.5	25.3	21.9	0.081 ± 0.0015

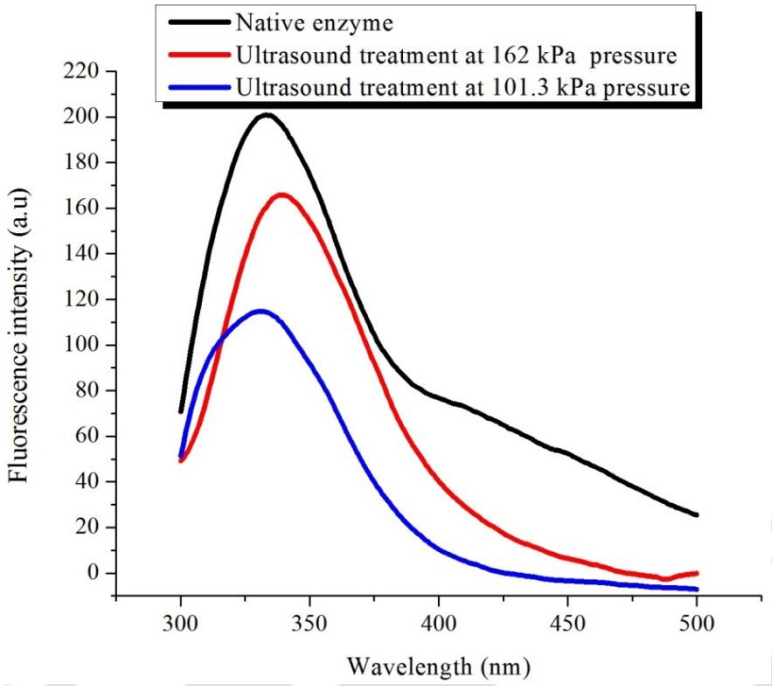

(A)

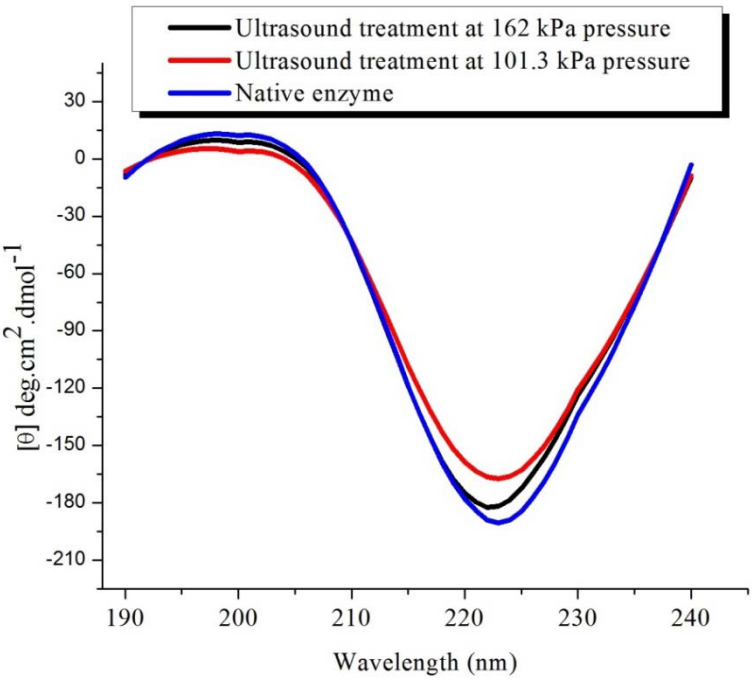

(B)

Figure 6.7: Analysis of the effect of ultrasound and cavitation on enzyme structure (ultrasound treatment time = 20 min). (A) Intrinsic fluorescence spectra of native enzyme and enzyme after sonication at pressure of 101.3 kPa and 162 kPa. (B) CD spectra of native enzyme and enzyme after sonication at pressure of 101.3 kPa and 162 kPa.

6.4 ANALYSIS AND DISCERNMENT OF PHYSICAL MECHANISM

Concurrent analysis of the time profiles and kinetics of desulfurization, Arrhenius and thermodynamic parameters, bubble dynamics simulations, and intrinsic fluorescence and CD analysis give an interesting insight into the physical mechanism of the sono–enzymatic desulfurization process. Given below are main inferences of this concurrent analysis:

(1) The highest desulfurization is obtained second experimental category of sono–enzymatic treatment at atmospheric pressure for which the activation energy (E_a) and enthalpy change (ΔH) have been the lowest. Quite interestingly, the frequency factor is also the least in this category. Reduction in activation energy and enthalpy change for desulfurization can be attributed to enhanced activity of the enzyme, as indicated by the results of intrinsic fluorescence spectroscopy and CD analysis described in greater detail in preceding section. The intense micro–convection generated by cavitation bubbles, in the form of micro–turbulence velocity and shock waves (as indicated by the results of simulation of cavitation bubble dynamics) cause conformational changes and unfolding of the secondary structure of the enzyme molecule, which leads to enhancement in the activity. The spontaneity of the desulfurization reaction also increases due to enhanced activity of the enzyme, as indicated by the highest ($-\Delta S$) values for sono–enzymatic treatment at atmospheric pressure.

(2) As noted earlier, thermal dissociation of gas and vapor molecules in the cavitation bubble can generate oxidizing radicals, which can independently attack the DBT molecules to convert them into DBT–sulfoxide and DBT sulfone. This phenomenon provides a parallel pathway for DBT oxidation. Moreover, DBT sulfoxide and DBT sulfone are also the intermediates in enzymatic desulfurization. Generation of these

intermediates in the reaction mixture boosts enzymatic desulfurization pathway leading to faster conversion of DBT sulfone into the final product of 4–methoxybenzoic acid. The overall manifestation of these phenomena is marked enhancement in kinetics of desulfurization. These radicals may also assist in rupture of the hydrogen bonds and hydrophobic interactions, causing molecular unfolding of proteins.

(3) A probable and plausible explanation for low frequency factor for sonoenzymatic treatments can be given as follows: As noted earlier, the micro–convection generated by cavitation bubble has two components, *viz*. micro–turbulence and shock waves. The former component is continuous in nature, while latter has discrete and random character. The phenomenon of transient cavitation is highly sporadic in time and space. The liquid forming shock waves (and also the contents of the liquid) undergo rapid and random motion in the bulk medium. In the present context, shock wave causes random and rapid movement of the enzyme and substrate (DBT) molecules, which reduces the probability of the interaction among them. This effect is more pronounced for reaction mixtures with dilute concentrations, as in case of present experiments, in which DBT concentration is in ppm. A direct consequence of this phenomenon is very low value of the frequency factor (or fruitful collisions between enzyme and substrate molecules leading to reaction). Thus, the shock waves also have an adverse effect on the desulfurization reaction–besides the beneficial effect of unfolding of enzyme structure causing enhancement in activity. This phenomenon puts a limit on the enhancement effect of sonication applied to enzymatic treatment for desulfurization. On the other hand, the highest frequency factor is seen for the category of enzymatic treatment with mechanical agitation. In this category, agitation by magnetic bar induces a volumetrically uniform and ordered fluid motion, which

assists in increasing probability of enzyme–substrate interaction.

(4) As indicated by the simulation results given in Table 6.3, the intensity of transient cavitation shows drastic reduction at elevated static pressure. There is no formation of shock waves as well as radicals. Despite this, there is marginal rise in the enzyme activity, as indicated by trends shown in Fig. 6.1, and the results of fluorescence spectroscopy and CD analysis. This is attributed to the phenomenon of micro–streaming, is stated in section 6.2.5. Micro–streaming also induces structural unfolding of the enzyme molecules; however, this effect is not as marked as the shock wave, as confirmed by the contents of the secondary structure in ultrasound treated enzyme depicted in Table 6.4. At elevated static pressure, the transient motion of the cavitation bubbles is transformed into small amplitude oscillatory motion. The micro-turbulence generated by such bubbles is weak, which further gets dampened with distance from the center of the bubble. However, if an enzyme molecule is located in the interfacial region of a bubble, the microturbulence generated by the bubble – although weak – can still contribute to limited conformational changes (unfolding of the proteins) in enzyme structure leading to minor increase in activity. Therefore, the values of activation energy and ΔH for the third experimental category of sono–enzymatic treatment at elevated static pressure are higher than those obtained in second experimental category at atmospheric pressure. Due to absence of shock waves and relatively more uniform convection induced by micro–streaming, the frequency factor shows almost 3× increase at elevated static pressure in third category as compared to atmospheric static pressure in second category.

Finally, comparison of the results of desulfurization under atmospheric and elevated static pressure clearly indicates that beneficial effect of protein unfolding induced by shock wave dominates over the adverse effect of reduction in frequency

factor – which is manifested in term of the highest desulfurization with the fastest kinetics in the category of sono–enzymatic treatment at atmospheric pressure.

6.5. CONCLUSION

The present study has revealed interesting mechanistic features of sono–enzymatic desulfurization. Intense micro–convection generated by ultrasound and transient cavitation induces conformational changes of reduction in α–helix and β–conformations, and increase in random coil content of the enzyme. This causes partial unfolding of proteins and exposure of inner hydrophobic groups and regions leading to ~26% increase in enzyme activity. The extent of enzymatic desulfurization shows ~2× increase with sonication, with reduction in activation energy and enthalpy change for desulfurization. However, random motion of enzyme molecules induced by shock waves limits the enhancement effect of sonication.

REFERENCES

Bale CW, Chartrand P, Degterov SA, Eriksson G, Hack K, Mahfoud, R.B., Melancon, J., Pelton, A.D., Petersen, S., 2002. FactSage thermochemical software and databases. *Calphad* 26(2), 189–228.

Bhasarkar JB, Chakma S, Moholkar VS. Mechanistic features of oxidative desulfurization using sono–fenton–peracetic acid (Ultrasound/ Fe^{2+}–CH_3COOH–H_2O_2) system. *Ind. Eng. Chem. Res*. 2013; 52: 9038–9047.

Brenner M, Hilgenfeldt S, Lohse D. Single–bubble sonoluminescence. *Rev. Mod. Phys*. 2002; 74: 425–484.

Chakma S, Moholkar VS. Investigations in synergism of hybrid advanced oxidation processes with combinations of sonolysis + fenton process + UV for

degradation of bisphenol–A. *Ind. Eng. Chem. Res*. 2014; 53: 6855–6865.

da Silva Madeira L, Santana Ferreira–Leitao V, da Silva Bon EP. Dibenzothiophene oxidation by horseradish peroxidase in organic media: Effect of the DBT:H_2O_2 molar ratio and H_2O_2 addition mode. *Chemosphere* 2008; 71: 189–194.

Eibes G, Cajthaml T, Moreira MT, Feijoo G, Lema JM. Enzymatic degradation of anthracene, dibenzothiophene and pyrene by manganese peroxidase in media containing acetone. *Chemosphere* 2006; 64: 408–414.

Eriksson G. Thermodynamic studies of high temperature equilibria—XII: SOLGAMIX, a computer program for calculation of equilibrium composition in multiphase systems. *Chem. Scr*. 1975; 8: 100–103.

Gogate PR, Tatake PA, Kanthale PM, Pandit AB. Mapping of sonochemical reactors: review, analysis, and experimental verification. *AIChE J*. 2002; 48: 1542–1560.

Grossmann S, Hilgenfeldt S, Zomack M, Lohse D. Sound radiation of 3 MHz driven gas bubbles. *J. Acoust. Soc. Am*. 1997; 102: 1223–1227.

Gulseren I, Guzzy D, Bruce BD, Weiss J. Structural and functional changes in ultrasonicated bovine serum albumin solutions. *Ultrason. Sonochem*. 2007; 14: 173–183.

Hirschfelder JO, Curtiss CF, Bird RB. Molecular Theory of Gases and Liquids. *Wiley, New York*, 1954.

Jadhav SH, Gogate PR. Intensification in the activity of lipase enzyme using ultrasonic irradiation and stability studies. *Ind. Eng. Chem. Res*. 2014; 53(4): 1377–1385.

Jambrak AR, Mason TJ, Lelas V, Herceg Z, Herceg IL. Effect of ultrasound treatment on solubility and foaming properties of whey protein suspensions. *J. Food Eng*. 2008; 86: 281–287.

Keller JB, Miksis MJ. Bubble oscillations of large amplitude. *J. Acoust. Soc. Am*. 1980; 68: 628–633.

Krishnan SJ, Dwivedi P, Moholkar VS. Numerical investigation into the chemistry induced by hydrodynamic cavitation. *Ind. Eng. Chem. Res*. 2006; 45: 1493–1504.

Malani RS, Khanna S, MoholkarVS. Sonoenzymatic decolourization of an azo dye employing immobilized horse radish peroxidase (HRP): a mechanistic study. *J. Hazard. Mater*. 2013; 256: 90–97.

Malani RS, Khanna S, Chakma S, Moholkar VS. Mechanistic insight into sono–enzymatic degradation of organic pollutants with kinetic and thermodynamic analysis. *Ultrason. Sonochem*. 2014; 21: 1400–1406.

Mogharrab N, Ghourchian H, Amininasab M. Structural stabilization and functional improvement of Horseradish Peroxidase upon modification of accessible Lysines: Experiments and simulation. *Biophys. J*. 2007; 92: 1192–1203.

Moholkar VS, Warmoeskerken MMCG. An integrated approach to optimization of an ultrasonic processor. *AIChE J*. 2003; 49: 2918–2932.

NIST Data Gateway (Chemistry Webbook) Home Page. http://webbook.nist.gov/chemistry.

Patidar R, Khanna S, Moholkar VS. Physical features of ultrasound assisted enzymatic degradation of recalcitrant organic pollutants. *Ultrason. Sonochem*. 2012; 19: 104–118.

Press WH, Teukolsky SA, Flannery BP, Vetterling WT. Numerical Recipes. Cambridge University Press, New York, 1992.

Reid RC, Prausnitz JM, Poling BE. Properties of gases and liquids. McGraw Hill, New York, 1987.

Sangave PC, Pandit AB. Ultrasound and enzyme assisted biodegradation of distillery wastewater. *J. Environ. Manage*. 2006; 80: 36–46.

Sivasankar T, Paunikar AW, Moholkar VS. Mechanistic approach to enhancement of the yield of a sonochemical reaction. *AIChE J*. 2007; 53: 1132–1143.

Sreerama N, Woody RW. Estimation of protein secondary structure from circular

dichroism spectra: comparison of CONTIN, SELCON, and CDSSTR methods with an expanded reference *Set. Anal. Biochem*. 2000; 287: 252–260.

Storey BD, Szeri AJ. Water vapor, sonoluminescence and sonochemistry. *Proc. R. Soc. Lond. Ser. A* 2000; 456: 1685–1709.

Subhedar PB, Gogate PR. Enhancing the activity of cellulase enzyme using ultrasonic irradiations. *J. Mol. Catal. B– Enzym*. 2014; 101: 108–114.

Toegel R, Gompf B, Pecha R, Lohse D. Does water vapor prevent upscaling sonoluminescence? *Phys. Rev. Lett*. 2000; 85: 3165–3168.

Toegel R, Lohse D. Phase diagrams for sonoluminescing bubbles: A comparison between experiment and theory. *J. Chem. Phys*. 2003; 118(4): 1863–1875.

Villasenor F, Loera O, Campero A, Viniegra–Gonzalez G. Oxidation of dibenzothiophene by laccase or hydrogen peroxide and deep desulfurization of diesel fuel by the later. *Fuel Proces. Technol*. 2004; 86: 49– 59.

Wang Z, Lin X, Li P, Zhang J, Wang S, Ma H. Effect of low intensity ultrasound on cellulase pretreatment. *Bioresource Technol*. 2012; 117: 222–227.

Whitmore L, Wallace BA. DICHROWEB, an online server for protein secondary structure analyses from circular dichroism spectroscopic data. *Nucleic Acid Res*. 2004; (Web Server issue): 668–73.

Whitmore L, Wallace B.A. Protein secondary structure analyses from circular dichroism spectroscopy: methods and reference databases. *Biopolymers* 2008; 89(5); 392–400.

भारतीय प्रौद्योगिकी संस्थान गुवाहाटी
Indian Institute of Technology Guwahati

Chapter 7

Overview and Suggestions for Future Research

Overview and Suggestions for Future Research

Deep desulfurization of the liquid transportation fuel is an urgent need of the hour, in view of the environmental pollution caused by SOx emissions from vehicular and other engine exhausts. The conventional technology of hydrodesulfurization is not able to achieve the prescribed limits of sulfur content of liquid fuels, and hence, past several years have witnessed quest for alternative technologies by scientists and engineers. Two technologies that have shown high promise for deep desulfurization of fuels are: oxidative desulfurization and biodesulfurization. In addition, these technologies also have other merits such as no requirement of expensive hydrogen during treatment, and much milder operating conditions and eco-friendly nature, as compared to hydrodesulfurization. More recently, these techniques have been coupled with sonolysis in order to enhance the kinetics and efficiency of sulfur removal. The ultrasound-assisted desulfurization techniques – collectively called as "sono-hybrid" techniques – have been proven to be far efficient on laboratory scale research. The exact physical mechanism of these processes has not been identified and established

yet. This thesis has made an attempt to deduce the physical mechanism of sono-hybrid techniques of through approach of concurrent analysis of experimental results and simulations of cavitation bubble dynamics. In this chapter, we take an overview of the findings of this research work. Given below is a summary of the main results of each of preceding 5 chapters. These results, when viewed and analyzed at a glance, present a cogent and coherent physical picture of the mechanism of sono-hybrid processes. Some remarkable similarities in physical mechanism of these processes - despite significantly different chemistry – are also evident.

- Chapter 2 treated the system of ultrasound-assisted oxidative desulfurization (UAOD) process using Fenton-Peracetic acid as oxidant. H_2O_2 was revealed to be the key component of oxidant, which balanced several competing pathways and reactions of overall oxidative desulfurization process. Addition of Fe^{2+} to peracetic acid had a beneficial effect while excess H_2O_2 has an adverse effect on the process. Transient cavitation was revealed to play a negative role in the desulfurization process, while ultrasound has a positive effect. The former effect is a consequence of scavenging of $HO_2^{\bullet}$ radicals in the aqueous phase by radicals generated by cavitation bubbles, while the latter effect is attributed to generation of fine emulsion between oxidant and toluene phases due to strong micro-mixing generated by ultrasound. This study clearly pointed out that lesser scavenging and effective interphase transfer of $HO_2^{\bullet}$ radicals is more crucial to utilization of $HO_2^{\bullet}$ radicals for desulfurization than mere generation of these radicals.

- In Chapter 3, physical mechanism of the oxidative desulfurization process simultaneously assisted by ultrasound and phase transfer agent (PTA) was deduced. A distinction was made among individual beneficial effects of PTA and ultrasound on the oxidative desulfurization system, and also the synergy between the effects of PTA

and ultrasound. Effect of PTA was more marked for mechanically stirred system due to mass transfer limitations, while intense emulsification due to ultrasound helps overcome the mass transfer limitations and reduces the extent of enhancement of oxidation by PTA. Despite application of PTA and ultrasound, the intrinsic factors and properties of the reactants such as polarity (and hence partition coefficient) and diffusivity were revealed to have a crucial effect on the extent of oxidation. The intrinsic reactivity of the oxidant also played a vital role, as seen from the extent of oxidation achieved with performic acid and peracetic acid. It was revealed that interfacial transport of oxidant in the form of oxidant–PTA complex reduced the undesired consumption of oxidant by the reducing species formed during transient cavitation in organic medium, which helped effective utilization of oxidant towards desulfurization.

- Chapter 4 presented further research on physical mechanism of phase transfer agent (PTA) assisted ultrasonic oxidative desulfurization process. Synergistic links between mechanisms of PTA and ultrasound/ cavitation were identified by coupling experimental results with simulations of cavitation bubble dynamics, and Arrhenius & thermodynamic analysis of reaction kinetics. It was revealed that ultrasonic oxidative desulfurization had radical–based mechanism with least activation energy. However, due to high instability of radicals, the frequency factor (or fruitful collisions among reactant species) was small leading to low DBT oxidation. PTA–assisted oxidative desulfurization had ionic mechanism with much higher activation energy. The synergistic effect of fine emulsification generated by micro–convection due to ultrasound and cavitation, and PTA–assisted interphase transport of oxidant resulted in almost complete oxidation of DBT. These results essentially established that synergy between mechanisms of ultrasound/ cavitation and PTA was predominantly

of physical nature. Moreover, effect of PTA was more marked for ultrasonic system than mechanically agitated system.

- Chapter 5 attempted to gain mechanistic insight into enhancement effect of sonication on biodesulfurization. The approach adopted in this chapter was that of fitting the Haldane kinetics model (substrate inhibition) to dibenzothiophene (DBT) metabolism and analyze trends in model parameters concurrently with simulations of cavitation bubble dynamics. Mechanistic synergy between sonication and biodesulfurization is revealed to be of both physical and chemical nature. Generation of micro-turbulence in medium by sonication has lead to fine emulsification and enhancement of DBT transport across organic/ aqueous interphase. Microturbulence also enhanced transport of substrate and product across cell wall that increases reaction velocity (V_{max}). However, Michaelis constant (K_m) and inhibition constant (K_I), being intrinsic parameters, remained unaffected by sonication. Radicals produced by transient cavitation independently oxidized DBT to DBT-sulfoxide and DBT-sulfone (intermediates of metabolism), which contributed to enhancement of biodesulfurization. However, high shear generated by ultrasound and cavitation had an adverse effect on action of surfactant β-cyclodextrin for enhancement of interphase transport of DBT.
- Chapter 6 treated the subject of ultrasound–assisted enzymatic desulfurization using system comprising Horseradish peroxidase enzyme and dibenzothiophene (DBT). Pathway for enzymatic desulfurization (comprising DBT–sulfoxide and DBT–sulfone as intermediates and 4–methoxy benzoic acid as final product) was established with GC–MS analysis. Intrinsic fluorescence and circular dichroism spectra of ultrasound–treated enzyme revealed conformational changes in the secondary structure of the enzyme (reduction in α–helix and β–conformations and

increase in random coil content) leading to enhancement in its activity. Concurrent analysis of desulfurization profiles, Arrhenius and thermodynamic parameters, and simulations of cavitation bubble dynamics revealed that strong micro–convection generated by sonication enhanced enzyme activity and desulfurization kinetics. Parallel oxidation of DBT by radicals generated from transient cavitation gave further boost to desulfurization kinetics. However, random motion of enzyme molecules induced by shock waves reduced the frequency factor (or fruitful collisions between reactant species) and put a limit on the ultrasonic enhancement of enzymatic desulfurization.

All of these results when viewed at a glance clearly reveal that in all sono-hybrid systems, physical effects of ultrasound and cavitation played dominant role in enhancing effect of the coupling technique – whether peracid, or Fenton-peracid or PTA-peracid or microbial or enzymatic. Among the individual effects of ultrasound and cavitation, the former is revealed to have more constructive effect on the system due to continuous nature of the micro-convection generated by micro-steaming. The physical effect of shock wave generated by cavitation is revealed to have a negative effect. In case of both PTA-assisted peracid oxidation and enzymatic treatment, low frequency factor was attributed to intermittent and sporadic nature of the shock waves. Nonetheless, shock waves did contribute to emulsification leading to higher interfacial area. In all systems, the activation energy of the desulfurization process has been revealed to reduce with application of ultrasound. Another striking similarity is in the synergism between chemical effect of cavitation and the microbial and enzymatic degradation of DBT. In both of these systems, the independent oxidation of DBT induced by the radicals generated by the transient cavitation gives rise to intermediates of the metabolic pathway – which assists faster conversion of the DBT

into the final product of either HBP or 4-methoxy benzoic acid. For enzymatic system, the shock waves have both beneficial and adverse effect. Strong microturbulence generated by these waves lead to conformational changes and unfolding of enzyme protein leading to higher activity, while random movements of the enzyme molecules induced by shock waves bring down the frequency factor leading to slowing down of kinetics, despite lower activation energy. Main cause leading to low contribution of the chemical effect of cavitation to enhancement of desulfurization process is highly sporadic nature of cavitation events in both space and time.

The results of this thesis also stimulate further research in mechanistic issues of ultrasound assisted (or sono-hybrid) processes for desulfurization of liquid fuels:

1. In all studies in this thesis, the frequency of the ultrasound has been kept constant. It would be worthwhile to conduct the same studies at different frequencies so as to ascertain the individual contributions of ultrasound and cavitation to the system.

2. Low frequency factors in case of sono-hybrid processes have been attributed to random fluid movement induced by shock waves. This hypothesis could be ascertained with high speed photographic studies using suitable tracers or model compounds.

3. In all of the systems, a single sulfur compound (DBT) has been used as model. A mixture of different sulfur compounds with varying reactivity could also be attempted. The preference of reduction in these compounds can give inputs towards effectiveness of either oxidative or microbial/enzymatic system for handling practical fuels.

4. In Chapter 6, it was revealed that ultrasound induces conformational changes in the structure of HRP enzyme leading to increase in its activity. This theme can be studied further with greater details. In addition to circular dichroism, X-ray crystallographic studies of the ultrasound treated enzyme can be carried out to reveal the exact 3-D structure of the enzyme after sonication treatment. This will help in putting the arguments reg. effect of sonication on enzyme activity presented in chapter 5 on a firmer basis.

4. Finally, the experiments reported in this thesis could also be attempted on higher processing scale – either bench or pilot scale. Large ultrasound baths available commercially could be directly used for these experiments.

Table 7.1: Summary of % DBT Oxidation Obtained in Different Systems

Chapter	Process	DBT oxidation (%)	k (min^{-1})	R^2
Chapter 2	US + CH_3COOH + H_2O_2 + Fe^{2+}	24.74 ± 0.28	3.62×10^{-3}	0.99
	US + CH_3COOH + H_2O_2 + Fe^{2+} (1.6 bar)	32.56 ± 0.78	8.01×10^{-3}	0.83
Chapter 3	US + FA + H_2O_2 + TOAB	42.00 ± 0.96	7.50×10^{-3}	0.93
	US + FA + H_2O_2 + TOAB (1.6 bar)	37.05 ± 0.59	2.11×10^{-2}	0.89
Chapter 4	MS +PFA + TBAB	63.5 ± 0.92	1.22×10^{-2}	0.96
	US +PFA + TBAB	96.65 ± 1.06	4.26×10^{-2}	0.97
	US + PFA+ TBAB + ESP (1.6 bar)	77.6 ± 1.32	1.52×10^{-2}	0.85
Chapter 5	Mechanical shaking with sonication (free cells)	57.4 ± 1.12	--	--
	Mechanical shaking with sonication (immobilized cells)	71.42 ± 1.20	--	--
	Mechanical shaking with sonication and β-CD addition (free cells)	64.44 ± 1.34	--	--
	Mechanical shaking with sonication and β-CD addition (immobilized cells)	75.56 ± 1.31	--	--
Chapter 6	Sono–enzymatic treatment (P_o = 101.3 kPa)	65.24 ± 1.10	1.83×10^{-4}	0.96
	Sono–enzymatic treatment (P_o = 162 kPa)	49.57 ± 1.18	1.25×10^{-4}	0.95

भारतीय प्रौद्योगिकी संस्थान गुवाहाटी
Indian Institute of Technology Guwahati

ACKNOWLEDGEMENTS

I owe my deepest gratitude to all those who made this thesis possible. The first and foremost appreciation goes to my supervisor **Prof. Vijayanand S. Moholkar** for his valuable suggestions, encouragement and constant support throughout my research work. He has been a true source of inspiration and spending his precious time for discussion by which I have gain immense skill of knowledge in terms of research.

I would like to acknowledge my sincere gratitude to my doctoral committee members, Dr. M. K. Purkait, Prof. P. Ghosh, and Dr. Debashish Das for their insightful advices and suggestions throughput the research.

My sincere thanks got to Prof. Pranab Goswami for their kind help.I am thankful to the Chemical Engineering Department and also to the faculty members for their constant support. The kind and constant help of the staff members of Department of Chemical Engineering, IIT Guwahati. I am also thankful to the **Indian Institute of Technology Guwahati** for providing me with the state of the art infrastructure for advance level of research.

I am thankful to my seniors Dr. Amrita Ranjan, Dr. Swati Khanna, Dr. Hanif Choudhury for their valuable guidance. I also extend my thanks to my colleagues and friends, Dr. Shuchi, Dr. Sankar, Pritam, Maneesh, Arup, Shyamali, Ritesh, Amit, for their constant help and enthusiastic company.

Finally, yet importantly, I would like to express my heartfelt thanks to GOD, my wife Mrs. Sonu Bhasarkar for her support, immense care and encouragement. At last but not the least, I am highly indebted to my Mummy Mrs. Arifa Bhasarkar and my father

for all the sacrifices they made for my better future and giving me freedom to take my own decision. My Ph.D. endeavor could not be completed without their endless love and blessing. Special thanks to my Mummy, this is all because of you.

Jaykumar B. Bhasarkar

January 2016, Guwahati

RESEARCH OUTPUT OF THE THESIS

PAPERS IN PEER REVIEWED INTERNATIONAL JOURNALS

(1) Bhasarkar JB, Chakma S, Moholkar VS. Mechanistic features of oxidative desulfurization using sono–Fenton–peracetic acid (Ultrasound/ Fe^{2+}–CH_3COOH–H_2O_2) system. *Industrial and Engineering Chemistry Research* 2013; 52: 9038–9047.

(2) Bhasarkar JB, Chakma S, Moholkar VS. Investigations in physical mechanism of the oxidative desulfurization process assisted simultaneously by phase transfer agent and ultrasound. *Ultrasonics Sonochemistry* 2015; 24: 98-106.

(3) Bhasarkar JB, Dikshit PK, Moholkar VS. Ultrasound assisted biodesulfurization of liquid fuel using free and immobilized cells of *Rhodococcus rhodochrous* MTCC 3552: A mechanistic investigation. *Bioresource Technology* 2015; 187: 369-378.

(4) Bhasarkar JB, Borah AJ, Moholkar VS. Mechanistic analysis of ultrasound assisted enzymatic desulfurization of liquid fuels using Horseradish Peroxidase. *Bioresource Technology* 2015; 196: 88-98.

(5) Bhasarkar JB, Singh M, Moholkar VS. Mechanistic insight into phase transfer agent assisted ultrasonic desulfurization. *RSC Advances* 2015; 5 (125): 102953-102964.

BOOK CHAPTER

Moholkar VS, Choudhury HA, Singh S, Khanna S, Ranjan A, Chakma S, Bhasarkar JB. Physical and chemical mechanisms of ultrasound in biofuel synthesis. In: Production of Biofuels and Chemical with Ultrasound (Z Fang, RL Smith, X Qi, editors), Biofuels and Biorefineries series (Vol. 4), Springer Science + Business Media, Dordrecht (2015), pp. 35–86.